AD-A037 412 DEVELOPMENT OF SANDWICH STRUCTURED PHOTOSENSITIVE FILMS FOR APPLICATION TO NON-CONTACT POTENTIOMETERS(U) NAVAL AVIONICS FACILITY INDIANAPOLIS IND G A MAGEE NOV 76 1/3

UNCLASSIFIED NAFI-TR-2148-REV-1 F/G 14/2 NL

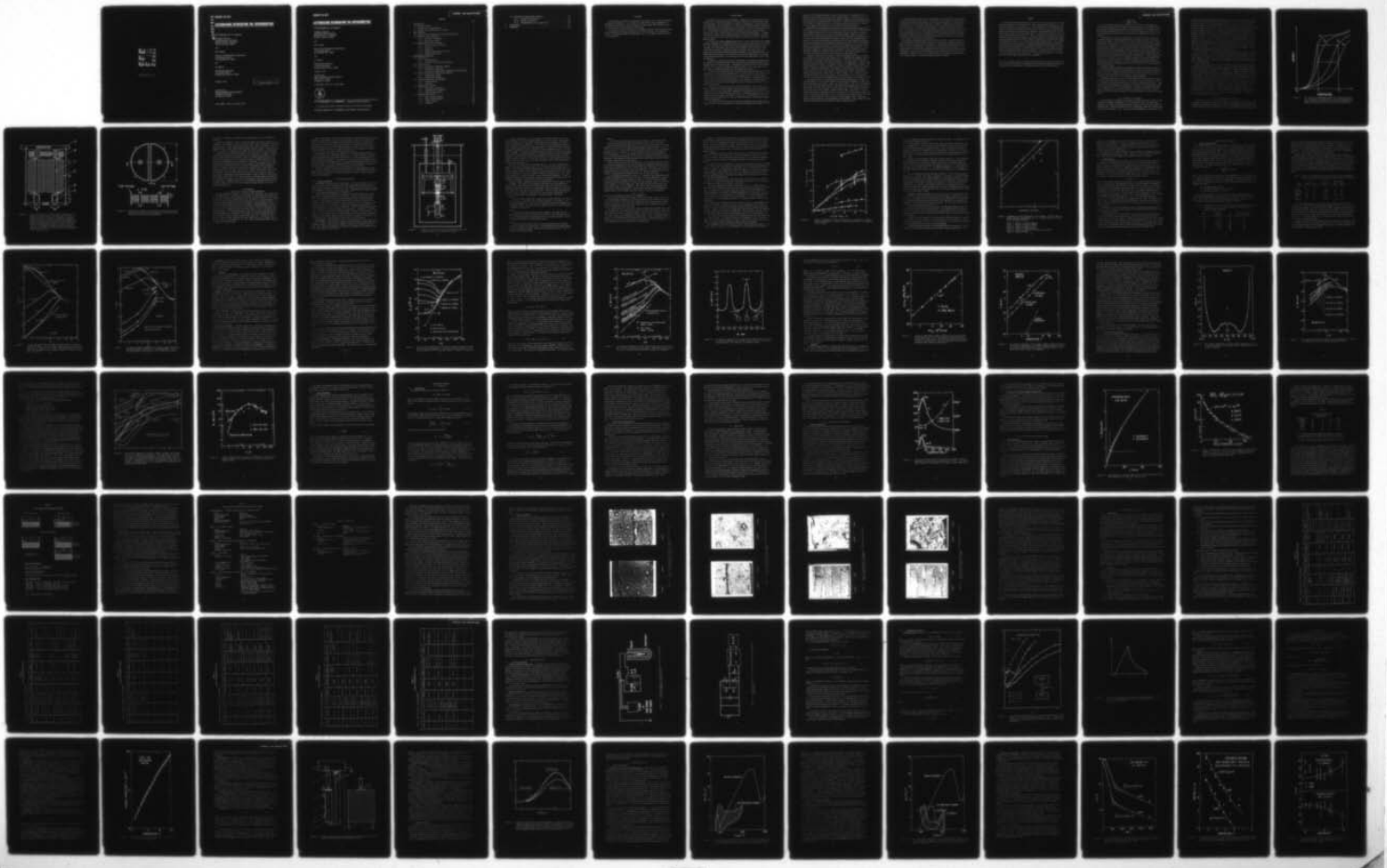

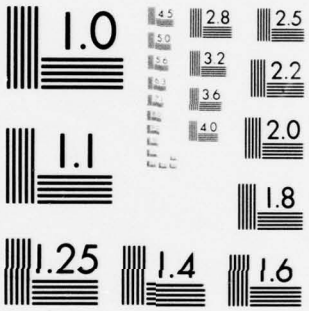

MICROCOPY RESOLUTION TEST CHART
NATIONAL BUREAU OF STANDARDS-1963-A

AD A037412

NBSIR 76-847

ELECTROCALORIC REFRIGERATION FOR SUPERCONDUCTORS

Ray Radebaugh and J.D. Siegwarth

Cryogenics Division
Institute for Basic Standards
National Bureau of Standards
Boulder, Colorado 80302

and

W.N. Lawless

Research and Development Laboratories
Corning Glass Works
Corning, New York 14830

and

A.J. Morrow

Development Laboratory
Corning Glass Works
Raleigh, North Carolina 27604

DISTRIBUTION STATEMENT A
Approved for public release;
Distribution Unlimited

February 1977

Sponsored by
Advanced Research Projects Agency
ARPA Order No. 2535
Arlington, VA 22209

Covers May 1, 1973 to June 30, 1975

NBSIR 76-847

ELECTROCALORIC REFRIGERATION FOR SUPERCONDUCTORS

Ray Radebaugh and J.D. Siegwarth

Cryogenics Division
Institute for Basic Standards
National Bureau of Standards
Boulder, Colorado 80302

and

W.N. Lawless

Research and Development Laboratories
Corning Glass Works
Corning, New York 14830

and

A.J. Morrow

Development Laboratory
Corning Glass Works
Raleigh, North Carolina 27604

February 1977

Sponsored by
Advanced Research Projects Agency
ARPA Order No. 2535
Arlington, VA 22209

Covers May 1, 1973 to June 30, 1975

U.S. DEPARTMENT OF COMMERCE, Juanita M. Kreps, Secretary

Dr. Betsy Ancker-Johnson, Assistant Secretary for Science and Technology

NATIONAL BUREAU OF STANDARDS, Ernest Ambler, Acting Director

PRECEDING PAGE BLANK-NOT FILMED

CONTENTS

		Page
1.	INTRODUCTION	1
	1.1. Purpose of Work	1
	1.2. Description of Refrigerator	1
	1.3. History and Organization of Project	2
2.	HEAT SWITCHES	6
	2.1. Types of Heat Switches and Minimum Requirements	6
	2.2. Mechanical Heat Switches	7
	2.2.1. Multiple leaf switch	7
	2.2.2. Helium gap switch	15
	2.3. Magnetothermal Heat Switches	16
	2.3.1. Survey of various metals	16
	2.3.2. Beryllium	20
	2.3.3. Magnesium	26
	2.3.4. Thermal conductance of joints	29
	2.3.5. Magnet requirements	35
3.	REFRIGERATION MATERIALS	36
	3.1. Theoretical	36
	3.1.1. Thermodynamics	36
	3.1.2. Criteria for materials selection	38
	3.2. Previous Work	39
	3.3. $SrTiO_3$ Glass-Ceramic Research Samples	40
	3.3.1. Dielectric properties	40
	3.3.2. Relation to capacitance thermometer manufacturing	42
	3.4. $SrTiO_3$ Glass-Ceramic Multilayer Samples	42
	3.4.1. Fabrication method	42
	3.4.2. Fabrication problems	51
	3.5. Alternate Materials Investigated	57
	3.5.1. Glass-ceramics	57
	3.5.2. Ceramics	57
	3.6. Experimental Methods	66
	3.6.1. Dielectric properties	66
	3.6.2. Thermodynamic properties	70
	3.6.3. Thermal conductivity	80
	3.7. Experimental Results	82
	3.7.1. $SrTiO_3$ glass-ceramics	82
	3.7.2. $KTaO_3$ glass-ceramics	108
	3.7.3. Single crystals	108
	3.7.4. Ceramics	113

3.8. Discussion of Experimental Results. 143
3.8.1. Dielectric Properties 143
3.8.2. Thermal Properties. 150
3.8.3. Recommendations for further work. 175
4. CONCLUSIONS. 176
5. REFERENCES 178

DISCLAIMER

Certain commercial materials are identified in this report in order to specify adequately the experimental procedure. In no case does such identification imply recommendation or endorsement by the National Bureau of Standards, nor does it imply that the material identified is necessarily the best available for the purpose.

The views and conclusions contained in this document are those of the authors and should not be interpreted as necessarily representing the official policies, either expressed or implied, of the Advanced Research Projects Agency, the U. S. Government, Corning Glass Works or its subsidiaries.

PROJECT SUMMARY

The purpose of this work was to investigate a technique for the refrigeration of superconductors at 4 K which has the potential of better reliability and lower cost than present 4 K refrigerators. The poor reliability in present 4 K refrigerators is a major handicap in the technological use of superconductors. In this project a solid-state type of refrigeration was investigated for use as the final stage of refrigeration to span the range between 4 and 15 K. This proposed new technique uses the electrocaloric effect in certain dielectric materials and is the electrical analog of cooling by adiabatic demagnetization. In essence, a high electric field is used to change the entropy of a paraelectric material. The advantage over the magnetic case is that electric fields in thin layers are easier to apply than magnetic fields.

A continuous refrigerator operating with a load at 4 K and a heat sink at 15 K is accomplished by separating the refrigeration material from the load and heat sink by heat switches. The original problems in the project were to develop appropriate heat switches for use on a prototype, 1-watt refrigerator and to develop the refrigeration material based on $SrTiO_3$ glass-ceramic technology. Preliminary studies had indicated that certain $SrTiO_3$ glass-ceramics would be the most promising refrigeration material in this temperature range. The program was well along before it was found that $SrTiO_3$ glass-ceramics would not be suitable as the refrigeration material; this conclusion then led to the investigation of other potential materials.

The heat-switch problem was attacked by investigating both mechanical and magnetothermal heat switches. The mechanical switch, which has moving parts, used forced contact between multiple leaves of gold-plated copper. Conductances on the order of 5 W/K could be achieved with about 10 such contacts and with on-to-off heat transfer ratios on the order of 1000. Such a ratio is significantly higher than the required value of about 30.

A literature review showed that both single crystal gallium and tungsten would be useful materials for the lower (between refrigerator and 4 K load) heat switch. Such materials show large changes in the thermal conductivity at low temperatures when a transverse magnetic field is applied. Switch ratios on the order of 100 are possible. The magnetothermal conductivity of single crystal beryllium was measured in this program and the results show that this material can be used for both the upper and lower heat switches with a switch ratio of about 100 in both cases.

A compilation of literature data on the thermal conductance of joints (solder, grease, adhesive, pressure) was made and revealed a lack of data between 4 K and room temperature on solder joints. Such joints have higher conductances at room temperature than any other type and would be used in the electrocaloric refrigerator. Measurements were made on the thermal conductance of indium solder joints between 2 K and 120 K. The conductance per unit area reached a peak of 100 W/cm^2K at 20 K, which is sufficiently high to eliminate most problems with joint conductances.

In any dielectric material the entropy change or refrigeration power brought about by a change in electric field is proportional to the change of polarization with respect to tem-

perature. When no remanent polarization occurs in the material, the polarization can be derived from the dielectric constant, an easily measured quantity. Therefore, early in the program the change of dielectric constant with respect to temperature was a primary quantity for estimating the refrigeration power of a material. The $SrTiO_3$ glass-ceramic showed a peak in the dielectric constant at about 30 K with a large positive slope below that. The positive slope implied cooling would occur when the electric field was increased.

Many manufacturing problems had to be overcome in making satisfactory multilayer $SrTiO_3$ glass-ceramics with large temperature derivatives of the dielectric constant and large electric field breakdown strengths and over half the experimental work on the program was devoted to these problems. Sample porosity was the major unsolvable problem. However, it was then discovered that the inherent electrocaloric effect in $SrTiO_3$ multilayer glass-ceramics at 4 K not only was very small and dominated by hysteretic effects, but that it probably had the wrong sign. Definite electrocaloric cooling was seen in the 10-40 K temperature range when the field was decreased, but the temperature changes were only about 0.03 K. Direct measurements of dc polarization were made on the samples and the results were consistent with the electrocaloric measurements but inconsistent with the dielectric constant behavior. The dc polarization showed only a negative slope with temperature, and the polarization became essentially independent of temperature below about 10 K. The dielectric constant, on the other hand, had a peak at about 30 K with a large positive slope below that.

Extensive dc polarization and dielectric constant measurements were made on the $SrTiO_3$ glass-ceramics as well as many other materials to try to understand the fundamental discrepancy between the two types of dielectric measurements. It was found that many dielectric materials show a broad peak in the dielectric constant at low temperatures. In the past such peaks have usually been taken as an indication of ferro- or antiferroelectric ordering. The model developed here to explain the peak in the dielectric constant is based on the electret behavior of impurity-vacancy dipoles in the material. Impurity levels in the parts per million range can give rise to such effects. Application of an electric field produces a remanent polarization which remains after the field is removed. It is a result of the electret behavior and not that of a ferroelectric. The polarization, and not the dielectric constant, is then the proper thermodynamic quantity for predicting the electrocaloric effects.

Many other materials were investigated by polarization, electrocaloric, and specific heat measurements to find a suitable material for electrocaloric refrigeration. These other materials included glass-ceramics, ceramics, and single crystals. Most of the investigations were on $SrTiO_3$ and $KTaO_3$ based materials. Other materials investigated were of the $Pb_2Nb_2O_7$ type ceramics, the polar PZT ceramics, and TlBr single crystal. The largest electrocaloric effects were seen in $SrTiO_3$ ceramics, followed closely by $KTaO_3$ single crystal. In $SrTiO_3$ ceramics electrocaloric temperature changes on the order of 0.5 K were observed at about 10 K. The effect decreased significantly at 4 K. For various practical reasons the electric fields applied to these samples were usually limited to relatively modest values. Without any existing theoretical model for the thermodynamics of the materials, it was uncertain how much larger the electrocaloric effects would be if higher fields were applied.

A theoretical model, based on the lattice dynamics of the materials, was then developed to explain the observed cooling effects. Dielectrically active materials are classified as either displacive type or order-disorder type. The materials studied in this program were of the displacive type since they are usually more active at low temperatures than the order-disorder materials. The theoretical model developed is valid for the displacive type materials. In this model only the entropy associated with transverse optic phonons can be altered with an applied electric field. The calculated temperature changes for $SrTiO_3$, $KTaO_3$, and TlBr agree reasonably well with the observed values. This model shows that at 4 K the maximum possible entropy changes in the displacive type materials are at least an order of magnitude too small to make a practical refrigerator.

The report is concluded by stressing the need to concentrate on a search for an appropriate order-disorder type of dielectric because the possible entropy changes are orders of magnitude higher than the displacive type materials. Unfortunately order-disorder materials order at rather high temperatures, thus removing the available entropy for cooling. It is suggested that for any future work thermodynamic studies be made on lithium thallium tartrate and $NH_4H_2PO_4$, which may be order-disorder materials with enough entropy at 4 K for useful refrigeration. However, at this time the basic physics of the dielectric materials must be better understood before a worthwhile development program could begin.

ABSTRACT

A solid state type of refrigeration, which utilizes the electrocaloric effect in certain dielectric materials, has been investigated. Such a refrigerator would operate with a load at 4 K and reject heat to a reservoir at 15 K. Heat switches for such a refrigerator were studied. One type was a multiple leaf contact switch. The other type was a magnetothermal switch utilizing single crystal beryllium. Based upon earlier preliminary work, the refrigeration material was to be a $SrTiO_3$ glass-ceramic. It was found here that such a material has no useful electrocaloric effect at 4 K. Many other materials were studied but none were found with sufficiently high reversible electrocaloric effects for a practical refrigerator. The largest effects were seen in $SrTiO_3$ ceramics, followed by $KTaO_3$ single crystal. Temperature reductions of about 0.5 K at 10 K were observed during depolarization. A theoretical model, based on the electret behavior of impurity-vacancy dipoles was developed to explain the observed dielectric behavior in the materials investigated. Another theoretical model, based on the lattice dynamics of displacive dielectrics, was used to explain the observed entropy and temperature changes seen in such materials. The model points out that displacive type materials have too low entropies at 4 K for practical refrigeration. An investigation of certain order-disorder dielectrics is suggested.

Key words: Beryllium; ceramics; cryogenics; dielectric-constant; electrets; electrocaloric effect; entropy; ferroelectrics; glass-ceramics; heat switches; magnetothermal conductivity; polarization; potassium tantalate; refrigeration; specific heat; strontium titanate.

PRECEDING PAGE BLANK-NOT FILMED

1. INTRODUCTION

1.1. Purpose of Work

One of the largest applications of cryogenics is in the area of superconductivity. These applications range from the low-power level devices employing the Josephson effect up to the large scale superconducting magnets and rotating machinery. These superconducting devices require temperatures below 15 K, and in most cases temperatures of about 4 K. In certain limited cases, infrared detection also requires 4 K temperatures or lower to gain sensitivity.

The unreliability of present 4 K refrigerators is probably the main reason for the relatively slow growth of applied superconductivity in commercial markets. A mean-time-between-failure (MTBF) of about 3000 hours is a typical figure for such machines. Specialized mechanics are required to work on such machines and their presence every few thousand hours serves as a reminder that 4 K is not easily achieved. Rotating compressors and expanders now offer some hope for a MTBF of about 10,000 hours for large 4 K refrigerators. The Stirling cycle and Gifford-McMahon cycle refrigerators can also achieve a MTBF of 10,000 hours even on a small size machine of about 1 watt. Unfortunately the regenerative heat exchangers used on such machines become ineffective below about 10 K. What is needed then to reach 4 K with such a machine is a very reliable last stage to span the gap between about 15 K and 4 K. In addition, this last stage should operate close to Carnot efficiency to maintain a good overall efficiency. A survey of cryogenic refrigerators[1] shows that 4 K refrigerators operate at the same fraction of Carnot efficiency as do 10-30 K refrigerators of the same power rating.

Preliminary studies[2] showed that a refrigerator utilizing the electrocaloric effect in certain glass-based materials would make a promising last stage to span the gap between 15 K and 4 K. Since it is inherently a solid state type of device, the reliability of the electrocaloric refrigerator should far exceed that of the 15 K upper stage. Thus 4 K can be reached with the reliability of a 15 K regenerative type refrigerator.

The purpose of this project was to study the feasibility of an electrocaloric refrigerator which would absorb roughly 1 watt at 4 K and reject the heat to a reservoir at about 15 K. Originally the refrigeration material was to have been a glass-ceramic of $SrTiO_3$. That choice was based on preliminary mea surements and calculations[2] of the thermodynamic properties of research samples of $SrTiO_3$ glass-ceramics. Subsequent measurements on multilayer samples manufactured from this material showed relatively small cooling effects and the program was altered to study the potential of using other materials with large electrocaloric effects.

1.2. Description of Refrigerator

The electrocaloric refrigerator is analogous to a magnetic refrigerator, which is often referred to as adiabatic demagnetization.[3] The difference is that in the electrocaloric refrigerator the entropy of the working material is changed by an electric field rather than a magnetic field. The first experiments with the electrocaloric effect were on Rochelle salt by Kobeko and Kurtschatov[4] in 1930. Since then several measurements of electrocaloric cool-

ing effects in various materials have been measured, but until now no attempt has been made to make a refrigerator utilizing the electrocaloric effect. Quasicontinuous refrigeration is achieved by taking the refrigerating material through a closed loop on an entropy versus temperature diagram. Such a path is shown in figure 1. The entropy of the material is shown for four different values of electric field. If we start at the temperature T_2 in a field of E_4 and then change the field to E_2, the material cools adiabatically to the temperature T_1. When going from the field E_2 to E_1 in an isothermal process, heat in the amount $Q_1 = T_1\Delta S$ is absorbed. The change in field from E_1 to E_3 causes the sample to heat adiabatically to T_2. An amount of heat $Q_2 = T_2\Delta S$ is then rejected to a thermal reservoir at T_2 during the field change from E_3 to E_4. The ratio of heat rejected at T_2 to the heat absorbed at T_1 is then simply the Carnot result $Q_2/Q_1 = T_2/T_1$ for the ideal cycle discussed here. If now two refrigerators are operated simultaneously such that at any time one or the other is in that part of the cycle where $T = T_1$, then continuous refrigeration at T_1 is achieved[2]. Preliminary studies[2] showed that cycle times on the order of 1 second would be optimum for a refrigerator of $SrTiO_3$ glass-ceramic operating between 4 and 15 K.

A schematic diagram[2] of an electrocaloric refrigerator capable of continuous refrigeration is shown in figure 2. The working material is separated from the reservoir at 15 K and the load at 4 K by heat switches. The working material has closely spaced metal fins in it, as in a capacitor, to provide heat transfer and a means of obtaining a high electric field with a reasonable voltage. The two halves can be made in the form of two half cylinders (see Fig. 2b) to conserve space.

A rather unique refrigeration cycle was proposed by van Geuns[5] which has applications to the electrocaloric refrigerator. His idea is to use high pressure helium gas as a regenerative material to change the temperature of a paramagnetic or paraelectric material between 15 and 4 K. In that case the adiabatic lines in figure 1 are replaced by constant field lines. In the real cycle, however, there must be a small adiabatic segment at the end of the cooling or heating step to account for the finite ΔT required between the helium gas and the refrigeration material. With this regenerative cycle the heat load due to the lattice heat capacity is nearly eliminated from each cycle, but the initial cool down from 15 K is then done in very small steps until equilibrium is established in the helium gas. The helium gas must be at a high pressure (above the critical pressure) to provide a high heat capacity. The high pressure can pose certain mechanical problems in displacing the gas with respect to the refrigeration material. Whether this type of mechanical device would be any more reliable than a mechanical 4 K refrigerator can only be determined by experiment. We have not pursued this type of cycle in this project. Instead the heat switch arrangement has been pursued since it can be made with no moving parts.

1.3. History and Organization of Project

Glass-ceramics of $SrTiO_3$ developed by Lawless[6] show large changes in dielectric constant with respect to temperature. Because of that behavior, such a material has been useful for low temperature capacitance thermometers.[6,7] Corning Glass Works and the Cryogenics Division of NBS collaborated on extending measurements of the capacitance thermometer to temperatures

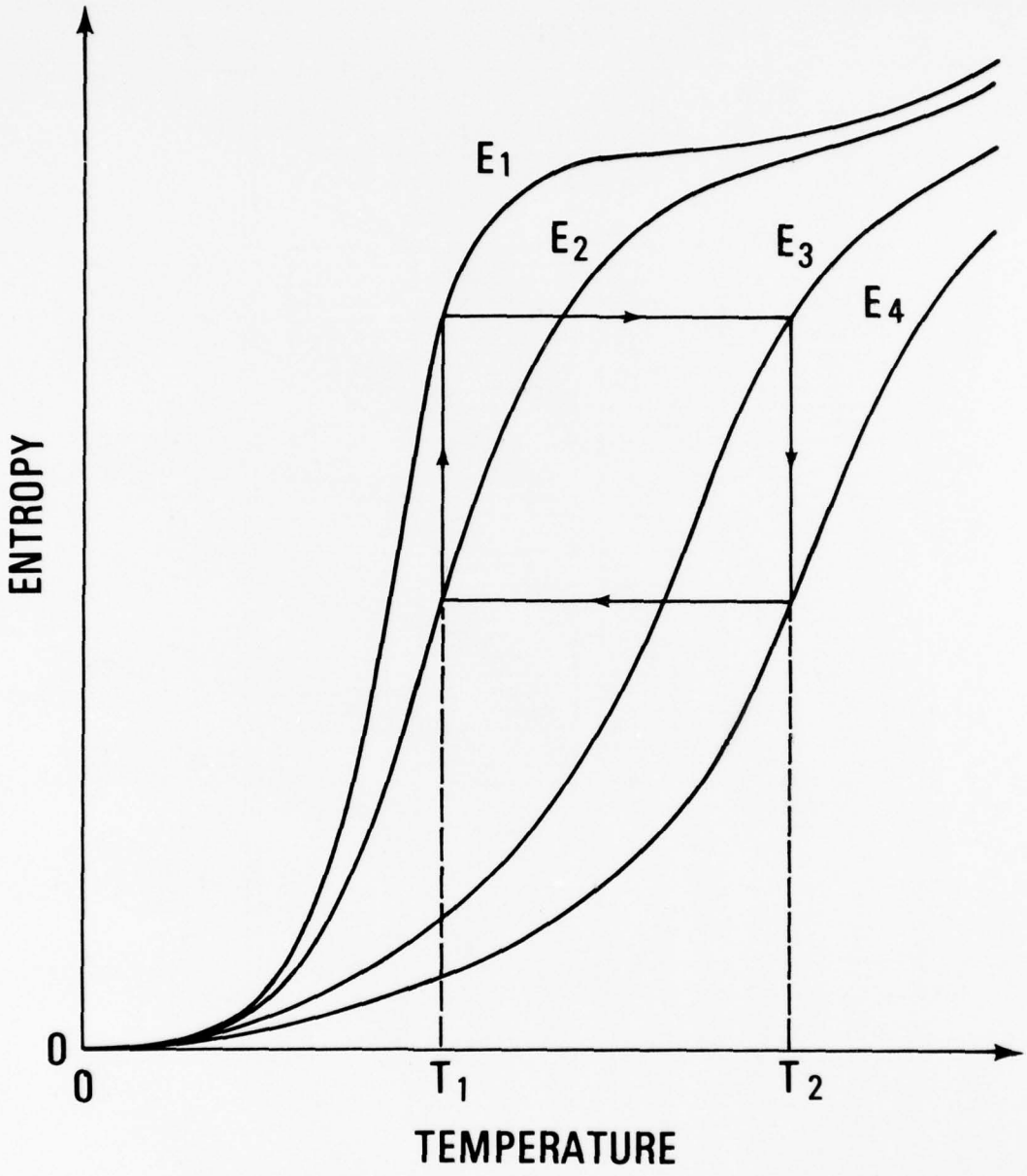

Figure 1. The entropy vs. temperature curves for a material useful for electrocaloric refrigeration. The ideal refrigeration cycle, shown by the arrows, is traced out by changing the electric field from E_1 to E_3 to E_4 to E_2 and back to E_1.

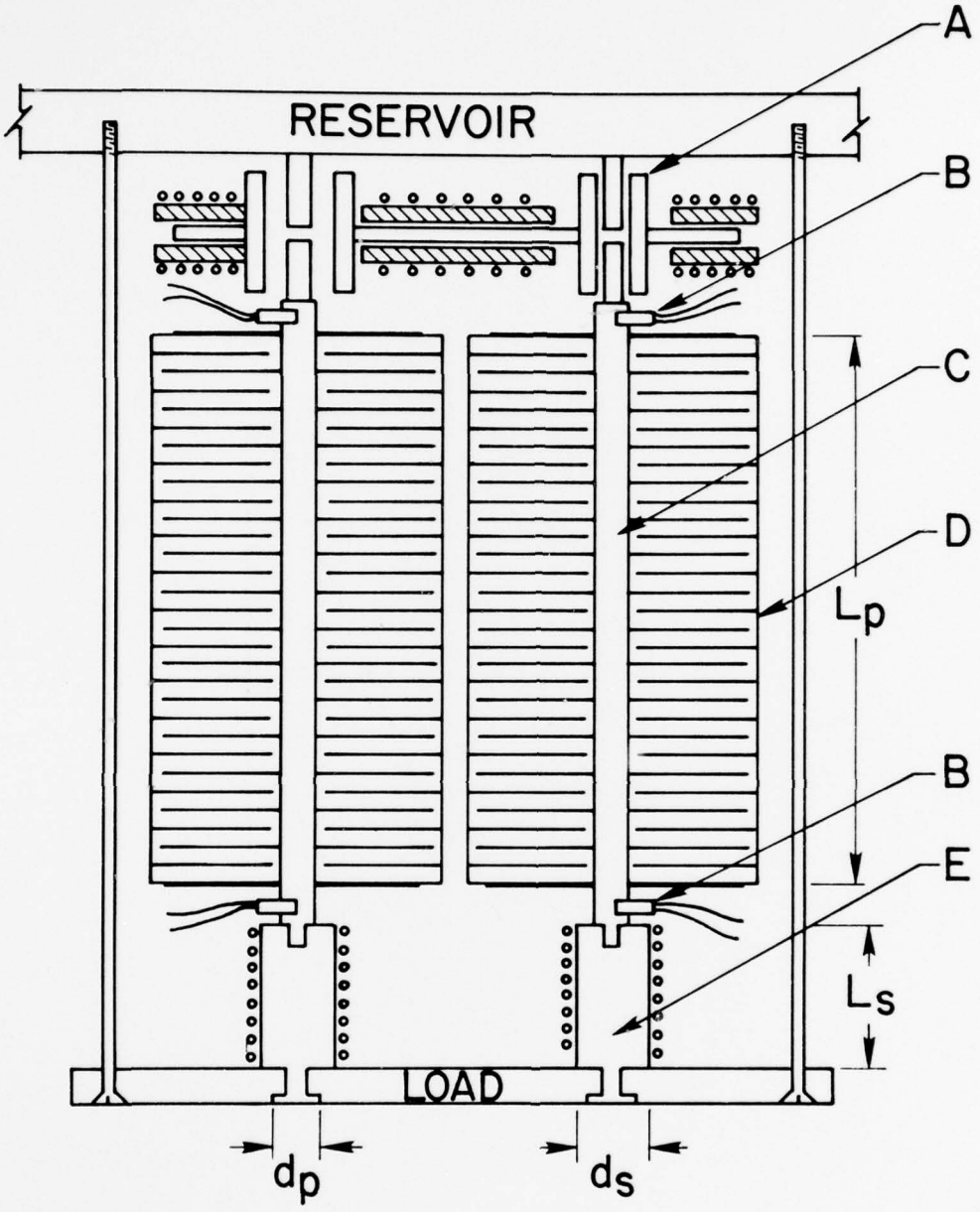

Figure 2a. Vertical cross section of the model refrigerator: (A) Mechanical thermal valve (left-hand valve is closed, right-hand valve is open); (B) Temperature sensors to monitor operation; (C) Metal post running lengthwise through the element and acting both as low voltage lead and heat conductor (see also Fig. 2b); (D) Dielectric element with interspersed metal electrodes (see also Fig. 2b); (E) Magnetic thermal valve which thermally connects or isolates the element from the load depending on the magnetic field.

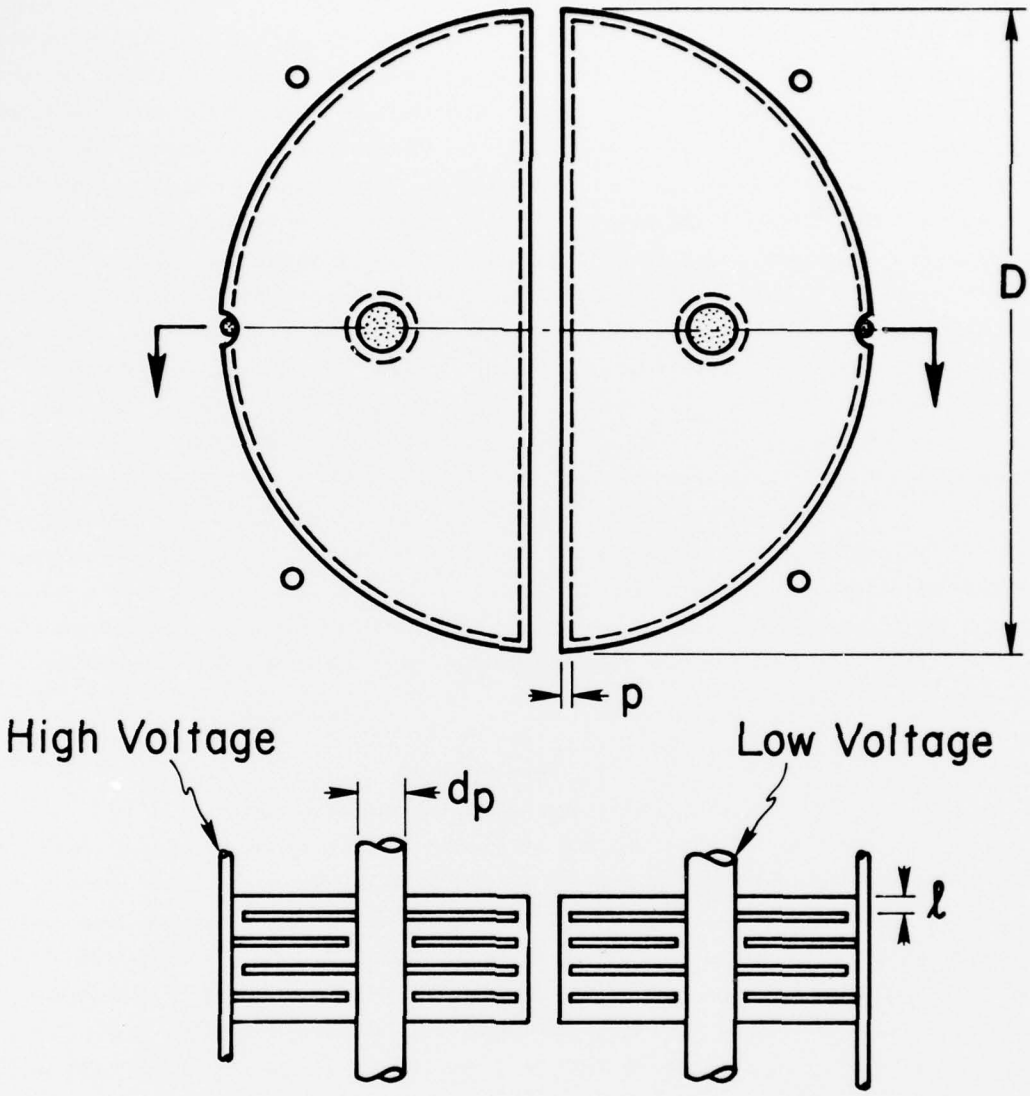

Figure 2b. Horizontal and partial vertical cross sections of the model refrigeration showing the arrangement of the metal post and electrodes with the dielectric material.

below 2.4 K[8]. In addition, the material has been proposed for use as a low temperature bolometer.[9]

Lawless then proposed[2,10] that the $SrTiO_3$ glass-ceramics be used as an electrocaloric refrigerator. This proposal was based on several factors. First, thermodynamic calculations[2] from the dielectric constant behavior showed large cooling effects would occur in the 4-15 K temperature range. Second, large breakdown strengths had been achieved in similar materials. Third, it is possible to fabricate glass-ceramic materials into almost any size and shape.

In addition to the refrigeration materials, the construction of an actual refrigerator required the development of heat switches and a general experience in cryogenics in order to put together an efficient refrigerator. Thus, a collaboration between Corning Glass Works and the Cryogenics Division of the National Bureau of Standards evolved as a sound approach to the development of the electrocaloric refrigerator. A two year project came about with ONR and ARPA funding for two men for two years. The Cryogenics Division subcontracted half of those funds to Corning Glass Works for manufacturing the refrigeration samples. In addition, Corning Glass Works and the Cryogenics Division each funded one additional man for the two years. Thus the project became a four man effort for two years. The Cryogenics Division was responsible for the heat switches, Corning Glass Works was responsible for manufacturing the refrigeration material, and Dr. Lawless of Corning Glass Works became a guest worker at the Cryogenics Division to make the properties measurements on the refrigeration samples and to oversee the development of the glass-ceramic processes and compositions. Subsequent problems with the refrigeration materials led the Cryogenics Division to change its effort in the last six months from heat switches to studies of refrigeration materials.

2. HEAT SWITCHES

2.1. Types of Heat Switches and Minimum Requirements

Two heat switches are required for the electrocaloric refrigerator, one to connect the cooling element with the 15 K reservoir, and the other to connect the cooling element with the 4 K load. The ratio of heat conducted in the "on" state of the switch to that conducted in the "off" case will be called the switch ratio and should be as high as possible. The switch ratio should probably be at least 30 to maintain a high refrigerator efficiency. In the "off" condition the switch must span the temperature difference between 15 K and 4 K. In the "on" case the upper heat switch will be at about 15 K whereas the lower heat switch will be at 4 K. The temperature drop across these switches in the "on" case should be as small as possible. As a first approximation we take this ΔT to be 1 K for both switches. For the refrigerator size considered in this project, the lower switch must then have an "on" conductance of about 1 W/K and the upper switch about 5 W/K. To achieve a switch ratio of 30 means that the conductance ratio must be about 11 x 30 = 330 because the ΔT in the "off" case is 11 times that of the "on" case. These switches must be able to operate at roughly one cycle per second.

There are several ways in which the switch conductance can be varied with some external parameter. These parameters could be such things as force, magnetic field, and electric field. We know of no other parameters which could reversibly change the conductance of a heat switch. An electric field controlled heat switch is especially attractive since electric fields are easy to establish and are already being used for the cooling element. Though the thermal conductivity of a material like $SrTiO_3$ can be changed with an electric field,[11] the effect is too small to make a useful heat switch.

Superconducting heat switches are commonly used for adiabatic demagnetization but their use is restricted to temperatures below about 1 K. A large difference in the normal state and superconducting state thermal conductivity occurs only for temperatures much below the transition temperature. The operation of the switch requires a magnetic field to drive the material into the normal state. The mechanical switches commonly used in calorimetry[12] will operate in the 4-15 K temperature range but their conductances are usually on the order of only a few milliwatts per kelvin instead of watts per kelvin.

Previously developed heat switches have been designed for lower temperatures, lower power levels, or longer cycle times than that required for this electrocaloric refrigerator. Hence, a program was necessary to develop the proper heat switches. Several types were investigated and compared.

2.2. Mechanical Heat Switches

2.2.1. Multiple leaf switch

Most pressed contact switches have conductances, k, of only a few mW/K at 4 K. Generally, the forces, F, applied have been only a few kg because opening the switch causes heating that increases with increasing forces. The conductance of a switch has been found to be dependent on F^n where n is usually less than 1. The conductance is generally independent of the macroscopic surface area of the contacts.[13,14]

Berman and Mate[14] have measured the conductance of solid gold contacts at 4 K that were closed at room temperature and found a value of 0.2 W/K at 4 K for a 43 kg closing force. This suggests that a mechanical contact type switch might achieve the desired conductance. The conductance of the gold switch might be expected to be qualitatively similar to copper,[14] so k is reduced by a factor of 4 when the switch is closed at 4 K and is proportional to $F^{3/4}$. This being the case, several hundred kilograms closing force would be required to achieve the desired conductance. High forces are undesirable because of the structural parts that must extend to room temperature. In addition, it is possible that the surfaces can be mechanically damaged causing a reduction in the conductance of the contact. It is conceivable that a high switch conductance could be achieved if the heat could flow through several independent contacts instead of one contact. The geometry could be arranged so that a single applied force could close all of the contacts.

Switch design: A switch designed to achieve high conductance with a low closing force is shown in figure 3. The contacts are stacked in parallel so that the single clamp mechanism closes several. When the clamp is opened, the spring of the leaves can move them apart. The stiffness and alignment of the leaves will determine how much residual closing force remains between contact surfaces.

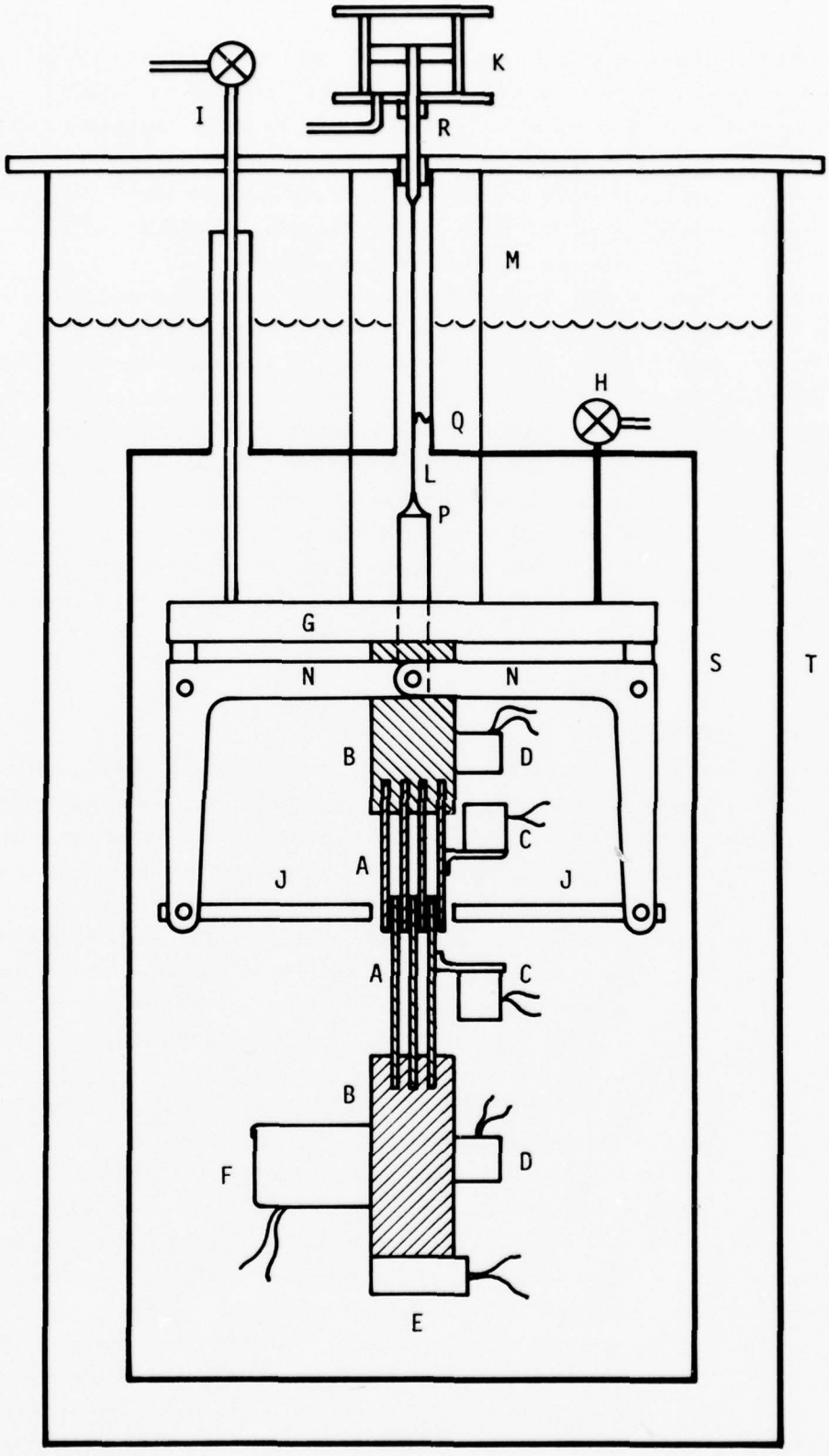

Figure 3. Schematic of heat switch and actuating mechanism; the conducting parts of the switch are hatched.

In figure 3 the leaves A, A are either copper with free ends gold plated or silver. They are soldered into slots in copper base blocks B, B with pure indium. Carbon thermometers are mounted either on copper tabs indium soldered to top and bottom outer leaves C, C, or on the copper blocks as shown by D, D, since only two carbon thermometers are used at a time. A heater E is attached to the lower copper block to establish the desired heat flux. A germanium thermometer F is used to calibrate the carbon thermometers in place. A second heater (not shown) is attached to the upper block and used to heat the whole switch assembly during calibration. The upper base block B is thermally anchored to the flat circular heat exchanger G. Liquid helium is admitted through needle valve H and the vapour is removed through the pump line and valve I. This line is jacketed to a point above the bath so the enthalpy of the gas as well as the latent heat can be used to cool the switch when measurements are being made above 4 K.

The switch is clamped shut by the two brass jaws J, J. The force is applied over an area of 3.2 mm times the leaf width, about 9 mm. The closing force is applied by an air piston K. The forces are transmitted through the wire L and a stainless steel tube M. The jaws are moved by two pairs of bell cranks N, N which are coupled to the pull wire L through an equalizing device P. The wire is thermally anchored with copper braid at Q at 4 K and vacuum jacketed so a sliding O-ring seal R can be placed at room temperature. The switch assembly is placed in a vacuum container S sealed by a Woods metal joint near the top. The vacuum can is immersed in liquid helium in a set of glass dewars T.

There are a number of questions that must be answered about the switch shown in figure 3. For example: Can a switch of this geometry be fabricated out of high conductivity materials? Can plated contacts be used or must they be solid gold? How high is the conductance when the switch is closed at low temperature? What is the effect of cycling the switch while cold? How large is the on-to-off ratio? Is there a surface cleaning problem? Can such a switch be adapted to a small dielectric cooling stage? These questions are resolved to varying degrees by measurements on four modifications of the switch.

Switch 1

This switch had 13 leaves made of copper with a residual resistance ratio (RRR) of 500. This ratio is the ratio of the electrical resistances at 300 K and 4 K. The leaves were approximately 0.33 mm thick, 8-1/2 mm wide, 25 mm long and arranged to give 12 parallel contacts. The contact ends were plated with about 2.5×10^{-3} mm thickness of commercial gold plating.

Switch 2

This switch had 3 leaves, hence two contact surfaces. The leaves were high purity copper with an RRR of 1900, and were 0.75 mm thick, about 10 mm wide and 18 mm long. The contact ends were plated with pure gold to a thickness of about 8×10^{-3} mm The leaves were mechanically polished before plating.

Switch 3

This switch was the same as switch 2 in every way except that the leaves and contacts were silver with an RRR of 1400. Silver contacts were tried because measurements at 77 K showed the contact conductance of silver higher than gold.[15] The contacts were mechanically polished.

Switch 4

This switch used identical leaves to those of switch 2. The base blocks were larger, made of high purity copper and there were 11 leaves, hence 10 contacts.

All the leaf materials were rolled from 6.3 mm or 9.5 mm rod and annealed. The switch 2 material was rolled to size, etched with HNO_3 and oxygen annealed at 1000°C in air at 5×10^{-4} torr for 24 hr. The high purity copper was annealed once during rolling, and annealed afterward at 750°C in a vacuum for 1 hr. The silver was rolled to size and annealed at 550°C in hydrogen for 1-1/2 hr. The residual resistance ratios were measured after all rolling and annealing was completed. All the leaves were soldered into the base blocks with pure indium. High temperature solders were not used to avoid damaging the contact surfaces or diffusing impurities into the leaf material.

Since the proposed electrocaloric refrigerator is to reject heat at about 15 K, most of the conductance measurements were made at that temperature. Temperature measurements were made either on the base blocks, to get the conductance of the whole switch, or at the leaves, so the results could be corrected to the contact conductance. The latter results can be compared directly to the pure gold contact results.[14] Because of the geometry of the leaf switches, the temperature drop between contacts cannot be directly measured.

For the temperature measurements on switch 1, a calibrated carbon thermometer was used to measure the temperature on one side of the switch. The carbon thermometer on the other side of the switch was calibrated against this each run. The switch was closed during calibration and heat was supplied by a heater on the heat exchanger, figure 3, to bring the switch assembly to a constant temperature. Under these conditions the heat flow in the switch should be zero. For the remainder of the switches, both carbon thermometers were calibrated by a germanium thermometer. The calibrations were done at three temperatures between 4 and 15 K, and the results were used to find A, B, and P of the equation[16]

$$\text{Log } R = A + BT^{-P}$$

where R is the thermometer resistance at the temperature T.

The conductance measurements were made by adjusting the needle valve, H, figure 3, to fix the heat exchanger temperature at the desired value while heat is applied to the opposite side of the switch. The heater power, temperatures and closing force were recorded when the temperatures reached equilibrium. The closing force was determined from the cylinder air pressure and area of the piston.

The switch contacts were cleaned with an abrasive copper-cleaning powdered soap, rinsed with distilled water, then rinsed with freon liquid and dried with freon gas. Switch 4 was also cleaned with freon in an ultrasonic cleaner. There was a slight increase in contact conductance. Switch 2 was cleaned only with freon liquid at first. The contact conductance was about 1/3 the conductance after cleaning with the soap. There was some variation in conductance from run to run and occasionally it was necessary to reclean the contacts. The higher conductance results are presented in the figures below.

Results: So that the switch conductances can be more readily compared to the measurements of Berman and Mate[14] for solid gold, the conductances are given in figure 4 as W/K per contact. Most of the measurements presented were done around 15 K since this was the temperature at which the switch was to be used. Data are shown for switch 3 at 4 K, however. The switches were cycled from 1 to 150 times while cold. Since there was no change observed in conductance after cycling the switch, the data are presented without specifying the number of cycles.

The conductance of switch 1 is shown by point 1 after it was cooled from room temperature to 15.2 K with a 54 kg closing force. The contact conductance is about 1/4 that of solid gold contacts. After opening and closing the switch at 15 K, the switch conductance per contact is shown by curve 1A. The measured conductance is from base block to base block.

The conductivity of the leaf material of switch 1 was measured and found to be 160 W/cmK at 12 K. This is high for an RRR of 500 when compared to other conductivity measurements on high purity copper.[17] This measurement indicated that most of the measured ΔT was in the contact. Cobalt or silver impurities are used in the commercial gold plating for hardening. Since this impurity could possibly affect the contact conductance, pure gold was used to plate the remaining switches. The indium joint conductance was estimated to be 10 W/K cm^2 from the conductivity measurements.

The contact conductance of pure gold plated contacts is shown by curve 2 of figure 4 for switch 2. The switch was closed with a 54 kg force before cooling. At 15 K the force was increased resulting in some increase in conductance.

The contact conductance of the switch, after cycling at 15 K, is shown by curve 2A. The conductance is reduced by slightly more than two by opening and closing the switch cold. There is a thermometer on both sides of the indium solder joint for this measurement, a carbon thermometer on the leaf and the germanium thermometer on the base block. If the ΔT is corrected for the leaf conductance and the conductance of the 0.9 cm square base block, then the conductance of the indium joint can be determined. This gave an indium joint conductance of ∞ to 20 W/K depending on whether 7 or 14 W/cmK was used for the OFHC copper conductivity.

The total switch conductance per contact is shown in curve 2B. The thermometers were mounted on the blocks. A correction has been applied to exclude the ΔT due to the base blocks since they can be made of a much higher conductivity material than the OFHC copper used here. There is only one set of low-temperature conductivity data[17] for OFHC copper and for that the state of work hardening is unspecified. The error bars on the data are for a 7 W/cmK minimum conductivity and a 14 W/cmK maximum conductivity for OFHC copper at 15 K.

The section of curve 2B showing little force dependence was measured while reducing the air cylinder pressure. This apparently different force dependence is due in large part to drag in the air cylinder and linkage to the switch. Applying the force with a spring scale brought the pressure applied and pressure released curves closer together.

The conductance of the silver contacts of switch 3 after opening and closing at 15 K is shown by curve 3A. The point 3 is the conductance of the switch after cooling closed to

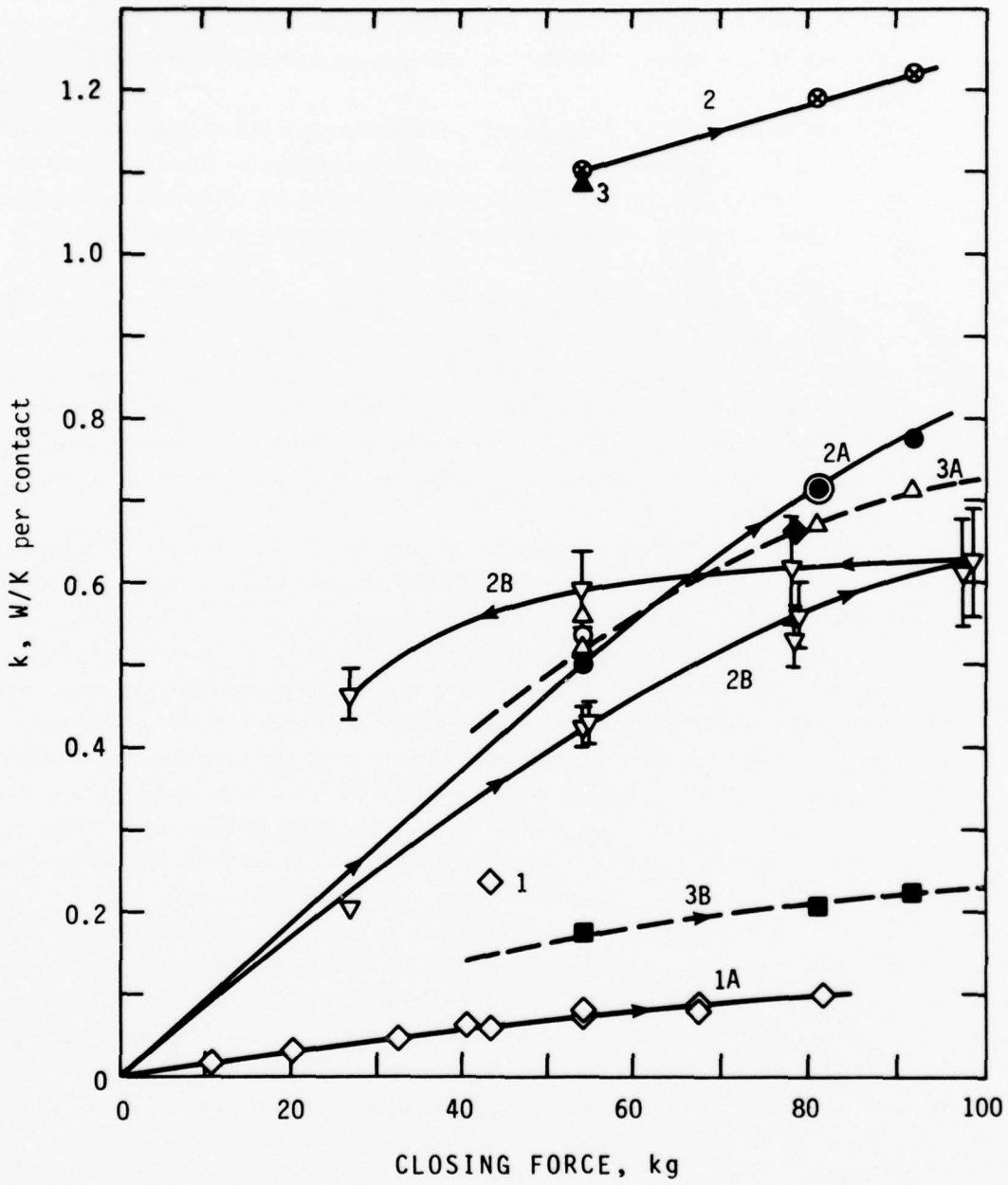

Figure 4. Contact conductances switch conductances as a function of closing force for switches 1, 2, and 3. All curves and points are normalized to one contact.

15 K. This conductance is about the same as for gold plated copper. The conductance of the silver at 4 K is shown by curve 3B.

The conductance per contact of switch 4 after cooling closed was essentially the same as for switches 2 and 3. The closed cold contact conductance, however, was only about 3/4 of the conductance observed in the earlier switches. This could perhaps result from the stiffness of the leaves or a movement of one set with respect to the other. If, for some reason, one or both of the leaves on which the thermometers were mounted made poorer contact than the next, the measured ΔT would be between the ΔT of the contacts and the ΔT of the whole switch.

In figure 5, the conductances of the switch contacts of switches 1, 2, and 3 (switches cooled from ambient while closed) are compared to the solid gold contacts of Berman and Mate. Switches 2 and 3 were cooled at a higher closing force so the conductance was corrected to a 43 kg closing force assuming the conductance varies as $F^{3/4}$. The conductances agree well with the results of Ref. 14. The temperature dependence of the conductance of the silver contacts, after cycling cold, was found to be proportional to T in agreement with Ref. 14.

On-to-off conductance ratios were measured for switches 1, 2 and 4 for closing forces around 90 kg. For switch 1, this ratio was about 2000. For switch 2, this ratio varied for different runs from 900 to 3000, probably depending on the alignment of the leaves. This ratio was actually measured for an open ΔT of about 10 K and no radiation corrections have been applied. Switch 4 had an on-to-off ratio of about 45. The low ratio is due to the impracticability of aligning a large number of relatively stiff leaves so there are no appreciable contact forces remaining when the switch is open. The longer and thinner leaves of the first switch were sufficiently flexible so that the open conductance was low in spite of the even larger number of leaves.

Discussion: A maximum conductance of 1.2 W/K at 15 K with a 90 kg closing force and a 10^3 on-to-off ratio was achieved with the switches reported above. Although 5 W/K at 15 K was desired, the obtained value is sufficient for testing a refrigerator. The conductances of both pure gold plated copper and silver contacts are comparable to the solid gold measurements[14] when the contacts are closed before cooling. The conductance after reclosing the switch cold is reduced by a factor of 2 or 3.

The pure gold plated contacts used for switch 2 were definitely superior to the commercial plating, which contained a dilute impurity. This difference may be caused by the presence of the impurity, but it should be noted that the leaves of switch 2 were mechanically polished before plating, and the plating was thicker, either of which may have caused the improvement.

The power, n, of the relation $k \alpha F^n$ for the contact conductances was found to be about 0.66 for switch 2 and 0.6 for switch 3 from log-log plots of k as a function of F. These slopes do not extrapolate to $k = 0$ at $F = 0$ on a linear plot. No corrections have been made to the indicated forces for friction in the switch mechanism.

The above measurements show that a high conductance switch (on the order of 1 W/K) can be made by plating and that the fabrication can be done using pure indium solder. The

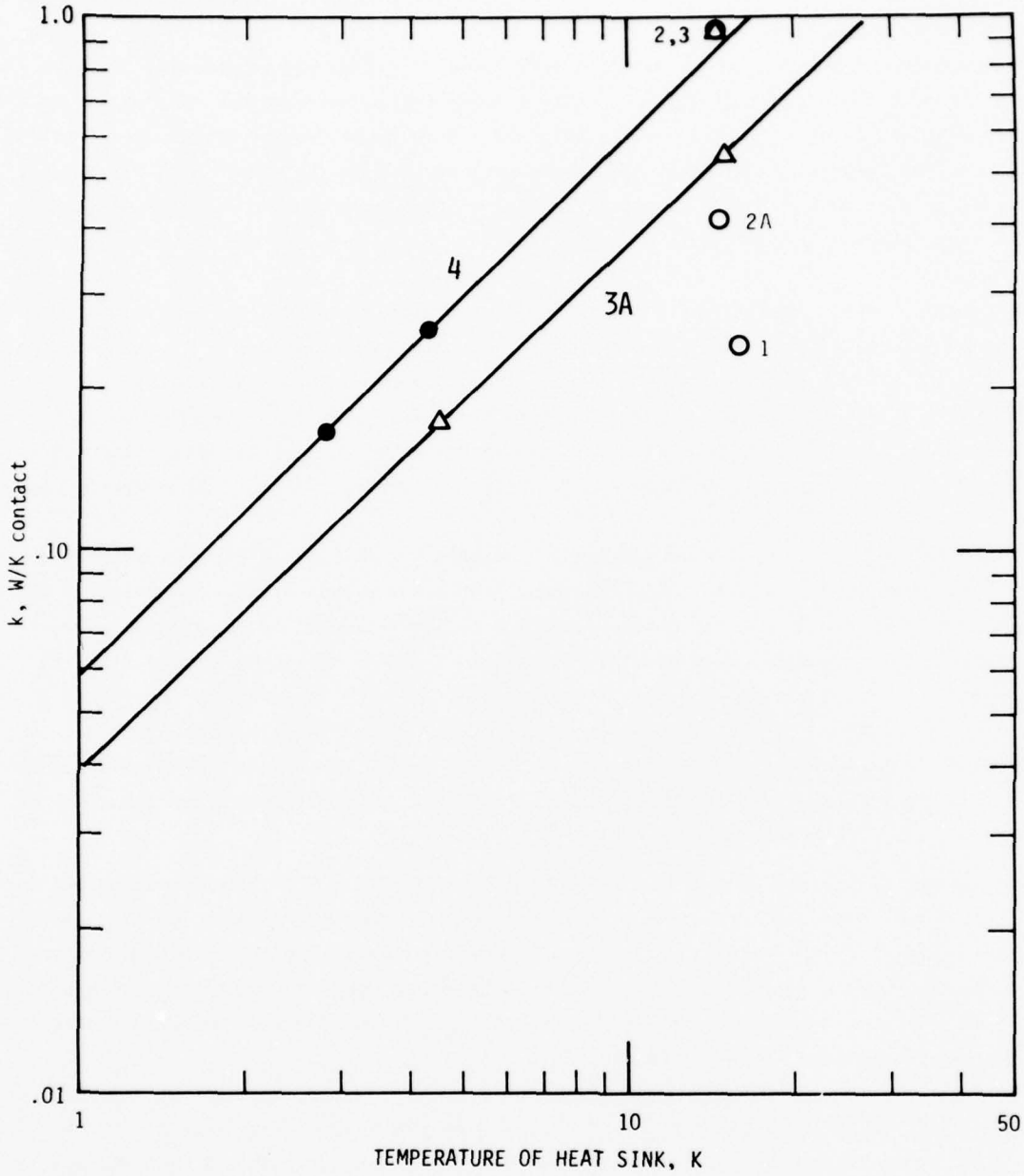

Figure 5. T dependence of the conductance of one contact. Curve 4, data of Berman and Mate extrapolated to 17 K. Closing forces are 43.0 kg unless otherwise specified.

Point 1 - Switch 1 closed at ambient
Point 2 - Switch 2 closed at ambient
Point 2A - Switch 2 closed at 15 K
Point 3 - Switch 3 closed at ambient
Curve 3A - Switch 3 closed at 15 K with a 54 kg force
Curve 4 - Berman and Mate

conductance is not degraded by cold cycling the switches 150 times. On-to-off ratios of greater than 10^3 are possible if the leaves are properly aligned (switches 2 and 3) or sufficiently flexible (switch 1). Cleaning and maintaining that cleanliness appears to be no problem. No heating was observed due to opening or closing the switch, which is not surprising due to the heat fluxes present.

The conductance of a switch of the above design can probably be increased by optimizing the leaf dimensions and the number of leaves. Probably, a switch with even higher conductance is possible using a more elaborate disengaging mechanism for the leaves.

2.2.2 Helium gap switch.

In order to transfer heat across contacts in a vacuum (previous section) large forces are required. A second mechanical switch considered uses a low pressure of helium gas around the contacts to provide good heat transfer without using high contact forces. The thermal conductivity of helium gas is independent of pressure until the pressure becomes so low that the mean free path of the molecules becomes comparable to the gap spacing. For a pressure of 1 torr the mean free path of helium gas is 1.1 μm at 4 K and 2.1 μm at 15 K. Therefore, for a gap of 5 μm or more the thermal conductivity of the gas will be the classical bulk value. The thermal conductance across the helium gap is simply

$$K = kA/\ell,$$

where k is the thermal conductivity of the helium, A is the cross sectional area of the gap, and ℓ is the gap spacing. The conductance can then be varied by changing the gap spacing. For the "on" case the two copper surfaces are brought into light contact. For reasonably smooth surfaces, the average gap spacing may be about 5 μm. The "off" condition is achieved by separating the two plates by a gap of about 5 mm. The conductance then decreases by a factor of 1000. For a ΔT of 11 K in the off case, the switch ratio would be $\ell_{off}/11\ \ell_{on}$ for k independent of temperature. Actually k varies from 0.084 mW/cmK at 4 K to 0.22 mW/cmk at 15 K,[18] so the switch ratio becomes $\ell_{off}/7.5\ \ell_{on} = 133$ for the upper switch and $\ell_{off}/19.4\ \ell_{on} = 52$ for the lower switch as ℓ changes from 5 μm to 5 mm. The biggest uncertainty is the "on" conductance since the spacing depends on the quality of the surfaces. In order to transfer 5 watts at 15 K with a ΔT of 1 K, a surface area of 11.4 cm^2 is required with a gap of 5 μm.

An apparatus to test the heat conductance across a helium gap was designed and built. However, a shift in emphasis from heat switches to refrigeration materials prevented a test of the helium gap heat switch.

An actual working heat switch would have a cycle time of about 1 second so that the heat absorbed from one surface during the first half second can actually be stored in a movable plate with a high heat capacity. During the next one half second the plate is moved to make contact with the upper reservoir and transfers its stored heat to it. Thus a simple solenoid could move the plate from one position to the other. A 200 g movable plate of lead could be used for an upper switch but a lower switch would require as much as 8 kg of lead. Thus such a helium gap heat switch would only be practical for the upper switch.

2.3. Magnetothermal Heat Switches

2.3.1. Survey of various metals.

The thermal conductivity of a metal is composed of the lattice and the electronic term, i.e., $k = k_\ell + k_e$. The electronic contribution can be reduced considerably in many metals by the application of a transverse magnetic field. The amount of reduction is proportional to the electrical magnetoresistive effect. A reduced Kohler diagram[19] of the transverse magnetoresistivity of most metals is very helpful in selecting those metals with high magnetoresistive effects. A high magnetoresistive effect also reduces the eddy current heating. However, additional conditions must be met to obtain a large change in thermal conductivity with a magnetic field. The zero field thermal conductivity, which should be high, is proportional to the residual resistivity ratio (RRR = ρ_{295}/ρ_0), where ρ_0 is usually measured at 4.2 K. The lattice thermal conductivity, which should be low, is given theoretically by the expression[20]

$$k_\ell = \frac{3.1 \times 10^2 k_\infty}{G N_0^2 \theta_0^2} T^2 \text{ (W/cm K)},$$

where k_∞ is the constant thermal conductivity at high temperatures, e.g., room temperature, G is a numerical factor which is about 70, N_0 is the number of free electrons per atom, and θ_0 is the Debye temperature at 0 K. From this expression it is obvious that a high θ_0 will give a low k_ℓ. The important properties of a metal which would make a good heat switch are summarized as follows:

(1) high magnetoresistive effect
(2) high residual resistance ratio (RRR $\geq$ 1000)
(3) high Debye temperature, $\theta_o \geq 300$ K.

Even though some materials, such as bismuth, have extremely high magnetoresistive effects, they are inappropriate as heat switches since they do not satisfy conditions (2) and (3) above. Table 1 lists the various metals which are known to satisfy all three conditions above and therefore would be potential heat switch materials.

Table I. A summary of metals which have the potential for making good magnetothermal heat switches in the 4-15 K range. The metals are listed in order of decreasing magnetoresistive effect.

Metal	highest RRR to date	θ_o (K)	sufficient literature data on k(T,H) exists
Ga	2×10^5	324	yes
Be	3×10^3	1160	no
Mg	$10^6 - 10^7$	342	no
W	3×10^4	405	yes
Fe	3×10^3	464	no
Ru	$> 10^3$	600	no

Of the six possible candidate materials only Be and possibly Ru have high enough θ_o to be potentially useful as the upper switch where the "on" temperature is about 15 K. The other materials would be useful only for the lower switch where the "on" temperature is 4 K. Until now, only Ga and W had been measured in enough detail to predict the heat switch performance. In fact Ga has already been used as a heat switch in the 1-4 K temperature range.[21] Our first efforts were then to make a switch of Ga.

Gallium: Figure 6 shows the behavior of the thermal conductivity of gallium as a function of temperature for various transverse magnetic fields. The H = 0 curves are from the work of Boughton and Yaqub,[22] and the $H \neq 0$ curves are from Engels, et al.[21] In the "off" state of the switch ($H \neq 0$) the temperature will be 15 K on one side of the switch and 4 K on the other side. The heat flow must be evaluated by integration over the k(T) curve. For $k \propto T^2$ the average conductivity is the value of k at about 11 K. For the lower switch, the switch ratio is then approximately $(1/11)k_4/k_{11}$ and for the upper switch the ratio is $(1/11)k_{15}/k_{11}$. Table 2 lists these switch ratios for gallium as well as for several other metals.

Table 2. Measured or estimated thermal conductivity at three different temperatures and the switch ratio for several heat switch metals. Units for k are W/cm K.

	H = 0		H = 14 k Oe	Switch Ratios	
Metal	k (4 K)	k (15 K)	k (11 K)	lower	upper
Gallium	200	5.0	0.20	91	2.3
Beryllium	23	73	0.040	52	166
Magnesium	60	28	1.6	38	18
Tungsten	800	115	0.45	162	23
Iron	50	70	$\sim$ 0.5	9	13
Ruthenium	50	80	0.1 - 0.3	15 - 45	24 - 73

Two gallium magnetothermal heat switches were made by growing a single crystal of 99.9999% Ga in a teflon mold like that described by Yaqub and Cochran.[23] Each crystal had relatively large diameter discs grown on each end to reduce the thermal resistance at the bond between gallium and copper. Both crystals broke upon cooldown. The first was subject to slight tension from the stainless steel support system, whereas the second was subject to compression from the teflon support system. Because of the brittleness and low melting point (29.9°C) of gallium, and because of the encouraging results obtained with beryllium, further work on gallium was abandoned.

Tungsten: The magnetothermal conductivity appears to be quite well characterized from the measurements by de Haas and de Nobel[24] and by Long.[25] Figure 7 shows the thermal conductivity behavior and table 2 gives the expected switch ratios. The results show that tungsten would make a satisfactory lower switch.

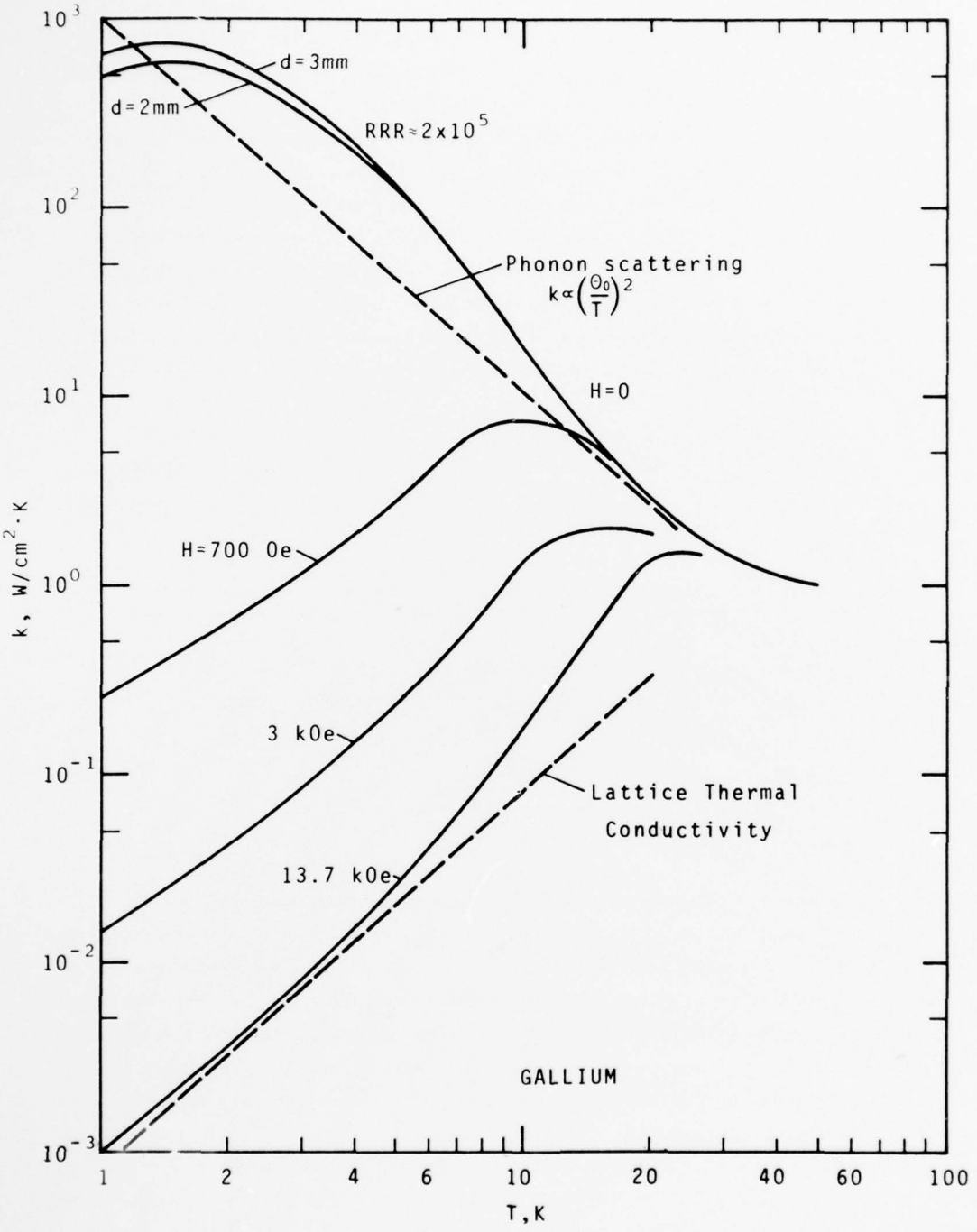

Figure 6. The thermal conductivity of single crystal gallium in transverse magnetic fields[21]. The heat flow is parallel to the a axis and the field is parallel to the c axis. The thermal conductivity in zero field is somewhat size dependent because of the long electron mean free path[22].

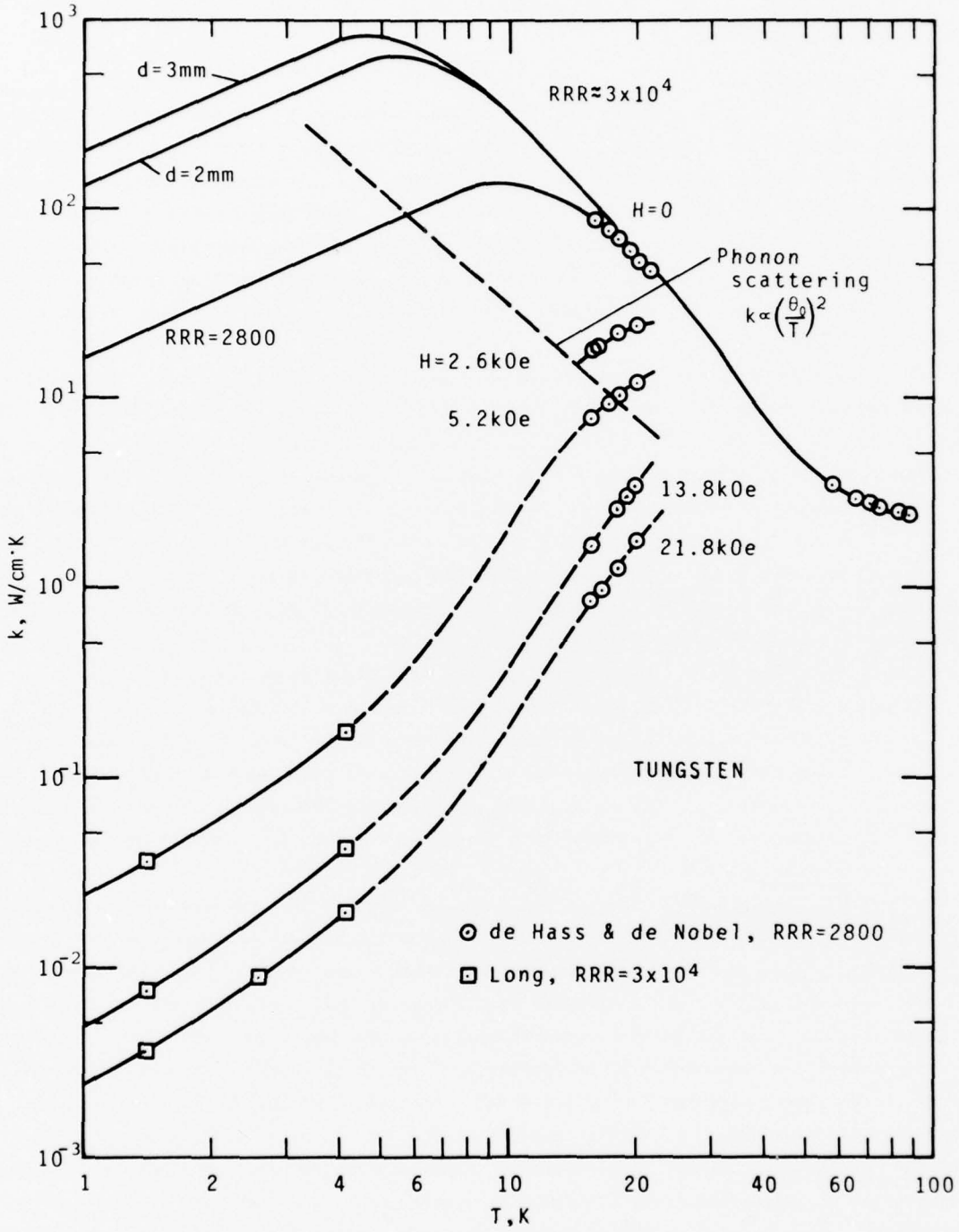

Figure 7. The measured thermal conductivity of single crystal tungsten in transverse magnetic fields[24,25]. A size dependence occurs at low temperatures in zero field for the higher purity sample.

Other metals: The rest of the metals listed in table 1 have not been measured in enough detail to permit an evaluation of them in regard to heat switches. Magnetothermal conductivity measurements were then made on two of these metals (beryllium and magnesium) to permit an evaluation of them. The estimates in table 2 show that it is not fruitful to study iron and ruthenium.

2.3.2. Beryllium.

Until now the only measurements of the thermal conductivity of beryllium in a magnetic field were those of Grüneisen.[26,27] His sample had a resistance ratio, ρ_{295}/ρ_0, of 948. He found that the maximum field effect occurred with the heat flow along the hexagonal c axis and the magnetic field along an a axis such as $\langle 11\bar{2}0 \rangle$. Unfortunately his measurements were made at only 23.5 K and 81 K. Our measurements on the magnetothermal conductivity of beryllium have shown this material to be superior to all other metals for heat switches in the 4-15 K temperature range. For that reason a fairly extensive study of its thermal and electrical conductivity was made.

Samples. Two different single crystal beryllium samples were measured. Most of the measurements were made on a very high purity sample, which we will denote as sample 1. This sample was loaned to us by Dr. R. J. Soulen of the Heat Division of the National Bureau of Standards. He in turn received the sample from Dr. W. Reed of Bell Telephone Laboratories. That sample was one of several that Dr. Reed cut out from a much larger single crystal grown by Nuclear Metals, Inc. The size of the crystal we received was 3 mm x 3 mm x 25 mm. The orientation of the crystal was determined from back scattered x-ray Laue photographs. The hexagonal c axis was along the long axis of the crystal to within one degree. The resistivity ratio, ρ_{295}/ρ_0, was found to be 1340.

Sample 2 was spark cut from a single crystal disc piece given to us by Dr. S. K. Sinha of Iowa State University. This sample was 2.3 mm x 3.7 mm x 16 mm with the c axis within two degrees of the long axis of the crystal. The resistivity ratio, ρ_{295}/ρ_0, was found to be 79. After the sample was spark cut, it was etched in a solution with composition: 26.5 ml conc. H_2SO_4, 450 ml conc. H_3PO_4, 53 g CrO_3, held at a temperature of about 70°C. The ends of this etched sample were then tinned with 99.99% pure indium using an ultrasonic soldering iron and zinc chloride flux.

Experimental techniques. The thermal conductivities of the two beryllium samples were measured by using the standard technique of observing the temperature drop across a portion of the sample while a steady heat current flowed through the sample. Carbon thermometers of 1/8 watt size and 220 Ω normal resistance with a flat ground on one side were used as temperature sensors. Two thermometers were varnished to the sample to measure the ΔT across it and one thermometer was mounted on the reservoir close to the sample. The reservoir thermometer then allowed measurements of the thermal resistance at the boundary between the sample and the reservoir. A constant current source and a digital voltmeter were used to read the carbon thermometers. A germanium thermometer, calibrated by the manufacturer, was also mounted on the reservoir to calibrate the three carbon thermometers. A capacitance thermometer,[6] also mounted on the reservoir, served to calibrate the other thermometers in a magnetic field. Between 100 K and 300 K thermocouples of type KP versus Au-0.07% Fe were

used for measurements of both T and ΔT. Published thermocouple tables[28] were used to convert voltages to temperatures.

An aluminum foil radiation shield surrounded the sample and was attached to the reservoir. The reservoir, made entirely of copper, was a 10 cm^3 pot suspended inside a vacuum can by a 6 mm diameter stainless steel pumping tube. Liquid nitrogen or liquid helium outside the vacuum can could be let into the reservoir through a stainless steel capillary tube with a valve in the liquid bath. With such an arrangement the reservoir could be cooled down to the bath temperature within a few minutes by opening the valve in the liquid bath while the pumping tube on the reservoir is vented to the atmosphere. Measurements below the bath temperature were made by closing the needle valve and pumping on the reservoir. Measurements above the bath temperature were made by first closing the needle valve and applying current to a reservoir heater to boil off the liquid in the reservoir. When the temperature rose to the desired point the needle valve was opened just enough to provide a cooling effect to nearly balance the heat input to the reservoir. The carbon thermometers were calibrated during that procedure. Next the power to the reservoir heater was turned off as the same power was applied to the sample heater for measurement of the thermal conductivity. This procedure gave rather rapid equilibrium times and usually yielded very stable temperatures.

The reservoir and vacuum can were made small in diameter so as to fit in the tails of nested glass dewars. These tails, in turn, were fit between the poles of an iron core electromagnet which could attain a field of 955 kA/m (12 kOe).

The high purity sample 1 was thermally anchored to the reservoir with a low temperature varnish. The heater was attached to the other end of the sample with varnish also. The thermal boundary resistance of the varnish joint was much higher than the thermal resistance of the sample in zero field. Thus accurate measurements in zero field were difficult to make because of the necessity for low power levels. That sample was to be used later for superconducting fixed point measurements and contamination with solder was not desirable. Sample 2 however was tinned with pure indium on each end as described previously. One end of this sample was then indium soldered to the reservoir and the heater mounting bracket soldered to the other end. The indium solder provided much better thermal contact for this sample.

The electrical conductivities of both beryllium samples were measured potentiometrically. Current and voltage leads were pressure contacts to the sample. Pointed screws were used for the voltage taps. Currents up to 2A were used when the sample conductivity was high. The same thermometers used for the thermal conductivity measurements were also used to determine the sample temperature during the electrical conductivity measurements.

Experimental Results. The temperature dependence of the electrical resistivity of sample 1 is shown in figure 8. These data are for the current along the hexagonal c axis and the magnetic field along the a axis. Previous measurements[26,29,30] in zero field on less pure samples are also shown for comparison. The total resistivity ρ_t is conventionally expressed as

$$\rho_t = \rho_i + \rho_r \qquad (2.1)$$

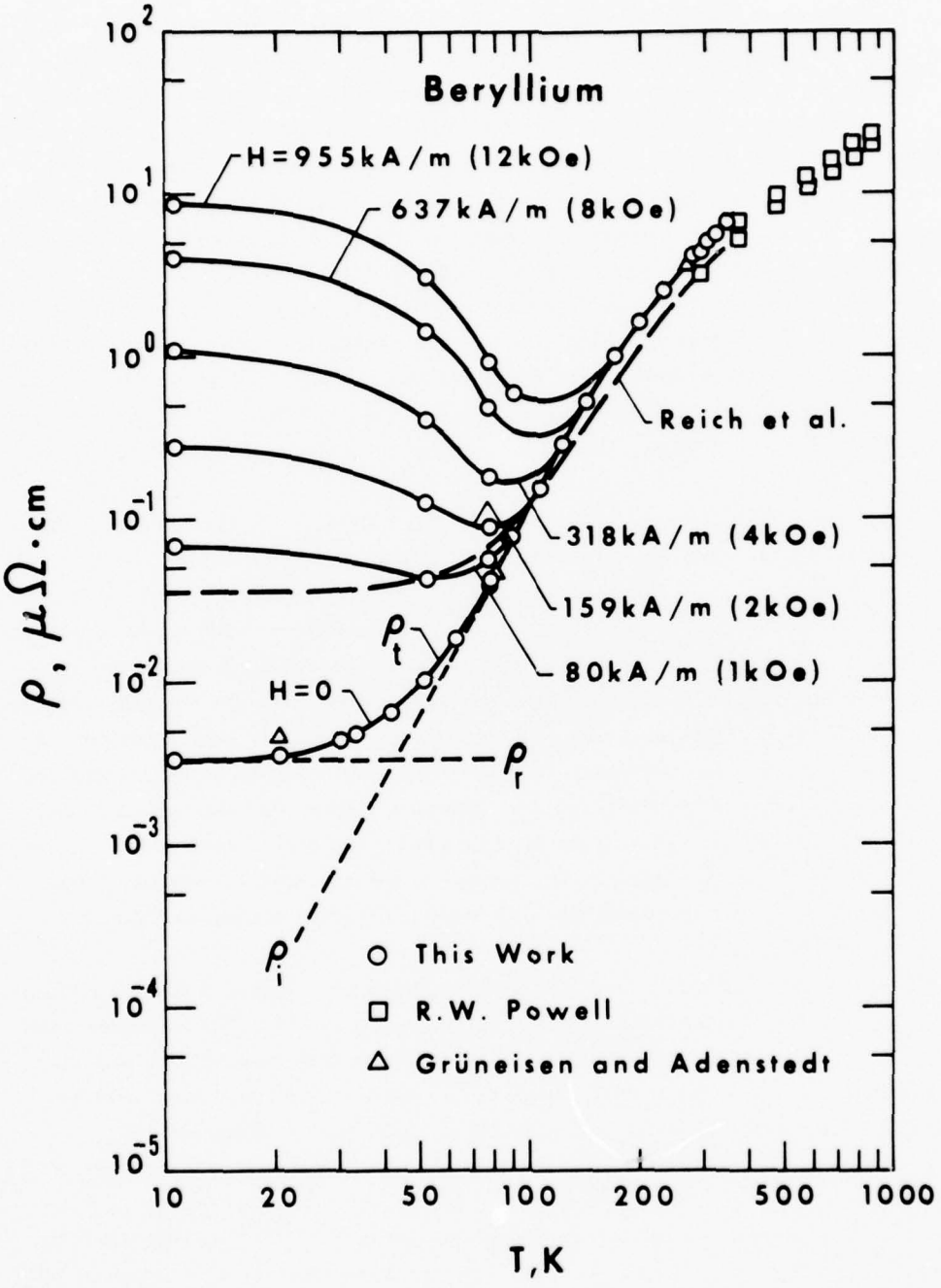

Figure 8. The electrical resistivity of high purity single crystal beryllium as a function of temperature in various transverse magnetic fields. Previous work[26,29,30] on less pure samples is shown for comparison.

where ρ_i is the intrinsic resistivity due to scattering of electrons by phonons and ρ_r is the residual resistivity due to impurity scattering of the electrons. For sample 1 we have $\rho_r = 3.35 \times 10^{-3}$ μΩ·cm and $\rho_i = 1.0 \times 10^{-9} T^4$ μΩ·cm. This expression for ρ_i is identical with that found by Reich, et al.[30] on a less pure sample. For our sample we find $\rho_{273.15\ K} = 3.69$ μΩ·cm and $\rho_{296.15\ K} = 4.48$ μΩ·cm. These data are in good agreement with the value $\rho_{273.15\ K} = 3.58$ μΩ·cm found by Grüneisen and Adenstedt.[26]

Figure 9 shows the thermal conductivity of beryllium sample 1 as a function of temperature for several magnetic fields. The heat flow was along the hexagonal c axis [0001] and the transverse magnetic field was along one of the a axes, e.g. $[11\bar{2}0]$, of the crystal. Such an orientation has been shown[26] to give the maximum field effect on the thermal conductivity. Figure 10 shows how the thermal conductivity varies with the angle of the magnetic field within the basal plane. As expected, a 60° symmetry exists. Such a plot was used to find the exact orientation of the a axis before taking the data shown in figure 9. The data taken near room temperature blend very well with the data of Powell[29] above room temperature on his purest sample in the annealed state. The data of Grüneisen and Adenstedt[26] on a less pure sample is shown for comparison. Their data is for H = 0 and H = 955 kA/m (12 kOe) and is consistent with the present data considering the differences in purity.

For H = 0 and T < 150 K the thermal conductivity of the high purity sample is dominated by electron conduction. For that range the data are fit very well by the theoretically expected form

$$W_e = W_i + W_o = \alpha T^2 + (\beta T)^{-1}, \qquad (2.2)$$

where W_e is the total electronic thermal resistivity, W_i is the ideal resistivity due to phonon scattering, and W_o is the resistivity due to impurity scattering. The data of figure 9 give $\alpha = 1.04 \times 10^{-5}$ cmW^{-1}K^{-1} and $\beta = 5.7$ W cm^{-1}K^{-2}. This was the first beryllium sample measured that was pure enough to allow a determination of the ideal thermal resistivity.

The total thermal conductivity, k, has a contribution from the electrons, k_e, and from the lattice, k_g, such that $k = k_e + k_g$. The electronic thermal conductivity is so easily reduced by the application of a transverse magnetic field that the lattice thermal conductivity can contribute a sizeable fraction to the overall conductivity in sufficiently high fields. The application of a magnetic field then allows a separation of the electronic and lattice components of conduction. Several methods exist for separating the two components from measurements in magnetic fields. In this work we use the method of Grüneisen and Adenstedt[26] in which they write

$$k(H) = k_e(H) + k_g \approx L_e T\sigma(H) + k_g, \qquad (2.3)$$

where L_e is the electronic Lorenz number and $\sigma(H)$ is the electrical conductivity in a magnetic field. In this expression L_e and k_g are assumed independent of magnetic field. A plot of k(H) versus $T\sigma(H)$ for different field strengths yields a rather straight line for H > 150 kA/m (2kOe). Thus L_e and k_g are determined simultaneously. This technique was used

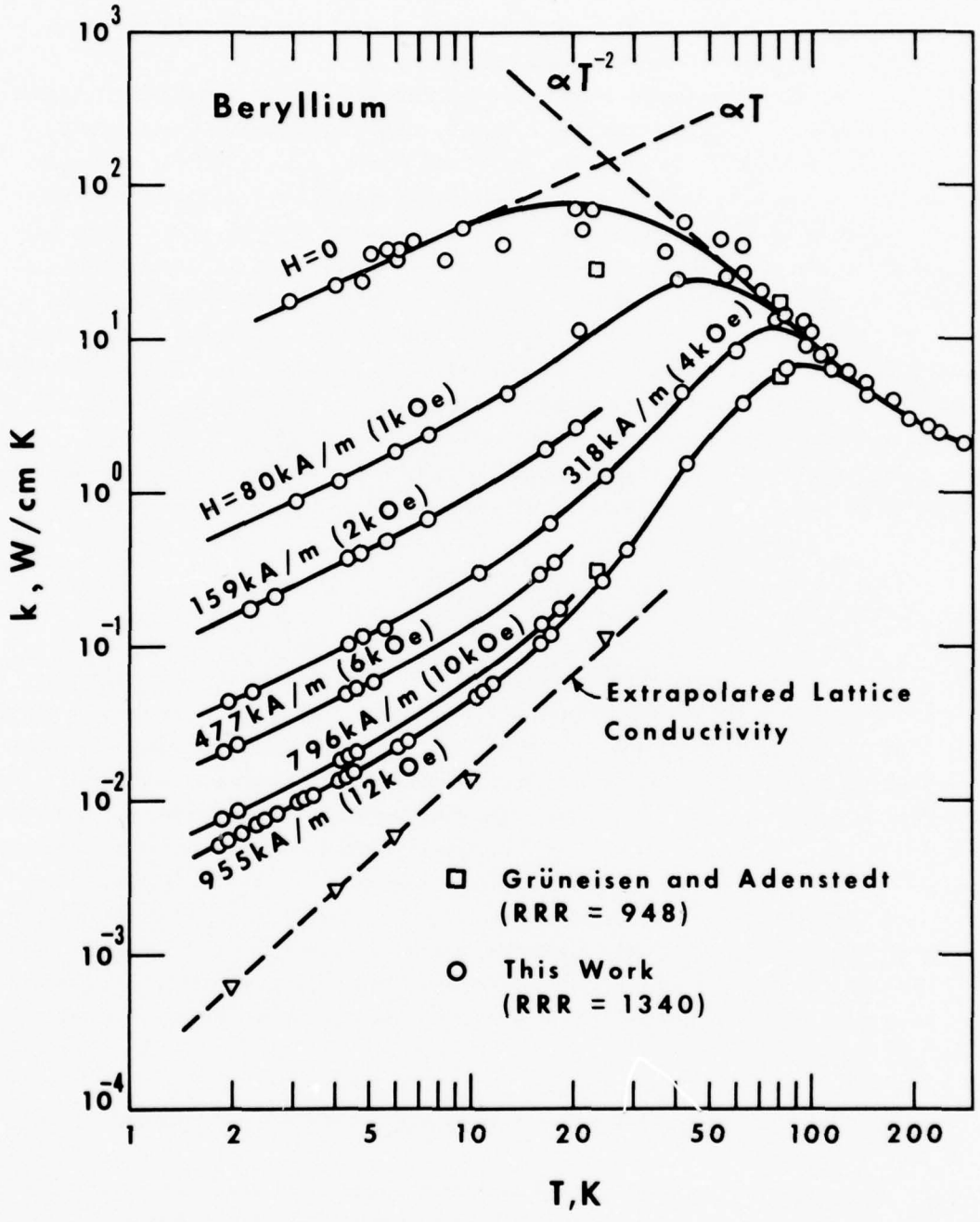

Figure 9. The thermal conductivity of high purity single crystal beryllium as a function of temperature for various transverse magnetic fields. The work of Grüneisen and Adenstedt[26] is shown for comparison.

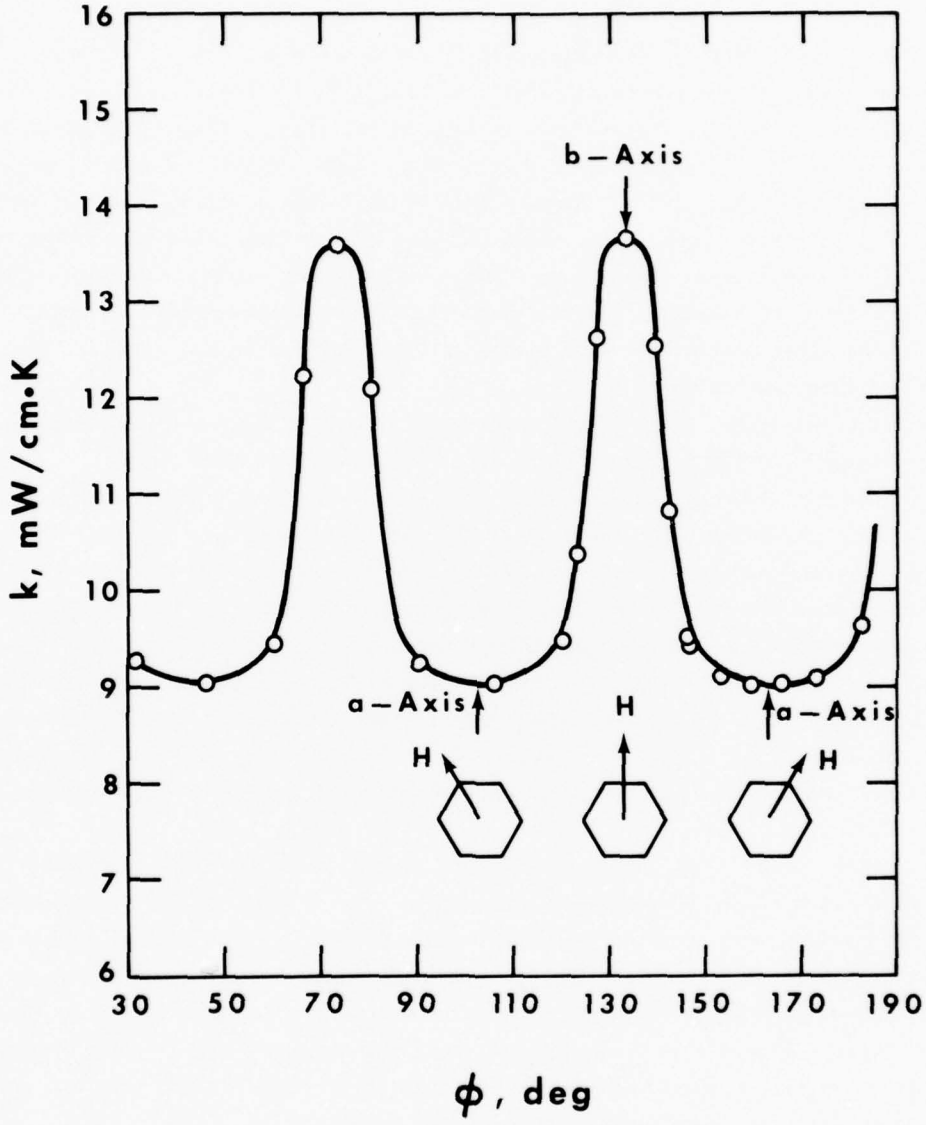

Figure 10. The thermal conductivity of single crystal beryllium at 2.1 K as a transverse magnetic field of 796 kA/m (10 kOe) is rotated about the basal plane. The angle $\emptyset$ is an arbitrary angle.

at several temperatures to obtain the lattice conductivity shown in figure 9. For T < 30 K for the lattice conductivity can be expressed as

$$k_g = \gamma T^2, \qquad (2.4)$$

where $\gamma = 1.6 \times 10^{-4}$ W/cm K^3. Powell, et al.[31] estimated $\gamma = 2.0 \times 10^{-4}$ W/cm K^3 from thermal conductivity measurements of beryllium alloys. The value of γ is lower than that of any other metal and is to be expected because of the high Debye temperature of beryllium.

For temperatures below about 20 K the thermal conductivity of this high purity beryllium sample can be changed by over three orders of magnitude with a magnetic field of 955 kA/m (12 kOe). This is roughly equivalent to going from the thermal conductivity of high purity copper to that of stainless steel. Table 2 lists the heat switch ratios which could be obtained with such a sample. As this table shows, beryllium is the only metal which can be used as the upper switch. It can be used as the lower switch also, but for that switch tungsten would be just as good.

The relative change of electrical resistivity at 4 K of beryllium sample 1 is shown as a Kohler diagram[32] in figure 11. This figure shows that $\Delta\rho/\rho_o \propto H^n$, where $n = 2.00 \pm 0.02$. This field dependence agrees with the theoretical value n = 2 for a compensated metal with no open orbits. Also shown in figure 11 is the relative change in electronic thermal resistivity. This change is nearly proportional to H^2 also, except that the coefficient of H^2 is smaller than for $\Delta\rho/\rho_o$. The difference, however, is about within the experimental uncertainty of $\Delta W_e/W_e(0)$. The biggest uncertainty is in $W_e(0)$, the electronic thermal resistivity in zero field. The rather small value of $W_e(0)$ at low temperatures along with the large cross section of the sample made it difficult to measure $W_e(0)$ accurately. The uncertainty in $W_e(0)$ for T < 70 K is about ± 25%. At higher temperatures and in magnetic fields the thermal resistivity increases considerably and the uncertainty eventually drops to about ± 5%.

The fact that $\Delta W_e/W_e(0)$ is proportional to $(H/\rho_o)^2$ points out the importance of using samples with a low ρ_o, i.e., high resistance ratio. A lower ρ_o not only means that a higher ratio between k(H = 0) and k_g can be attained but also that a lower field can be used to make k(H) approach k_g, the lattice thermal conductivity. Such behavior is evident in figure 12, which shows the magneto-thermal conductivity of sample 2, a less pure beryllium single crystal (RRR = 79). The thermal conductivity for H = 0 is considerably lower than for sample 1, but also the thermal conductivity for H = 955 kA/m (12 kOe) is considerably higher for this sample than that for sample 1.

Beryllium crystals with resistance ratios as high as 3000 were made several years ago for a government contract, but these samples (our sample #1 is one of those) are now essentially all gone. About $5,000-$15,000 would be required to establish facilities for growing more of these crystals.

2.3.3. Magnesium

The magnesium sample measured in this work was kindly grown for us by R. Reifenberger of the University of Arizona. It was a rather small crystal with dimensions 0.5 mm × 1.0 × 5.0 mm. The long axis was along the $[11\bar{2}0]$ direction and the rectangular sides were {0001}

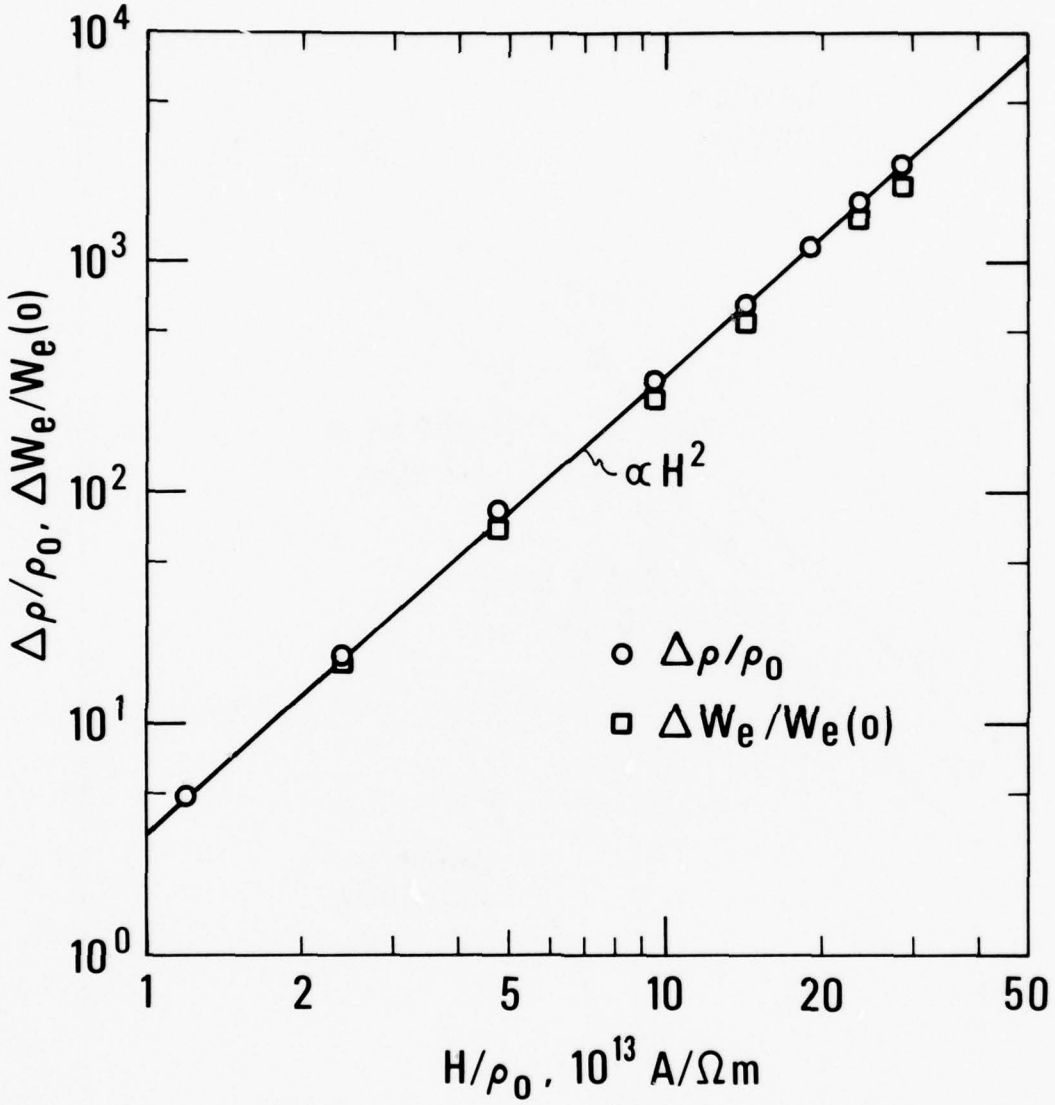

Figure 11. Electrical and thermal Kohler diagram for high purity single crystal beryllium at 4 K. The relative change in electrical resistivity, $\Delta\rho/\rho_o$, and of the electronic thermal resistivity, $\Delta W_e/W_e(0)$, are shown as a function of magnetic field divided by the residual electrical resistivity.

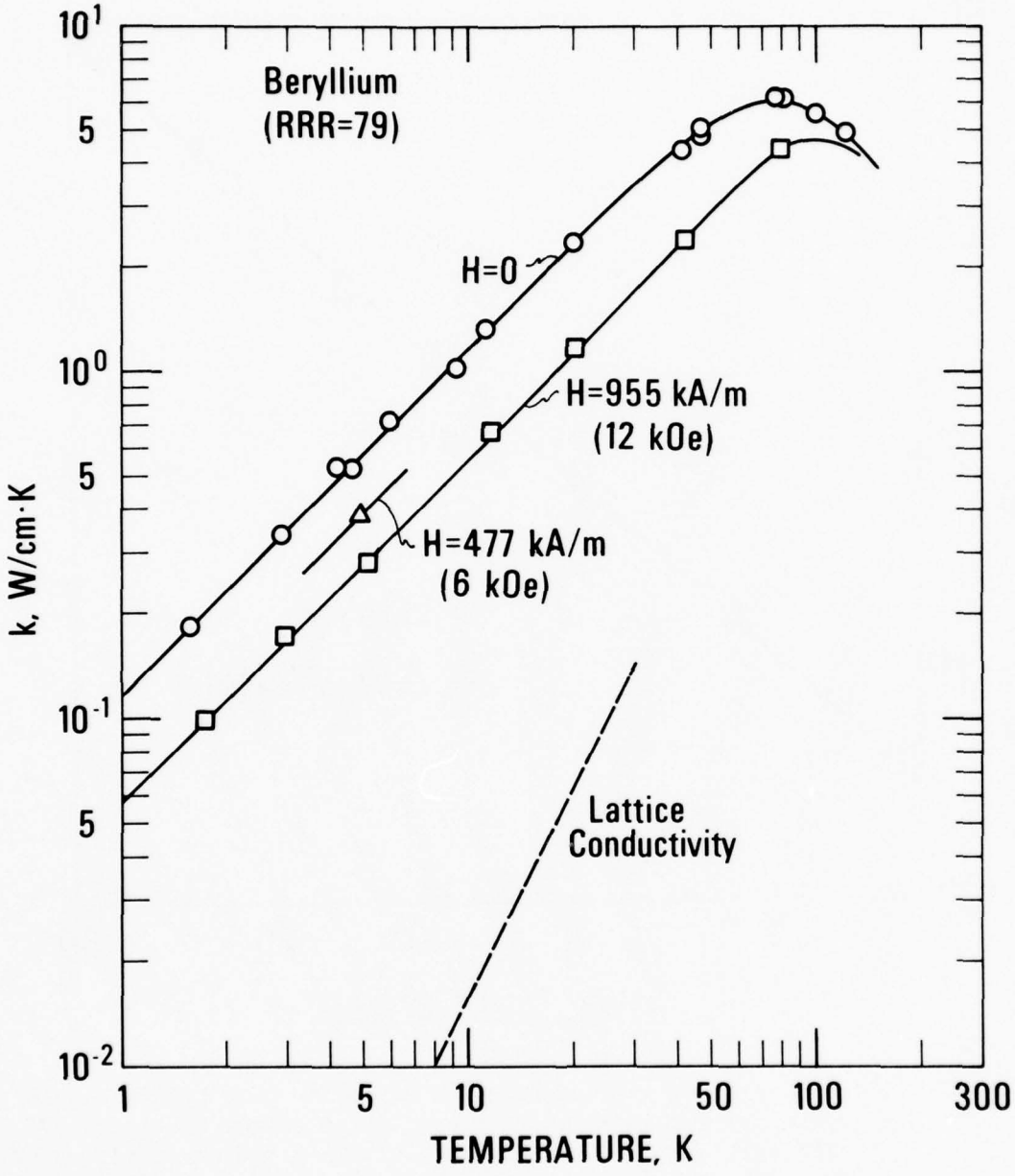

Figure 12. The thermal conductivity of low purity single crystal beryllium as a function of temperature for various transverse magnetic fields. The lattice conductivity derived from the measurements on high purity beryllium is shown for comparison.

and $\{10\bar{1}0\}$ type crystal faces. The resistance ratio of similar crystals were greater than 10^6, which makes these crystals among the purest substances known to man.[33] These crystals were grown from the vapor phase by a vacuum sublimation technique.[33] Copper was sputtered onto the ends of the sample to provide a base for indium solder.

The crystal was indium soldered to the copper reservoir of the thermal conductivity apparatus described previously. The holder for the heater was indium soldered to the other end. Small copper spots had been sputtered on the side of one of the {0001} faces but it was not possible to tin those spots. Consequently, a low temperature varnish was used to mount the two carbon thermometers on the {0001} face. These thermometers were mounted by first varnishing them to a piece of 0.05 mm thick copper foil. The copper foil had a narrow tab ($\sim$ 0.4 mm) which was wound around the sample and varnished in place. The two thermometers were placed 2.1 mm apart on the sample. Because of the small size of the sample the measurement inaccuracy was at least 15%. In zero magnetic field where the thermal conductivity is extremely high the inaccuracy is even greater.

Figure 13 shows how the thermal conductivity of magnesium at 4 K varies with the angle of the magnetic field. In this case the heat flow is along the $[11\bar{2}0]$ axis (a axis) and the field is rotated in the plane perpendicular to this axis. The minimum thermal conductivity occurs when the angle of the magnetic field is halfway between the c and b axes. A somewhat larger transverse magnetic field effect may occur for heat flow along the hexagonal c axis as in the case in beryllium.[26] The data in figure 14 were taken with the magnetic field aligned so as to give the minimum thermal conductivity. The zero field thermal conductivity below about 10 K was so high that it could hardly be measured in this small sample. The data above 30 K agree to within experimental error with previously published data for H = 0. Until now there has been no measurement of the thermal conductivity of magnesium in a magnetic field. The thermal conductivity shown in figure 14 for a given magnetic field is not as low as those for beryllium, gallium, or tungsten. However, even at 955 kA/m (12 kOe) there is no indication that the thermal conductivity is approaching the lattice conductivity. Thus it may be as much as an order of magnitude below the highest field curve in figure 14.

For heat switches made of very high purity magnesium, the switch ratios would be approximately those given in table 2. As is evident from this table, magnesium would not make as good a heat switch as beryllium or tungsten.

2.3.4. Thermal conductance of joints

Any low temperature apparatus is composed of many parts. In the electrocaloric refrigerator there will be a 15 K reservoir, refrigeration element, heat switches, and load. Each of these parts must be joined together in some fashion that will allow large amounts of thermal power to be transferred between these parts. An improperly designed joint may have a thermal resistance which could be larger than most other resistances in the system. The electrocaloric refrigerator has a cyclic operation mode so that the mass of material connected to the cyclic element must be kept small enough to prevent its heat capacity from thermally overloading the system. This is accomplished by using a small amount of high purity copper for the transfer of heat. The size of a magnetothermal heat switch also

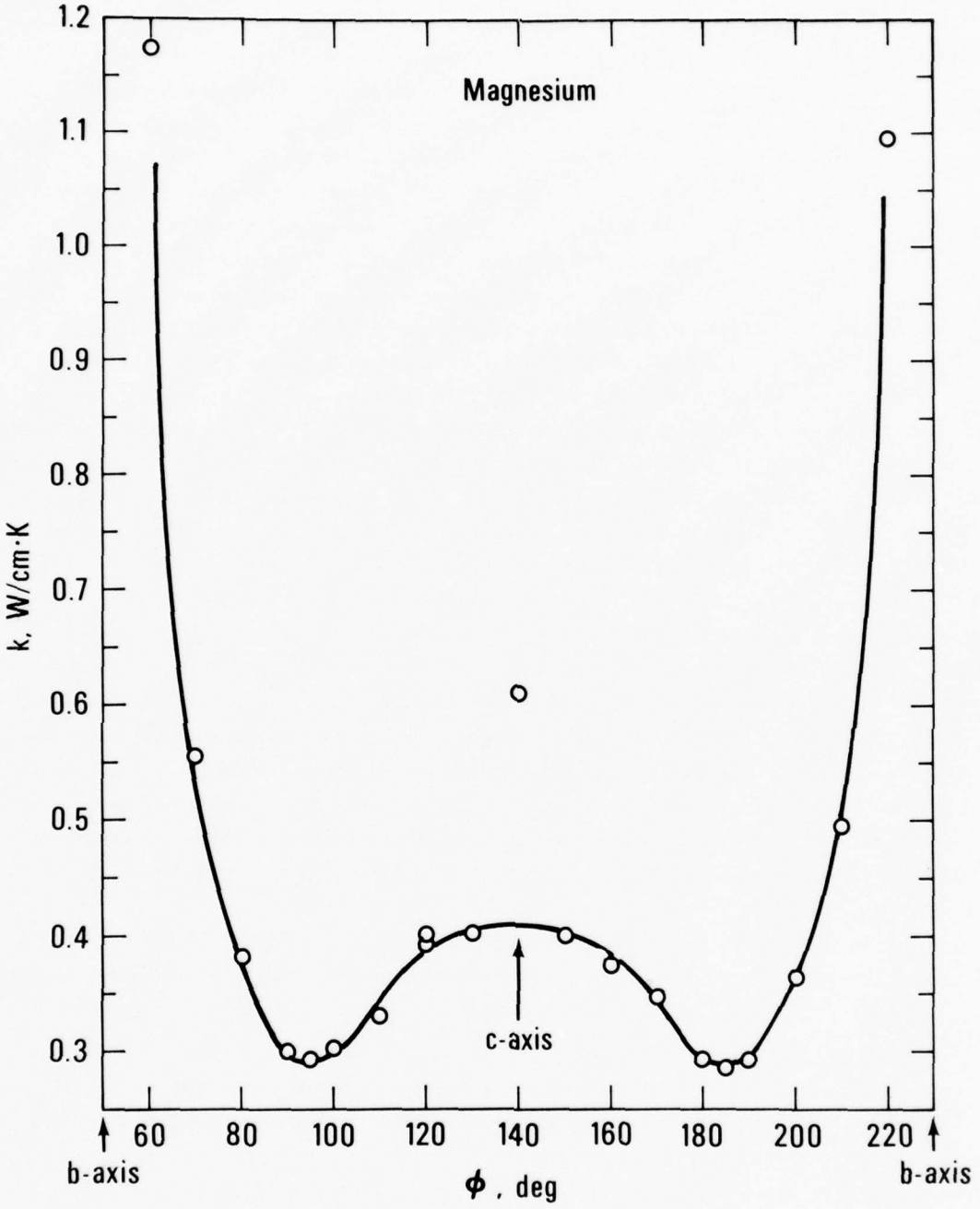

Figure 13. The thermal conductivity of single crystal magnesium at 4.3 K as a transverse field of 955 kA/m (12 kOe) is rotated through the arbitrary angle ϕ.

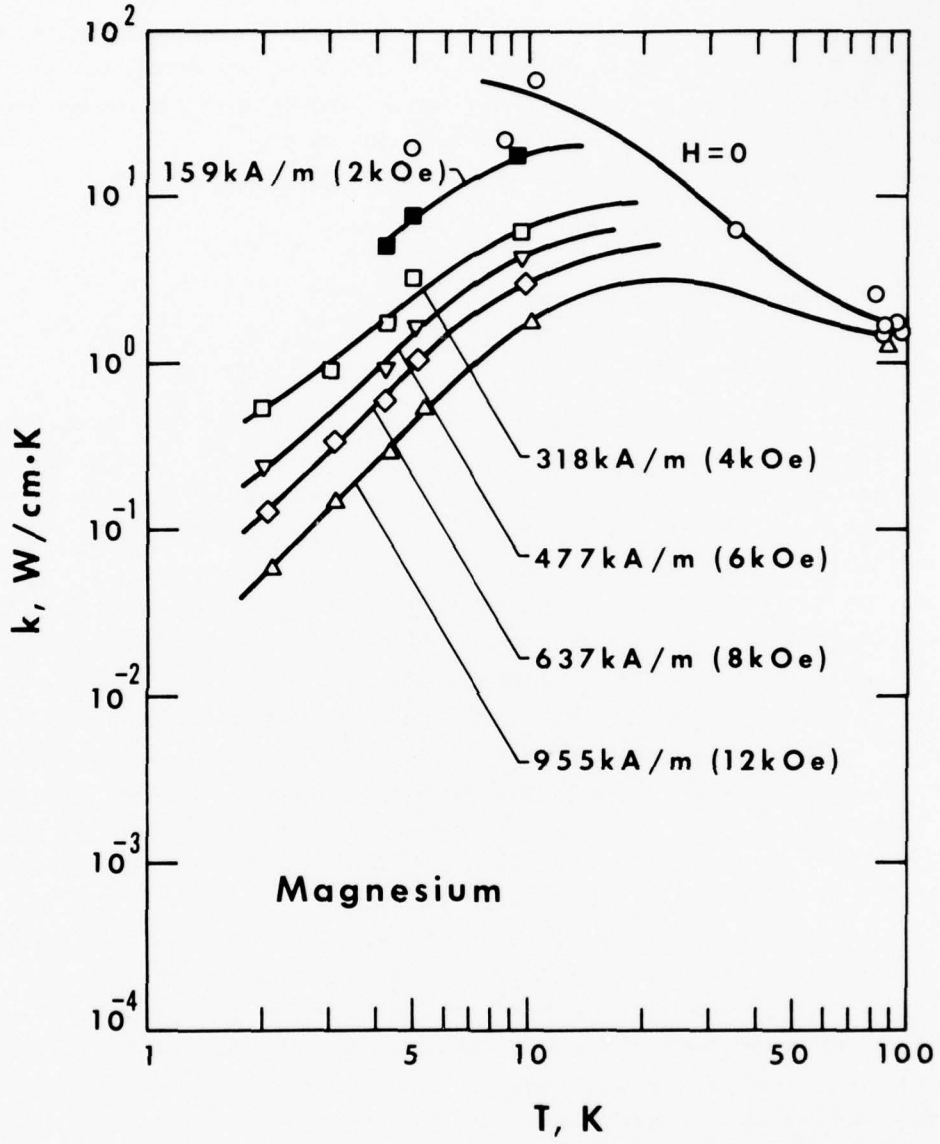

Figure 14. The thermal conductivity of single crystal magnesium as a function of temperature for various transverse magnetic fields.

needs to be kept small for the additional reason that the magnet size should be small. The small volumes of copper and of the magnetothermal switch material mean that the surface area of the joints will necessarily be quite small and therefore may have high joint resistances.

Figure 15 is a compilation of existing data on the thermal conductance of solder joints, grease joints, and pressure joints. In the case of the pressure joints the thermal conductance, in units of W/K, is for the whole joint, independent of the surface area. For the grease and solder joints the thermal conductance is for 1 cm^2.

The curves shown in figure 15 are taken from the following references:

Solder joints ($T < 1$ K): ref. 34,35
Solder joints (1 K $< T <$ 4 K): ref. 36,37
Solder joints (room temperature): ref. 38
Grease and adhesive joints: ref. 34,39-42
Pressure contacts: ref. 12,14,41-43.

It is rather amazing that there are no data in the literature on the thermal conductance of solder joints in the region between 4 K and room temperature. But rough interpolations (shown by the dashed lines in figure 15), based somewhat on values of the bulk thermal conductivity of certain solders, suggest that solder joints are superior to all other joints in the region above 4 K.

Because of the importance of and uncertainty of the thermal conductance in solder joints, measurements were made on such joints in this work. Indium solder was chosen since it has a higher thermal conductivity than alloy solders. Indium of 99.99% purity was used for these tests. Two joints were measured. The first was between beryllium sample 2 and an ETP copper surface. The second joint was between an annealed 99.999+% pure copper sample and the same ETP copper surface. Each joint was made by first tinning the two surfaces with generous amounts of indium. The parts were than pushed and rubbed together as heat was applied to the joint. The excess indium was trimmed off with a razor blade. The resultant joint thickness was on the order of 25 μm.

Figure 16 shows the thermal conductance of the two indium solder joints. These conductances were measured during the same time the thermal conductivity of each sample was being measured. It was necessary to extrapolate the temperature gradient in the sample to the surface. This correction was less than 10% for temperatures below 30 K with the annealed 99.999+% pure copper sample. For the beryllium sample, however, this correction amounted to as much as 90% for temperatures around 10 K. Thus only the high temperature data for beryllium is fairly reliable. With that in mind, the two sets of data (beryllium and copper) are in good agreement with each other. This agreement shows that even though it is difficult to wet beryllium with the indium, successful solder joints can still be made to it. The thermal resistance of the joint is more than an order of magnitude larger than that expected across a 25 μm thick pure indium sample. The increased resistance, which is typical in solder joints, is probably due to imperfections both in the solder layer and in the actual bond.

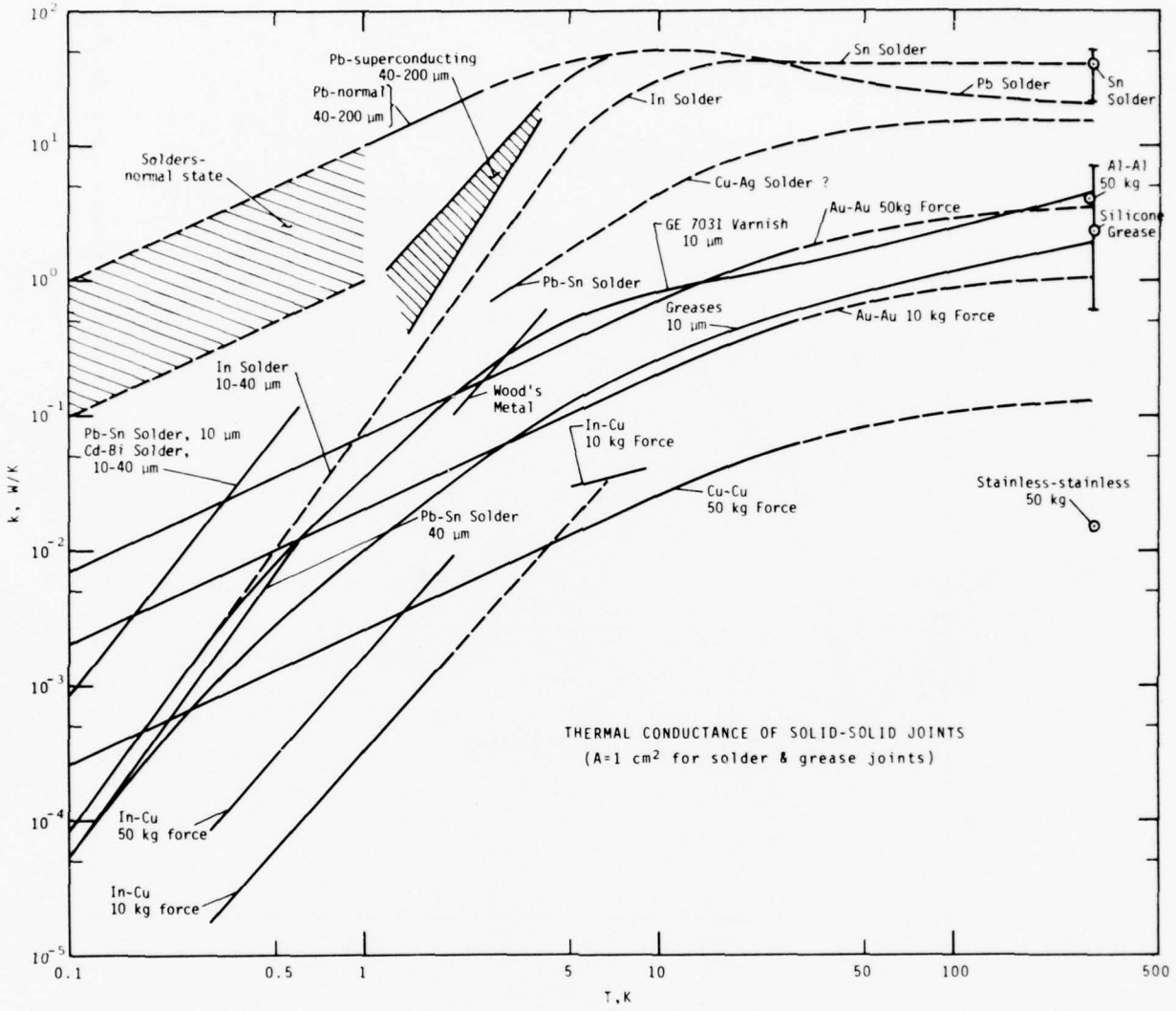

Figure 15. The thermal conductance of grease, adhesive, solder, and pressure joints as a function of temperature. The conductance is per cm^2 of contact for the grease, adhesive, and solder joints. However, the curves for the pressure joints give the total conductance of the joint, independent of the area, but dependent on the total force applied. The dashed lines are our estimates of the conductance in areas where no data exist.

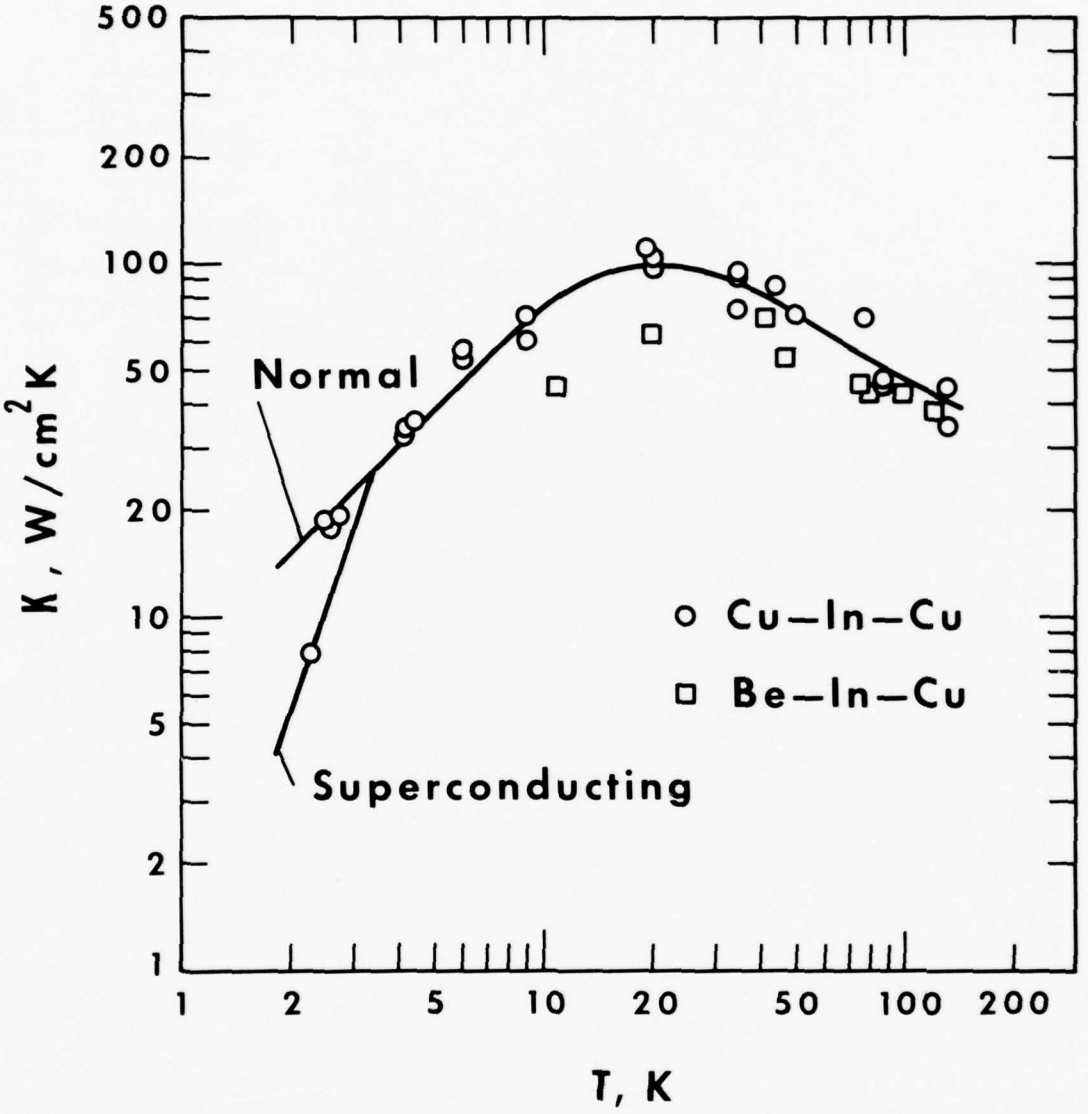

Figure 16. Thermal conductance as a function of temperature for two indium soldered joints. The normal state is produced by applying a magnetic field.

The indium joint conductance in the 4-15 K temperature range is considerably higher than estimated in figure 15. In order to transfer 5 W of power with a ΔT much less than 1 K would require a joint area on the order of 0.1-0.5 cm^2.

2.3.5. Magnet requirements

The magnetothermal switches require a transverse magnetic field on the order of 1200 kA/m (15 kOe) to operate them. This is low enough that iron can be used for most of the magnetic flux path. A gap in the iron on the order of 1 cm in length would be large enough to fit around, but not touch, the heat switch material. The magnet must be able to operate at 15 K, since it will be thermally anchored to the upper reservoir. Even if it were attached to the load, it would have to start operation at 15 K. Other requirements for the magnet are that the heat load to the 15 K reservoir be small compared with 5 W and that the rise time of the magnetic field be much less than 1 s.

The magnet wire could be made superconducting if Nb_3Sn were used. It has a transition temperature of about 18 K. The only heat load would be from heat conduction down the leads but this could be made much less than 5 W. It should be possible to apply or take off the field in a Nb_3Sn magnet in less than one second in light of the present superconducting magnet technology. However, tests were not made of the possible cycle times in a Nb_3Sn magnet.

For resistive windings the power dissipation in an air core solenoid can be expressed as[44]

$$W = \frac{\rho r}{\lambda} \left(\frac{H}{G}\right)^2, \qquad (2.5)$$

where ρ is the resistivity in ohm-cm, r is the inside radius of the magnet coil in cm, λ is the fraction of coil volume occupied by conductor, H is the field in Oe, G is a geometry factor typically in the range 0.15 to 0.2, and W is the power in watts. For commercial purity copper at 15 K, for r = 0.5 cm, and for H = 1200 kA/m (15 kOe), the power dissipation is about 200 watts. The use of an iron core with a 1 cm gap can reduce the power to about 2 watts. High purity copper wire could reduce the power dissipated by another order of magnitude. A commercial iron core transformer was modified to make a C-type magnet capable of generating the required fields. The copper wire in the coil was 0.5 mm diameter. The rise and fall times for generating the field were on the order of 0.2 s.

The magnets for the magnetothermal heat switches could be made of copper windings and it would be certain to work. The power dissipated in that case would be higher than desired unless high purity copper were used. The use of Nb_3Sn would probably be better but there is the uncertainty of how fast the field can be changed.

3. REFRIGERATION MATERIALS

3.1. Theoretical

3.1.1. Thermodynamics

The general TdS equation for a dielectric material is

$$TdS = C_E dT + T(\partial P/\partial T)_E dE, \tag{3.1}$$

where C_E is the specific heat in the electric field E and P is the polarization of the sample. The refrigeration absorbed during the isothermal step from E_2 to E_1 in figure 1 is given by

$$\dot{Q}_L = T_1 \Delta S = T_1 \int_{E_2}^{E_1} (\partial P/\partial T)_E dE. \tag{3.2}$$

The temperature change during the adiabatic step from E_4 to E_2 is best determined by equating the entropy changes along a fictious path from E_4 to E_2 at the temperature T_2 and then from T_2 to T_1 along the field line E_2. These entropy changes are given by

$$\int_{T_1}^{T_2} \left(\frac{C_E}{T}\right)_{E_2} dT = \int_{E_4}^{E_2} (\partial P/\partial T)_{T_2} dE. \tag{3.3}$$

The specific heat in an electric field is given by[45]

$$C_E = C_O + T \int_O^E \left(\frac{\partial^2 P}{\partial T^2}\right)_E dE, \tag{3.4}$$

where C_O is the specific heat in zero field. Equations (3.2) to (3.4) point out the fact that the thermodynamic behavior of a dielectric material can be determined entirely from $C_O(T)$ and P(T,E). This fact can be visualized by considering the entropy in figure 1 as a surface in (T, E) space. The entropy at a point (T_1, E_1) is found by integrating (3.1) from (0, 0) where S=0. One may choose any integration path, but the path considered at the moment follows the E=0 plane from T=0 to T=T_1 and then along the T_1 plane from E=0 to E=E_1. Each of the two segments of the path use only one of the terms in eq. (3.1) because first the field is held constant and then the temperature is held constant. The total entropy is then given as

$$S(T_1,E_1) = \int_0^{T_1} \frac{C_O}{T} dT + \int_0^{E_1} \left(\frac{\partial P}{\partial T}\right)_{T_1,E} dE .$$

The dielectric constant ε of a dielectric is given as $\varepsilon = (\partial P/\partial E)_T$ so that the polarization can be derived from the dielectric constant by the expression

$$P(T,E) = \varepsilon_O \int_O^E K'(T,E')dE' + P(T,0), \qquad (3.5)$$

where ε_O is the dielectric constant of free space and K' is the relative dielectric constant. The last term accounts for any remanent polarization in the material. A material with any remanent polarization is normally referred to as a pyroelectric. If the direction of polarization can be reversed, then it is called a ferroelectric. Dielectric absorption, or the storage of charges, can also make a contribution to any measured remanent polarization. In addition, at low temperatures there may be some very long dipole relaxation times which can given rise to a measured remanent polarization. These last two contributions were not considered at the beginning of this program. Much has been learned about the charge storage and relaxation mechanisms during this project, but there still remains much to be learned. The presence of a remanent polarization usually implies irrversibility in P(T,E). Therefore, P(T,E) would no longer be a state function from which other thermodynamic properties could be derived. Irreversibility in P(T,E) would also give rise to hysteretic heating.

The temperature-entropy diagram of a dielectric material can also be determined entirely from specific heat measurements without recourse to polarization measurements. This can be done by choosing the integration path for eq. (3.1) to be first along the T=0 plane from E=0 to E=E_1 and then along the E_1 plane from T=0 to T=T_1. In that case the total entropy is given as

$$S(T_1,E_1) = \int_0^{E_1} \left(\frac{\partial P}{\partial T}\right)_{E,T=0} dE + \int_0^{T_1} \frac{C_{E_1}}{T}\, dT,$$

which must be the same as that derived from any other path. The third law of thermodynamics requires S=0 at T=0, so the first term for $S(T_1,E_1)$ must be zero, i.e., $(\partial P/\partial T)_E = 0$ at T=0. The entropy in any electric field is then simply given as

$$S(T,E) = \int_O^T \frac{C_E}{T'}\, dT'. \qquad (3.6)$$

To use this type of expression for the entropy requires measurements of the specific heat in electric fields down to temperatures much less than T_1 in figure 1. In that case, the uncertainty in the entropy due to the extrapolation of the specific heat down to 0 K is usually negligible. Equation 3.6 includes the lattice entropy, so that field-induced entropy changes small compared with the lattice entropy would be difficult to detect from eq. (3.6). Because of that reason and because specific measurements are time-consuming, polarization measurements were used more often in this work to find ΔS upon a field change via eq. (3.2). The uncertainty in ΔS determined from $\partial P/\partial T$ is unaffected by the size of the lattice entropy.

Large entropy changes upon a change in the field will occur at temperatures not too far removed from a transition. The entropy curves shown in figure 1 are indicative of a zero field transition near T_1. Such a transition in a dielectric could be associated with a change from a ferroelectric or antiferroelectric state to the paraelectric state. The minimum entropy change required at T_1 can be roughly estimated. In going from T_2 to T_1 in figure 1, the dielectric material must be able to cool itself as well as metallic heat conductors and any inactive dielectric. If we assume that the metallic parts and the inactive dielectric occupy about 10% of the total volume of the refrigeration material, then the entropy change in the active dielectric would be on the order of 1 mJ/K cm^3 in cooling down the other materials from 15 K to 4 K. The lattice entropy at 15 K of the active dielectric would also be about 1 mJ/K cm^3. Therefore, the entropy available at T_1 needs to be somewhat larger than 2 mJ/K cm^3 if any isothermal refrigeration is to be performed. In terms of the gas constant we require $S_4 \geq 10^{-2}R$. If the cool-down from 15 K to 4 K is to be done in a regenerative mode or in several stages instead of one, then the entropy at 4 K can be smaller than $10^{-2}R$. Since the lattice specific heat of the dielectric material increases as T^3, the upper limit of refrigeration cannot be much above 15 K.

3.1.2. Criteria for materials selection

The previous section established the thermodynamic groundwork upon which criteria were established for selecting materials to try for electrocaloric cooling effects. It should be mentioned at this point that much was learned during the course of this project in regard to the criteria for selection of materials. For instance the original set of criteria was not adequate and the material ($SrTiO_3$ glass-ceramics) originally chosen turned out to be unsatisfactory.

Originally it was thought that the P(T,0) term in eq. (3.5) would be zero or negligibly small for a paraelectric or antiferroelectric material. In that case the dielectric constant could be used to find P(T,E) and the related thermodynamic properties. From eq. (3.1) it is evident that large refrigeration effects require a large $\partial K'/\partial T$. The original set of criteria then consisted of the following points: (1) a large zero field $\partial K'/\partial T$ in the 4-15 K temperature range, (2) the term $\partial K'/\partial T$ must remain sufficiently high up to the maximum field to be used, (3) a high breakdown strength to provide wide limits of integration in eq. (3.2), (4) negligible hysteresis in K'(T,E), and (5) the phonon-dipole relaxation time be much less than 1 s. Experimental results before the program began on research samples and on small plant manufactured samples of $SrTiO_3$ glass-ceramics indicated that all these conditions could be met. However, only the plant-manufactured multiple layer samples could give the high breakdown strengths. Considerable effort was then put into making large (about 5 cm^2 area) multilayer samples with process variable that maximized both $\partial K'/\partial T$ at zero field and the 4 K breakdown strength.

After it was found that cooling effects did not exist at 4 K in the $SrTiO_3$ glass ceramics, measurements of the DC polarization were made on these samples. These measurements showed a relatively large P(T,0) term in the total polarization. The resulting temperature dependence of this total polarization turned out to be considerably different from that derived from the dielectric constant at ac frequencies greater than 100 Hz. The dc

polarization showed zero temperature dependence at 4 K in the $SrTiO_3$ glass-ceramics, consistent with the electrocaloric measurements. A negative slope in P vs T did occur in the 10-15 K temperature range and some cooling effects were observed there.

Several variations in the $SrTiO_3$ glass-ceramics were then tried to try to understand the origin of the remanent polarization. These variations included changing the crystallization temperature, which changes the $SrTiO_3$ crystallite size and changing the composition of the glass phase. It was felt that these variations would determine if the remanent polarization came from the glass phase or the $SrTiO_3$.

We also decided to measure the DC polarization and the electrocaloric effect in several other candidate materials. The hope was to find a material with a large enough $\partial P/\partial T$ at 4 K to make an effective refrigerator. The study of the other materials would also allow us to obtain a more general understanding of the behavior of dielectrics in an electric field. In general, the alternate materials chosen had high dielectric constants which showed a temperature dependence near 4 K. Several of the materials chosen were reported in the literature to have a transition to either the ferroelectric or antiferroelectric state in the vicinity of the 4-15 K temperature range. Various solid solutions in $SrTiO_3$ and $KTaO_3$ were tried in the hopes that such solutions may lower the temperature at which the dc polarization still shows a temperature dependence.

3.2. Previous Work

The first measurements[4] of the electrocaloric effect were done in 1930, only four years after the first measurements[46] of the magnetocaloric effect. The magnetocaloric effect was utilized for adiabatic demagnetization below 1 K within a few years after the first measurements. However, further work on electrocaloric effect was not done until some twenty years later, probably because so little was known at that time of the dielectric behavior of materials. After the ferroelectric state was better understood, several more measurements[47] of the electrocaloric effect were made on such materials. The electrocaloric measurements on these ferroelectric materials were all done near room temperature. Granicher[48] first suggested the use of $SrTiO_3$ for electrocaloric cooling at low temperatures. His suggestion was based on his dielectric constant measurements of $SrTiO_3$. This material has a large negative temperature derivative around 20 K even though it does not become ferroelectric. At 3 K and below[49] the dielectric constant of $SrTiO_3$ is independent of temperature. That behavior is consistent with Barrett's theory[50] and means that no transition to the ferroelectric state occurs.

Hegenbarth[51] was the first to make electrocaloric effect measurements on $SrTiO_3$, which in that case were ceramic samples. With an electric field of 8 kV/cm, he saw adiabatic depolarization cooling of 6 mK at 78 K and 60 mK cooling at 17.5 K. Somewhat larger effects were seen in later measurements[52,53] on single crystal $SrTiO_3$, but these cooling effects disappeared below about 4-5 K. The temperature changes observed in the single crystal $SrTiO_3$ were in reasonable agreement with values calculated from the specific heat and the observed dielectric constant versus temperature and electric field.[52,54] The uncertainty in the calculation was dominated by that of the specific heat, since no accurate specific heat data existed in the liquid helium temperature range.

Electrocaloric cooling at still lower temperatures was first demonstrated in OH doped KCl by three independent investigations.[55-57] Cooling to 0.36 K from a starting temperature of 1.3 K was reported.[57] Various theoretical studies[45,58] and experimental investigations[59,60] on other doped alkali halides followed shortly. Cooling to as low as 0.05 K was demonstrated in CN doped RbCl.[60] Electrocaloric refrigeration using KCl:OH has been used[61] for thermostating crystals below 1 K while they were being radiated with short light pulses. Patents have been issued[62,63] for electrocaloric refrigeration with doped alkali halides as the refrigerant.

Of all the materials studied previously, none showed large enough electrocaloric effects to be useful as a refrigerator in the 4-15 K temperature range. The doped alkali halides appear to be quite powerful for temperatures below 1 K. However, because of the very low ordering temperature and the limit of about 10^{20}-10^{21} impurities per cm^3, these materials have only very small cooling effects in the 4-15 K range. The studies on $SrTiO_3$ (single crystal and ceramic) indicate that material is better suited for cooling at higher temperatures than the doped alkali halides. Unfortunately it tends to order at too high a temperature so that almost no cooling is available at 4 K. Development of a practical 4 K electrocaloric refrigerator was then dependent upon the discovery of a more suitable material.

3.3. $SrTiO_3$ Glass-Ceramic Research Samples

3.3.1. Dielectric properties

A new class of dielectric materials were discovered recently by one of the authors (WNL).[6] The dielectric properties of these materials in the 1-20 K temperature range appeared ideal for an electrocaloric refrigerator operating in this temperature range. A patent[10] was issued for an electrocaloric refrigerator utilizing such materials. These new dielectric materials are the $SrTiO_3$ glass-ceramics. The useful glass-ceramics are select compositions in the SrO-TiO_2-Nb_2O_5-Al_2O_3-SiO_2 system, where the Al_2O_3-SiO_2 component is the glass phase. The initial work on these materials was done with bulk material ground down into thin sheets. The field of the glass chemistry of crystallized glasses has grown steadily following the work of Stookey[64] at the Corning Research Laboratory, and the reader is referred to the literature[64,65] for a detailed account of the preparation of these materials. In brief, crystals of $SrTiO_3$ about 5-10 μm in size are grown *in situ* at about 50 volume percent in an alumino-silicate glass matrix at temperatures near and above 900°C

The $SrTiO_3$ glass-ceramics exhibit large changes in the dielectric constant with respect to temperature below 20 K, as shown in figure 17. For some research samples $\partial K'/\partial T$ was as high as 25 K^{-1}. The positive value of $\partial K'/\partial T$ at low temperatures is in marked contrast to that found in single crystal $SrTiO_3$,[49,54,66-69] which has only a negative derivative. The dielectric constant in figure 17 follows a Curie-Weiss law from room temperature down to approximately the temperature of the peak at 33 K. The loss tangent (tan δ) has a maximum at 20 K. The lattice parameter data from the two diffraction lines shown in figure 17 were identical above 77 K but showed a splitting at and below 50. This structural transformation was tentatively identified as cubic→tetragonal, but the data were too limited to determine the c/a ratio. Measurements of the loss tangent as a function of frequency indicated the dipole-lattice relaxation times were much less than 1 second.

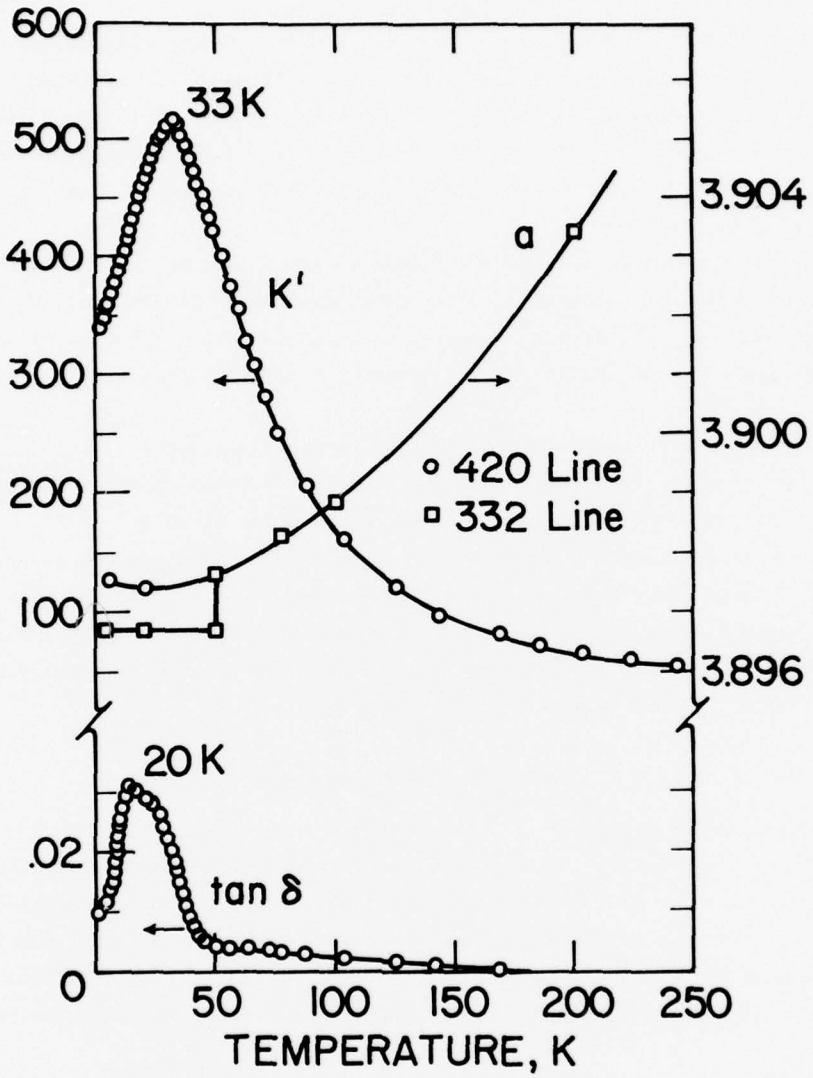

Figure 17. Dielectric data (K' and tan δ) and lattice parameter data (a) measured on a $SrTiO_3$ glass ceramic from 2 to 250 K. The Curie-Weiss behavior of K' extends to, and above, normal temperature.

A serious problem with the bulk samples was that the breakdown strength was extremely low (a few hundred V/cm) due to minute cracks in the ground glass. Thus the hysteresis and field dependence of $\partial K'/\partial T$ could not be measured in these samples.

3.3.2. Relation to capacitance thermometer manufacturing

A similar $SrTiO_3$ glass-ceramic material has been developed previously for a low temperature capacitance thermometer.[6] This material has a value of $\partial K'/\partial T$ which is nearly independent of temperature over a wide range, but the value is much less than 25 K^{-1}. The thermometer-manufacturing process is similar to the process used to fabricate multilayer samples to be discussed in the next section. With this process breakdown strengths in excess of 300 kV.cm have been achieved.

Hysteresis measurements, shown in figure 18, were made on the thermometer type samples at 4.2 K by numerically integrating K'(E) data measured at 100 Hz. As the curve indicates, very little hysteresis is present except for the region below about 40 kV/cm. From such results the polarization appears to be essentially reversible as required for the thermodynamic analysis.

An electric field reduces $\partial K'/\partial T$ rapidly as shown in figure 19, although calculations[2] based on the results in figure 19 show that the refrigeration power is sufficiently high for practical use, provided that $(\partial K'/\partial T)_{E=0}$ is on the order of 25 K^{-1}.

The problem which had to be investigated in this project was the use of the research material with high $(\partial K'/\partial T)_{E=0}$ in the multiple layer process to provide the high breakdown strength. Such a step would also be a test of the prototype manufacturing process. The material made in this process was then expected to meet all the criteria discussed in section 3.1.2.

3.4. $SrTiO_3$ Glass-Ceramic Multilayer Samples

3.4.1. Fabrication method

The term "glass-ceramic multilayer sample" refers to a capacitor fabricated using the Corning Glass K II process.[70] Essentially it consists of alternate layers of glass-ceramic and precious metal electrodes sealed under heat and pressure to form a monolithic unit. The ease of forming using this process far exceeds conventional ceramic methods and was, therefore, a good candidate process for use in the fabrication of the proposed refrigerator elements.

The initial phases of the fabrication process were performed at Sullivan Park Research and Development Laboratory, Corning, New York. The constituent oxides and/or carbonates were mixed by J. E. Sage in a mason jar in 1000 g batches, then melted by the Melting Technology Department in platinum-crucibles, cocktail-mixed, and quenched between two water cooled rollers to produce a tinted ribbon glass which was slightly reduced due to the high melt temperature. The ribbon glass was subsequently oxidized by heating to approximately 700°C in air for 3-4 hours which is well below the nucleation temperature. The oxidized glass was a lighter shade of yellow to greenish-brown. This concluded the portion of work which was performed at the laboratory in Corning, New York. The ribbon glass was next shipped to the Capacitor Product Development laboratory at the Corning Glass Works Plant in Raleigh, North Carolina.

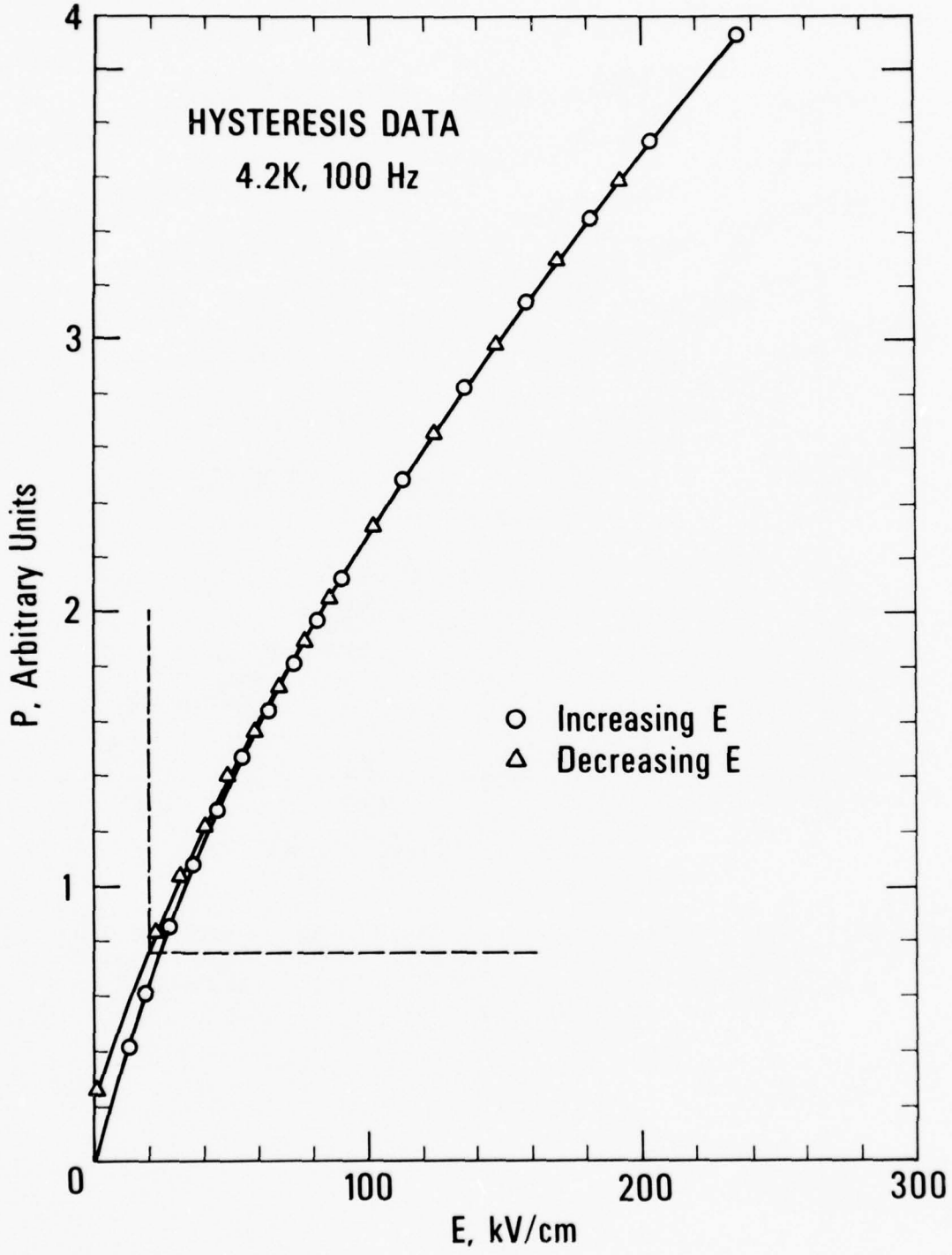

Figure 18. Polarization vs. electric field at 4.2 K for $SrTiO_3$ glass-ceramic from integration of dielectric constant data.

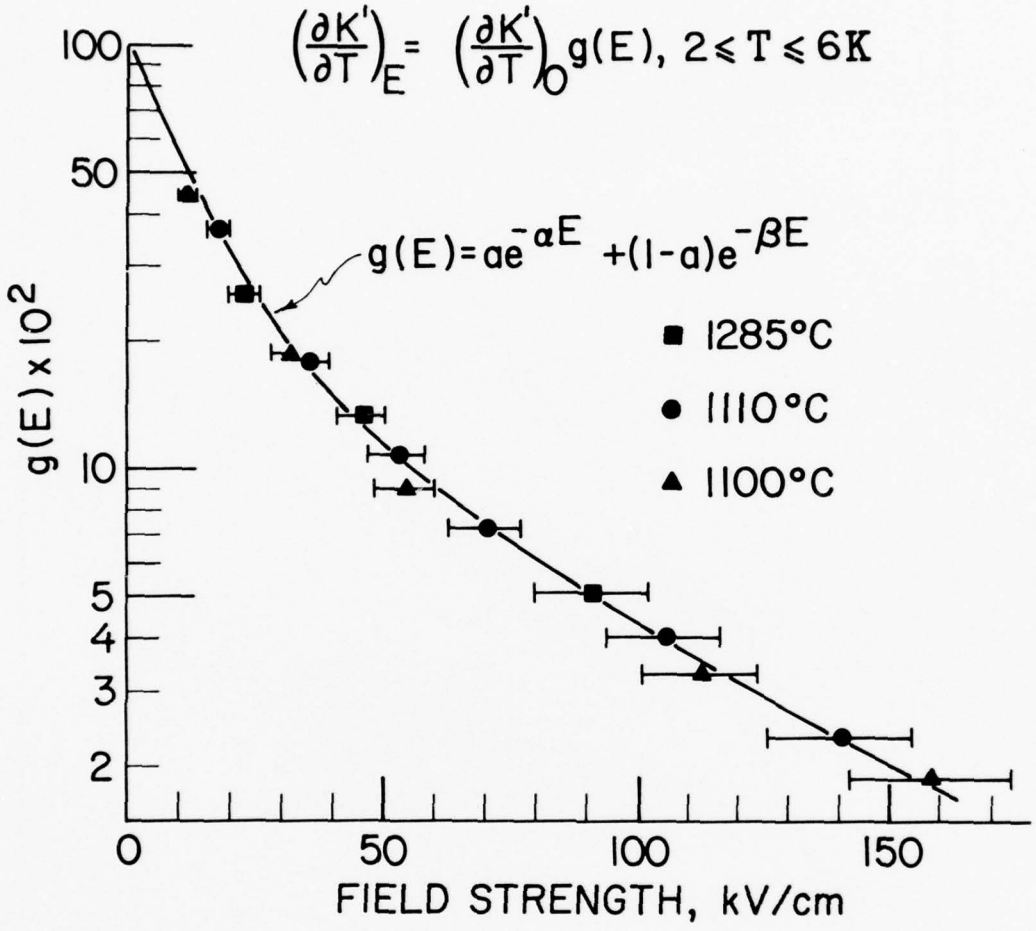

Figure 19. Empirical dependence of $\partial K'/\partial T$ on field strength for three glass-ceramics, $2 \leq T \leq 6$ K. The solid curve through the points is a plot of the $g(E)$ function shown. Samples cerammed at three different temperatures were measured.

The work in Raleigh was performed by A. J. Morrow, R. P. Ruddock, and W. D. Claborn. The first step was to grind the ribbon glass in water in a 1.33 gallon carburundum ball mill with Al_2O_3 cylindrical media. A grind of 44 hours at 60 rpm reduced the glass to a particle size of 2.75 μm. It was dried overnight, mixed with an aqueous binder system, and ball milled for 4 more hours. The resulting slurry was de-aired for 16 hours and cast into a thin film which, when fired, was approximately 28 μm thick.

In order to produce capacitors, a wet stacking method was used in which the electrodes are screened onto the dielectric film. The screen is shifted after each application to effectively produce several capacitors in parallel. The electrode metals used are listed in table 3.

TABLE 3

Electrode Metal Compositions[a]

Weight Percent

Manufacturer's Number	Pt	Au	Pd	Vehicle
A-2664	4.5	42	13.5	40
A-2860	49	12	--	39
9545[b]	48	12	--	40
A-2721	--	45	15	40

[a]All inks manufacturered and composition information supplied by Engelhard Industries, 1 W. Central Avenue, E. Newark, New Jersey.

[b]A different (and less satisfactory) vehicle was used for this ink.

A-2664, Pd-Pt-Au, was used as a standard metal throughout most of the work. Normally, 8 weight percent glass frit was added to the paste using a 3 roll mill. The geometry of the samples for this project was limited in large part by the screening operation. Since an 11.5 x 11.5 cm area is the maximum practical area which can be screened, the maximum sample which could be made would be approximately 10 x 10 cm. This size is impractical, however, since only one sample is produced per stack. Therefore a 1.9 x 1.9 cm sample was agreed upon which would yield 25 samples per stack and yet give a thermally efficient volume. In the original design (Fig. 20) a so-called "floating electrode" was inserted in the center of each effective capacitor and a generous "pullback" was allowed. It was thought that it would be possible to apply larger voltages with these modifications. In a later design, the "floating electrode" was removed, the pullback was reduced to increase the amount of dielectric exposed to the electric field, and the dielectric thickness was increased. The thicker dielectric layers were made by pressing 11.5 cm squares of green film together at a pressure of 30 psi. This procedure allowed a uniform thickness of film to be used and also made it highly

FIGURE 20

GLASS-CERAMIC MULTILAYER SAMPLE DIMENSIONS*

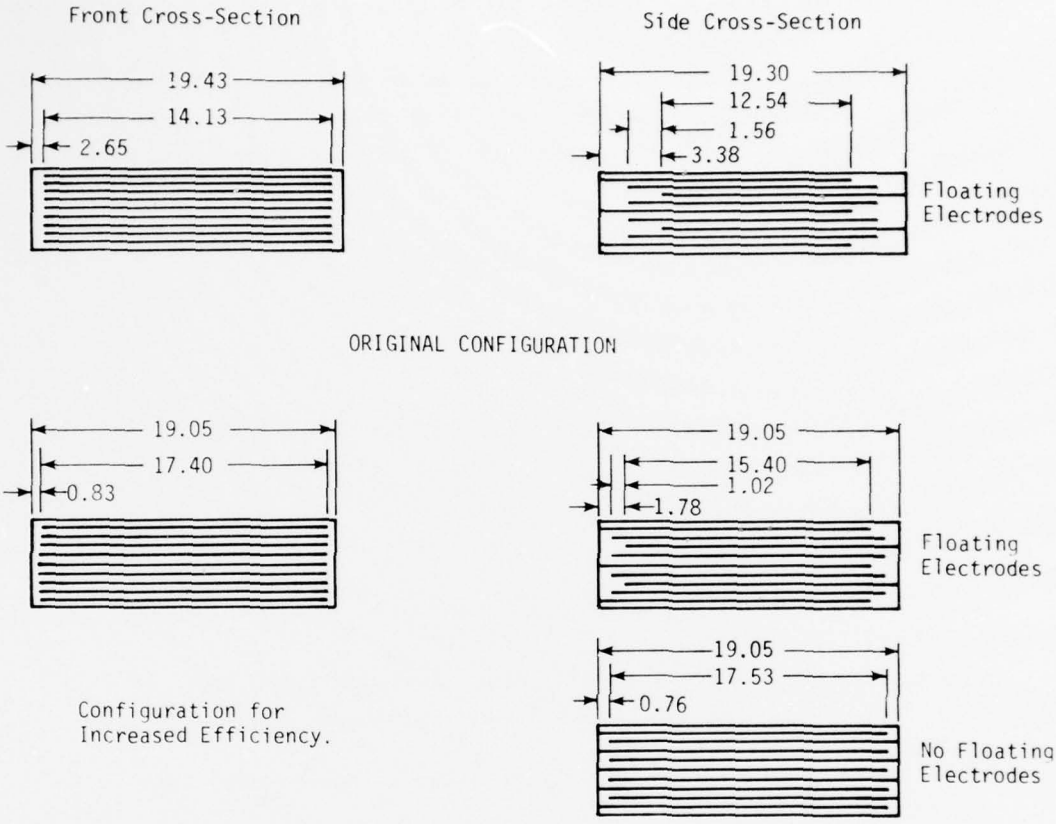

BOTH CONFIGURATIONS:

Glass Thickness: 0.028 mm/pieces
Electrode Thickness: 3.81 μm

ORIGINAL CONFIGURATION:

15 effective layers of 0.056 mm, 2.06 cm^2 (15 floating layers)

NEW CONFIGURATION:

Floating: 15 eff. of 0.056 mm, 2.87 cm^2 (15 floating layers)
.002 Type: 15 eff. of 0.056 mm, 3.05 cm^2
.003 Type: 10 eff. of 0.084 mm, Same area as above
.004 Type: 6 eff. of 0.112 mm, Same area as above
.006 Type: 5 eff. of 0.168 mm, Same area as above

* All measurements in millimeters.

unlikely that a pinhole in the film could extend from one electrode to another, reducing the probability of shorts and increasing the resistance to breakdown under voltage.

At the end of the stacking operation an 11.5 x 11.5 cm stack containing 25 samples was fabricated. The next step effected the removal, through oxidation, of the organic binder, and the fusing of the stack into a dense glass plate. The first portion of this operation, "burn-out", was a 20-hour cycle in which the temperature of the stack was very gradually raised to 350°C, then to 600°C in a drop-bottom furnace. The stack, sandwiched between layers of mica (to prevent sticking) and stainless steel plates, was then removed from the burn-out furnace at 600°C and transferred quickly to the press-ceram furnace at 725°C. A pressure of 100 psi was applied using an air cylinder. The furnace was maintained at 725°C for one hour, in the standard cycle, then raised at 135°C/hour to 915°C where it was held for 2 hours. The entire assembly, pressure plates, mica, and stack, was then removed and placed in an oven to cool.

A diamond saw was used to cut the samples apart. They were checked for shorts by dipping the exposed electrodes in Du Pont 8225 silver and air drying. This procedure made it possible to determine whether shorts were being formed in the press-ceram or firing operations.

Due to temperature limitations of the press-ceram furnace, the final firing step was performed in an ordinary box furnace. Variables were rate, soak time, and soak temperature. The normal procedure was to sandwich the samples between polished plates of fused silica protected by 2.5 x 2.5 cm x 25 μm pieces of platinum foil to prevent reaction. A weight of 400 g/sample was applied to prevent curling. After firing, the ends of the samples were ground on 600 grit SiC paper to ensure good electrode exposure. Dupont 8225 was applied to the electrodes and fired at 620°C for 10 minutes in a drop-bottom furnace.

The ac capacitance and dissipation factor were measured on an automatic bridge at 1 KHz and 1 VAC. On some samples, measurements were also made at 77 K by immersion in liquid nitrogen. A teflon fixture allowing the simultaneous immersion of 10 samples was constructed for this purpose.

Both to optimize properties and to eliminate processing problems a large number of variations were made in the process during the project. Table 4 is a summary of parameters varied. The experimentation breaks down chronologically into several distinct matrices primarily involving a particular glass composition.

The first work done used the 899 FEP glass and was exploratory in nature. After elimination of a host of problems, including batching and film casting problems and the major problem of substrate adherence during firing, manufacture of the first FEP matrix was carried out. There were 64 matrix elements altogether including 2 electrode metal, 4 press-ceram, 2 firing rates, and 4 firing temperature variations. Feeling that several of these variables had been acceptably eliminated, the second matrix, using 899 FEL glass, was carried out using 2 electrode metals and 6 firing temperature variations while holding other factors constant. This conclusion turned out to be somewhat premature; therefore, a second FEP matrix was fired in which 3 firing rates, 2 electrode metals, 2 press-ceram cycles, 6 firing temperatures, and 3 soak times were varied. In addition, three configurations were made: 28 μm layers with floating electrodes, and samples without floating electrodes having dielectric thicknesses of 56 and 84 μm.

Table 4

Glass-Ceramic Multilayer Experimentation Summary

Initial Matrix: Sticking Problem Solved, 9 Samples Tested.

Glass:	899 FEP
Firing Temperature:	1075-1200°C
Press-Ceram:	Seal A (Standard)
Firing Rate:	150°C/Hr. (2 Hr. Soak)
Metals:	A2664
Floating Electrodes	
Firing Substrates:	ZrO_2, Mica, BN, Al_2O_3, SiO_2, Graphite, Platinum Foil.

FEP-1: 132 Samples Tested.

Glass:	899 FEP
Firing Temperature:	1100, 1120, 1140, 1160°C
Press-Ceram:	Seals A, B, C, D (Variation in Soak Time at 725°C and 915°C)
Firing Rates:	100, 150°C/Hr. (2 Hr. Soak)
Metals:	A2664, 9545
Floating Electrodes	

FEL-1: Porosity Problem First Identified, 78 Samples.

Glass:	899 FEL
Firing Temperature:	1100, 1120, 1145, 1160, 1180, 1215°C
Press-Ceram:	C
Firing Rate:	150°C/Hr. (2 Hr. Soak)
Metals:	A2664, 9545, A2860 (Detective)
Floating Electrodes	

FEP-2: 209 Samples

Glass:	899 FEP
Dielectric Thickness:	.001" Layers Floating Electrodes .002" Layers .003" Layers New Artwork (Better Efficiency)
Firing Temperature:	1080-1200°C
Firing Rate:	30, 60, 90°C/Hr.
Firing Soak Times:	2, 8, 20 Hours
Metals:	A2664, A2860, A2721
Electrode Fritting:	0, 8 (Normal), 12% by Weight
Press-Ceram:	Normal (A), High Pressure, Extended Pressure

FHJ-1: Processing Matrix, Approximately 400 Samples.

Glasses:	899 FHJ (Primarily), 899 FEL (Control), 899 FEP
Firing Temperature:	1100-1200°C
Firing Rates:	30, 60, 90°C/Hr. (10 Hr. Soak)
Samples:	Multilayer (.002"), Bulk Glass, Unelectroded Samples, Small Samples
Burnout:	Normal, Extra Long
Metals:	A2664, A2721, A2860
Binder:	Aqueous, Toluene (FEP), Methacel (FEP)
Press-Ceram:	Capacitance Thermometer (DXO) Variations (involves application of pressure during cycle and soak times) AVC Suggested Variations (rates and temperature changes).

Table 4 (Continued)

FEL-2: 75 Samples Tested.

Glass:	899 FEL
Firing Temperature:	1080-1200 in 10° Increments 60°C/Hr. (10 Hr. Soak)
Samples:	.003", .004", .006" Layers 3/4", 1-3/8", 2" Square Samples
Metal:	A2664

FEP-FHN: Approximately 100 Samples.

Glasses:	899 FEP and 899 FHN (Niobium-Free)
Firing Temperature:	1100, 1115, 1130, 1145, 1160
Samples:	.003" Dielectric, A2664 Metal 60°C/Hr. (10 Hr. Soak)
Press-Ceram:	Low Temperature (825, 850°C Max. Temp.) (FEP)

FHS-FID: Boroaluminosilicates, 20 Samples Tested.

Glasses:	899 FHS, 899 FID (Niobium-Free)
Firing Temperature:	No Fire, 1100°C
Samples:	.003" Dielectric, A2664 Metal. 60°C/Hr. (10 Hr. Soak)

A great deal of experimentation was performed in an attempt to solve specific problems (e.g., excessive porosity). The primary matrix involved in this work used the 899 FHJ glass (FEL batched using carbonate-free starting batch powders). Nearly every variable in the process was varied in this matrix which sought a solution to the porosity problem. This work will be detailed in a later section.

When it became clear that no process variation was likely to eliminate porosity altogether, a second FEL matrix was fabricated wherein most variables were fixed. A standard processing procedure was determined at this time: a 60°C/hour rate combined with a 10 hour soak at temperature using Pd-Pt-Au (A2664) electrode metal. The major variables were firing temperature and geometry. Samples having dielectric thicknesses of 0.11 mm and 0.17 mm and external dimensions of 3.5 cm and 5.1 cm square were made for the first time. The larger samples were never fired but were press-ceramed showing that samples this size could be made.

After the discovery of the irreversible heating effect in multilayer samples, an attempt was made to reduce or eliminate the effect through glass composition. The first matrix along this line involved 899 FEP and a niobia-free version of FEP: 899 FHN. Samples were made using the standard process referred to above.

In order to help pin down the cause of the heating effect, a series of samples were also made in which the press-ceram peak temperature was varied from 825°C to the normal 915°C. Some of these samples were fired at low temperatures, for example 1000°C, after press-ceram.

Later, a second matrix was performed using 899 FHS and 899 FID which were boroaluminosilicate compositions with and without niobia, respectively.

A final phase of the fabrication method involved work in Raleigh to bond multilayer samples together with an eye to the finished refrigeration unit. High purity foils of silver, tungsten, and copper in 25 μm and 254 μm thicknesses were used along with several bonding agents: epoxy (Epibond 100-A), Corning glass code 750 AGB devitrifying glaze, and DuPont 8225 glass gritted organic silver paste. Bonding samples were fabricated from previously tested multilayer samples. A stainless steel fixture was devised to hold the sandwiched multilayers together during processing. All foils were used with the epoxy, which was a one component, thermally activated bonding agent. The epoxy was heated to 175°C and spread on the chips which were then held together until hard using the fixture. Producing a thin uniform layer was the only difficulty encountered. Due to the temperature involved, only silver foil was tested with the DuPont 8225 and the Corning 750 AGB. Using the same configuration, the application of these materials was made easier by the ability to work at room temperature. The bonded layers were fired in a drop-bottom furnace. The DuPont 8225 was fired at 620°C for 10 minutes; 750 AGB was fired at 350°C and 560°C each for 30 minutes. The 750 AGB glass, supplied in frit form was converted to a slurry using Reusche Oil, an organic vehicle. Results for all the above techniques were tested by cycling the bonded units between liquid nitrogen and warm water. The only failures were found in the DuPont 8225 samples which was therefore not recommended.

It is obvious that a large number of samples were fabricated during this project. The process involved is a sensitive one and yields often fell below 50% for a given stack. In addition, most of the variations, both in configuration and process, had never been attempted

previously. However, among the dozens of problems encountered, and for the most part overcome, two stand out as having the greatest significance, which are considered in detail below.

3.4.2. Fabrication problems

Two critical problems were encountered in the fabrication of the cooling samples, 1) substrate adherence during the final firing operation, and 2) porosity. The former was aggravated by the fact that the initially recommended firing temperatures were high and caused considerable softening in the samples. After experimenting with a variety of materials, including mica, BN powder, SiO_2, Al_2O_3 powder and substrate, ZrO_2, SiC, graphite, and solid Pt, the idea of using the Pt foil was suggested. Although some sticking was still encountered, the foil was flexible enough to be peeled off. The solution to this problem allowed the fabrication of high quality samples, which previously had not been possible.

The problem of porosity was considerably more difficult. Especially when fired at relatively high temperatures (1120°C or above), pores in the samples increased drastically in size so that at 1160-1200°C they were easily visible to the naked eye. On the electrode edges of the samples which had been ground, the pores looked like pits in the surface, but scanning electron microscope work (Figs. 21-24) showed clearly that their origin was internal.

An intensive effort was made to determine the cause of this porosity in both Raleigh and Sullivan Park. Diverse theories to account for the formation of the pores led to several widely varying investigations which break down into roughly three areas, 1) electrode variations, 2) composition changes, and 3) process variations.

As the pores tended to form along the metal electrodes, it was suspected that the electrodes were the cause of the problem. Dr. Andrew Herczog (Sullivan Park) suggested a possible mechanism whereby the platinum in the electrode could be causing porosity through the formation of $PtTiO_3$ at intermediate temperatures. To test this theory, Pd-Au (A2721) and Pt-Au (A2860) electroded samples were made. No differences in porosity was observed. In a definitive experiment, samples without electrodes were made which showed the same porosity as electroded samples and shifted emphasis to other possible causes. Dr. Brent Wedding (Sullivan Park) also did DTA and TGA analyses of electrode pastes and observed no gassing at firing temperatures.

Dr. I. Lachman (Sullivan Park) successfully fabricated honeycombed structures of FHN by an entirely different fabrication process than the one used in Raleigh. However, measurements on these samples at helium temperatures proved disappointing.

Carbonates were used in the original glass melts for electrocaloric refrigeration glasses (899 FEP, 899 FEL) but not for the capacitance thermometer glass (899 DXO), a similar glass which had been used for multilayer samples previously. It appeared from SEM photos that there was less porosity in the DXO samples than in FEP or FEL samples. A batch was prepared using no carbonates (899 FHJ) having the same nominal composition as FEL to test the possibility that carbon or carbon-dioxide could be remaining in the glass after melting and resolidifying the starting materials. This glass was also used for an extensive processing matrix in Raleigh.

Among the parameters varied, which are listed in table 4, many were part of the press-ceram cycle which had not been extensively investigated previously. The incentive for this

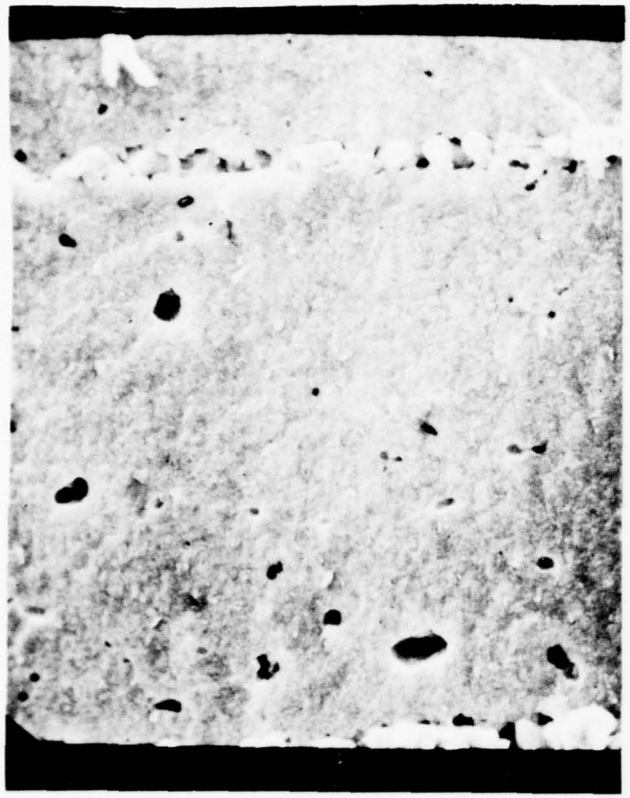

1100°C 1200X

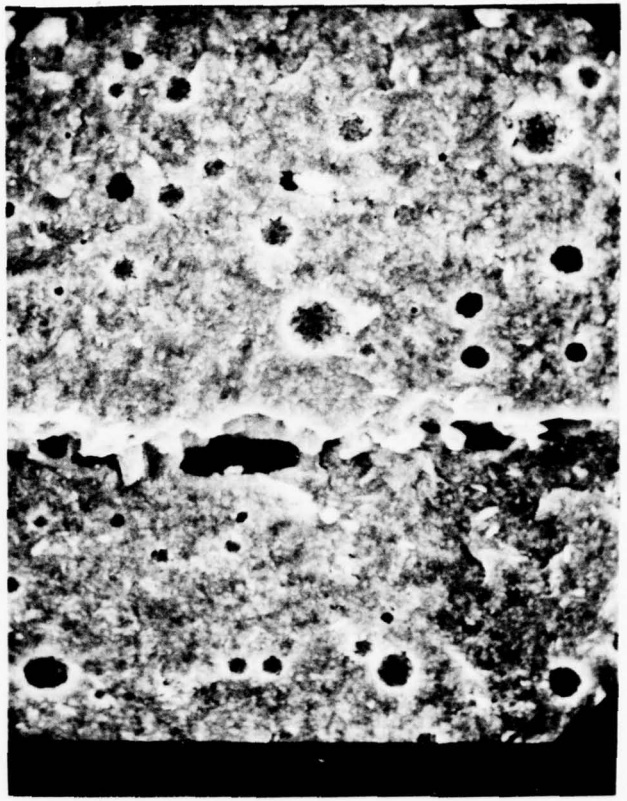

1130°C 800X

Figure 21. Electron micrographs of the edge of a 899 FEP multilayer glass-ceramic sample cerammed at 1100 and 1130°C.

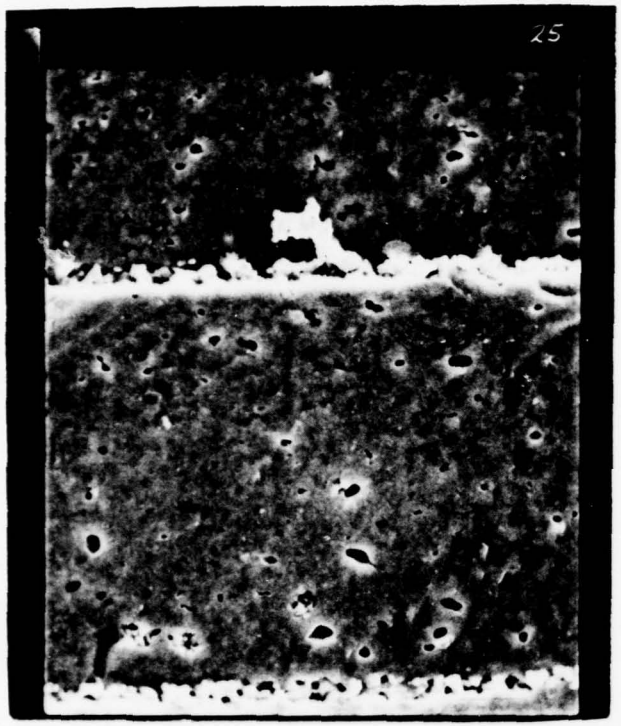

1100°C 671X

1100°C 2013X

Figure 22. Electron micrographs of the edge of a 899 FEL multilayer glass-ceramic sample cerammed at 1100°C.

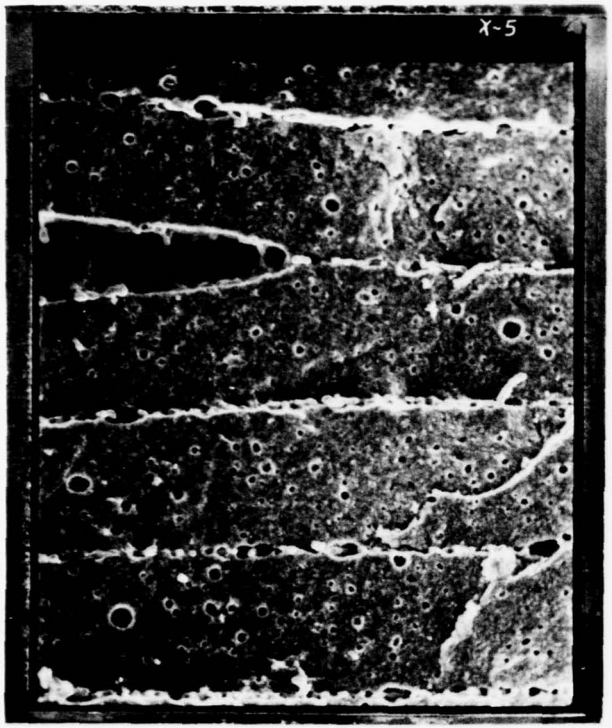

1180°C 228X

1180°C 2282X

Figure 23. Electron micrographs of the edge of a 899 FEL multilayer glass-ceramic sample cerammed at 1180°C.

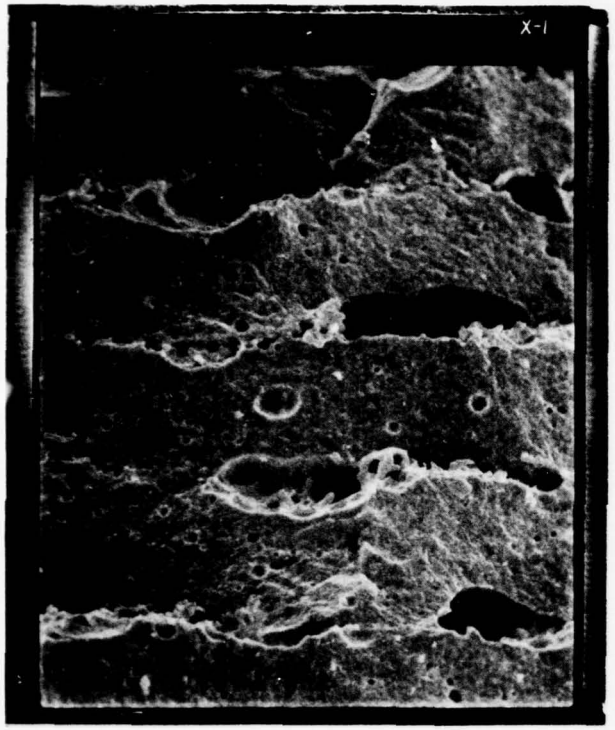

1200°C 204X

1200°C 2039X

Figure 24. Electron micrographs of the edge of a 899 FEL multilayer glass-ceramic sample cerammed at 1200°C.

research was the observation that DXO produced lower porosity samples than did FHJ. Aside from a slight difference in composition, the major difference in the processing of this glass involved the application of pressure and soak times in the press-ceram cycle. Samples of FHJ produced using the so-called "DXO Cycle" did in fact produce lower porosity samples than those produced using the so-called "ECR Cycle" described previously. However, these samples exhibited no capacitance; the electrodes were apparently discontinuous. A search to reproduce the low porosity effect without loss of capacitance was performed by exhaustively varying all differences between the two cycles. The result was that all variations produced higher porosity chips with capacitance.

Also involved in the processing matrix was a change in binder system. FEP glass was used and a slurry was developed using a toluene base. The resulting samples showed increased porosity compared to the normal aqueous batch.

In a third approach, 152 μm sheets of glass 1.27 cm square were fabricated from solid glass at Sullivan Park by John Sage. Platinum electrodes were sputtered onto both sides of the squares in the typical pullback configuration. In Raleigh, each square was sandwiched between two layers of cover glass and 3 samples were press-ceramed at approximately normal pressure using the standard press-ceram furnace. The resulting samples, which were electrically satisfactory after press-ceram, lost capacitance during the final firing. Apparently the thickness of the platinum was not sufficient to maintain continuity at elevated temperatures. By the time this experiment had been completed, the irreversible heating effect was discovered by Dr. Lawless in Boulder. It was therefore not repeated using thicker electrodes.

Other variations in the process were suggested by work done in Sullivan Park by R. J. Colegrove using the Automatic Viscosity Control (AVC) furnace. The rate of increase in temperature in this device is controlled by a feedback loop to the viscosity of a piece of sample glass in the furnace. A minimum limit of viscosity can be maintained using this system. It was discovered that significant crystallization occurred at 960°C, above the final press-ceram temperature. Therefore, a new press-ceram cycle was devised having 960°C as its upper limit. No improvement was observed in Raleigh samples using this cycle. Several samples fired under viscosity control appeared less porous than average and were measured, however.

Chips without electrodes were made from FHJ and showed the same porosity as FEL. This eliminated the possibility that the carbonates were causing the problems. Despite the fact that blisters formed on the surface of samples during firing were shown to be carbon dioxide by Dr. Hans Holland at Sullivan Park using mass spectragraphic analysis, no evidence of carbon could be found in the unfired chips.

It is evident from the above that a considerable amount of effort was devoted to solving the fabrication problems associated with making these larger samples, an effort which involved manpower and resources at Corning Glass works in excess of what the contract called for.

In the final analysis, undeniable progress was made in learning how to make these samples, which involved temperature ranges, composition fields, and plate sizes previously not attempted.

3.5. Alternate Materials Investigated

3.5.1. Glass-ceramics

Aside from the variations in the strontium titanate aluminosilicate and boroaluminosilicate systems discussed above, one completely new glass ceramic system was investigated: the potassium tantalate-aluminate system. Work on this system was suggested by results obtained using a potassium tantalate single crystal and it was hoped that by formulating a glass ceramic, multilayer samples could be fabricated.

The initial work on this system was performed at Sullivan Park by John Sage. Using the same basic processes as were used for the original research samples, compositions in the systems $KTaO_3$-Al_2O_3, $KTaO_3$-Al_2O_3-$6SiO_2$, and $KTaO_3$-ZrO_2-SiO_2 were melted in Corning and the low-temperature properties measured in Boulder. The most promising appeared to be the $KTaO_3$-Al_2O_3 system; therefore, a 10 pound batch of ribbon glass was made by John Sage, with the assistance of Dr. A. A. Erickson, and shipped to Raleigh for processing into multilayer samples.

In Raleigh, an attempt was made to process the new glass (899 FIL) in the same manner as previous glasses. However, it was found that no sealing was taking place in the press-ceram operation. Higher and lower sealing temperatures were tried, but the result in every case was a plate which showed no glassy properties and which cracked very badly when pressure was removed.

A possible explanation of this phenomenon based upon experience with similar glasses was proposed by Dr. R. D. McBrayer, Raleigh. He suggested that a reaction may be occurring in the aqueous batching operation producing a cement-like ceramic from the glass. In order to test this theory a non-aqueous toluene-based batch was prepared (the same as was used with 899 FEP to test the effect on porosity). The results after press-ceram were essentially the same. No explanation for this effect has as yet been advanced and no multilayer samples could be produced for testing.

3.5.2. Ceramics

After the irreversible heating effect was observed in glass-ceramic samples, it was decided to eliminate the glass matrix and make pure ceramic samples. At first, only the strontium titanate and potassium tantalate systems were attempted. Later, however, solid solutions of other oxides in the above systems and new compositions in the lead-pyroniobate family were made.

The following general procedure was used in the preparation of all ceramic compositions:

(1) The composition was calculated in weight percent from the chemical formula.

(2) Using an "00" size porcelain ball mill with porcelain media, the reagent grade powders were ground for 6 hours at a speed of 73 rpm. Loading was 350 g powder to 350 ml of liquid media (methanol, water, or acetone).

(3) The mixture was dried and ground with a mortar and pestle, then put into ZrO_2 saggers and calcined.

(4) The calcined material was reground in the mortar and pestle.

At this stage, a decision was made whether to use a cast film approach to make samples or to press pellets. This depended on the compatibility of the ceramic chemically to the

aqueous batch and the volatility of the ceramic expected during firing (e.g., $KTaO_3$ had to be covered in its own powder to minimize K_2O loss and therefore was unsuitable for multilayer samples).

The process used for multilayer samples without electrodes (often called K-Squares) was as follows:

(1) The powder above was ground in a "00" size ball mill with an aqueous binder for 6 hours.

(2) Film was cast from the resulting slurry to produce fired film of approximately 33 μm thickness.

(3) Twenty 11.4 cm square pieces of film were laminated using pressure and heat into a solid plate.

(4) The plate was cut into 25 samples 1.9 cm square using a razor blade.

(5) Samples were placed on a ZrO_2 pallet and prefired at 450°C to remove the binder then fired in a box furnace. For the strontium titanates, Pt foil was used to prevent reaction between the ceramic and the pallet.

(6) Electrodes were applied using DuPont 8225 silver to the top and bottom surfaces of the K-Square. A small margin was left around the edges to decrease the possibility of voltage breakdown. The silver was fired at 700-800°C in a continuous furnace.

(7) Room temperature capacitance and dissipation factor were measured and dielectric constant calculated.

The process used for pressed pellet samples was as follows:

(1) A 5% by weight addition of Carbowax, dissolved in acetone, was made to the powder.

(2) Pellets, .95 cm in diameter, were pressed from 3 g of material.

(3) The pellets were fired in a box furnace on ZrO_2 pallets. A special atmosphere was produced when necessary by burying the pellet in its own powder (e.g., $KTaO_3$).

(4) The fired pellets were sliced using a diamond saw into rectangular samples approximately 254 μm thick by cutting in a direction parallel to their axis.

(5) The samples were silvered, silver fired, and measured as described above.

X-ray diffraction analysis was performed at Sullivan Park by Dr. Hans Holland on all successfully fired samples, and determined that the desired phase had been produced in all cases.

The ceramics produced fall into three general types: strontium titanate and solid solutions, potassium tantalate and solid solutions, and lead pyroniobate and related compounds. The specific processing information for each of these compositions is compiled in table 5.

The $SrTiO_3$ compositions were all fabricated into K-Squares. This appeared to be a reasonable course since no volatile components were included (with the possible exception of V_2O_5) and considerable experience was available on the batching of this material. It was discovered early that the samples curled during firing due to reaction with ZrO_2 and therefore Pt foil was used (as with the glass-ceramic samples).

The $KTaO_3$ compositions were more difficult. A calcination temperature which would react the K_2CO_3 and Ta_2O_3 without causing K_2O loss had to be determined. It was also clear

TABLE 5.

CERAMIC EXPERIMENTATION SUMMARY

GROUP A - Strontium Titanate & Solid Solutions

LOT NUMBER	INTENDED COMPOSITION	COMPONENTS Wt. %	GRINDING MEDIUM	CALCINE TEMPERATURE	TEST CONFIGURATION	FIRING TEMPERATURES	FIRING CONDITION	COMMENTS
ST-1	$SrTiO_3$	TAM 505 Commercial Grade	Pre-Ground	Pre-Calcined	K-Squares	1350°C (2 Hr)	ZrO_2 Pallet Pt Foil On ZrO_2 Pallet	Reacted with ZrO_2 pallet.
ST-2	$SrTiO_3$	TAM 854 C.P. Grade	Pre-Ground	Pre-Calcined	K-Squares	1350°C (2 Hr) 1400°C (2 Hr) 1450°C (2 Hr)	Pt Foil On ZrO_2 Pallet	Only 1450°C firing was densely sintered.
ST-3	$SrTiO_3$	$SrCO_3$-64.9 TiO_2-35.1	H_2O	1200°C 12 Hrs	K-Squares	1450°C (2 Hr)	Pt Foil On ZrO_2 Pallet	Curled during firing.
STN(10)-1	$0.9SrTiO_3$ - $0.1Sr_{\frac{1}{2}}NbO_3$	$SrCO_3$-62.2 TiO_2-31.9 Nb_2O_5-5.9	H_2O	1200°C 12 Hrs	K-Squares	1450°C (2 Hr)	Pt Foil On ZrO_2 Pallet	
STN(20)-1	$0.8SrTiO_3$ - $0.2Sr_{\frac{1}{2}}NbO_3$	$SrCO_3$-59.5 TiO_2-28.6 Nb_2O_5-11.9	H_2O	1200°C 12 Hrs	K-Squares	1450°C (2 Hr)	Pt Foil On ZrO_2 Pallet	
STN(30)-1	$0.7SrTiO_3$ - $0.3Sr_{\frac{1}{2}}NbO_3$	$SrCO_3$-56.7 TiO_2-25.3 Nb_2O_5-18.0	H_2O	1200°C 12 Hrs	K-Squares	1450°C (2 Hr)	Pt Foil On ZrO_2 Pallet	Analyzed as solid solution.

TABLE 5.

CERAMIC EXPERIMENTATION SUMMARY

GROUP A - Strontium Titanate & Solid Solutions

LOT NUMBER	INTENDED COMPOSITION	COMPONENTS Wt. %	GRINDING MEDIUM	CALCINE TEMPERATURE	TEST CONFIGURATION	FIRING TEMPERATURES	FIRING CONDITION	COMMENTS
STN(2)-1	$0.98SrTiO_3$- $0.02Sr_{\frac{1}{2}}NbO_3$	$SrCO_3$-64.4 TiO_2-34.5 Nb_2O_5-1.2	Methanol	1200°C 12 Hrs Repeated Twice	K-Squares	1450°C (2 Hr) 1500°C (4 Hr)	Pt Foil On ZrO_2 Pallet	Both firings too low.
STV(10)-1	$0.9SrTiO_3$- $0.1Sr_{\frac{1}{2}}VO_3$	$SrCO_3$-63.4 TiO_2-32.5 V_2O_5-4.1	Acetone	1200°C 12 Hrs.	---	---	---	Over calcined.
STV(10)-2	$0.9SrTiO_3$- $0.1Sr_{\frac{1}{2}}VO_3$	$SrCO_3$-63.4 TiO_2-32.5 V_2O_5-4.1	Methanol	1000°C 6 Hrs	K-Squares	1350°C (1 Hr)	Pt Foil On ZrO_3 Pallet	
STV(20)-1	$0.8SrTiO_3$- $0.2Sr_{\frac{1}{2}}VO_3$	$SrCO_3$-61.8 TiO_2-29.7 V_2O_5-8.5	Acetone	1200°C 12 Hrs.	---	---	---	Over calcined.
STV(20)-2	$0.8SrTiO_3$- $0.2Sr_{\frac{1}{2}}VO_3$	$SrCO_3$-61.8 TiO_2-29.7 V_2O_5-8.5	Methanol	1000°C 6 Hrs	K-Squares	1350°C (1 Hr)	Pt Foil On ZrO_2 Pallet	
STV(2)-1	$0.98SrTiO_3$- $0.02Sr_{\frac{1}{2}}VO_3$	$SrCO_3$-64.6 TiO_2-34.6 V_2O_5-0.8	Methanol	1100°C 6 Hrs	K-Squares	1350°C (2 Hr) 1450°C (2 Hr)	Pt Foil On ZrO_2 Pallet	1350°C firing optimum.

TABLE 5.

CERAMIC EXPERIMENTATION SUMMARY

GROUP A - Strontium Titanate & Solid Solutions

LOT NUMBER	INTENDED COMPOSITION	COMPONENTS Wt. %	GRINDING MEDIUM	CALCINE TEMPERATURE	TEST CONFIGURATION	FIRING TEMPERATURES	FIRING CONDITION	COMMENTS
STS(5)-1	$0.95SrTiO_3$- $0.05Sr_{\frac{1}{2}}SbO_3$	$SrCO_3$-63.4 TiO_2-33.4 Sb_2O_3-3.2	Methanol	1100°C 6 Hrs	K-Squares	1350°C (2 Hrs) 1450°C (2 Hrs)	Pt Foil On ZrO_2 Pallets	1450°C firing optimum.
BT-1	$BaTiO_3$	Transelco Reagent Grade 219-2	Pre-Ground	Pre-Calcined	K-Squares	1300°C (1 Hr)	ZrO_2 Pallet	

TABLE 5.

CERAMIC EXPERIMENTATION SUMMARY

GROUP B - Potassium Tantalate & Solid Solutions

LOT NUMBER	INTENDED COMPOSITION	COMPONENTS Wt. %	GRINDING MEDIUM	CALCINE TEMPERATURE	TEST CONFIGURATION	FIRING TEMPERATURES	FIRING CONDITION	COMMENTS
KT-1	$KTaO_3$	K_2CO_3-23.8 Ta_2O_5-76.2	Methanol	980°C 1 Hr.	Pellets	1200°C (2 Hr) 1250°C (2 Hr) 1300°C (2 Hr)	On ZrO_2 Buried in Powder-Wrapped In Foil	Best results obtained by firing in powder @ 250°C/hr rate to 1250°C.
KT-2	$KTaO_3$	K_2CO_3-23.8 Ta_2O_5-76.2	Methanol	1000°C 6 Hrs	Pellets	1250°C (2 Hr) 1300°C (2 Hr)	On ZrO_2 Buried in Powder-Wrapped in Foil	Did not fire as well as KT-1.
KTV(10)-1	$0.9KTaO_3$ - $0.1KVO_3$	K_2CO_3-24.9 Ta_2O_5-71.8 V_2O_5-3.3	Methanol	980°C 1 Hr.	Pellets	1200°C (2 Hr) 1250°C (2 Hr) 1300°C (2 Hr)	Buried In Powder	250°C/Hr rate.
KTV(20)-1	$0.8KTaO_3$- $0.2KVO_3$	K_2CO_3-26.2 Ta_2O_5-66.9 V_2O_5-6.9	Methanol	980°C 1 Hr.	Pellets	1200°C (2 Hr) 1250°C (2 Hr) 1300°C (2 Hr)	Buried In Powder	250°C/Hr rate.
KTS(5)-1	$0.95KTaO_3$- $0.05KSbO_3$	K_2CO_3-27.6 Ta_2O_5-70.0 Sb_2O_3-2.4	Methanol	980°C 1 Hr.	Pellets	1200°C (1 Hr) 1300°C (1 Hr) 1350°C (1 Hr)	Buried In Powder	1200°C-Underfired 1300°C - Porous 1350°C - Melted
KTN(10)-1	$0.9KTaO_3$- $0.1KNbO_3$	K_2CO_3-28.0 Ta_2O_5-67.5 Nb_2O_5-4.5	Methanol	980°C 1 Hr.	Pellets	1200°C (1 Hr) 1300°C (1 Hr) 1350°C (1 Hr)	Buried In Powder	1200°C-Underfired 1300°C - Porous 1350°C - Melted

TABLE 5.

CERAMIC EXPERIMENTATION SUMMARY

GROUP C - Lead Pyroniobate & Related Compounds

LOT NUMBER	INTENDED COMPOSITION	COMPONENTS Wt. %	GRINDING MEDIUM	CALCINE TEMPERATURE	TEST CONFIGURATION	FIRING TEMPERATURES	FIRING CONDITION	COMMENTS
PN-1	$Pb_2Nb_2O_7$	$PbSO_4$-69.5 Nb_2O_5-30.5	H_2O	1100°C 2 Hrs.	K-Squares & Pellets	1150°C 1 Hr.	ZrO_2 Pallet Stacked K-Squares	No significant loss of Pb.
PCN-1	$Pb_2Cd_{2/3}Nb_{4/3}O_6$	$PbSO_4$-69.8 CdO-9.8 Nb_2O_5-20.4	Methanol	1100°C 2 Hrs.	---	---	---	Over calcined.
PCN-2	$Pb_2Cd_{2/3}Nb_{4/3}O_6$	$PbSO_4$-69.8 CdO-9.8 Nb_2O_5-20.4	Methanol	1000°C 1 Hr.	Pellets	1150°C (1 Hr) 1200°C (1 Hr)	ZrO_2 Pallet	Very porous, pallet staining.
PZN-1	$Pb_2Zn_{2/3}Nb_{4/3}O_6$	$PbSO_4$-72.4 ZnO-6.5 Nb_2O_5	Methanol	980°C 1 Hr.	Pellets	1050°C (1 Hr) 1150°C (1 Hr)	ZrO_2 Pallets	Very porous, pallet staining.
PCMN-1	$Pb_2Cd_{\frac{1}{2}}Mn_{\frac{1}{2}}NbO_6$	$PbSO_4$-72.0 CdO-7.6 Mn_2O_3-4.7 Nb_2O_5-15.7	Methanol	1100°C 2 Hrs.	---	---	---	Over calcined.
PCMN-2	$Pb_2Cd_{\frac{1}{2}}Mn_{\frac{1}{2}}NbO_6$	$PbSO_4$-72.0 CdO-7.6 Mn_2O_3-4.7 Nb_2O_5-15.7	Methanol	980°C 1 Hr.	Pellets	1050°C (1 Hr) 1150°C (1 Hr)	ZrO_2 Pallets	Very porous, pallet staining.

TABLE 5.

CERAMIC EXPERIMENTATION SUMMARY

GROUP C - Lead Pyroniobate & Related Compounds

LOT NUMBER	INTENDED COMPOSITION	COMPONENTS Wt. %	GRINDING MEDIUM	CALCINE TEMPERATURE	TEST CONFIGURATION	FIRING TEMPERATURES	FIRING CONDITION	COMMENTS
PGN-1	Pb_2GaNbO_6	$PbSO_4$-72.8 Ga_2O_3-11.2 Nb_2O_5-15.9	Methanol	980°C 1 Hr.	Pellets	1050°C (1 Hr) 1150°C (1 Hr)	ZrO_2 Pallets	Very porous, pallet staining.
CCN-1	Cd_2CrNbO_6	CdO-55.1 Cr_2O_3-16.3 Nb_2O_5-28.5	Methanol	1100°C 2 Hrs.	K-Squares	1300°C (1 Hr) 1250°C (1 Hr)	ZrO_2 Pallets	Pallet staining.
PCTT-1	$Pb_2Cd_{\frac{1}{2}}Ti_{\frac{1}{2}}TaO_6$	$PbSO_4$-65.1 CdO-6.9 TiO_2-4.3 Ta_2O_5-23.7	Methanol	1100°C 2 Hrs.	---	---	---	Over calcined.
PCTT-2	$Pb_2Cd_{\frac{1}{2}}Ti_{\frac{1}{2}}TaO_6$	$PbSO_4$-65.1 CdO-6.9 TiO_2-4.3 Ta_2O_5-23.7	Methanol	1000°C 1 Hr.	Pellets	1150°C (1 Hr) 1200°C (1 Hr)	ZrO_2 Pallets	Very porous, pallet staining.

PRECEDING PAGE BLANK-NOT FILMED

that K-Squares were unsuitable due to the "soft" calcine and necessity of firing the samples in an atmosphere. Considerable experimentation in firing procedure eventually produced dense $KTaO_3$ ceramic samples.

The $PbO-Nb_2O_5$ system also had the disadvantage of a volatile component, PbO. However, this was not as severe a problem as with $KTaO_3$. Two niobates: $Pb_2Nb_2O_7$ and Cd_2CrNbO_6 were produced in K-Squares although significant loss of PbO in the former and probably Cr_2O_3 and CdO in the latter caused considerable staining of the ZrO_2 pallets upon which they were fired. The remainder of the niobates were made using pressed pellets, often producing somewhat porous samples (perhaps due to low temperature calcination). Some compositions would not fire to a dense ceramic at the conditions tried and had to be abandoned. $PbSO_4$ was used in all Pb compositions due to its high temperature of decomposition. It was thought that this would allow better reaction during calcine with the very refractory Nb_2O_5.

3.6. Experimental Methods

3.6.1 Dielectric properties

Dielectric constant and derivative: The quantity $(\partial K'/\partial T)_{E=0}$ was the main property of the multilayer samples to be tested. Such measurements had to be made on hundreds of these samples to test the effects of various manufacturing procedures. A cryostat insert was made whereby a fifteen sample teflon holder was mounted on the end of the stainless steel tube. The holder was immersed in a bath of liquid helium which could be pumped down to about 1.5 K. A germanium thermometer was used to measure the temperature of the helium bath, which was controlled with a manostat. Each of the fifteen samples were connected in turn to a commercial capacitance bridge operating at 1 kHz. The capacitance of each sample was measured at 4.2 K and at a few lower temperatures. The data were computer analyzed to find K' and $\partial K'/\partial T$ for each sample.

For measurements of the dielectric constant at temperatures above 4 K, the specific heat apparatus was used. In that apparatus (described in section 3.6.2) only two samples could be run at the same time.

Breakdown strength at 4 K: The breakdown strengths of the glass ceramic capacitors were measured at 4 K in liquid helium. The dewars used were unsilvered so any external breakdown could be observed. The breakdown voltage was applied to the capacitor and monitored using the simple circuit shown in figure 25. The leakage current appears on the ammeters placed in the ground return leads. Currents of about 1 μA could be detected. A 1.5 megohm current limiting resistor was placed in the high voltage lead.

DC polarization: As shown in section 3.1.1. on thermodynamics, the polarization P(T,E) is used to determine the refrigeration power. When a remanent polarization is present, P(T,E) can no longer be determined from the dielectric constant but must be measured directly with a dc technique.

The circuit in figure 26 was built to measure P(T) directly. A similar technique has recently been used by Gesi.[71] This circuit can be used to measure both $P(T)]_E$ and $P(E)]_T$. A voltage, V, is applied across a series combination of the unknown capacitor C_1 and a known and much larger capacitor, C_s. Both capacitors must have very low leakage, $RC > 10^5$ sec

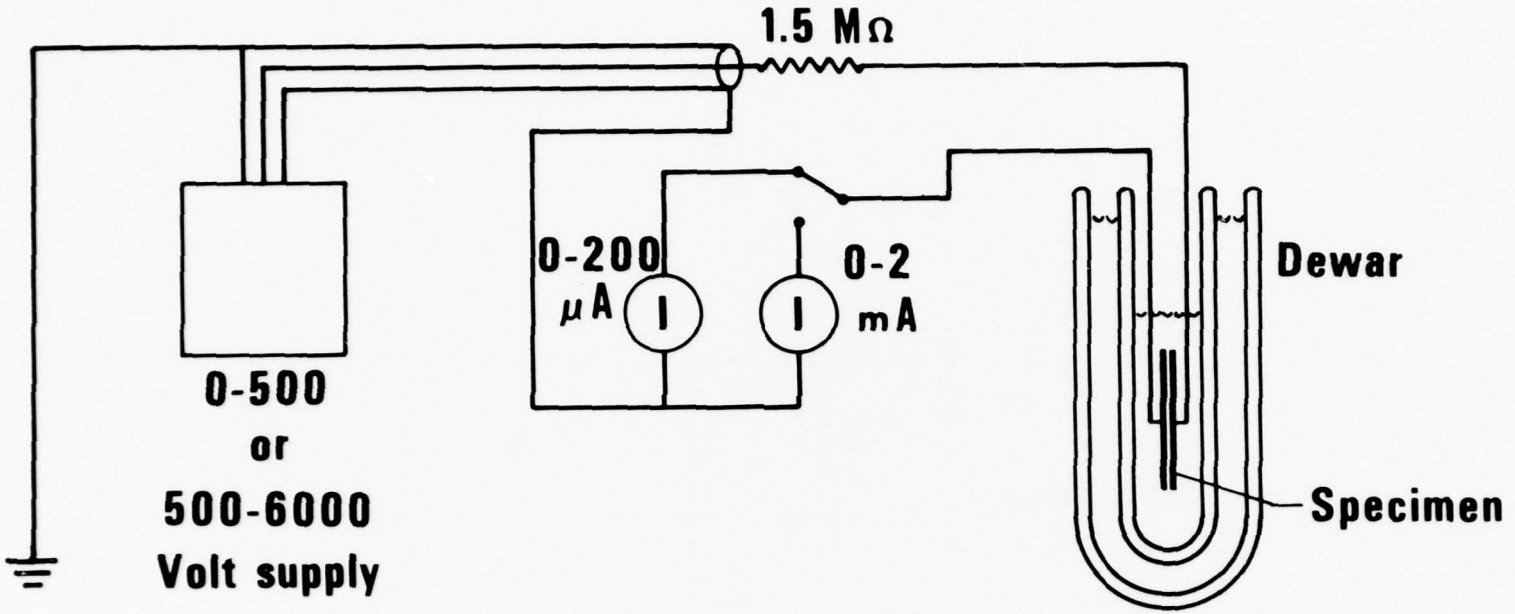

Figure 25. Schematic diagram of current limiting circuit for measurement of field breakdown strength at 4 K.

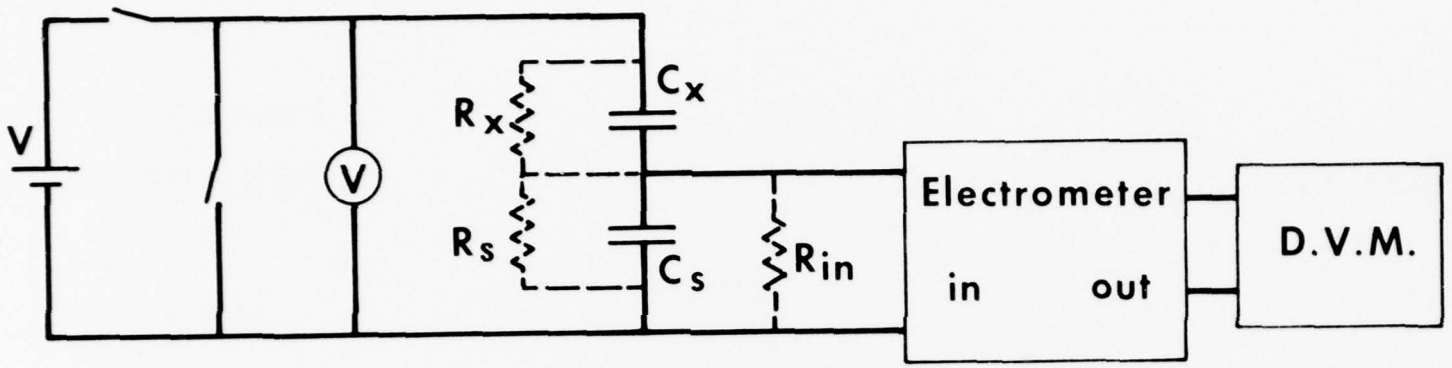

Figure 26. Schematic diagram of the circuit used for the DC polarization measurements.

for this system to work. When the ratio of $C_1/C_s \ll 1$ the voltage across C_1, i.e., V_1, is very nearly the applied voltage V. The voltage, V_s on C_s is measured with a vibrating reed electrometer. The input impedance, R_{in}, is so high that $R_{in}C_s \gg 10^5$ sec. The output of the electrometer is measured with a digital voltmeter. The precision of the measurement is about 0.01% for the larger capacitors measured.

For the capacitors connected in series with no leakage,

$$q_1 = q_s = C_s V_s = C_1 V_1.$$

For parallel plate geometry,

$$D = q/s,$$

where D is the electric displacement and s is the plate surface area. Since $P = D - \varepsilon_o E$, then

$$P = q_1/s_1 - \varepsilon_o E \cong C_s V_s/s_1 \text{ for } \varepsilon/\varepsilon_o \gg 1. \qquad (3.7)$$

The quantity P is the total induced polarization and will be called P_t.

If any ferroelectric ordering takes place or an electret is formed when the field is applied, then a charge will remain on V_s when V is removed. Then

$$P_r = [C_s V_s/s_1]_{V=0}$$

where P_r is the remanent polarization. An AC measurement of polarization will presumably measure $P_t - P_r$.

A liquid helium cryostat was used for these measurements. The samples were mounted in a vacuum can on a heat exchanger through which liquid helium could be valved. After a desired temperature was reached, the valve was closed. A carbon resistor sensor coupled to a heater by an electronic feedback circuit kept the temperature constant. The cryostat was the same as used for the multi-leaf switch measurements.

Most of the $P_t(T)$ measurements, where $P_t(T)$ is the total polarization observed when a field is applied, were made by applying the field to the sample around 77 K then cooling it to 4 K and recording P_t at several temperatures between. The temperature was brought to equilibrium at each point. Then the field was removed and P_r, the remanent field, was measured by warming the sample back to about 77 K. Hysteresis loops were measured by recording V_s while switching through E values at a constant T and calculating P_t from eq. (3.7).

The dielectric constant at low frequencies could be measured with the same system by measuring hysteresis loops as a function of T. The high frequency measurements were done by connecting a commercial capacitance bridge to the leads in place of the polarization system.

Most all of the materials on which measurements of P_t and P_r were desired had a sufficiently high R such that the decay time was negligible.

3.6.2. Thermodynamic properties

Measurement theory: From eq. (3.1) the thermodynamic state function can be written as

$$(\partial P/\partial T)_E = -C_E \beta_E / T, \tag{3.8}$$

where $\beta_E = (\partial T/\partial E)_S$, the electrocaloric coefficient. The function $(\partial P/\partial T)_E$ is then determined from measurements of C_E and β_E.

Since the field-dependent quantities C_E and β_E are involved, the experimental arrangement has to be compatible with handling large voltages. For this reason, the sample with voltage hookup leads should not be subjected to motion. Also, the use of helium exchange gas is proscribed for electrical discharge reasons. Consequently, a rigid system was adopted where the sample is secured to the reservoir by a thermal link in a high-vacuum environment. This situation is illustrated in the inset of figure 27.

Consider first the specific heat case. The heat flow is described by the equation

$$\dot{Q} = \mathcal{C}_E (dT/dt) + \mathcal{K}(T - T_o), \tag{3.9}$$

where $\dot{Q}$ is the power dissipated in the sample, $\mathcal{C}_E$ is the heat capacity of the sample (including addenda), $\mathcal{K}$ is the thermal conductance of the thermal link, T_o is the resevoir temperature, and T(t) is the sample temperature. Equation (3.9) is simply a power-balance equation, and it is assumed that steady-state conditions are involved. This is a reasonable assumption at the low temperatures of interest because thermal diffusivities are generally large.

A specific-heat datum by the pulse method consists of two parts, shown in figure 28: A heat energy pulse of duration Δt, followed by a temperature decay through the thermal link back to the reservoir temperature T_o. It is found experimentally that during the (short) heat pulse, the sample temperature rises linearly with temperature,

$$T(t) \cong \theta + (\theta - T_o)t/\Delta t, \tag{3.10}$$

and the corresponding solution to eq. (3.9) is

$$\mathcal{C}_E = \frac{\dot{Q}\Delta t}{(\theta - T_o)(1 + \Delta t/2\tau)} \tag{3.11}$$

where

$$\tau \equiv \mathcal{C}_E/\mathcal{K}. \tag{3.12}$$

The factor $(1 + \Delta t/2\tau)^{-1}$ in eq. (3.11) accounts for the heat energy flowing into the reservoir through the thermal link during the pulse duration Δt.

At the end of the pulse, $\dot{Q} = 0$ and the solution to eq. (3.9) is

$$T - T_o = (\theta - T_o)e^{-t/\tau}. \tag{3.13}$$

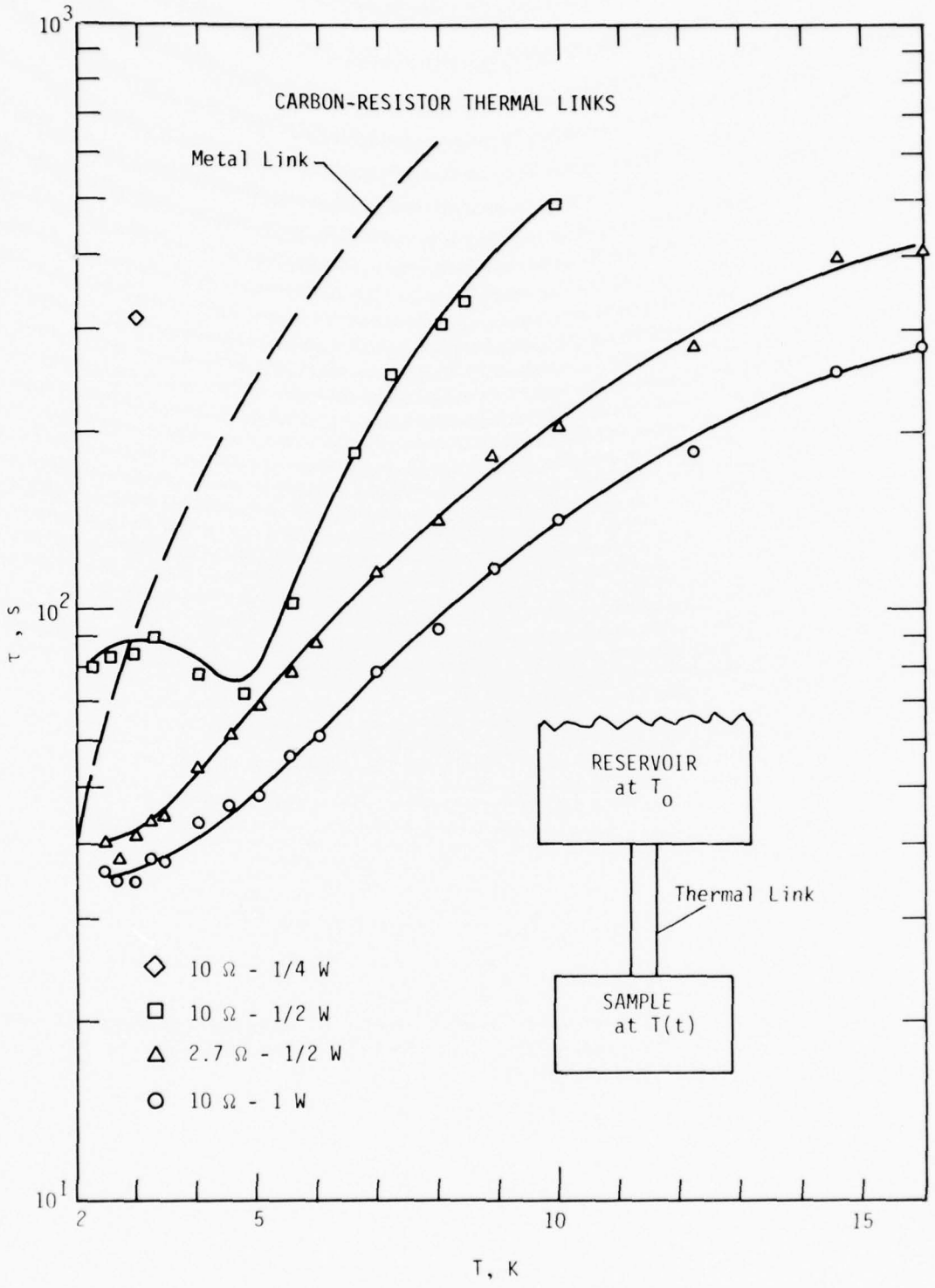

Figure 27. Time constant characteristics for various resistor thermal links between 2 - 20 K. Glass samples varied 3 - 5 gm. A hypothetical metal link is shown, and the inset illustrates the experimental arrangement.

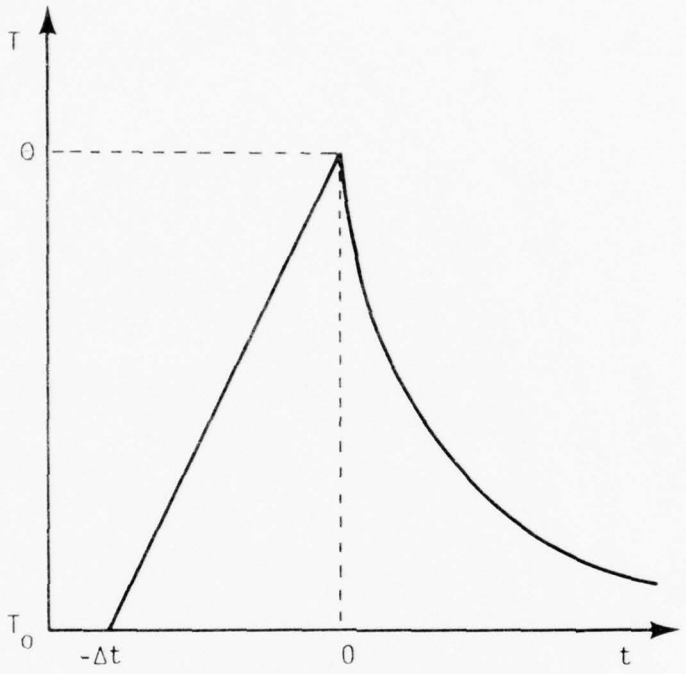

Figure 28. A specific heat datum. Heater power is applied between $t = -\Delta t$ to $t = 0$. The temperature rise decays exponentially to T_o following the heat pulse.

That is, the sample temperature decays exponentially to the reservoir temperature with the time constant τ, eq. (3.12).

Therefore, measuring $\dot{Q}$, Δt, T_o and determining θ and τ from a T - t plot, the heat capacity of $\mathcal{C}_E$ can be determined from eq. (3.11). Finally, the specific heat of interest, $C_E(T)$, is obtained from $\mathcal{C}_E$ by making the addenda correction,

$$C_E(T) = (\mathcal{C}_E(T) - \sum m_j C_j(T))/m, \tag{3.14}$$

where m is the mass of the dielectric sample, and the $m_j C_j(T)$ are mass times specific heat of the addenda.

Considering next the electrocaloric coefficient, β_E, the experimental situation is to make a field change ΔE about E and measure a temperature change, ΔT. A special consideration here is the phonon-polarization relaxation time. That is, following a polarization change the phonon spectrum will come into equilibrium with the polarization exponentially with a characteristic time called the phonon-polarization relaxation time. For the type of dielectric materials of interest, this relaxation time is faster than 10 μs.[2,72] This fact insures that adiabatic conditions are fulfilled in the experiment [i.e., $\beta_E \approx (\partial T/\partial E)_S$].

Therefore, for the time scales involved experimentally the dielectric material exposed to the field instantaneously changes in temperature from $T_o \to T_i$, whereas $(\theta - T_o)$ is the temperature change of the entire sample. The energy balance condition is

$$T_i - T_o = (\theta - T_o)[mC_E(T) + \sum m_j C_j(T)]/mC_E(T), \tag{3.15}$$

and it is important to recognize that m in eqs. (3.14) and (3.15) refers to the mass of the dielectric exposed to the field. Those portions of the dielectric not exposed to the field are included in the addenda.

Following the temperature change due to ΔE, eq. (3.9) with $\dot{Q} = 0$ applies, so the sample temperature decays back to T_o with the time constant τ, as in the specific heat case, eq. (3.13). The electrocaloric coefficient is then given by

$$\beta_E = (T_i - T_o)/\Delta E = \frac{(\theta - T_o)[mC_E(T) + \sum m_j C_j(T)]}{mC_E(T)\Delta E}. \tag{3.16}$$

The eqs. (3.14) and (3.16) describe the means for measuring C_E and β_E, respectively, from which the state function $(\partial P/\partial T)_E$, eq. (3.8), can in principle be determined. Note that the zero-field specific heat has to be known for the dielectric so that the addendum correction can be made for the dielectric material not exposed to the field. Also the field-dependent specific heat $C_E(T)$ has to be known to determine the electrocaloric coefficient, eq. (3.16).

We will now describe a scheme for considerably expediting these measurements. Suppose that a sample has been fixtured and wired for field-dependent measurements, and suppose that the zero-field specific heat has been measured. These measurements will yield $\mathcal{C}_o(T)$ from eq. (3.11) and $\tau(T)$ from fitting the T - t data. Consequently, the thermal link is calibrated,

$$\mathscr{H}(T) = \mathscr{C}_o(T)/\tau(T), \tag{3.17}$$

and it is important in what follows to recognize that $\mathscr{H}(T)$ is field-independent.

Without altering the sample fixturing, the field-dependent properties are measured. Specifically, a field change ΔE about E leads to temperature change $(\theta - T_o)$ followed by an $\exp(-t/\tau)$ decay. If the resulting T-t data are analyzed for τ, then

$$\mathscr{C}_E(T) = \tau\mathscr{H}(T) \tag{3.18}$$

where $\mathscr{H}(T)$ comes from the calibration, eq. (3.17). Substituting in eq. (3.14),

$$C_E(T) = [\tau\mathscr{H}(T) - \textstyle\sum m_j C_j(T)]/m, \tag{3.19}$$

and in eq. (3.16),

$$\beta_E(T) = \frac{(\theta - T_o)\tau(T)}{\Delta E[\tau\mathscr{H}(T) - \sum m_j C_j(T)]} . \tag{3.20}$$

Finally, combining eqs. (3.8), (3.19), and (3.20),

$$(\partial P/\partial T)_E = -(\theta - T_o)\tau\mathscr{H}(T)/mT . \tag{3.21}$$

The measurement scheme then is to measure first the zero-field specific heat, thus calibrating the link, eq. (3.17). Then, from a single ΔE-ΔT event, the field-dependent specific heat, eq. (3.17), the electrocaloric coefficient, eq. (3.20), and the state function, eq. (3.21), can all be determined at those T- and E- values.

The result eq. (3.21) is particularly attractive because it means that the state function, which is of primary interest, can be measured directly rather than by synthesizing β_E and C_E data. The cancellation of the addenda corrections in arriving at eq. (3.21) is fortunate experimentally, because these corrections, though small, are difficult to determine to high accuracy.

The application of the method for measuring zero-field specific heat will be emphasized, because measurements of the field-dependent properties are a straightforward extension of the zero-field methods.

Cryostat insert: The calorimeter is a two-can system where the inner can is a temperature-controlled isothermal shield, and the vacuum spaces of the two cans are connected. Hookup leads (0.015-cm manganin) run from an interchange can at room temperature down the pumping line and are heat sunk to a copper collar bolted onto the flange of the outer can. The highvoltage leads are encased in Teflon sleeving and are heat sunk to a sapphire rod mounted in the collar with varnish.

The lid of the inner can is suspended from the flange with copper straps, chosen to give 77→4 K cooldown times of about 12 hr. A second heat-sinking station and interchange is mounted on the underside of this lid and a sapphire rod is provided for heat-sinking the voltage leads. In this fashion, all leads to the samples are tempered to the reservoir

temperature, T_o. The inner can bolts onto this lid (both copper), and a heater wire is spiralled on the outside of this can. A temperature controller powers this heater using the signal from a silicon diode thermometer mounted on the lid. Finally, the sample and thermal link are mounted on a copper fixture which bolts onto the bottom of the heat-sinking station and interchange.

Thermal links: The time constant $\tau = \mathcal{K}/\mathcal{C}$ in eq. (3.12) depends on the thermal conductance of the link, $\mathcal{K}$, and the heat capacity of the sample, $\mathcal{C}$. It is not practical to have τ smaller than about 30 seconds nor larger than about 600 seconds. Also, as will be seen below, a portion of the thermal link is an addendum, so its mass should be kept small.

Now, $\mathcal{C} \propto T^3$ and for a metal link, $\mathcal{K} \propto T$. so that a metal link would have $\tau \propto T^2$ (approximately) in the temperature range of interest. This would lead to an unacceptably small (large) τ at 2 K (20 K) associated with an acceptable τ at 20 K (2 K). Different metal links could of course be used spanning overlapping temperature ranges.

It has been reported[73] that radio resistors have $\mathcal{K} \propto T^2$ (approximately) at low temperatures. Some available Allen-Bradley resistors were studied for possible thermal links: 10 Ω, 1W; 10 Ω, 1/2W; 10 Ω, 1/4W; and 2.7 Ω, 1.2W. The phenolic resin was machined off these resistors, the leads trimmed to 2 mm, and they were attached to glass or glass-ceramic samples in the manner described below. The sample weights chosen were 3-4 gm. The τ-data were measured as a function of temperature by heat-pulsing the samples through attached heaters and measuring the exponential time decay on a chart recorder. The results of these measurements are shown in figure 27. Also shown in figure 27 is a hypothetical metal link for which τ = 40 seconds and 2 K. These data reveal that τ is approximately proportional to T, as expected, and that the 10 Ω, 1W and 2.7 Ω, 1/2W resistors have favorable ranges of τ-values. The 2.7 Ω, 1/2W resistor was selected because of its smaller mass.

In the above section, the technique for determining C_E, β_E, and $(\partial P/\partial T)_E$ from a single ΔE-ΔT datum hinges on determining $\mathcal{K}(T)$ for the thermal link accurately from the zero-field specific heat measurements, eq. (3.17). The $\mathcal{K}(T)$ data so determined from two different specific heat runs are shown in figure 29.

Thermometry: The small 220 Ω, 1/8W Allen-Bradley resistors were chosen for sample thermometers because of their 2-20 K sensitivity. These were calibrated against a germanium resistance thermometer mounted on the reservoir. From 2 to 20 K, the R-T could be fitted to[16]

$$\log R = A + BT^{-P}, \qquad (3.22)$$

where typically the residual standard deviation was about 10 mK. Typical parameter values are A ≈ 2.37, B ≈ 3.47, P ≈ 0.78.

The thermometry procedure adopted was as follows: At the equilibrium temperature before a heat pulse or field change, $T = T_o$, and the resistor thermometer on the sample and a standard thermometer on the reservoir were measured. These data collected during the run were curve-fitted according to eq. (3.22), but only the B and P coefficients were retained. Then, at each equilibration point, the coefficient A was repeatedly determined from the reservoir temperature T_o and the B and P coefficients. This procedure makes use of eq.

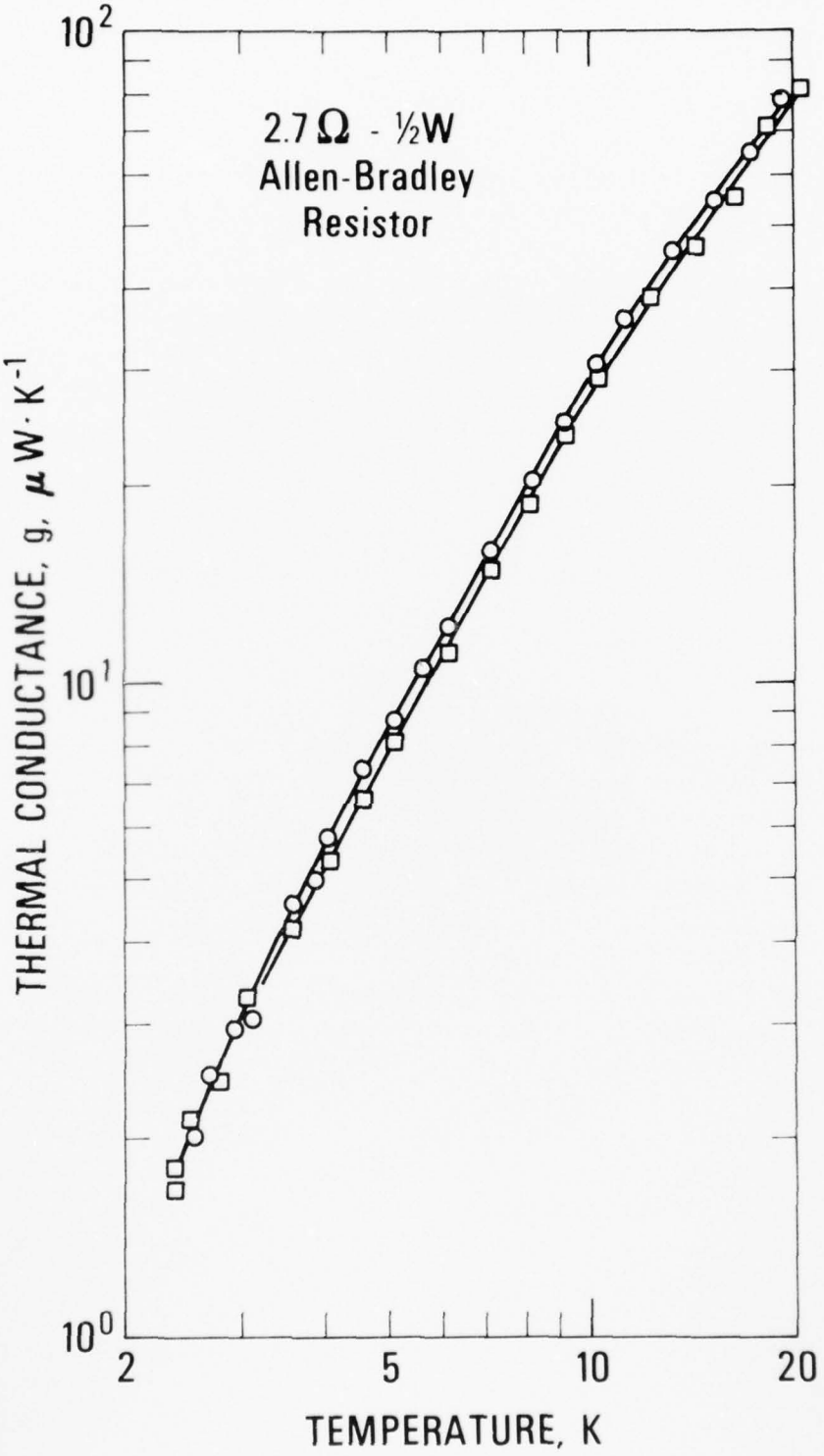

Figure 29. Variation of the thermal conductance, $\mathcal{L}$, with temperature for 2.7Ω, 1/2W resistor thermal links.

PRECEDING PAGE BLANK-NOT FILMED

(3.22) in such a way that the temperature changes ΔT reflect the accuracy of the overall fit while insuring that at equilibrium the sample thermometer matches exactly the standard thermometer.

Sample fixturing: A schematic of the fixtured sample is shown in figure 30 (voltage leads are not shown). The sample consists of two plates (labelled J) varnished together with a heater wire (G,H) sandwiched between. A thin layer of fritted silver (DuPont 8225) is fired (680°) on a portion of one edge of each plate (C). The manganin heater wire is next mounted on the face of one of the samples with varnish, and this step requires considerable care because of the relatively large specific heat of the varnish ($\sim$ 30 times larger than that of copper) and its dependence on curing conditions.

The fired-on silver section (C) is indium-soldered to the thermal link (B) and the solder joint (D) is trimmed with a knife. The machined-down resistor thermometer (F) is varnished to the sample, and short portions (about 1 cm) of the hookup leads (E) are tempered to the sample with varnish. Finally, the other end of the thermal link is indium-soldered to the reservoir (A).

The addenda weights are determined by cumulative weighings. The weight of the manganin heater wire is determined by measuring the room-temperature resistance and using the calibration, 5.7×10^{-5} g/Ω. Typically the heat capacity of the addenda amounted to about 4% of that of the sample above 10 K and about 20% at 2 K.

The components attached to both the sample and reservoir involve two types of corrections: A temperature gradient is established across, say, the thermal link, and it is easy to show that one-half the mass of the link is "on" the sample as an addendum. The second consideration involves the power flow in the manganin hookup leads (I). Note that if these leads were copper, they would constitute the thermal link. Neighbor[74] has shown that to a very good approximation, one-half the power generated in these leads flows to the sample. This means that one-half the resistance of these hookup leads has to be added to the heater resistance to obtain the total effective heater resistance at room-temperature.

Instrumentation: For the specific heat case, the heat dissipated in the sample is

$$Q = i^2 R_H(T) \Delta t \qquad (3.23)$$

where i is the d.c. current, $R_H(T)$ is the heater current, and Δt is the pulse duration. The current supply was a 9-volt battery bank and the current was measured by measuring the voltage drop across a 1 kΩ standard resistor. A switching panel was assembled where the pre-set current could be applied to the sample heater by depressing a relay switch which also triggered a digital clock. Releasing the switch stopped both the current flow and the clock.

The exciting current to the resistor thermometer on the sample was battery-supplied and measured by measuring the voltage drop across a 1 kΩ standard. The current was adjusted during the run to maintain the thermometer voltage at $\sim$ 20 mV, and this signal level produced negligible self-heating. All but 1 mV of this voltage signal was "bucked" potentiometrically, and the residual voltage was displayed on the 1 mV scale of a strip-chart

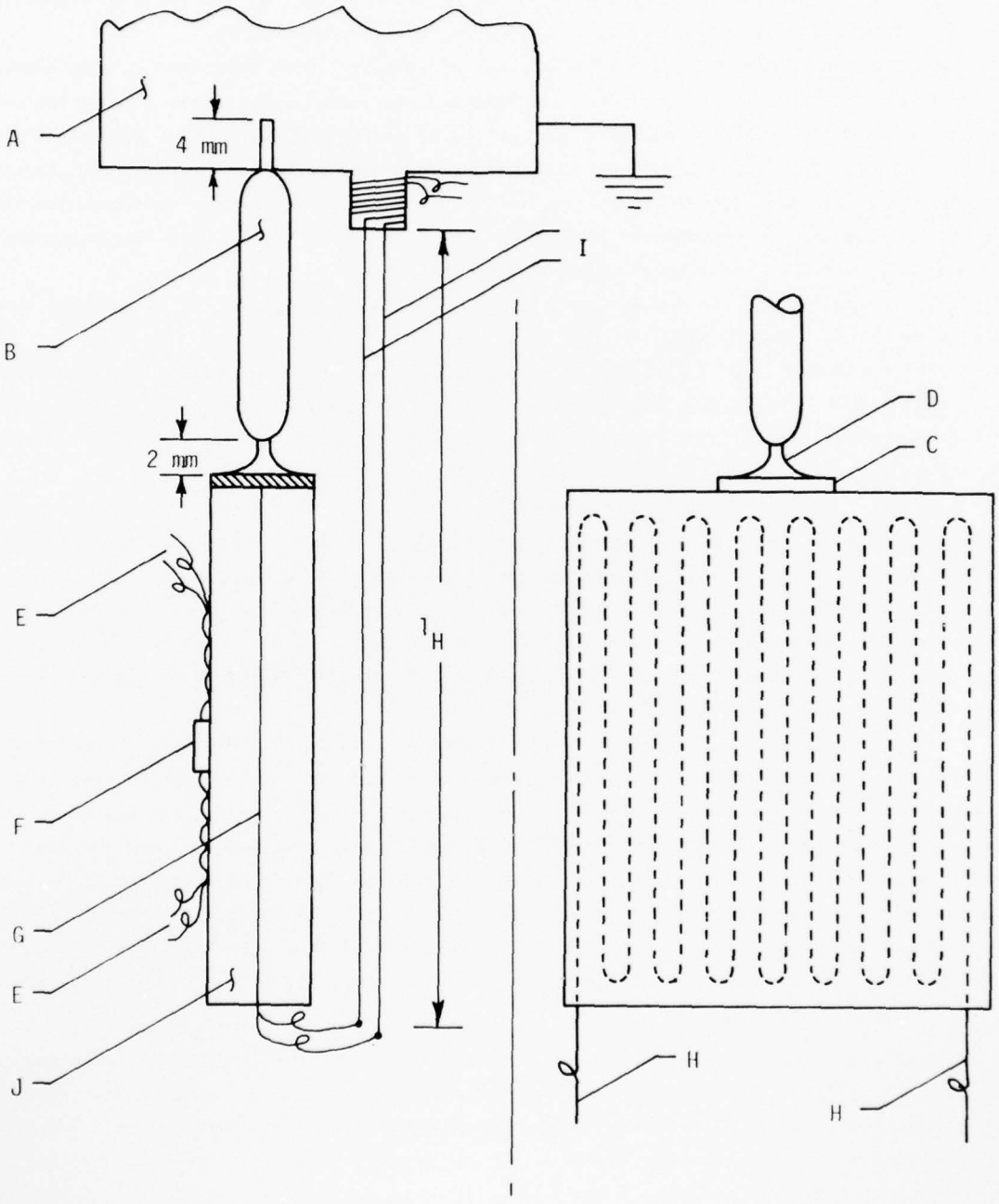

Figure 30. Schematic drawing of sample fixturing for measurement of specific heat and electrocaloric coefficient (see text).

recorder. For a specific heat datum, the heater current was interrupted when the chart pen deflection reached 0.5-0.8 mV, and this $\Delta V/V$ corresponded to $\Delta T/T$ values $\sim$ 2-4%.

Electric fields were produced by applying a voltage to the samples from a decade high voltage dc power supply. The power supply could provide up to 3000 volts. Step changes in field were produced by changing the decade setting on the power supply.

Accuracy of the method: The major sources of error in the method are: (1) The addenda corrections, $\sim \pm$ 0.5%, including some imponderables such as solder joints; (2) The heater resistance, $R_H(300)$, $\sim \pm$ 1%, due to uncertainties in correcting for hook-up leads; (3) The uncertainty in determining t = 0 from the chart trace which translates into an uncertainty in computing the intercept θ, $\sim \pm$ 2%; and (4) The curve-fitting uncertainties both in the $\exp(-t/\tau)$ fits and the thermometer handling according to eq. (3.22). These uncertainties reflected in τ and θ are believed to be no greater than $\sim \pm$ 2%.

The uncertainty in t = 0 does not affect τ, because this uncertainty is absorbed in the amplitude in the curve-fitting.

The repeatability of the method is an approximate measure of precision. At the same reservoir temperature, a sample was pulsed ten times using different heater currents, pulse times, and chart speeds. The resulting zero-field specific-heat values agreed to $\pm$ 2%. This repeatability is about the value expected from the t = 0 uncertainty.

The inaccuracy of the method was expected to be $\sim \pm$ 5%. An attempt was made to verify this by measuring the zero-field specific heat of SiO_2. A sample of Corning fused silica, Code 7940, was measured and these data are shown in figure 31 plotted as CT^{-3} vs T. Also shown in figure 31 are literature data for I. R. Vitreosil[75] and vitreous silica.[76] The position of the peak in CT^{-3} agrees well with the literature data, $\simeq$ 10 K but the height of the peak is $\simeq$ 16% higher than the literature data. At 3 and 20 K, the measured and literature data agree to 1.5% and 6.5%, respectively.

The difference in the heights of the CT^{-3} peaks in figure 31 appears to be much larger than the experimental error in the method. This difference is believed due to the different sources of SiO_2. That is, the temperature of the peak in the CT^{-3} curve is related to the frequency at which the phonon density of states reaches its first maximum, and the height of the peak correlates with the number of phonon modes in the density of states peak.[77] Low-frequency defect modes related to the open structure of SiO_2 are believed responsible for this departure of the specific heats of amorphous materials from a T^3 law. Consequently, the height of the CT^{-3} peak can be expected to depend on the pre-history of the SiO_2 samples.

3.6.3 Thermal conductivity

Knowledge of the thermal conductivity of the glass-ceramic was needed for eventual prototype design, so a method for measuring thermal conductivity in the range 2-20 K was established in parallel with the above specific heat-electrocaloric coefficient. The two methods involve much of the same equipment and thermometry handling. The conventional techniques of using two carbon thermometers on the sample with a heater attached to one end of the sample was used in the initial runs. The carbon thermometers were calibrated against a germanium resistance thermometer mounted on the reservoir. From the first set of measurements it was determined that the thermal resistance of the heater-sample joint and the

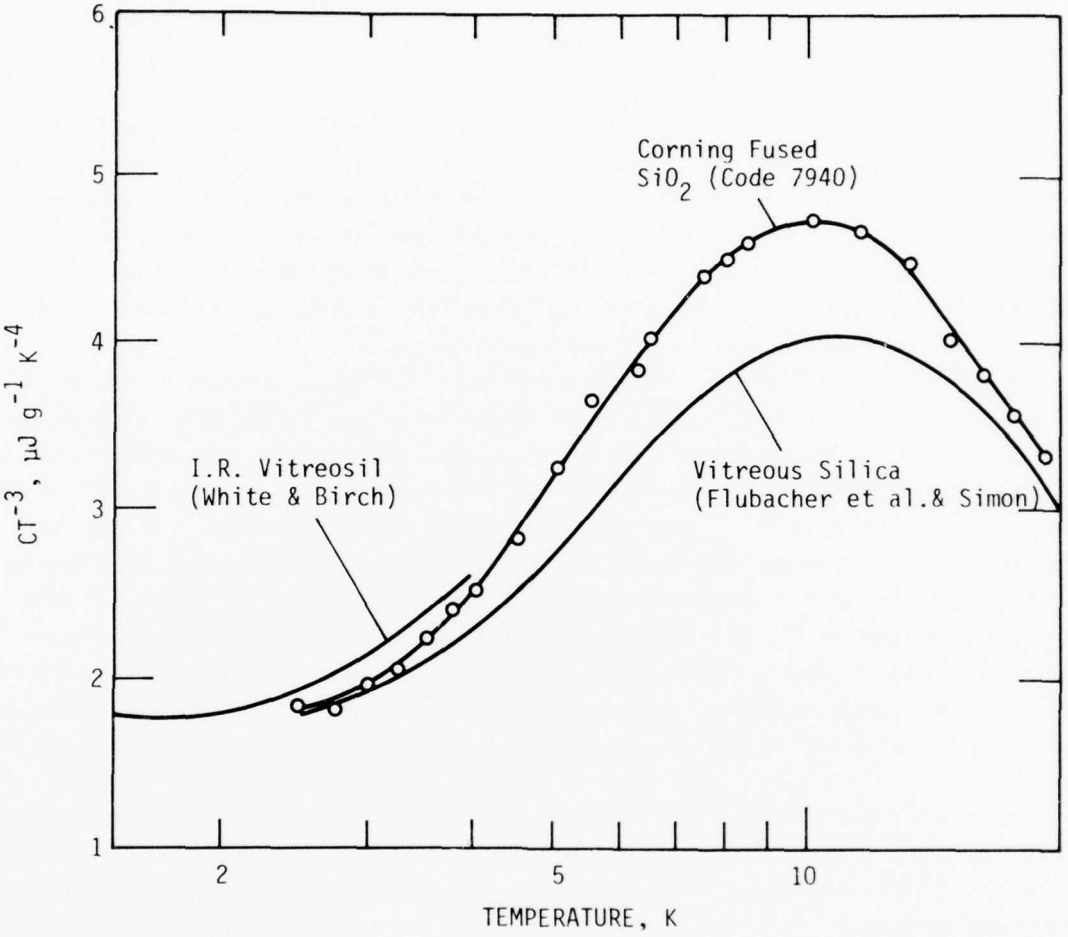

Figure 31. Comparison of specific heat data measured on a sample of SiO_2 with literature data. The difference between the measured and literature data at the maximum in CT^{-3} is too large to be attributed to experimental uncertainty but is believed due to differences in the number of low frequency phonon modes in the different samples of SiO_2.

sample-reservoir joint were negligible. Subsequent measurements were then done with the thermometers permanently mounted on the heater and reservoir. That procedure greatly simplified the mounting procedures.

3.7 Experimental Results

3.7.1. $SrTiO_3$ glass-ceramics

Maximizing $(\partial K'/\partial T)_0$ and the breakdown strength: The quantity $(\partial K'/\partial T)_0$ at 4 K was measured for over 200 samples in the FEP composition series. The series consisted of a preliminary matrix and two main matrices. About 64 different combinations of fabrication variables were used in these matrices. The most important variable was the ceram temperature and so the plot in figure 32 is of $(\partial K'/\partial T)_0$ vs the ceram temperature. The figure compares $(\partial K'/\partial T)_0$ for the FEP matrices with that of the bulk research samples. All the data for the matrices lie within the cross-hatched region.

Two features are immediately evident from figure 32. First, the high values of $(\partial K'/\partial T)_0$ as seen in the research samples could not be duplicated in the FEP matrices. Second, for low ceram temperatures the FEP values are higher than that of the research samples, but the FEP values drop abruptly for ceram temperatures above 1100°C. As discussed in section 3.4 it is just that temperature at which pitting in the samples began to occur. A plot of $d\ln K'/dT$ increases smoothly through the pitting regime which indicates the sudden drop of $\partial K'/\partial T$ is probably not an intrinsic material behavior. Most likely the pits cause the rapid decrease in K' and $\partial K'/\partial T$. The maximum value of K' at 4 K is about 250 and also occurs just before the onset of pitting. There appears to be only a slight correlation between $\partial K'/\partial T$ and the other process variables. Slower heating rates and longer soak times have the most influence in increasing $\partial K'/\partial T$. The use of seal A with paste A2664 gives a slightly higher $\partial K'/\partial T$.

The first measurements of voltage breakdown strengths on 0.025 mm thick samples showed three types of behavior: (i) conducting at all voltages, (ii) conducting above a certain voltage, and (iii) a classical breakdown with a sudden appearance of large current flow at the breakdown voltage. Arcing was often seen in this last case. It is difficult to define a breakdown strength for the first two cases, but it was arbitrarily taken as that field strength where 10 μA of current was drawn. If each element in the refrigerator drew that much current, then the heating effect would be comparable to the refrigeration power desired. As defined, the breakdown strength ranged from less than 10 kV/cm for the first case to as high as 600 kV/cm for the third case.

A study of the breakdown data for this first matrix suggested that flaws or pin holes clear through the 0.025 mm dielectric layer could account for the conducting behavior seen in many of the samples. It was then suggested that two or more layers of dielectric between the electrodes be used. With two or more layers the chances of having two pinholes line up to penetrate straight through the dielectric becomes essentially negligible. The second FEP matrix was then made with many samples containing two and three layers of the basic 0.025 mm thick dielectric and with no floating electrodes between the layers. For the cases where pitting did not occur, the breakdown strengths of these samples averaged about 550 kV/cm,

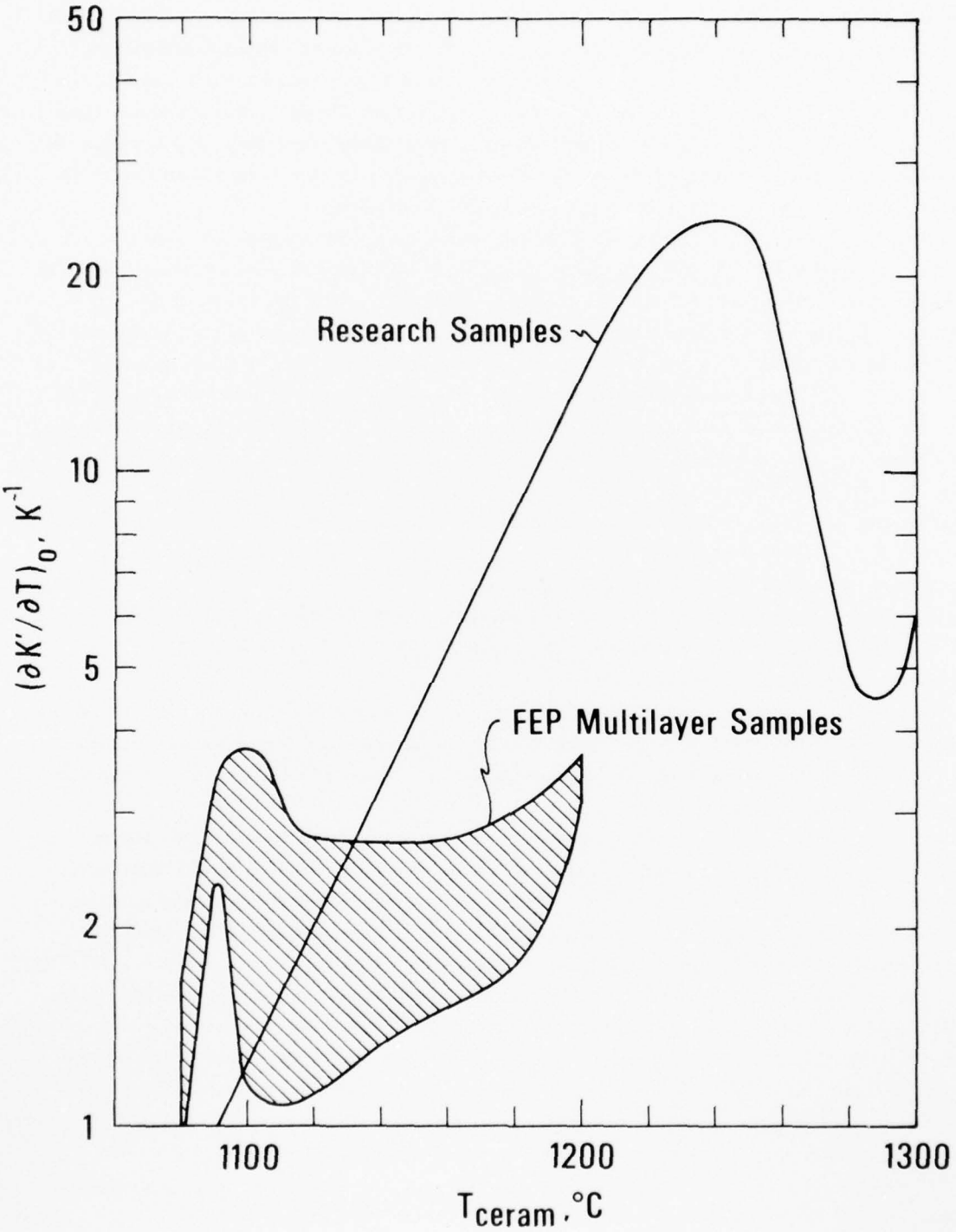

Figure 32. The temperature derivative at 4 K of the dielectric constant for the FEP multilayer samples as a function of the ceram temperature. Shown for comparison is the results on a bulk research sample.

whereas that of the samples with floating electrodes between the layers was about 160 kV/cm. The other process variables appeared to have little effect on the breakdown strengths. The 550 kV/cm is well above the 300 kV/cm strength used in the original design calculations.[2]

It was found that some correlation existed between the loss factor, tan δ, in the dielectric constant and the breakdown strength. Large values of tan δ, i.e., greater than about 0.01, are associated with low breakdown strengths although very small tan δ values do not necessarily mean large breakdown strengths. Measurements of tan δ were then useful in eliminating most of the samples which had low breakdown strengths.

A second series of samples with a different composition (FEL series) was made to test the effect of composition on the dielectric properties. The only difference between the FEP and FEL compositions is that FEP has a SiO_2/Al_2O_2 ratio of 4 while FEL has a ratio of 3. The FEL series also consisted of two matrices with essentially the same process variables as used with the FEP series. The results of measurements on $(\partial K'/\partial T)_o$ at 4 K are shown in figure 33 as a function of the ceram temperature. The behavior is somewhat similar to the FEP series in that the maximum $(\partial K'/\partial T)_o$ values are about 3.5 K^{-1} and that a rapid decrease in $\partial K'/\partial T$ occurs above a certain ceram temperature where pitting occurs. The onset of pitting for the second FEL matrix occurred at about 1160°C compared with 1100-1110°C for the FEP series and the first matrix of FEL. Extensive tests on the composition of the two FEL matrices showed no differences between the two, although there was a difference in color. No satisfactory explanation could be found for the difference in behavior. In any case, the maximum $(\partial K'/\partial T)_o$ values still did not exceed 3.5 K^{-1}, which is about an order of magnitude below that of the bulk research samples. The largest values of K' at 4 K are about 250, which are the same as for the FEP series.

The results of breakdown measurements on the FEL series gave similar results as for the FEP series except that there were far fewer samples which were conducting at low voltages. The average breakdown strength for the better samples was about 650 kV/cm, which is slightly higher than the FEP series.

As discussed in section 3.4 the FEP and FEL series contain 2 mole % $SrNb_2O_6$ doping. To test the effect of this niobium doping, the FHN series was made which is just FEP without the niobium oxide. The resulting K' and $(\partial K'/\partial T)_o$ values are decreased by about a factor of three and two, respectively. Consequently, niobium has a rather strong effect on $(\partial K'/\partial T)_o$.

One approach to solve the pitting problem was to inhibit strontium feldspar crystallization. This was accomplished by adding B_2O_3. Single layer research samples were made from this material and are known as the $SrTiO_3$ boroaluminosilicates. Two compositions were tested, FHS, which has 1% niobate and FID, which is niobate free. The ceram temperatures were mainly 1050 and 1100°C. For the FHS composition with 1100°C ceram temperatures the K' and $(\partial K'/\partial T)_o$ values were about 550 and 10 K^{1}, respectively. The dielectric constant reached a peak of about 600 at a temperature of 50 K. The niobate free FID samples had K' and $(\partial K'/\partial T)_o$ values of about 300 and 3 K^{-1}, respectively. Since these were only single layer research samples the breakdown strengths would be very low and were not even measured.

Further attempts to increase $(\partial K'/\partial T)_o$ were halted when electrocaloric and polarization measurements showed that $(\partial K'/\partial T)_o$ was not the relevant parameter as far as predicting cooling effects at 4 K.

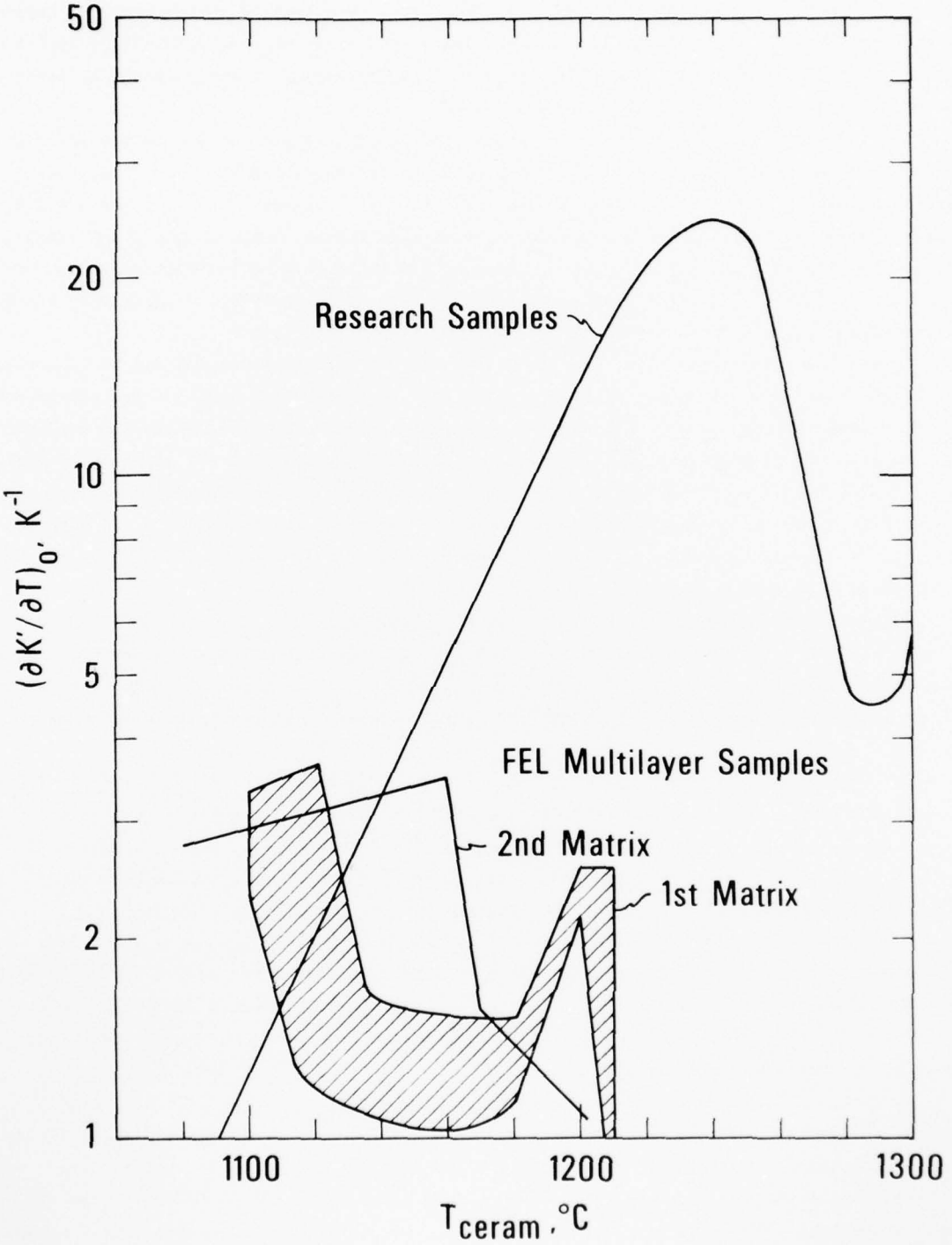

Figure 33. The temperature derivative at 4 K of the dielectric constant for the FEL multilayer samples as a function of the ceram temperature. Shown for comparison is the results on a bulk research sample.

Electrocaloric measurements: Considerable time was spent trying to solve the pitting problem. Finally it was decided to make electrocaloric measurements on the best FEL samples cerammed at 1100°C under optimum conditions. Two such samples were mounted in the apparatus for measurement of specific heat and electrocaloric coefficient. These samples are designated as ECR3 and ECR6.

The first observation was that the initial voltage application at 4 K caused heating rather than the expected cooling. Moreover, this heating persisted for very long times. Data are shown in figure 34 for two samples where at t = 0 the field was switched 0 → 239 kV/cm. These data were obtained by analyzing T(t) data knowing thermal conductance data $\mathscr{G}(T)$ for the thermal links. For times of about 40 min., the heating has fast and slow components with time constants of about 2 min. and 20 min., respectively. Considerable energy is dissipated in this process (about 0.1 - 0.2 J/cm^3 from figure 34).

It was found experimentally that once these initial mechanisms stabilized at some field value, the field could then be reduced, cycled, etc. without re-triggering these mechanisms.

The next observation was that at 4 K, where $(\partial K'/\partial T)_E$ was observed to be the largest, heating was seen on both positive and negative field changes ΔE about E. The samples were first stabilized as mentioned above, and data on this heating are shown in figure 35. The actual heat input was calculated using measured values of the specific heat. The results are shown as dashed lines in figure 35 corresponding to ΔQ = 1.90 and 6.37 μJ/cm^3. Here ΔQ was assumed temperature independent.

Electrocaloric measurements were also made on the same two stabilized samples between 20-40 K, and these ΔT-data are shown in figure 36. In the range 20-40 K, reversible electrocaloric heating ($\Delta E > 0$) and cooling ($\Delta E < 0$) are observed for the two samples. The dashed curves in figure 36 were drawn to represent exactly reversible electrocaloric temperature changes.

The deviation of the position ΔT points between 20-25 K from the dashed curve in figure 36 probably result from the hysteretic-heating effects (note that the field changes in figure 36 are considerably larger than the figure 35 field changes). That is, hysteretic heating would raise both the positive and negative ΔT points. Due to the uncertainty of the ΔT's, no attempt was made to correct the data for hysteresis effects.

The ceram temperature has a large effect on the resultant $SrTiO_3$ crystallite size. The possible effects of crystallite size on the electrocaloric properties were tested by measuring FEL samples cerammed at 915°C and 1160°C. The two samples measured previously were cerammed at 1100°C. The crystallite size changes from a few angstroms for 915°C samples to about 0.7 μm for 1160°C samples.

In figure 37 are shown temperature decays at 4.0 K following the first and second voltage pulses for FEL 1160 and FEL 915. The long time-constant self-heating appears absent in both samples because the τ's match the link time-constants. Also, the 0→E and E→0 τ's are essentially the same. There is hysteretic heating present in the uncrystallized FEL 915 sample, and both samples in figure 37 show evidence of depolarization cooling superimposed on the more dominant hysteretic heating.

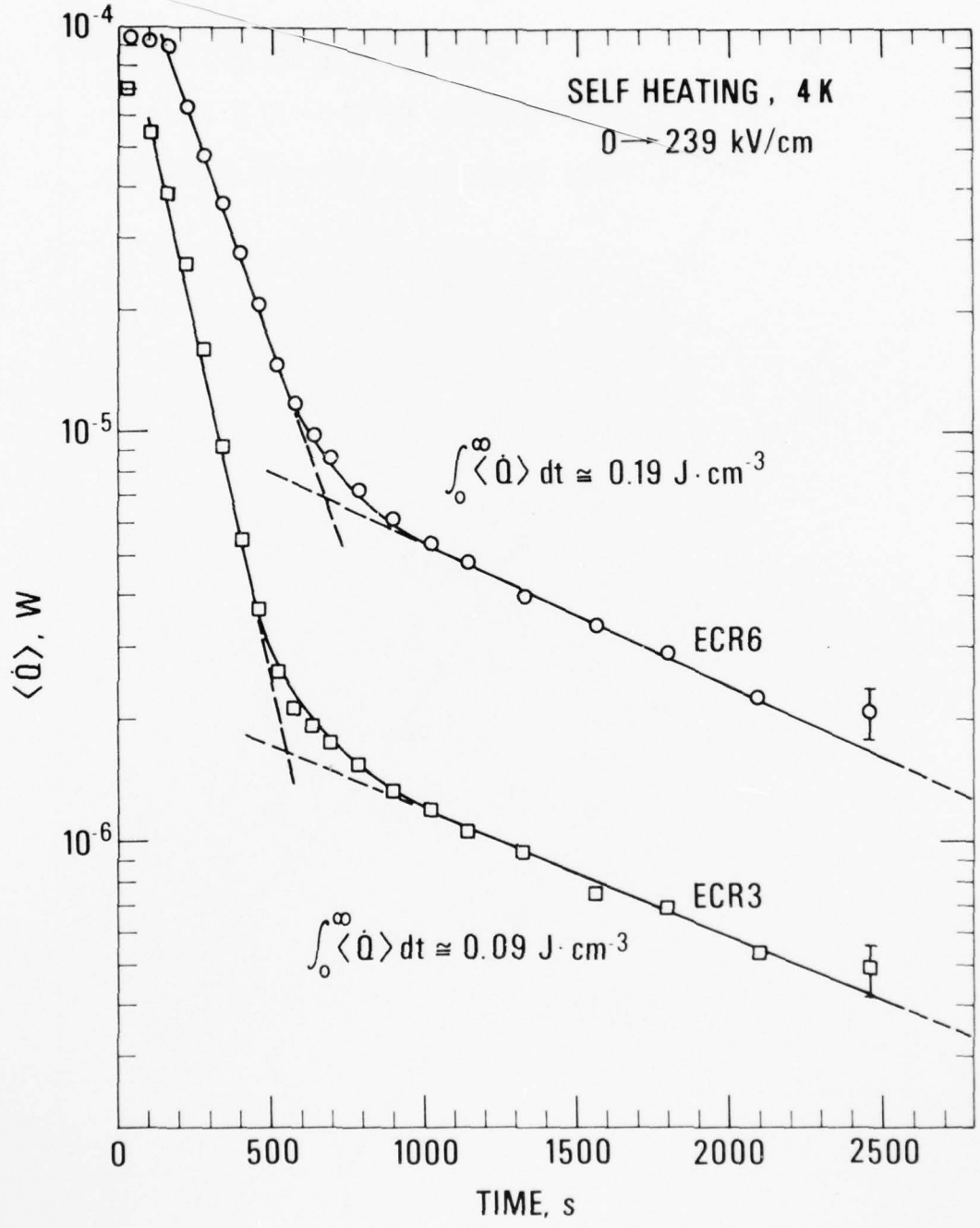

Figure 34. The time dependence of self heating in two FEL glass-ceramic after an electric field is first applied to the samples at 4 K. Both samples had ceram temperature of 1100°C.

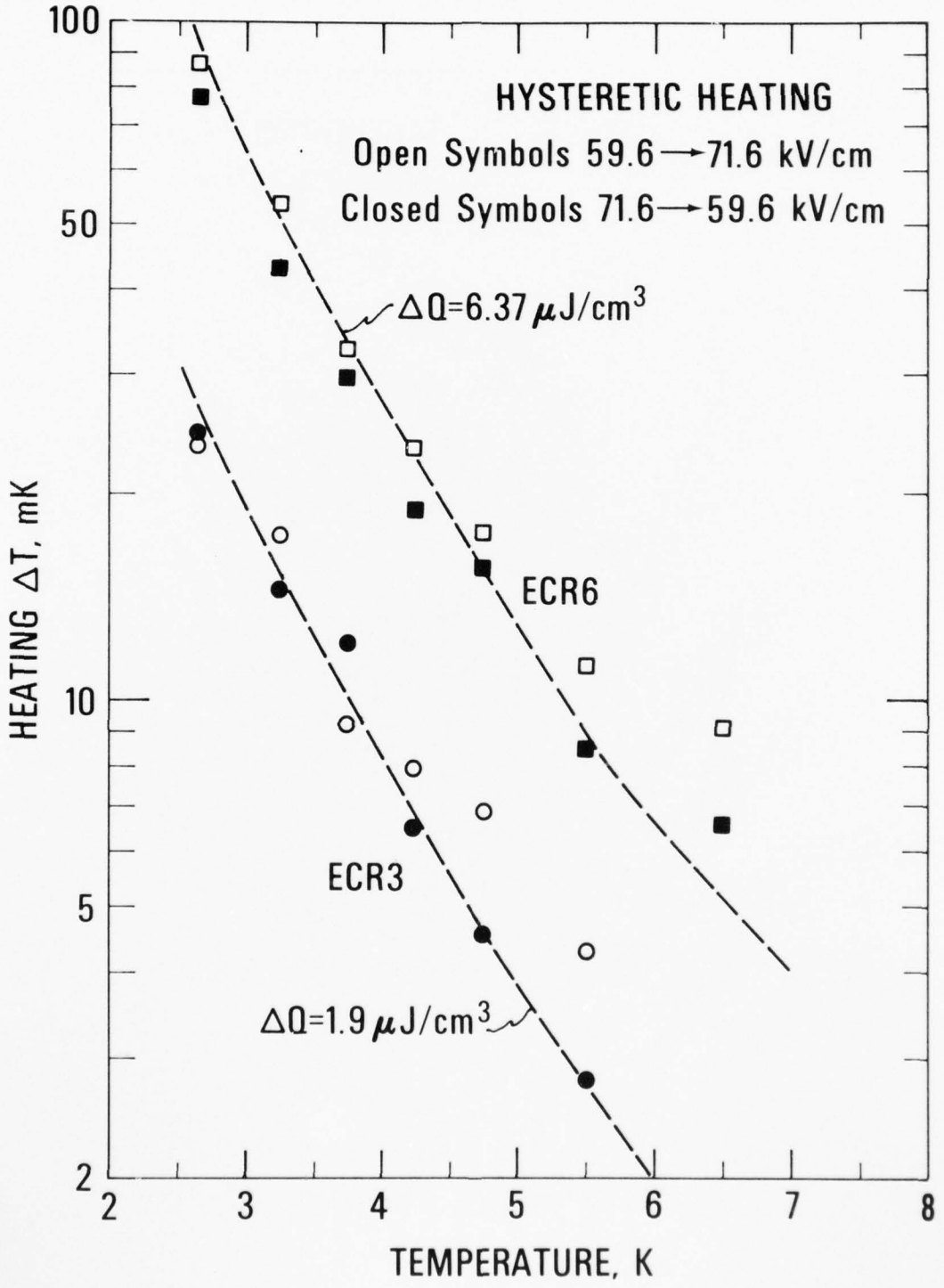

Figure 35. The temperature rise in two previously polarized FEL samples during a change in the electric field. The open symbols are for an increase in field and the closed symbols are for a decrease in field.

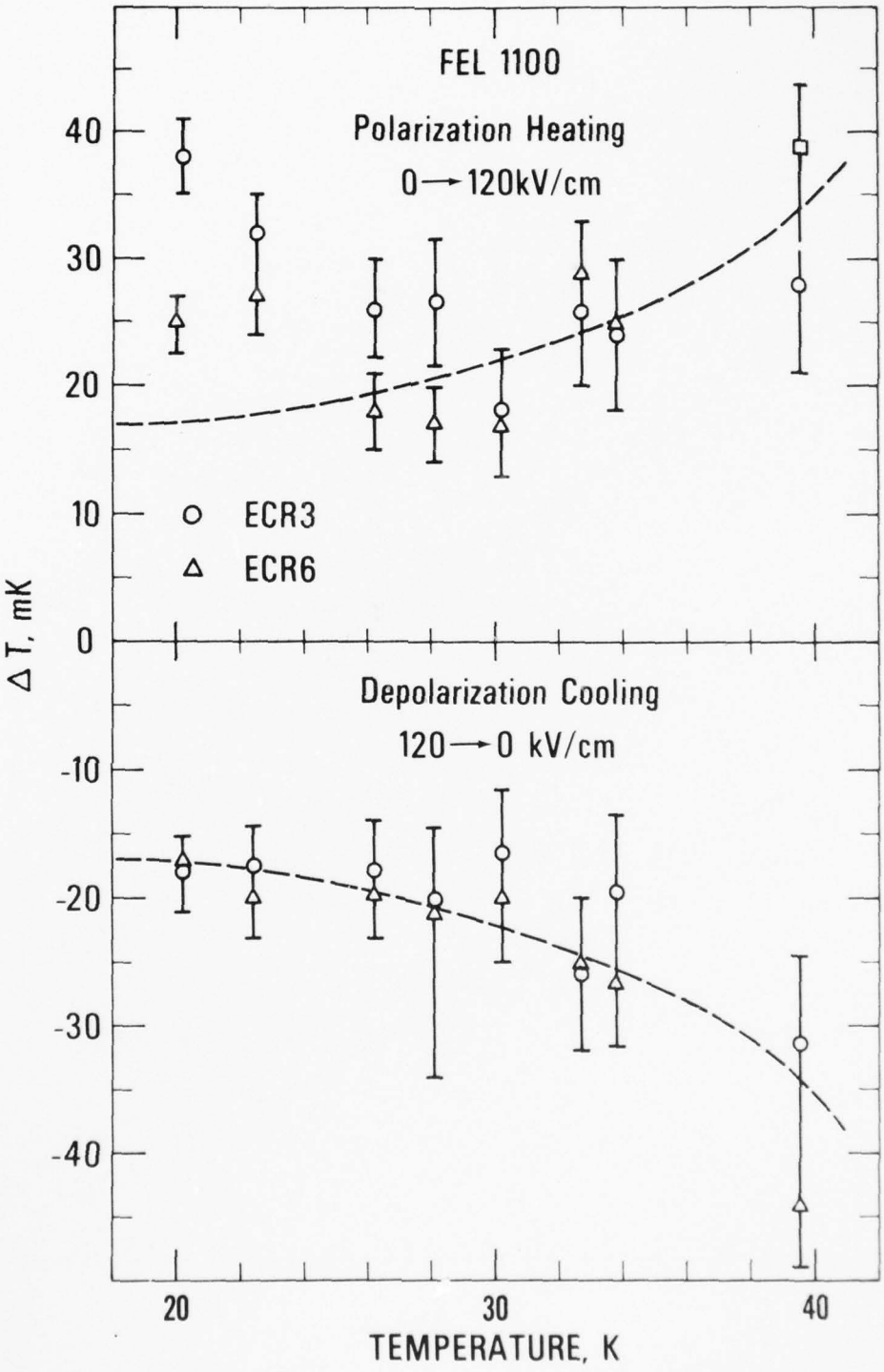

Figure 36. The temperature change in two previously polarized FEL samples during a change in the electric field. This data is for the 20 - 40 K temperature range where cooling is seen for a decrease in field.

AD-A037 412 DEVELOPMENT OF SANDWICH STRUCTURED PHOTOSENSITIVE FILMS FOR APPLICATION TO NON-CONTACT POTENTIOMETERS(U) NAVAL AVIONICS FACILITY INDIANAPOLIS IND G A MAGEE NOV 76

UNCLASSIFIED NAFI-TR-2148-REV-1 F/G 14/2 NL

2/3

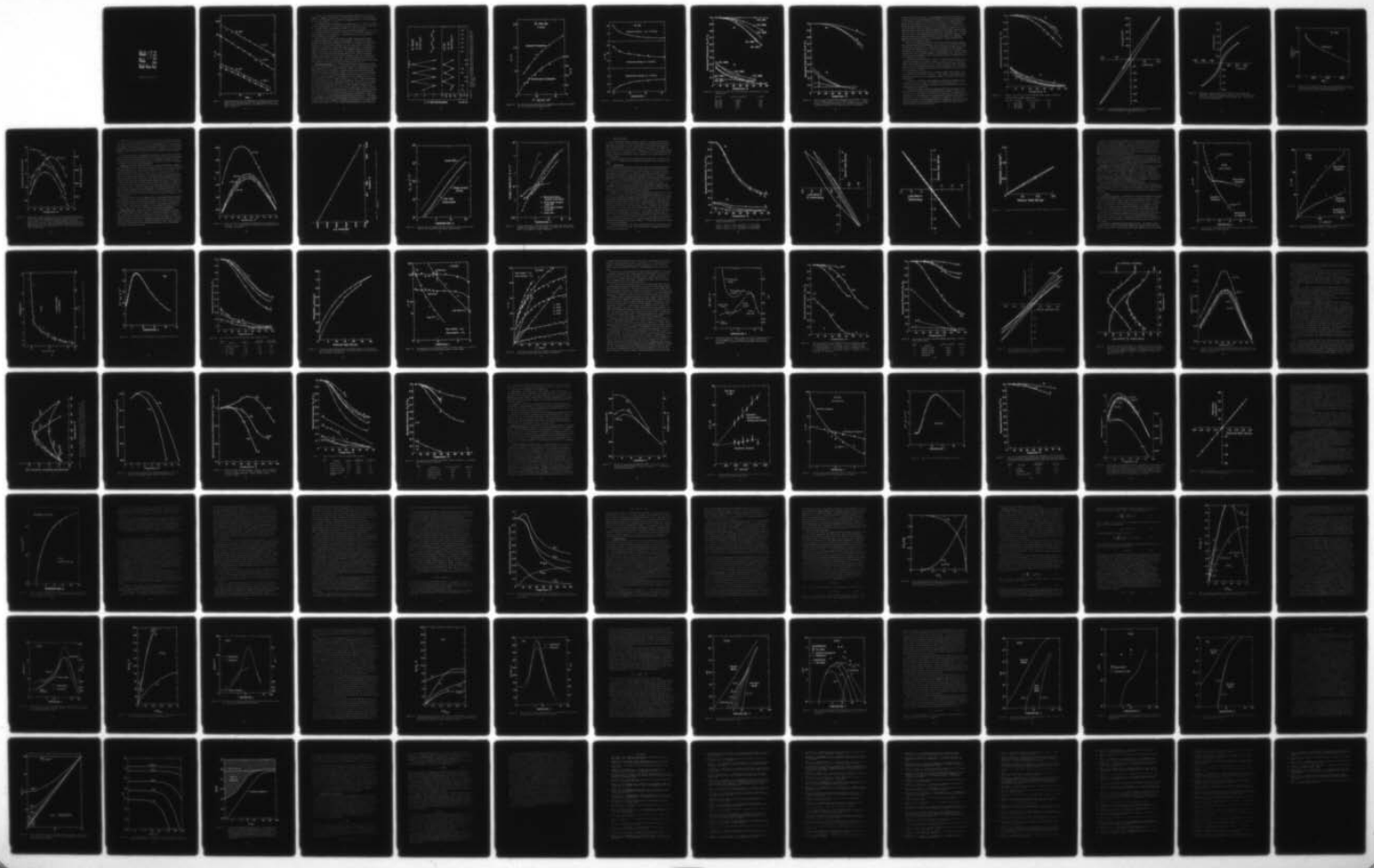

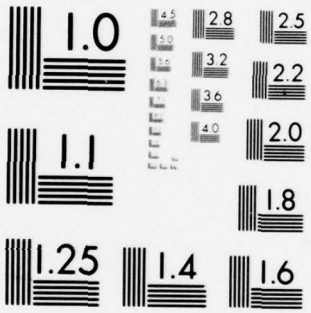

MICROCOPY RESOLUTION TEST CHART
NATIONAL BUREAU OF STANDARDS-1963-A

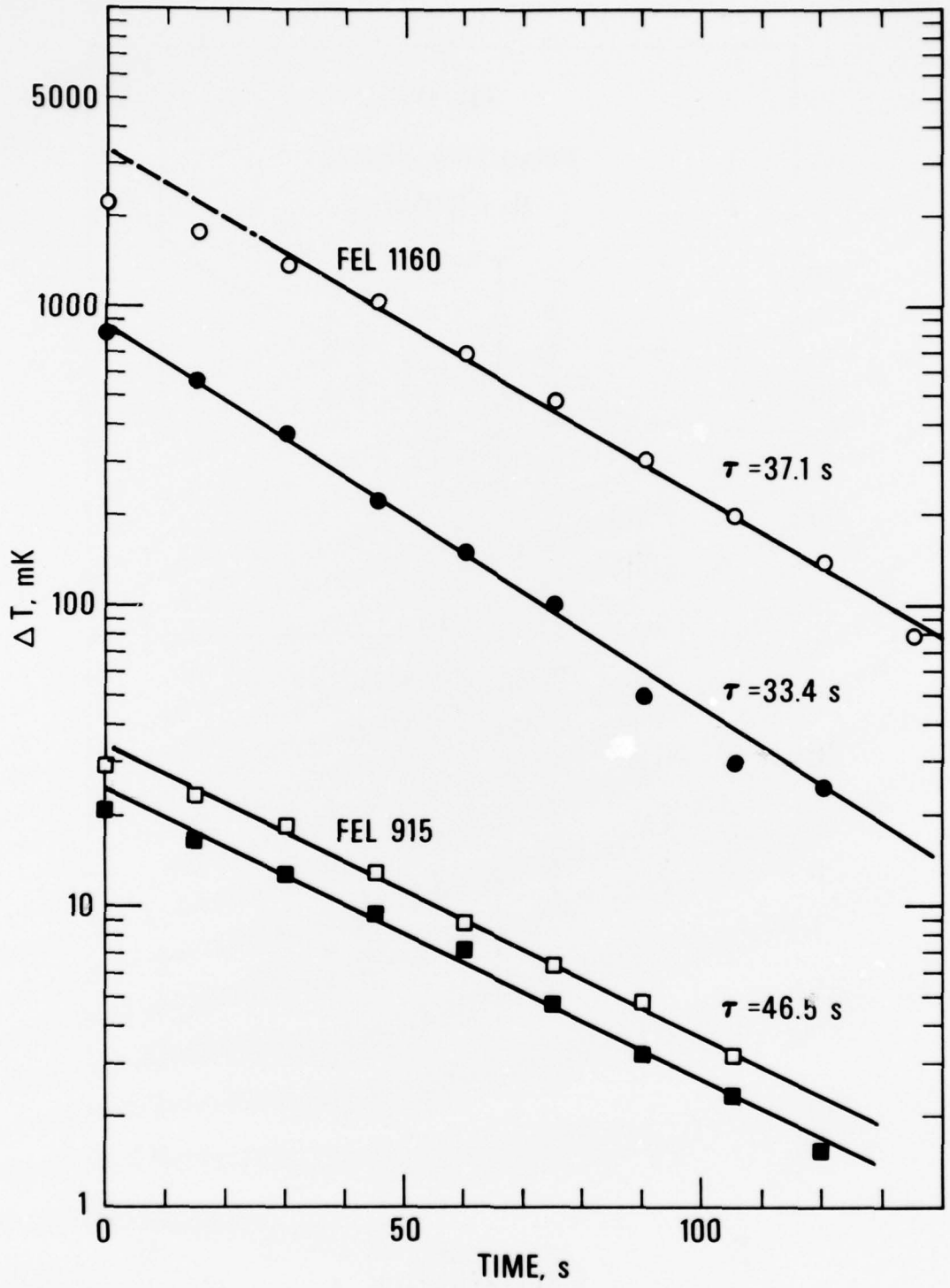

Figure 37. Temperature decays at 4 K following the first and second voltage pulses for FEL 1160 and FEL 915. The open symbols are for the first pulse, 0 → 72 kV/cm and the full symbols are for the second pulse, 72 kV/cm → 0.

In figure 38 are shown data on the effects of polarity reversal at 4.0 K for the two samples. For example, on switching 0→ + 72 kV/cm, FEL 1160 heated 2.2 K; after decay back to 4.0 K, the field change + 72 → 0 resulted in a temperature rise ΔT = 0.8 K; the subsequent 0→ - 72 switch yielded ΔT = 3.5 K, etc.

The residual polarization $+P_r$ remaining in the sample after a +E → 0 switch is reversed to $-P_r$ on the subsequent 0 → -E switch and results in the large ΔT = 3.5 K in FEL 1100. The ±E → 0 switch involves a smaller amount of heating, ΔT = 0.8 K for FEL 1160.

Also shown in figure 38 for FEL 1160 are the ΔT's obtained on subsequent 0 → +E → 0 → +E, etc., switches (measured in a second run). The initial 0 → +E switch gives a larger ΔT (2.2 K) than subsequent 0 → +E switches (ΔT = 1.2 K) provided polarity is not changed (this initial ΔT decays quickly, figure 37).

The FEL 915 data in figure 38 track the FEL 1160 data, implying that the heating mechanisms are qualitatively the same in these end members. In figure 39 are shown the hysteretic and electrocaloric components for FEL 1160 at 4.0 K plotted vs E^2. These data show that at 4.0 K the hysteretic component is not only larger than the electrocaloric component but is apparently increasing more rapidly with applied field. The electrocaloric component is defined as the reversible part of the temperature change and the hysteretic component is that which always causes heating. This definition assumes the hysteretic heating is the same for both increasing and decreasing fields. Because the hysteretic component is much larger than the electrocaloric component in figure 39, the inaccuracy of the electrocaloric component is rather large. The first resolvable cooling effects were seen at about 7 K. By 15 K, electrocaloric heating and cooling effects are well established, and electrocaloric data are shown in figure 40 on FEL 1160 from 15 to 31 K.

Polarization measurements: All the $SrTiO_3$ glass ceramics show qualitatively the same behavior for $P_t(T)$ and $P_t(E)$, where P_t is the total polarization. The most extensive polarization studies were done on the FEL glass ceramics, however, so the representative curves shown will be mostly for this material. Measurements of dc polarization for FEL glasses crystallized at different temperatures are shown in figure 41 for a 3.6 kV/cm field applied around 77 K. This $P_t(T)$ data and most subsequent $P_t(T)$ data are normalized to $P_t(T)$ = 1 at 4 K so the temperature dependence can be compared easily. The normalized values of P_t and P_r are designated P_{tN} and P_{rN}, respectively, where $P_{rN} = P_r/P_t(4\ K)$. There is no maximum in $P_t(T)$ evident above 4 K for any crystallization temperature. The slope of P_t does increase with increasing crystallization temperature since $P_t(4)$ and $\partial P_{tN}/\partial T$ increases with increasing crystallization temperature up to 1150°C. The 1160°C glass has a slightly smaller $\partial P_t/\partial T$ because the maximum value of P_t is smaller even though $\partial P_{tN}/\partial T$ is larger. The maximum $\partial P_t/\partial T$ with crystallization temperature cannot be confirmed without more samples measurements. None of the materials show any appreciable change of P_t with temperature below 10 K, unlike that of K'. All of the materials with any temperature dependence of P_t displayed a 25 to 30% remanent at 4 K when the field was removed after cooling from 77 K. This remanent was quasi-stable; a very slow but detectable decay was observed at constant T. This remanent rapidly decreased as T was increased. The remanent curves approach P_r = 0 assymptotically at some value of T above 77 K. Figure 42 shows normalized polarization curves measured at 3

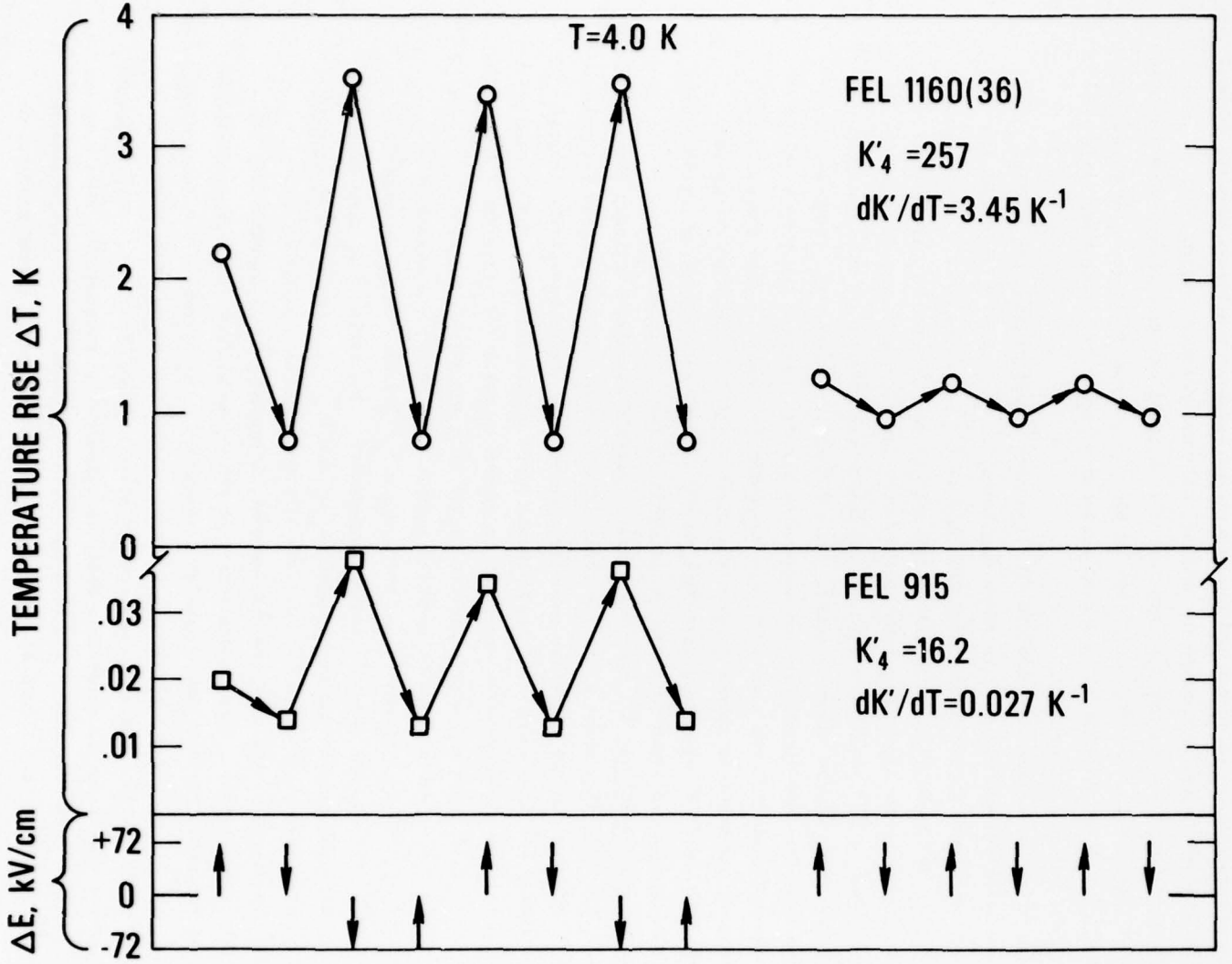

Figure 38. Effects of field changes and polarity reversal at 4 K for FEL 1160 and FEL 915. The lower part of the figure shows the direction of field change.

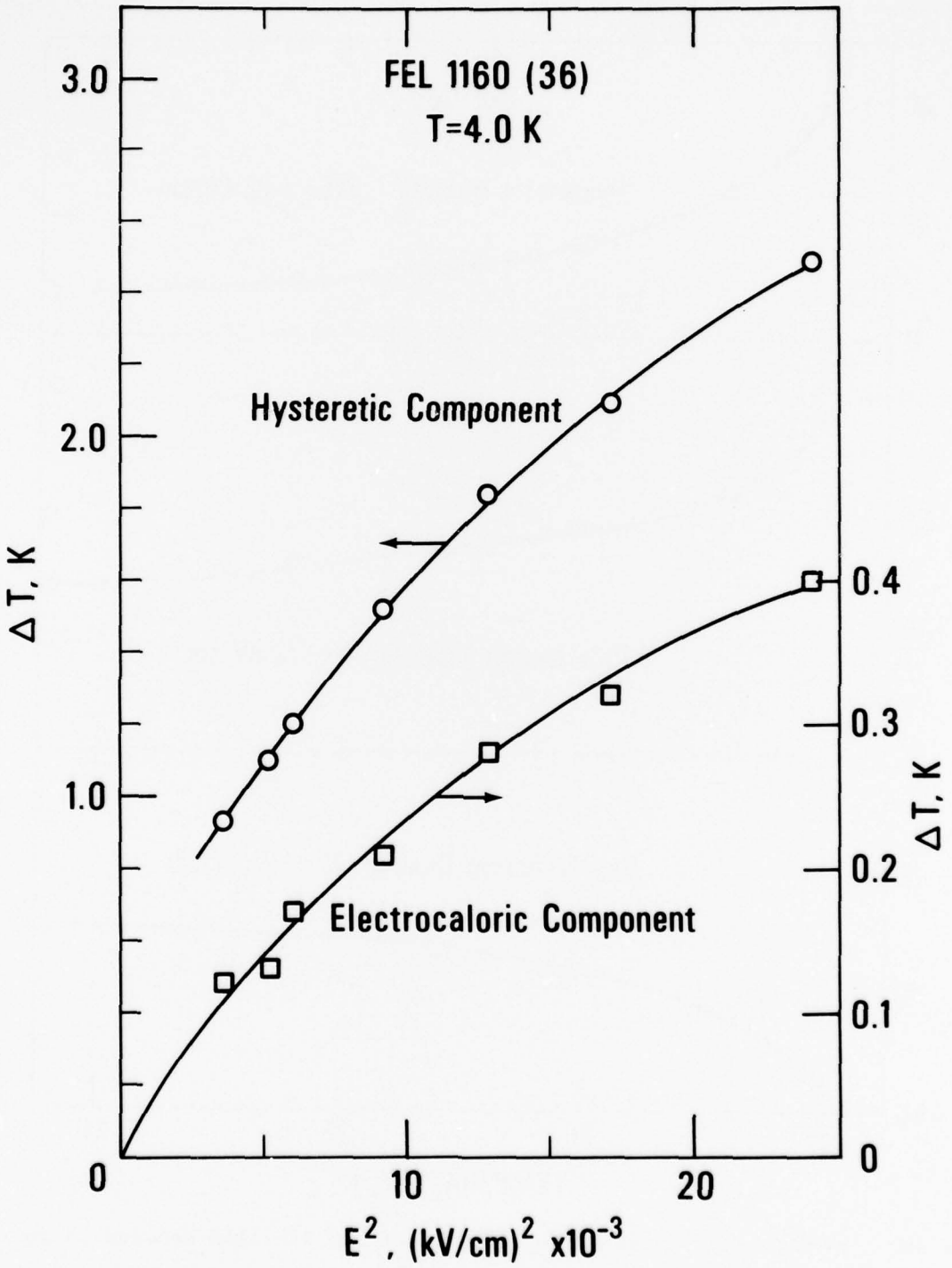

Figure 39. The hysteretic and electrocaloric components of temperature changes at 4 K as a function of electric field.

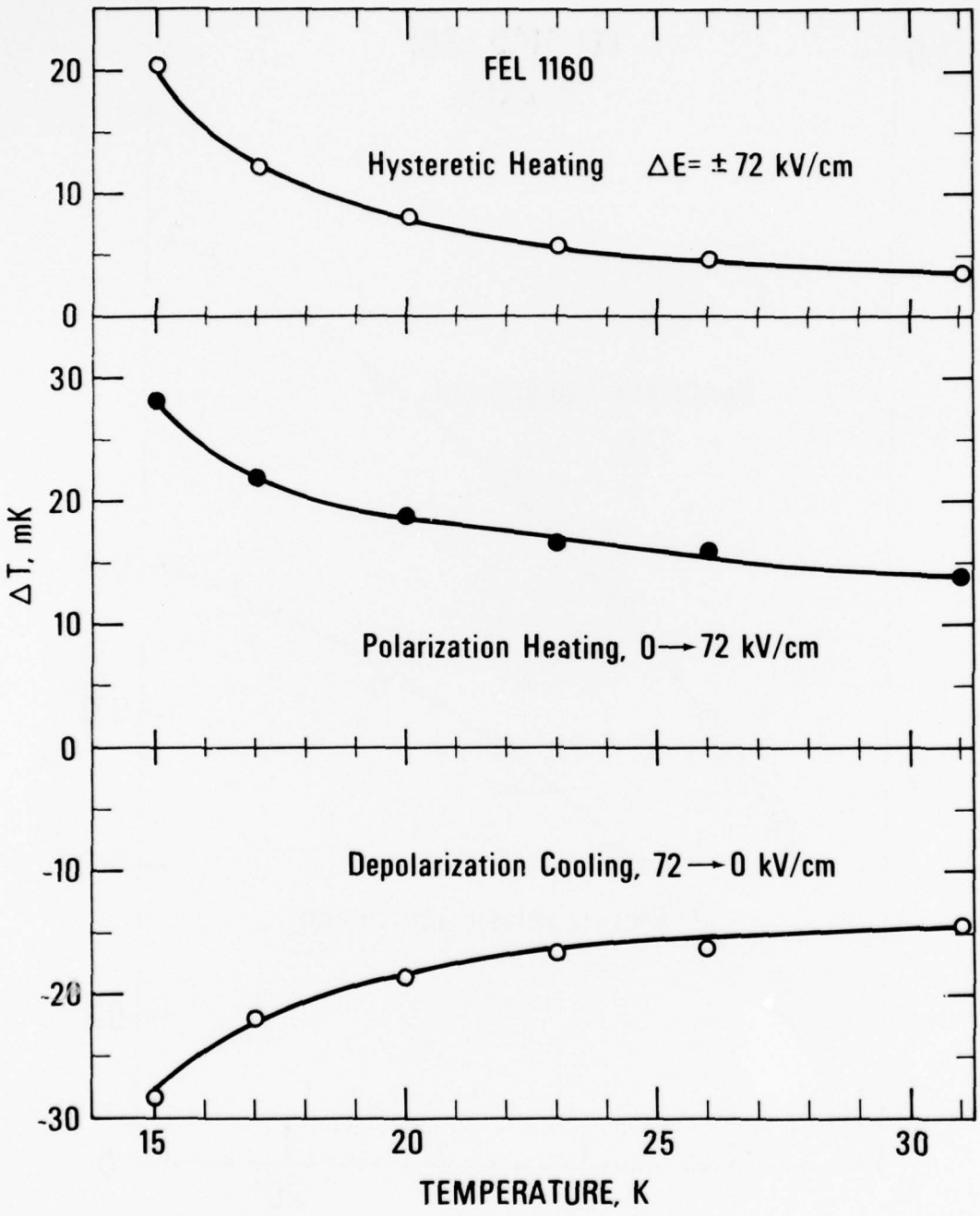

Figure 40. Electrocaloric and hysteretic effects in FEL 1160 between 15 and 31 K.

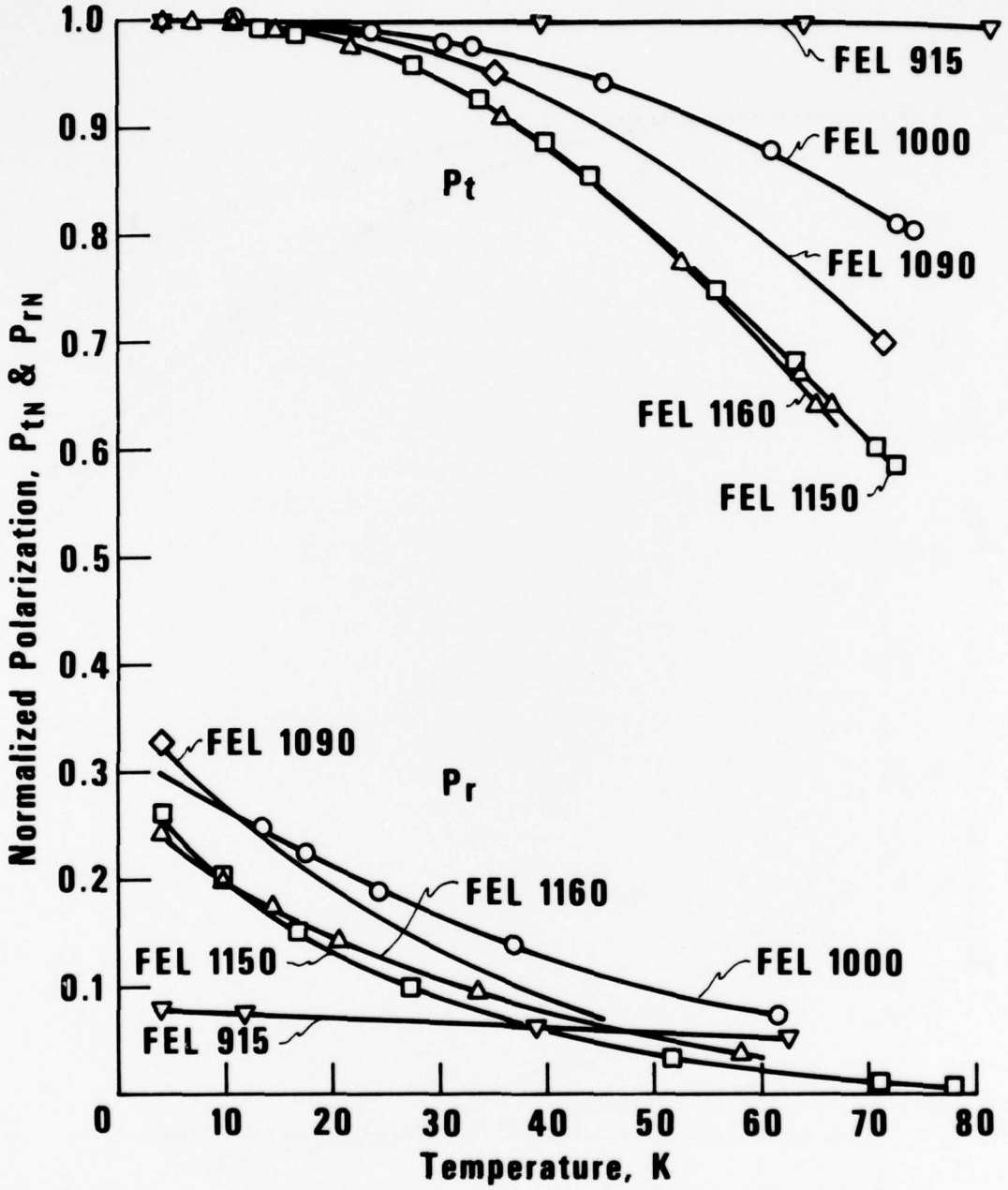

Figure 41. Curves of P_{tN} and P_{rN} for FEL materials crystallized at various temperatures.

Specimen	P_t(4 K), μcoul/cm^2	E, kV/cm
FEL 915	0.0058	3.63
FEL 1000	0.046	3.66
FEL 1090	0.116	3.66
FEL 1150	0.141	3.66
FEL 1160	0.118	3.64

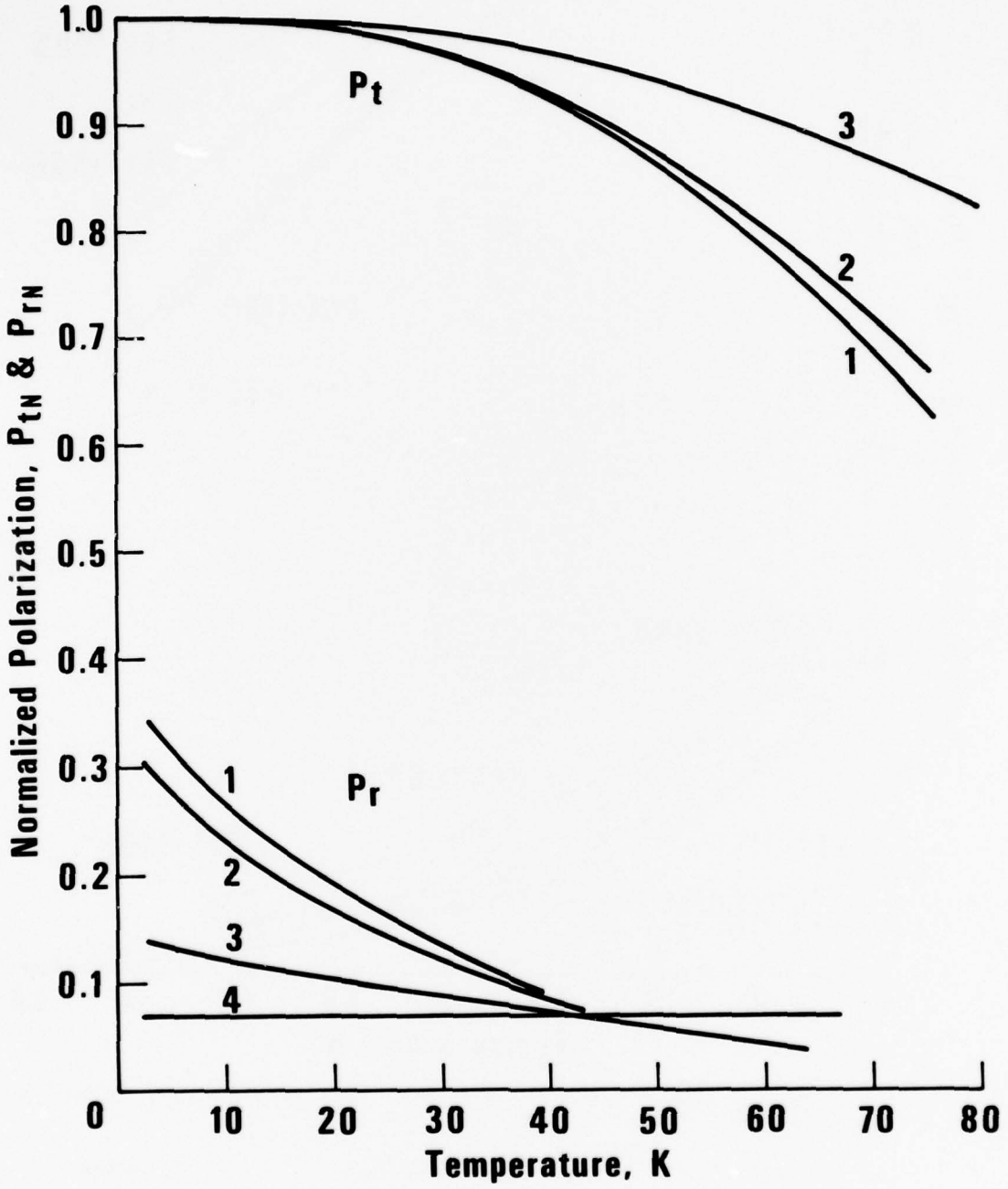

Figure 42. Curves of P_{tN} and P_{rN} for FEL 1090 and various fields. Curve 1, E = 3.7 kV/cm, P_t(4 K) = 0.11 μcoul/cm^2; Curve 2, E = 7.3 kV/cm, P_t(4 K) = 0.18 μcoul/cm^2; Curve 3, E = 59 kV/cm, P_t(4 K) = 0.89 coul/cm^2; Curve 4, E = 167 kV/cm, P_t(4 K) = 1.6 μcoul/cm^2.

different field values for FEL 1090°C. The normalized slope decreases in magnitude with increasing field. The relative magnitudes of P_r compared to P_t at 4 K for voltages applied at 77 K decreases from about 33% to about 14% as E is increased. The remanent appears to approach the same percentage around 70 K for all three field values. The remanent was measured once after applying a field of 167 kV/cm to the sample at 4 K. There was only a very slight decrease, one part in nearly 700, in P_r upon warming the samples to 67 K. This remanent may have resulted from a momentary breakdown of the FEL capacitor during the application of the field. Such occurrences were observed during the breakdown tests. This would leave a net charge on the standard capacitor when the high voltage lead is shorted. However, sufficient remanent would be expected to remain on the FEL capacitor for a temperature dependence to be observed even though it is superimposed on a leakage generated charge. This question was not pursued any further.

Figure 43 shows normalized $P_t(T)$ and $P_r(T)$ curves for three other glasses of approximately the same crystallization temperature. The P_t curves of FEP 1130 and FEL 1150 curves are essentially co-linear though P_r is larger for FEL. Removing the niobate from FEP (FHN 1130) reduces the T dependence of P_t. The DXO 1199 glass ceramic (used for capacitance thermometers) is unfairly displayed. It has twice the field applied to it because the plate spacing was half that of the other capacitors. A rough estimate of the P_t curve at half the field using the field dependent P_t data of figure 42 would bring the high temperature end of this curve down to the FHN curve.

Hysteresis loops for FEL glasses to a field of ± 2.2 kV/cm are shown in figure 44. In figure 45 the hysteresis loop is shown to fields of ± 228 kV/cm. The 0 to +345 kV/cm hysteresis loop which has been offset by P_t = 1.0 μcoul/cm^2 in figure 45, shows a very small opening. This is further reduced if the field is not brought below 60 kV/cm. The maximum field in the $SrTiO_3$ is probably less than 30 kV/cm due to the presence of the glass matrix with a low dielectric constant.

The half width of the hysteresis loop in figure 44 is about 0.0034 μcoul/cm^2. This would be about 0.006 μcoul/cm^2 for a field of 3.7 kV/cm. When 3.7 kV/cm is applied while cooling the sample from 77 to 4 K, the remanent is about 0.035 μcoul/cm^2, which is about 5 times larger.

For a period of time after a field is applied, the polarization increases with time. In figure 46, $P_t(\infty) - P_t(t)$, where t is time and $P_t(\infty)$ is the estimated P_t at $t = \infty$, is plotted as a function of time after E is raised to 300 kV/cm from 240 kV/cm. The curve can be approximated by two exponentials.

A maximum was observed in polarization measurements made while decreasing T if the electric field was switched off at each temperature point to measure P_r. Figure 47 shows the results of a P_t measurement of FEL 1150 for E first applied at 4 K and measured as T is increased to 56 K. The temperature then was decreased and P_t measured without changing the applied field. A peak is observed in P_t measured while increasing T. The 4 K to 56 K section of the curve is a quasiequilibrium curve as P_t increases slowly with time up to the peak, then decreases slowly with time above the peak. The peak of P_t occurs around 25 K while the peak of K' at 1 kHz occurs at 35 K.

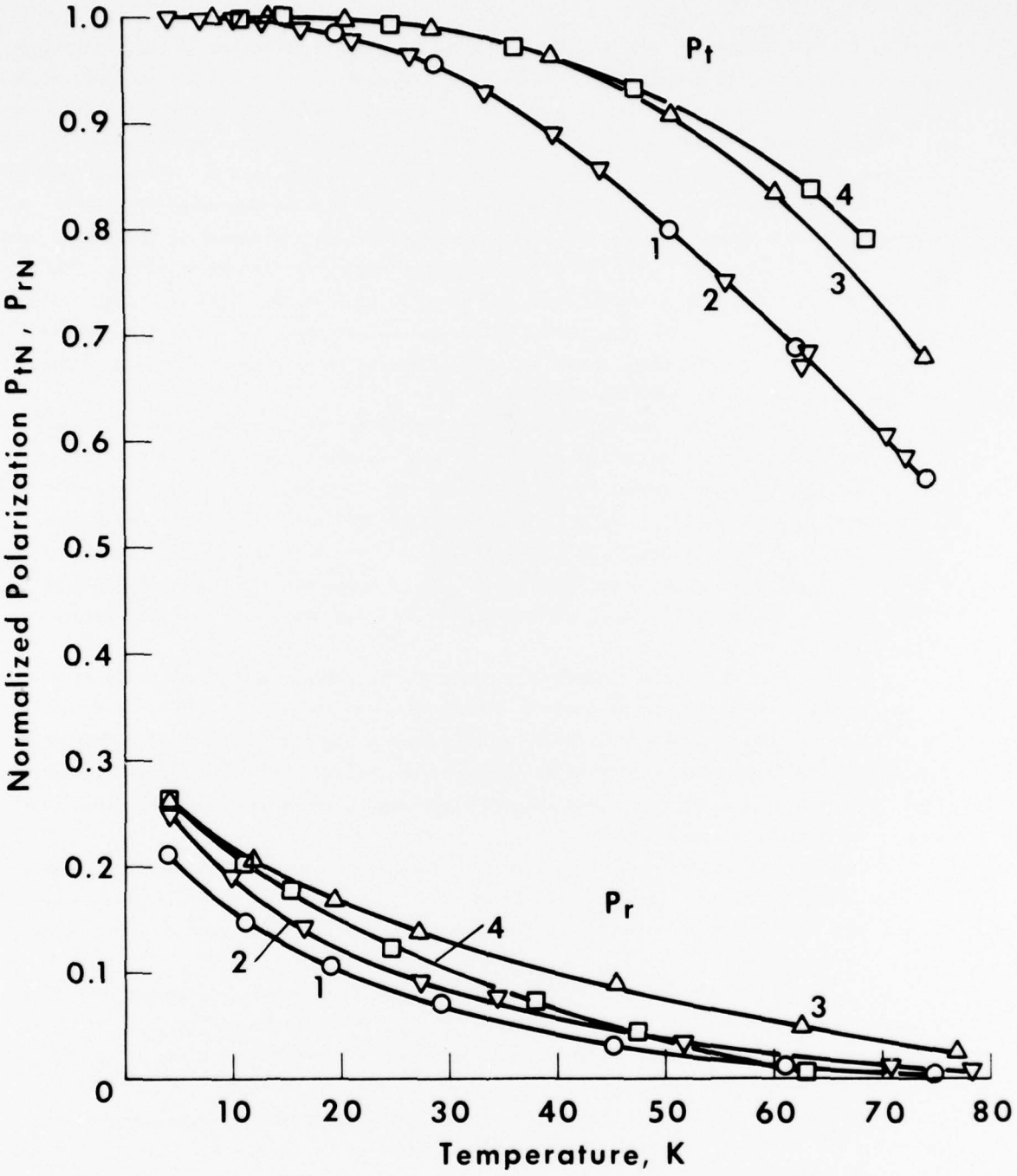

Figure 43. Curves of P_{tN} and P_{rN} for four different glass ceramic capacitors crystallized at similar temperatures.

Curve No.	Specimen	P_r(4 K) μcoul/cm^2	E kV/cm
1	FEP 1130°C	0.113	3.6
2	FEL 1150°C	0.141	3.7
3	FHN 1130°C	0.094	3.6
4	DXO 1100°C	0.12	7.1

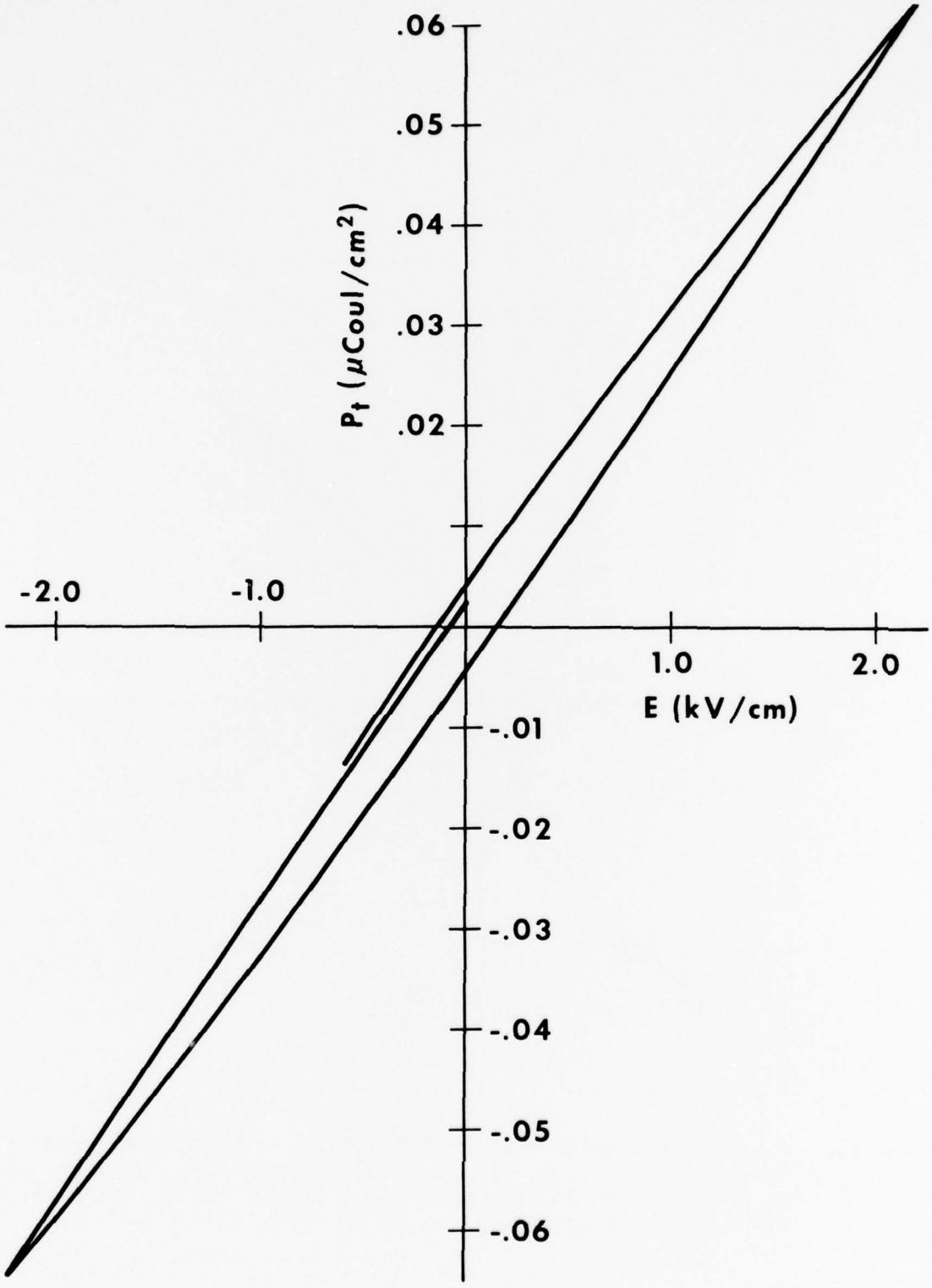

Figure 44. A $P_t(E)$ hysteresis loop for FEL 1150°C at 5 K for small fields. The cycle frequency is approximately 10^{-3} Hz.

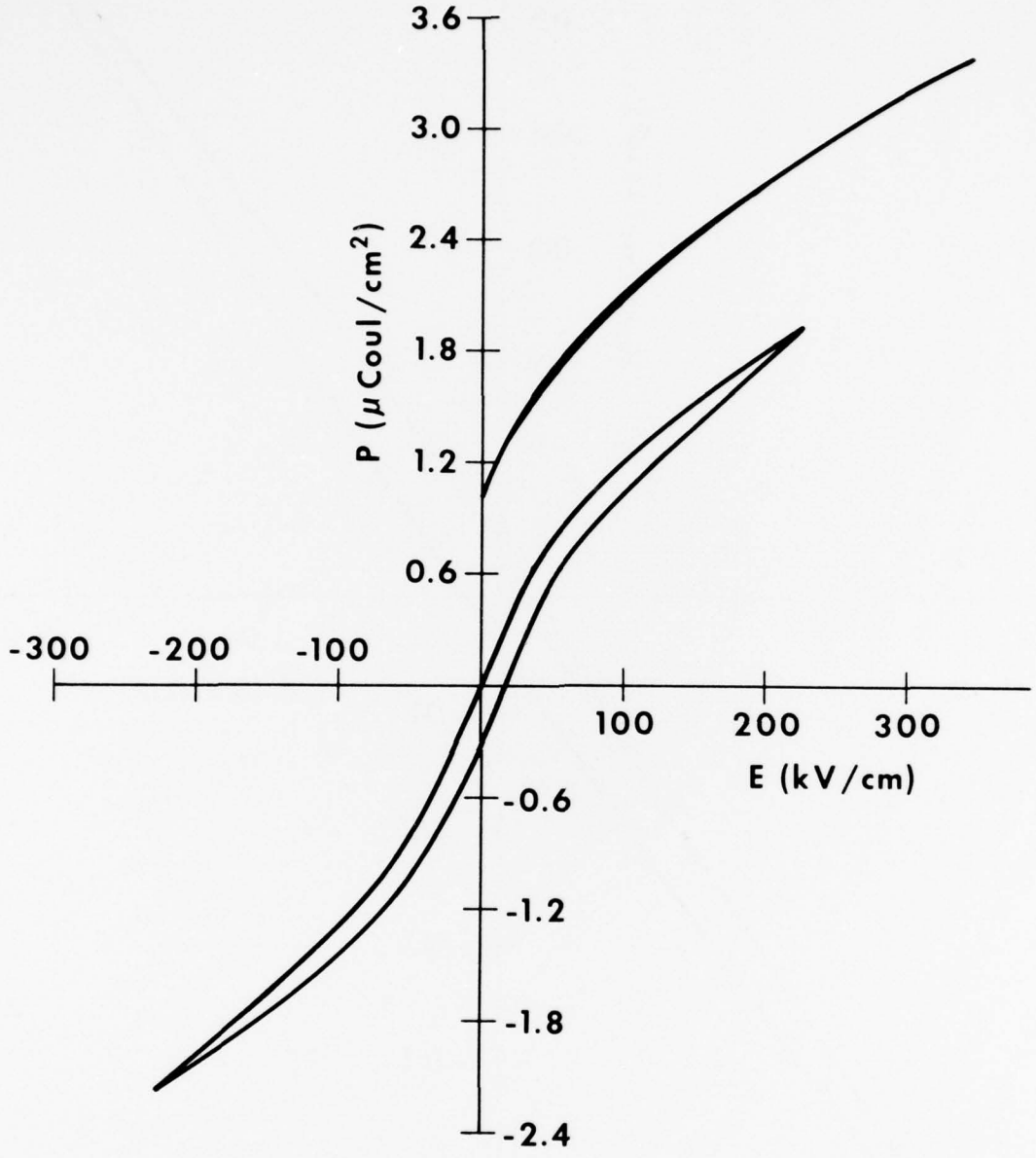

Figure 45. Hysteresis loops of $P_t(E)$ for FEL 1090 at 4 K and high field strengths. The cycle frequency is about 10^{-3} Hz. The upper curve is $P_t(E)$ for cycling E between 0 and maximum field. The zero of the P_t scale is arbitrary.

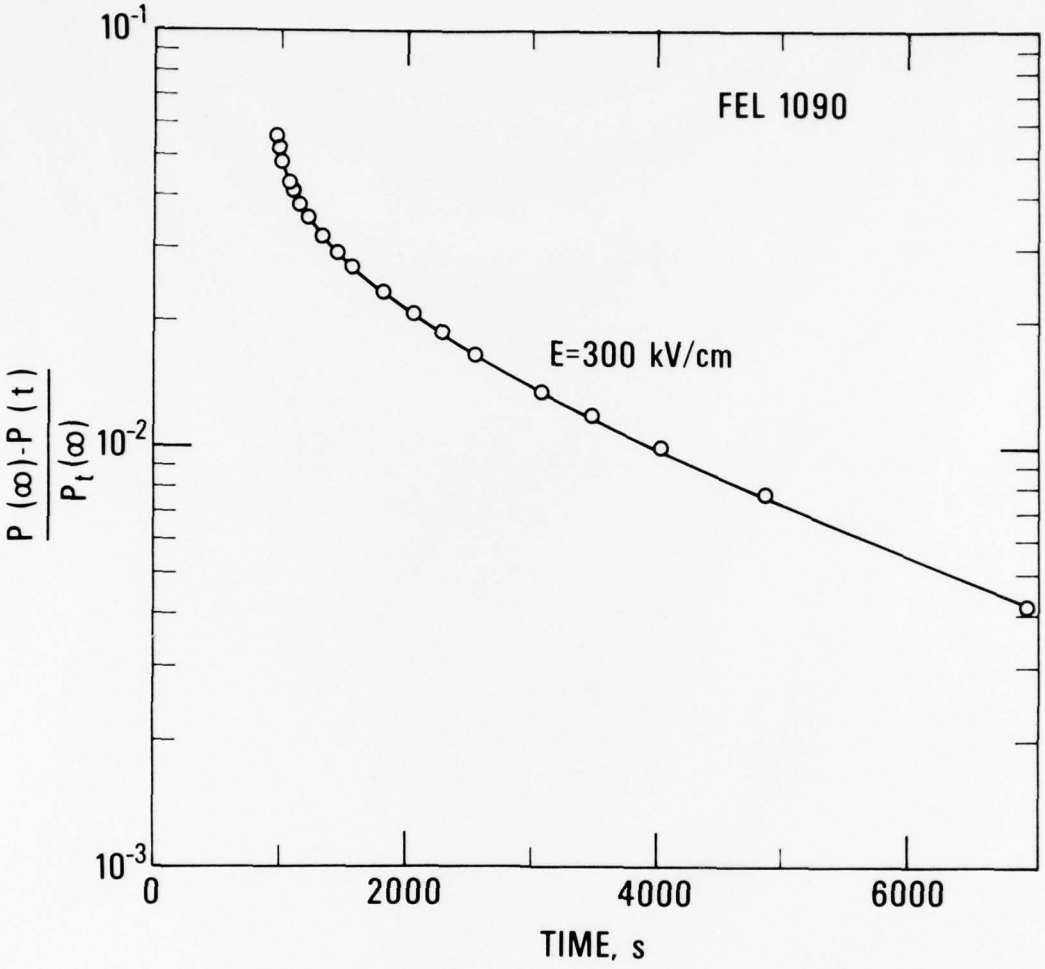

Figure 46. Change of P_t of FEL 1090 with time after increasing the field to 300 kV/cm from 240 kV/cm. The data are plotted as $[P_t(\infty) - P_t(t)]/P_t(\infty)$ where $P_t(\infty)$ is the estimated maximum value of P_t.

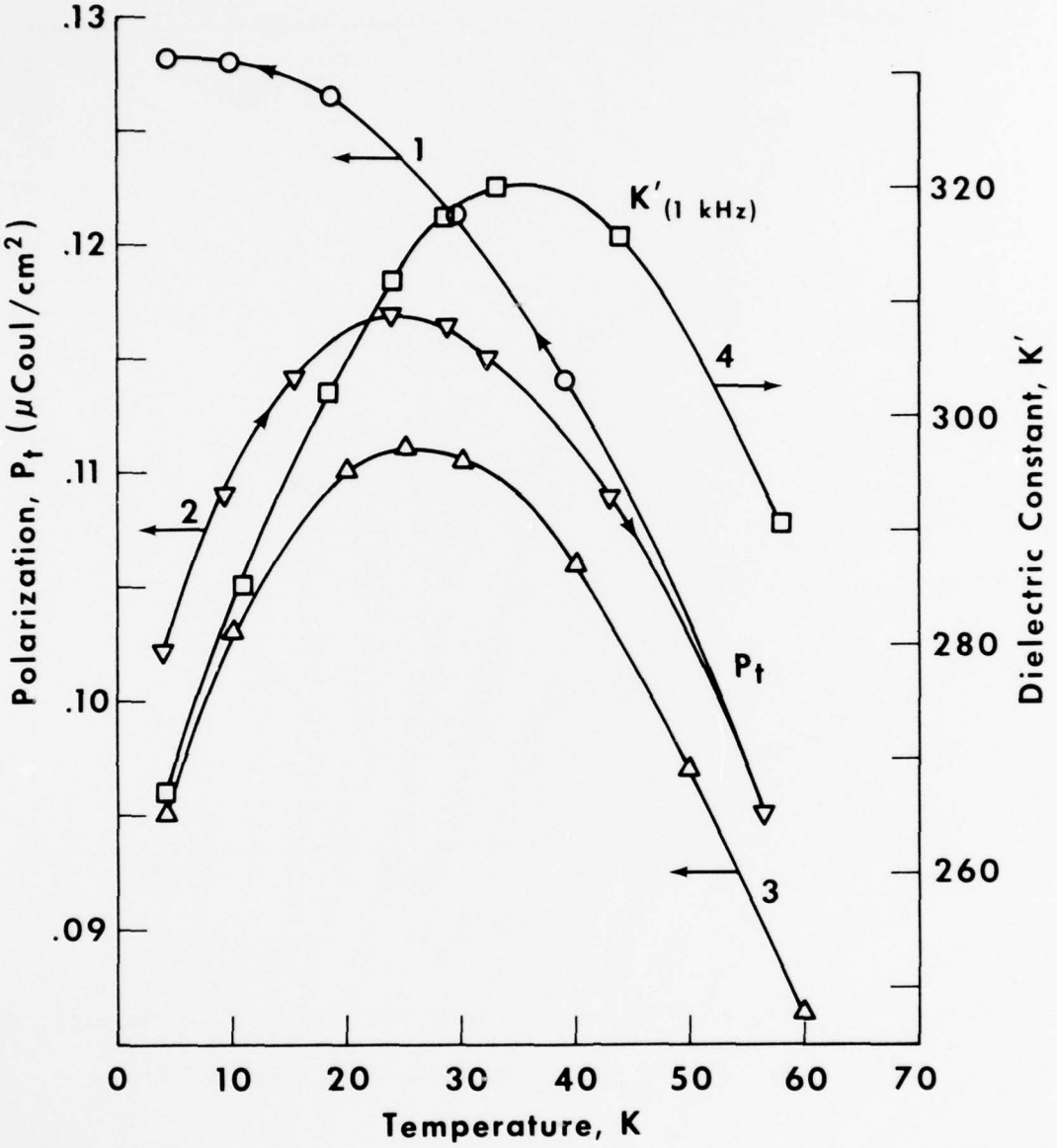

Figure 47. Polarization curves for FEL 1150 in a 3.7 kV/cm field showing the difference in $P_t(T)$ depending on whether the sample is heated from 4 K or cooled to 4 K after the field is applied. Curve 3 is $P_t(T) - P_r(T)$. Curves 2 and 3 are nearly identical in shape. The magnitude of curve 3 is lower by the amount of remanent polarization obtained when the field is applied at 4 K. Curve 4 shows K'(T) at 1 kHz and 0.36 V/cm.

Judging from the results of K'(T) measured for FEL (1090) for four frequencies between 0.01 Hz and 10 kHz, figure 48, the peak in K'(T) for 0.01 Hz could be about 10 K lower than the 1 kHz peak for FEL 1150 bringing it down to the same temperature as the observed peak in $P_t(T)$ warming. The curves of K'(T) of FEL (1090) show obvious dispersion. The loss tangents measured were small and probably dominated by lead losses. Dispersion exists in other glass ceramics as shown by the plot of C as a function of f in figure 49 for a DXO glass ceramic at 3 K.

No cooling is possible in the temperature region where P_t has a positive slope (curve 2 in Fig. 47) since the field must be applied to cause cooling, but the $P_t(T)$ curve would then follow a negative slope curve similar to curve 1. Only adiabatic depolarization cooling is possible since $P_t(T)$ always has a negative slope when the material is cooled. Such behavior is consistent with the electrocaloric measurements.

Specific heat: The zero field specific heat of an unelectroded FEP sample cerammed at 1100°C is shown in figure 50. Specific heat measurements between 3 and 5 K on an unelectroded FEL sample cerammed at 1100°C gave essentially identical results as the FEP sample. This figure also shows the specific heat of a glass, fused SiO_2, and the specific heat of a single crystal $SrTiO_3$. The single crystal $SrTiO_3$ specific heat curve is from unpublished data by J. H. Colwell of NBS, Washington. The FEP glass-ceramic is approximately 50% $SrTiO_3$ and 50% glass phase, though the glass phase is an alumino silicate rather than fused SiO_2. The specific heat of the FEP glass-ceramic appears consistent with what would be expected of a mixture of $SrTiO_3$ and glass. The data show no indication of an anomaly in the range 3-20 K. A transition from an antiferroelectric state (or ferroelectric state) to a paraelectric state would give rise to a peak in the specific heat at the transition temperature. Such peaks are usually spread out somewhat in temperature, but the specific heat of FEP at 20 K shows no apparent indication of any approaching peak at 33-40 K. The possibility of a sharp peak at 33-40 K cannot be ruled out until zero field specific heat data are obtained in that temperature range.

The specific heats of the two FEL samples used in the electrocaloric effect experiments were measured at 4.4 K as a function of electric field. For an electric field of 220 kV/cm the specific heat decreased less than about 5% compared with the zero field specific heat. Thus the change in entropy at 4 K with electric field is also probably less than about 5%. From eq. (3.4) it can be seen that a decrease of C_E with electric field implies $\partial^2 P/\partial T^2 < 0$. A negative value of $\partial^2 P/\partial T^2$ at 4 K is also seen in the polarization measurements.

Thermal conductivity: The results of thermal conductivity measurements on several different glass-ceramics are shown in figure 51. The results are typical of values seen in glass or some plastics. Results on fused SiO_2 are also shown in figure 51. The amount of glass phase decreases from FEP to FEO to Code 9658. These results suggest that the ceramic component contributes significantly to the thermal conductivity above about 7 K. Though the thermal conductivity values are low in comparison with metals or single crystal dielectrics, the values are sufficiently high that thermal equilibrium times in thin sections between electrodes are much less than 1 second.

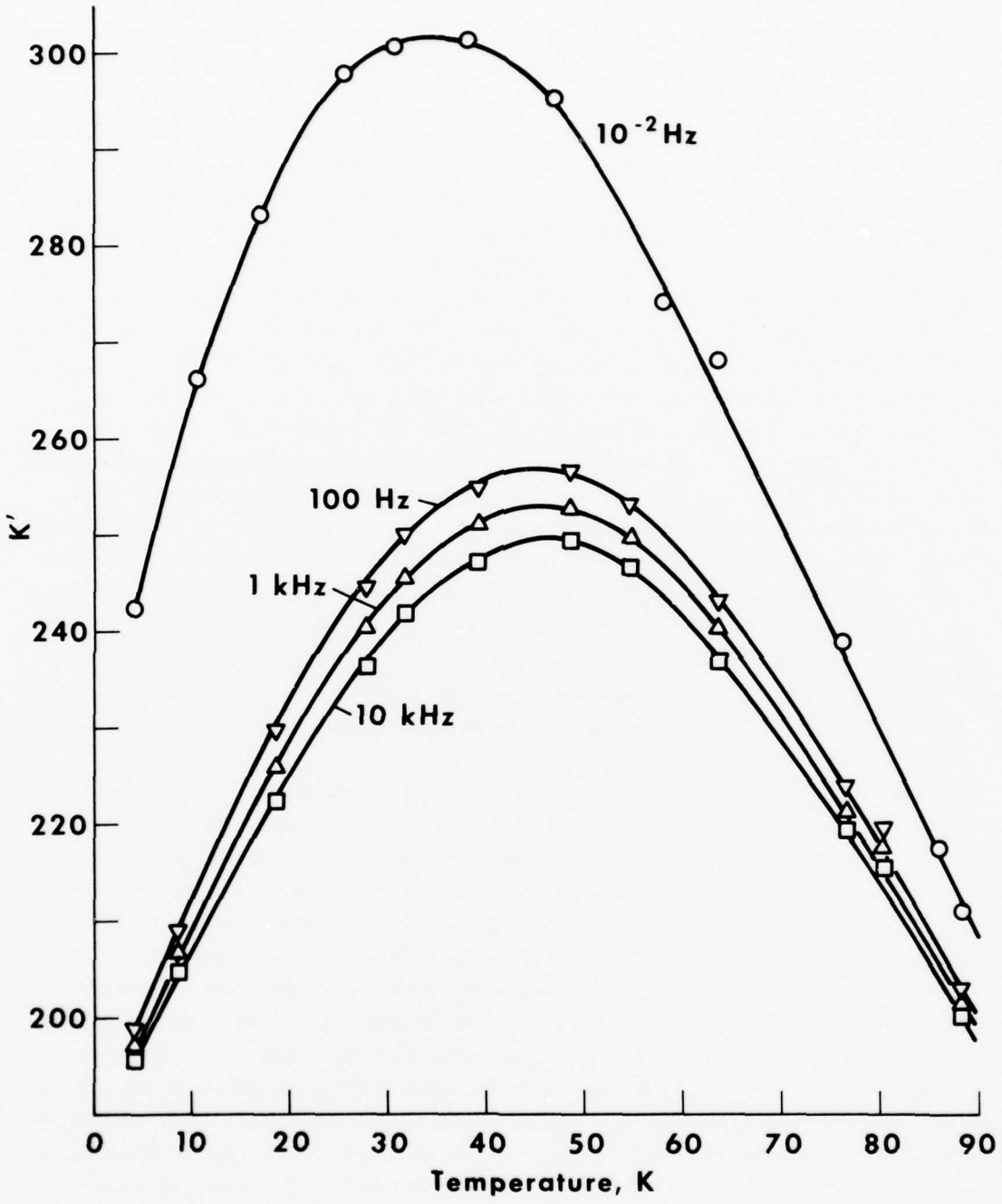

Figure 48. Curves of K'(T) at 4 frequencies between 0.01 Hz and 10 kHz for FEL 1090. E = 3.6 kV/cm max. at 0.01 Hz and 0.036 kV/cm max. at the higher frequencies.

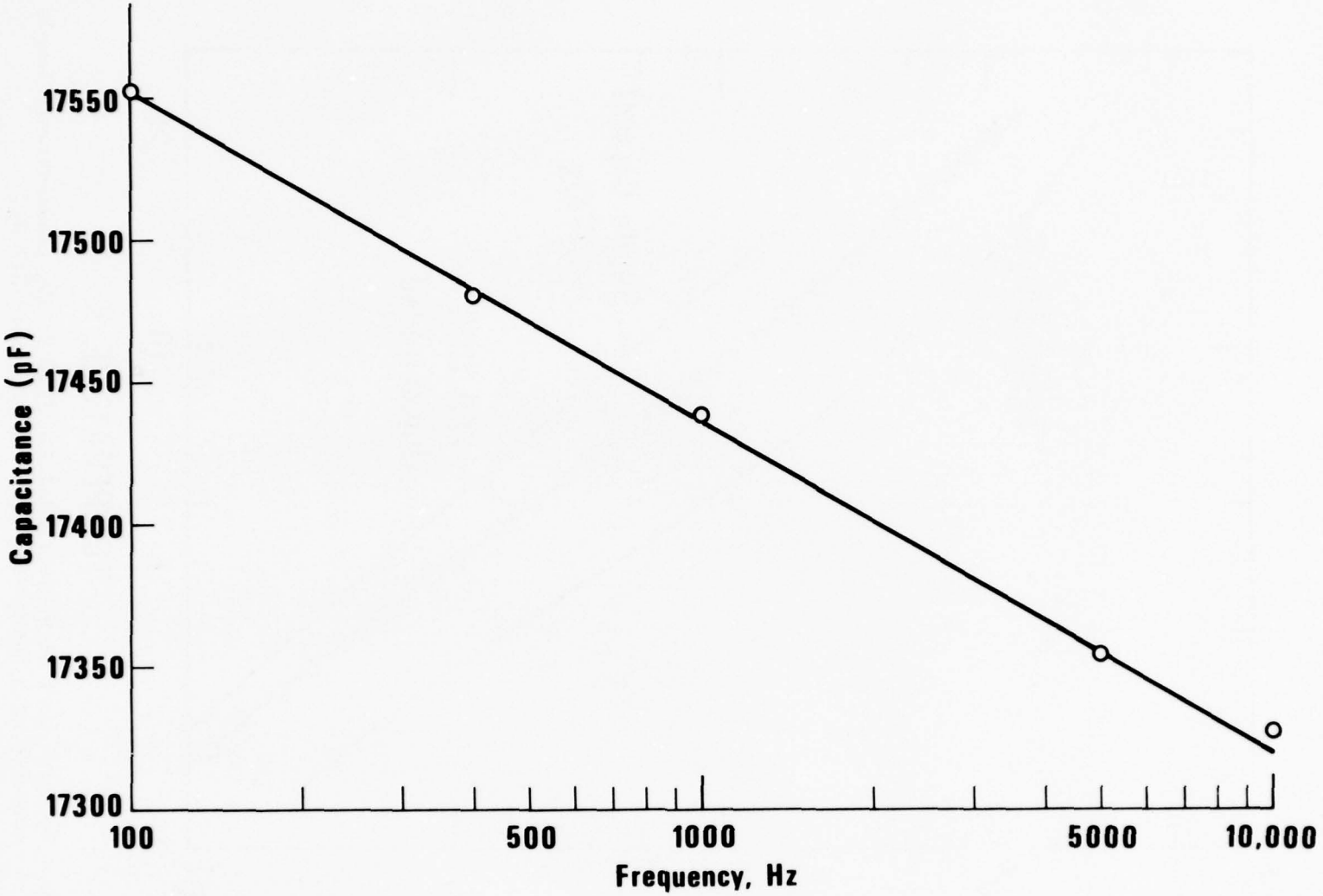

Figure 49. Capacitance of a DXO glass ceramic at 3 K as a function of measuring frequency.

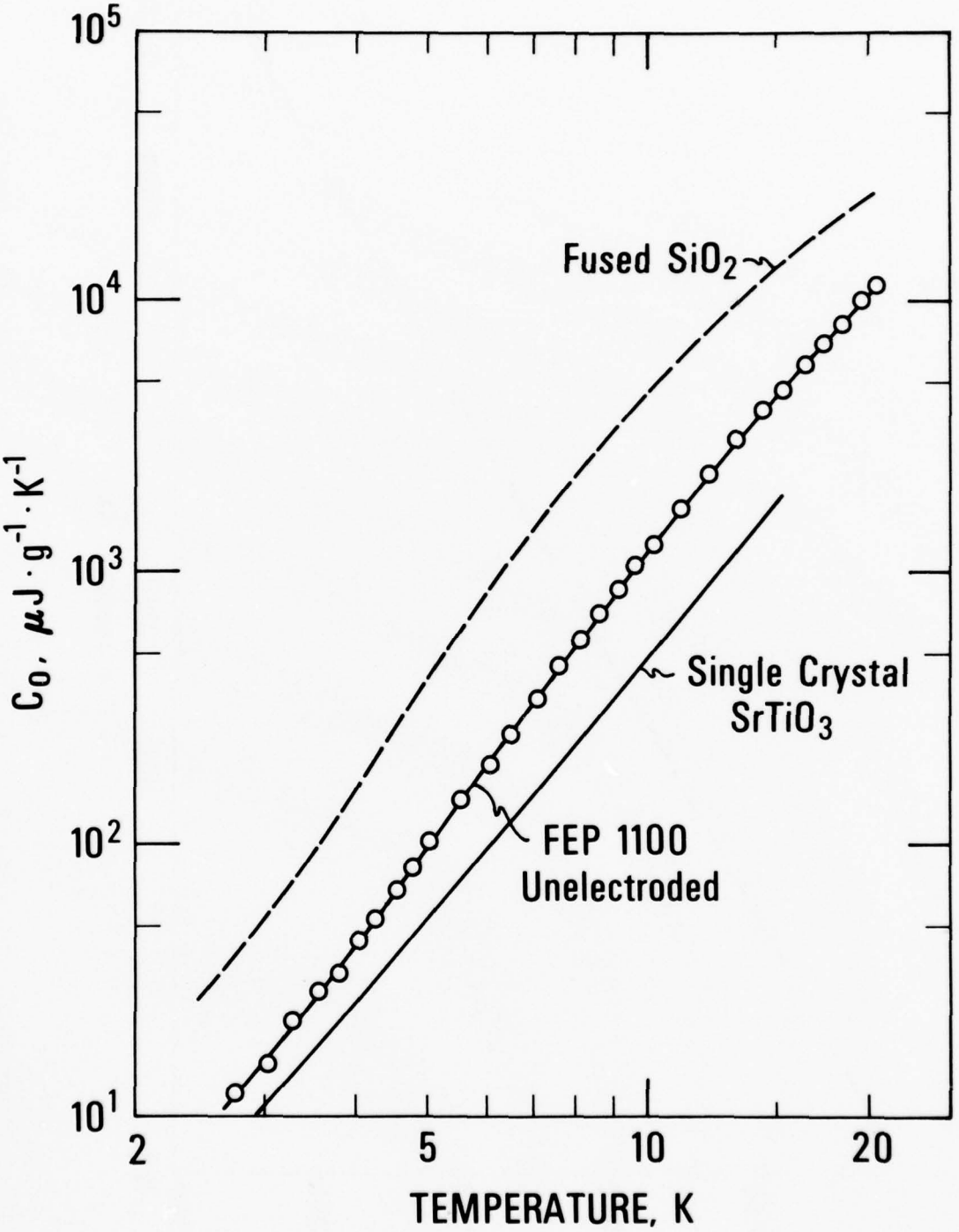

Figure 50. Specific heat of unelectroded FEP 1100 $SrTiO_3$ glass-ceramic sample compared with fused SiO_2 and single crystal $SrTiO_3$.

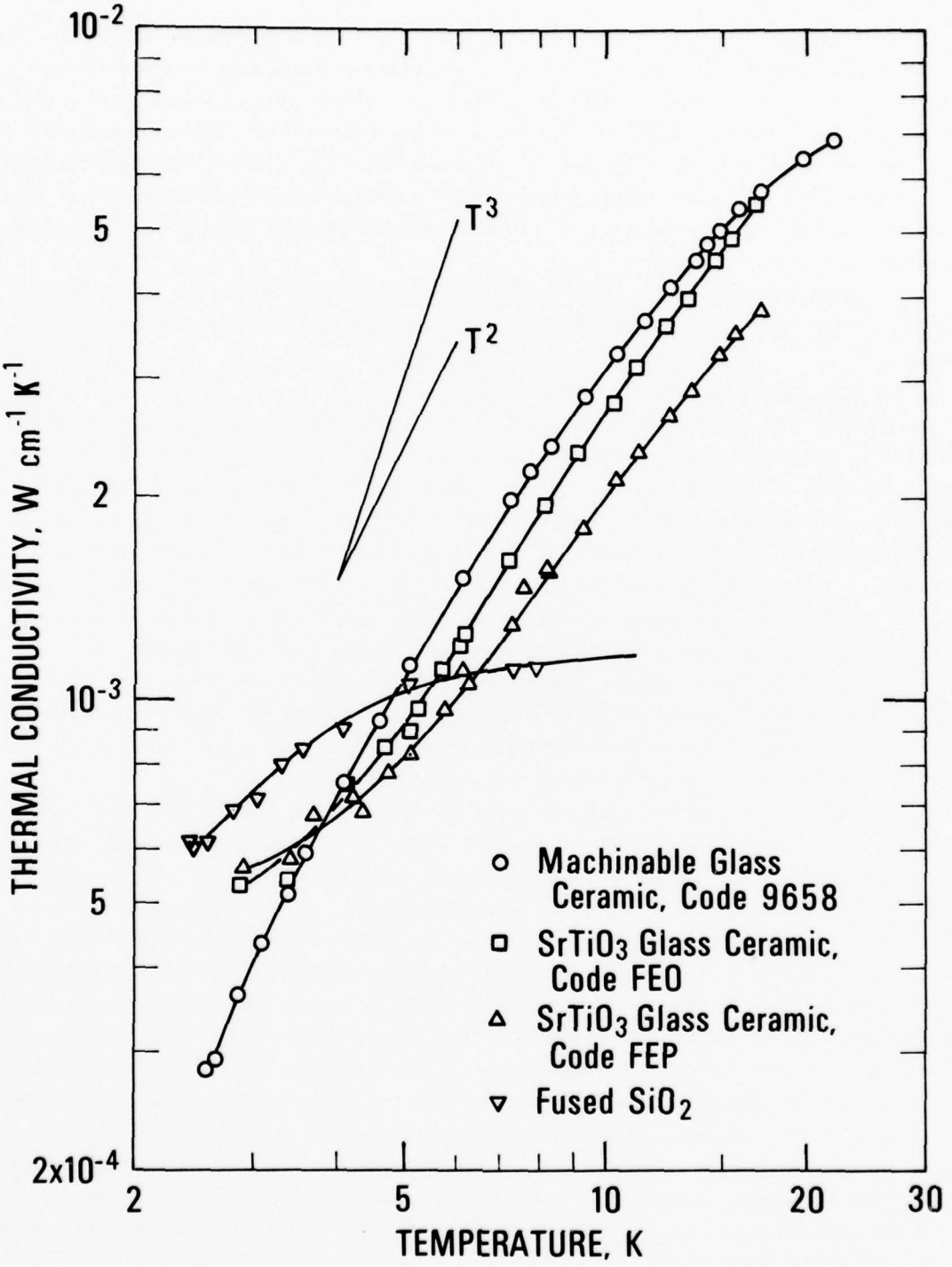

Figure 51. Thermal conductivity of three different Corning Glass Works glass-ceramics as compared with fused SiO_2. The slopes for T^2 and T^3 are shown in the graph for visual comparison.

3.7.2. $KTaO_3$ Glass-Ceramics

Large crystallization yields of $KTaO_3$ were realized in the glass-ceramic system K_2O-Ta_2O_5-Al_2O_3. The dielectric constants and their temperature derivatives were measured for three different compositions, 75%, 80%, and 85% $KTaO_3$. The 80% composition had nearly an order of magnitude higher K' and $\partial K'/\partial T$ as the other two compositions. This composition gave K' and $\partial K'/\partial T$ at 4 K of 731 and 9.4 K^{-1}, respectively. The dielectric constant reached a peak of about 800 at a temperature of 19.6 K. The behavior is thus qualitatively the same as that of the $SrTiO_3$ glass-ceramics. The loss tangent of 0.006 is quite low for this type of research sample.

Polarization measurements on these samples were not possible due to the low dc resistance ($< 10^{12}$ Ω). Likewise reliable electrocaloric measurements could not be made on such samples.

3.7.3. Single crystals

The difficulties in growing single crystals would make the proposed refrigerator more difficult but not necessarily impractical. A study of some single crystals was done to better understand the fundamentals of the dielectric behavior. In the case of the $SrTiO_3$ glass-ceramics, measurements of $P_t(T)$ showed that $\partial P_t/\partial T$ approaches zero well above 4 K. Thus cooling at 4 K would not be expected, in agreement with the actual electrocaloric measurements. Polarization measurements are much easier to make than electrocaloric measurements, thus many of the subsequent materials were tested only by polarization. A material with a relatively large $\partial P_t/\partial T$ at 4 K would then be a good candidate for cooling.

$KTaO_3$: A $KTaO_3$ single crystal obtained from Dr. Lou Grabner, NBS Washington, was first tried in the $P_t(T)$ apparatus and found to be conducting over the temperature range of interest. All the measurements presented below for a single crystal were made on a single crystal obtained from Dr. George Samara of Sandia Corporation.

In figure 52, $P_t(T)$ and $P_r(T)$ are shown for the $KTaO_3$ single crystal from 77 to 2 K at fields of 0.25, 0.84, and 4.05 kV/cm. The polarizations again are normalized to $P_t = 1.0$ at 4 K. The data were taken without warming the crystal above 77 K after the initial cooldown. Some hysteresis curves were run before the data for curves 2 and 3 were taken, then 2 and 3 were measured using the opposite polarity from 1. The application of a high field before measuring the remaining two $P_t(T)$ curves is most probably responsible for the relationship of the P_{rN} curves and the fact that P_{tN} is higher at 77 K. In any case, there is a fairly large remanent in this crystal also. There would be maxima in ITC,[78] the ionic thermal current, which is proportional to $\partial P_r/\partial T$, in the 13 to 18 K range, unlike the glass ceramics in which any ITC maximum appears to be below 4 K. The hysteresis was measured at 4 K at about 0.001 Hz. The loop was wide initially then closed down by a factor of 6 after two cycles. No saturation effects were evident at either 4 or 77 K, figures 53 and 54, and only a very slight hysteresis appears at 77 K. Hysteresis was measured when the field on the crystal was cycled between 0 and 3 kV/cm in figure 55. This loop opens more than the similar loop for the FEL glass ceramic.

The change in temperature of the crystal estimated from $P_t(T)$ for a field reduced from 15 kV/cm to 0 at 10 K is $\Delta T = 0.26$ K. This can be compared to the measured value of about 0.3 K, which is discussed below.

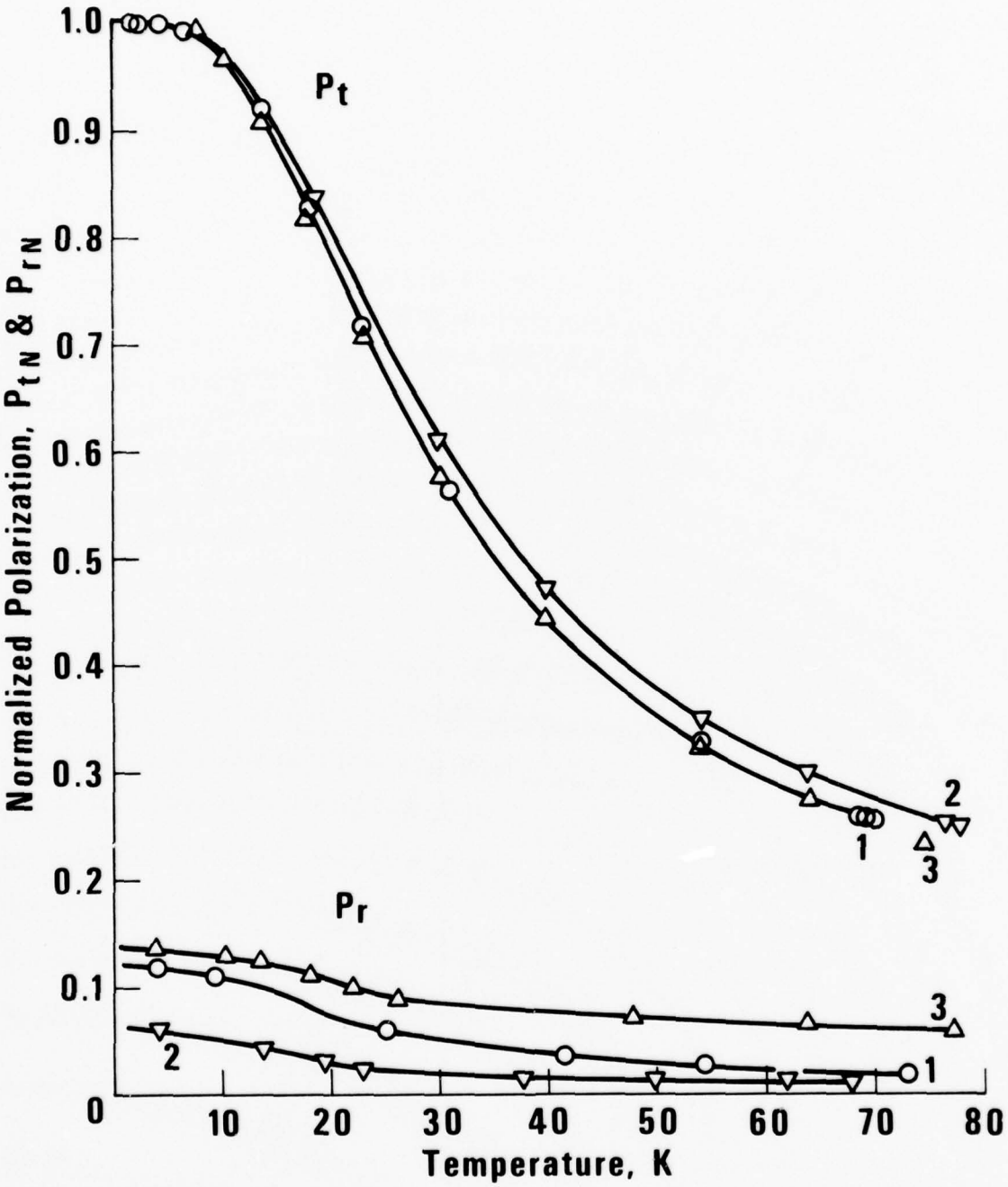

Figure 52. Polarization temperature curves for the $KTaO_3$ single crystal for various applied fields.

Curve 1, P_t(4 K) = 0.076 μcoul/cm^2, E = 0.25 kV/cm;
Curve 2, P_t(4 K) = 0.23 μcoul/cm^2, E = 0.84 kV/cm;
Curve 3, P_t(4 K) = 1.27 μcoul/cm^2, E = 4.05 kV/cm.

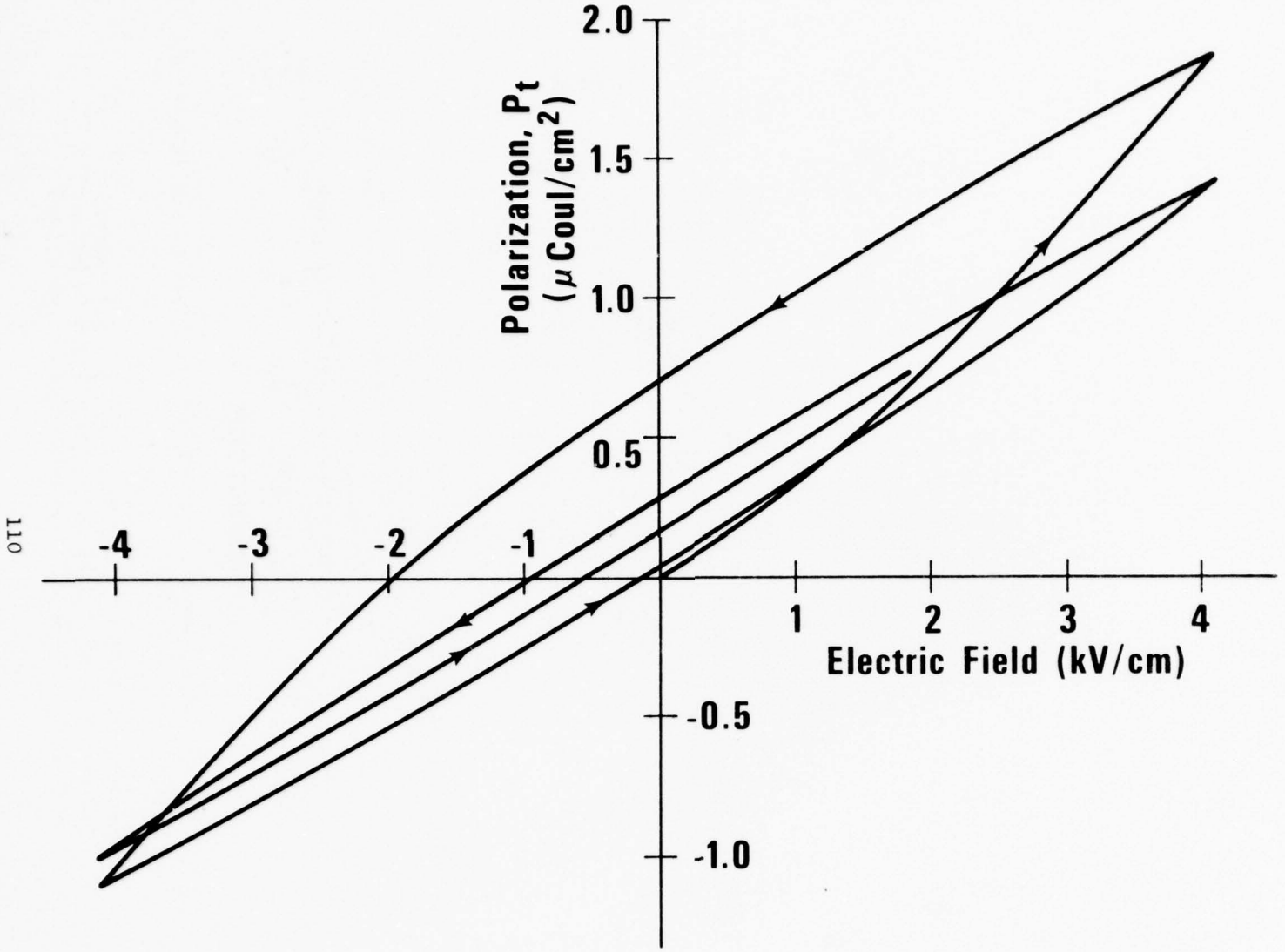

Figure 53. $P_t(E)$ hysteresis curve for $KTaO_3$ single crystal at T = 4 K and 10^{-3} Hz. The enclosed area shrinks as the loop is repeated.

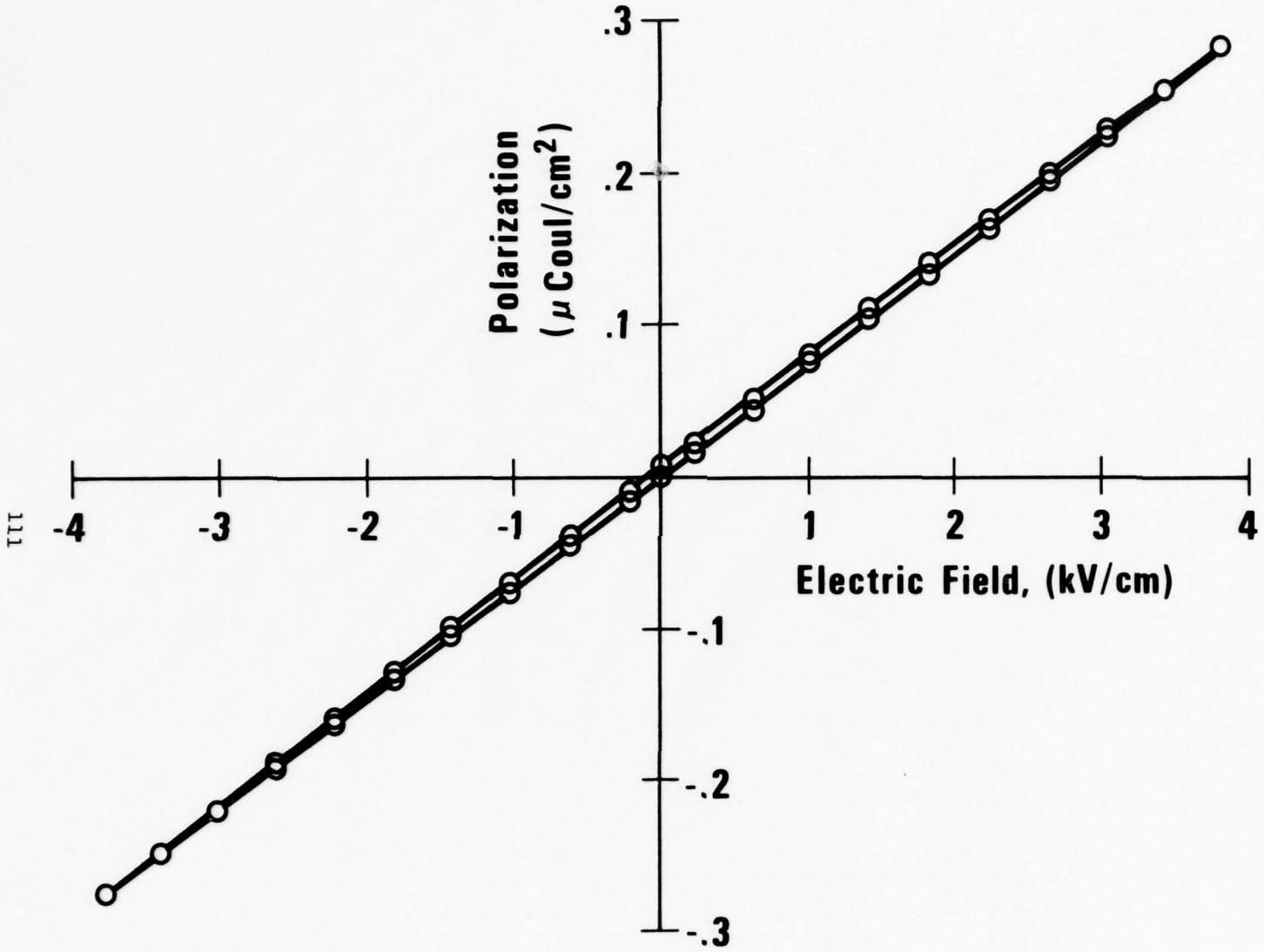

Figure 54. A $P_t(E)$ hysteresis loop for $KTaO_3$ at 77 K and 10^{-3} Hz.

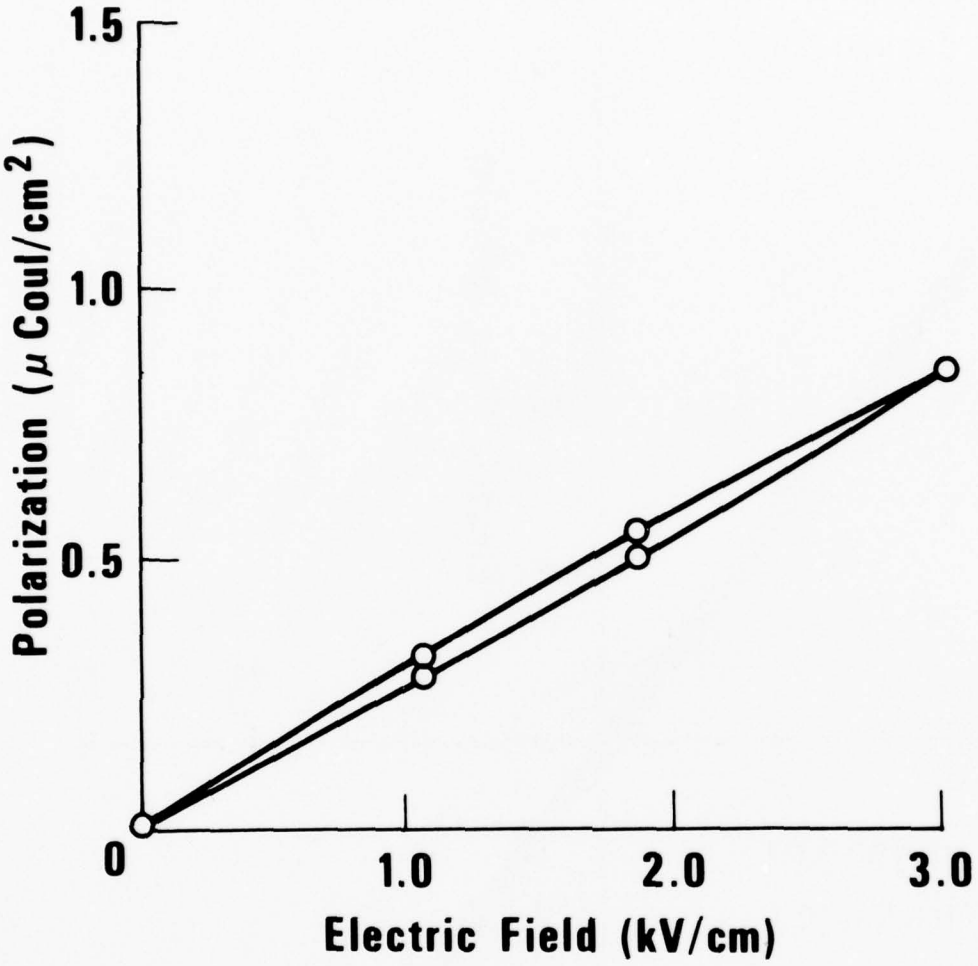

Figure 55. A $P_t(E)$ hysteresis loop for $KTaO_3$ for fields between 0 and +3 kV/cm at 4 K.

Results of the electrocaloric measurements on the same $KTaO_3$ single crystal are shown in figure 56 as a function of temperature. The results are separated into the hysteretic and reversible electrocaloric components. Addenda corrections have not been made for this data, but such a correction could give intrinsic values about twice that shown. Figure 57 shows the same data as a function of electric field at T = 10 K. These electrocaloric effects are considerably larger than those seen in the $SrTiO_3$ glass-ceramic and about comparable to published values for single crystal $SrTiO_3$.

The specific heat of the $KTaO_3$ single crystal was measured with the results shown in figure 58. A rapid increase in C/T^3 is observed from 2 K to 8 K, but such behavior is quite typical of many solids in this temperature range.[79] Both adiabatic and pulse methods were used as described in section 3.6.2. The agreement between the two methods serves as a check on the accuracy. The results are expected to be accurate to about 5%.

TlBr and TlCl: The dielectric constants of TlBr, TlCl, and TlI were measured by Samara[80] between 76 and 400 K. All three materials show very similar behavior of the dielectric constant, which increases with a decrease in temperature. At 76 K and below values of $\partial K'/\partial T$ are the order of $-0.02\ K^{-1}$ compared to about $-80\ K^{-1}$ for $SrTiO_3$. Measurements in this laboratory on TlCl between 0.015 and 10 K show that the dielectric constant levels off and becomes independent of temperature below about 3 K. The dielectric constant of TlBr is expected to behave the same way in that temperature range. Such behavior is typical for a material which remains paraelectric at all temperatures down to 0 K.

The electrocaloric effect in both TlCl and TlBr were undetectable. This was to be expected because of the small value of $\partial K'/\partial T$. The specific heat of each of these materials was measured between 2 and 20 K. The results for TlBr are shown in figure 59 and are similar to that of TlCl. The peak in C/T^3 is typical of most solids and will be discussed more in section 3.8.

3.7.4. Ceramics

$SrTiO_3$ and solid solutions: The polarization as a function of temperature was measured for various $SrTiO_3$ ceramics. Curves of $P_t(T)$ and $P_r(T)$ are shown in figure 60. The slope, $\partial P_{tN}/\partial T$, of the $KTaO_3$ single crystal is larger over the whole region below 40 K, though $\partial P_t/\partial T$ of $SrTiO_3$ ceramics is larger by virtue of a higher value of P_t at 4 K. Unfortunately, $\partial P_t/\partial T$ is essentially zero at 4 K and so refrigeration at 4 K is not possible. All the materials show a remanent though the temperature dependencies vary somewhat. The unique feature of P_r of the $SrTiO_3$ ceramics is that in three cases, P_r apparently changed sign.

A partial hysteresis loop for a $SrTiO_3$ ceramic at 4 K is shown in figure 61. The material seems to be less prone to breakdown than the $KTaO_3$ single crystal so data could be taken to higher fields. The first time the fields were applied momentary breakdowns appeared at 14 and 24 kV/cm as shown. Subsequent cycles showed no further discontinuities. The hysteresis loops for E between 0 and +30 kV/cm had small areas such as observed in the glass ceramics.

Electrocaloric measurements were made on sample ST2(1450). The hysteretic heating component and the reversible electrocaloric component were separated from the results and shown in figures 62 and 63. The reversible electrocaloric component for this $SrTiO_3$ ceramic

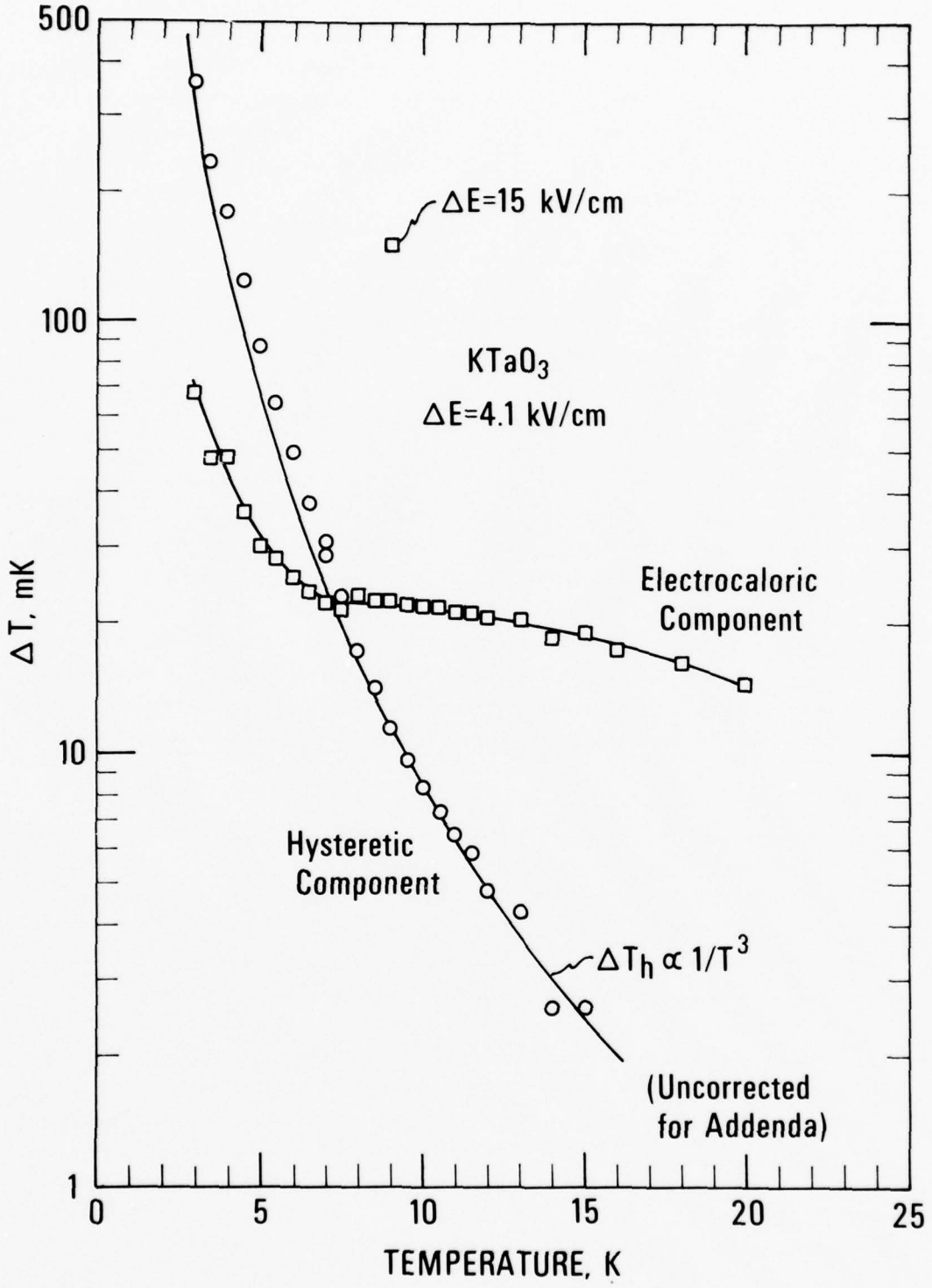

Figure 56. Electrocaloric and hysteretic effects in $KTaO_3$ single crystal for a field change of 4.1 and 15 kV/cm.

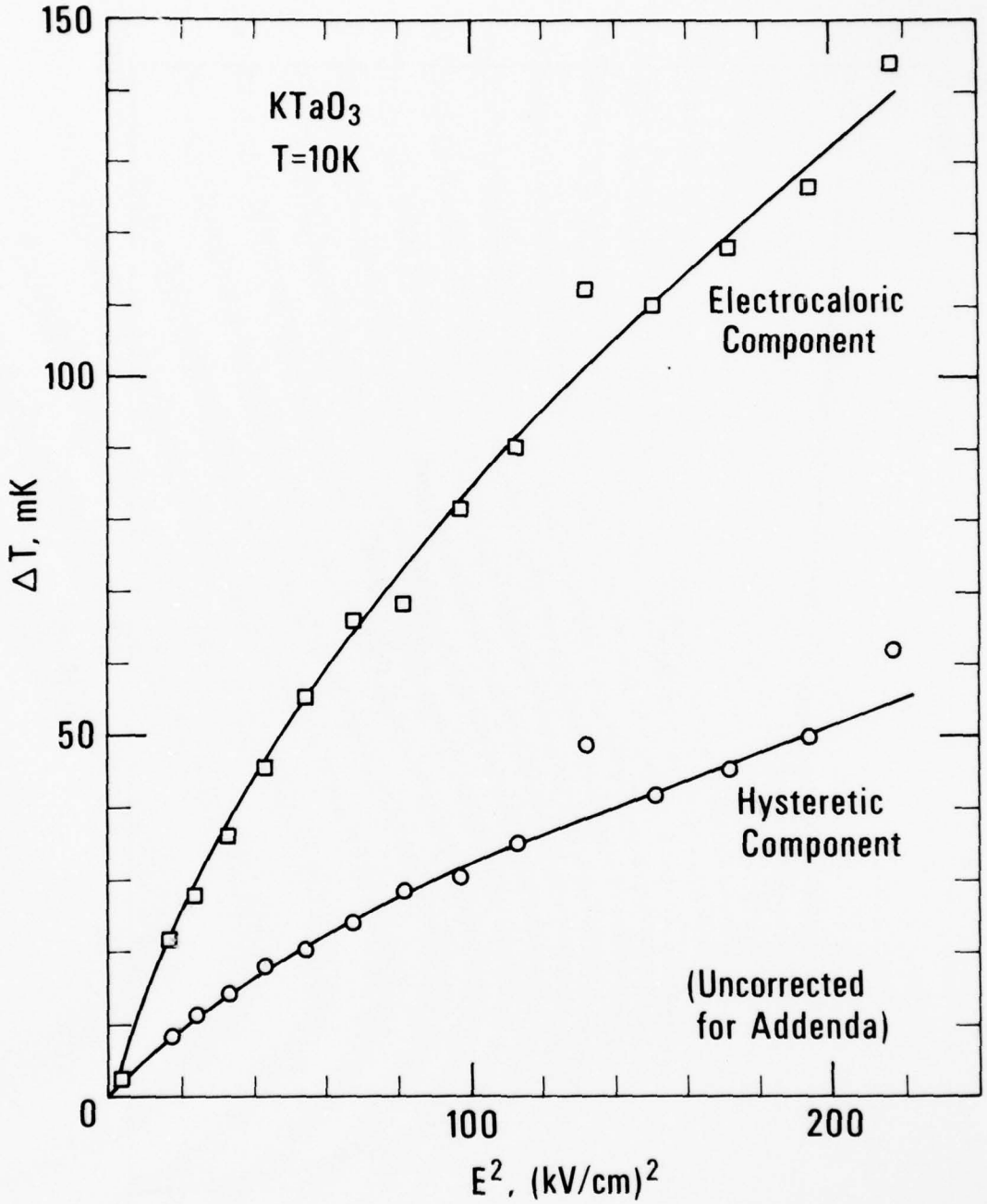

Figure 57. Electrocaloric and hysteretic effects in $KTaO_3$ single crystal at 10 K as a function of electric field change.

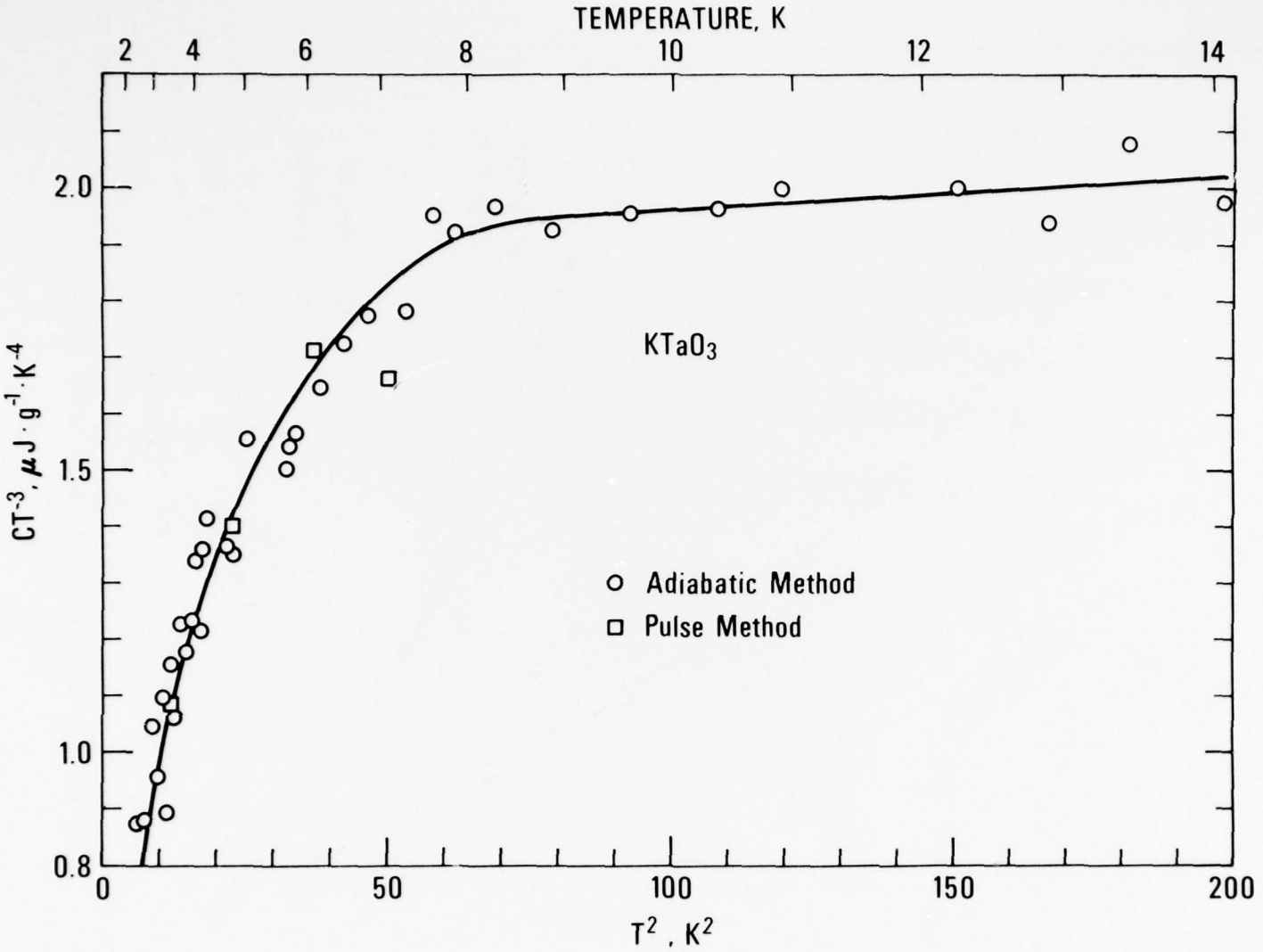

Figure 58. Specific heat of $KTaO_3$ single crystal between 2 and 14 K.

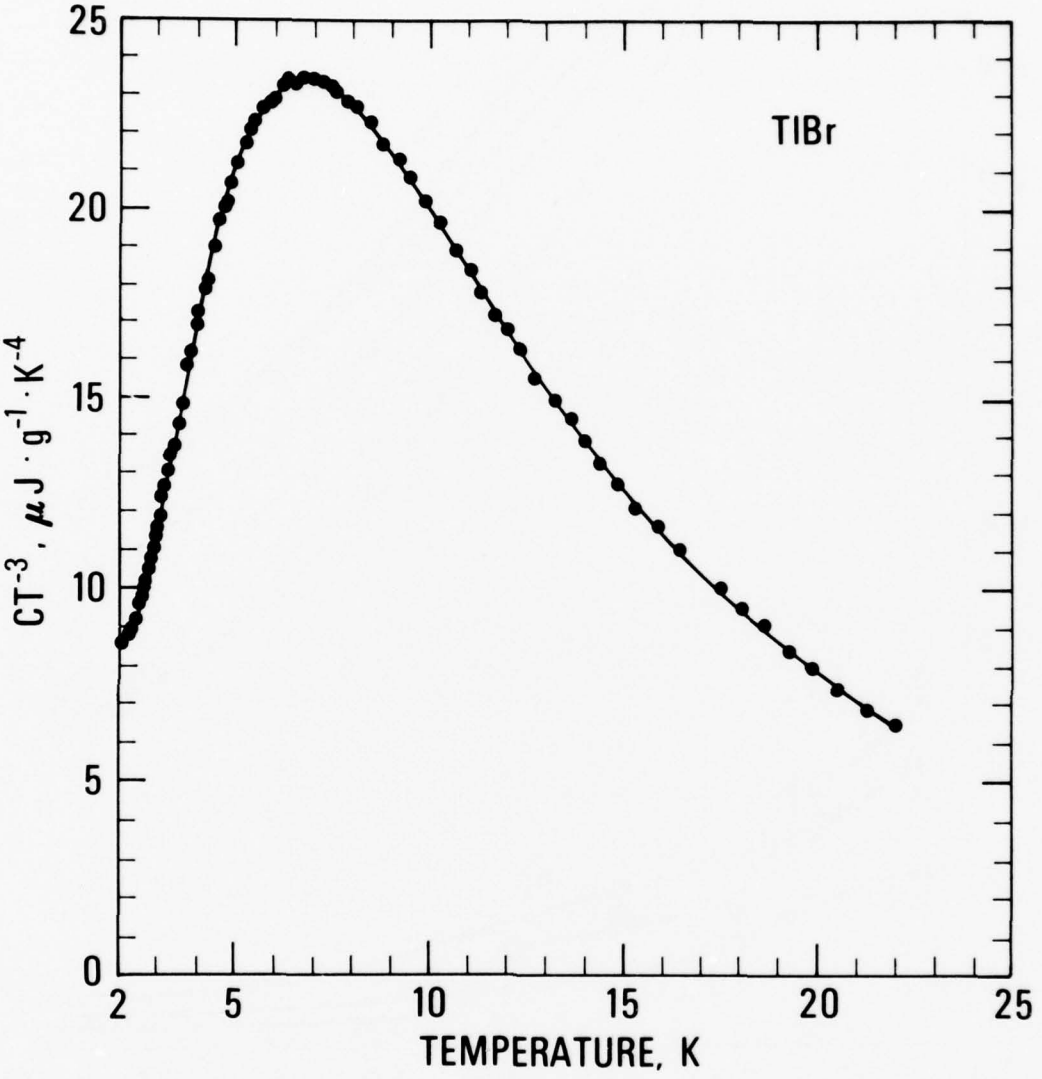

Figure 59. Specific heat of TlBr single crystal between 2 and 22 K.

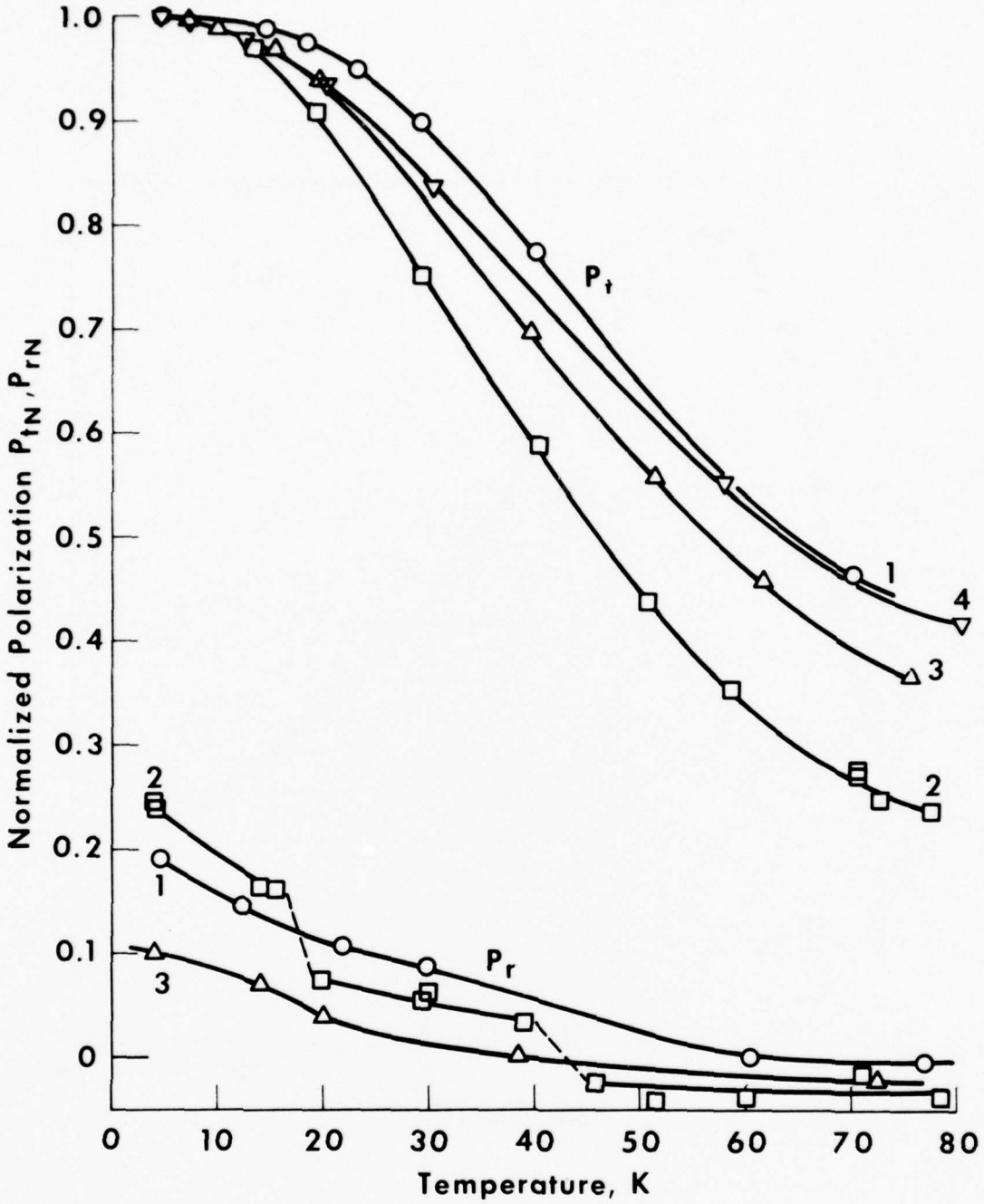

Figure 60. $P_t(T)$ and $P_r(T)$ curves for various $SrTiO_3$ ceramic samples.

Curve No.	Specimen	E (kV/cm)	P_t(4 K) (μCoul/cm^2)	P_t(4 K)/E (μCoul/kV cm)
1	Commercial grade	0.53	0.21	0.40
2	ST2 (1450)	0.46	0.33	0.71
3	ST2 (1350)	0.39	.064	0.16
4	ST3 (1450)	0.34	.068	0.20

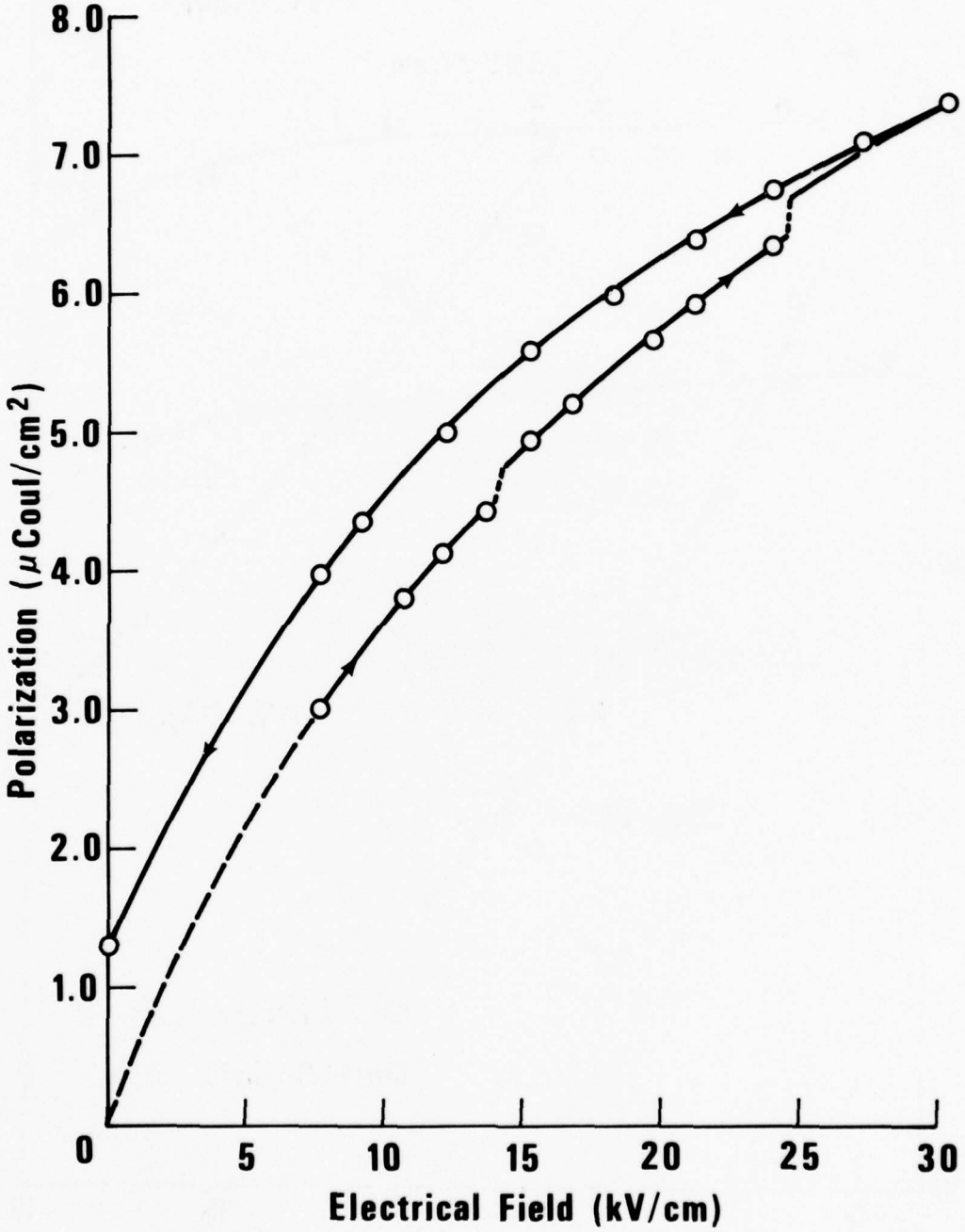

Figure 61. A partial $P_t(E)$ hysteresis loop for $SrTiO_3$ ceramic ST2 (1450) over the field range 0 to +30 kV/cm. Discontinuities are due to momentary charge leakage or breakdowns.

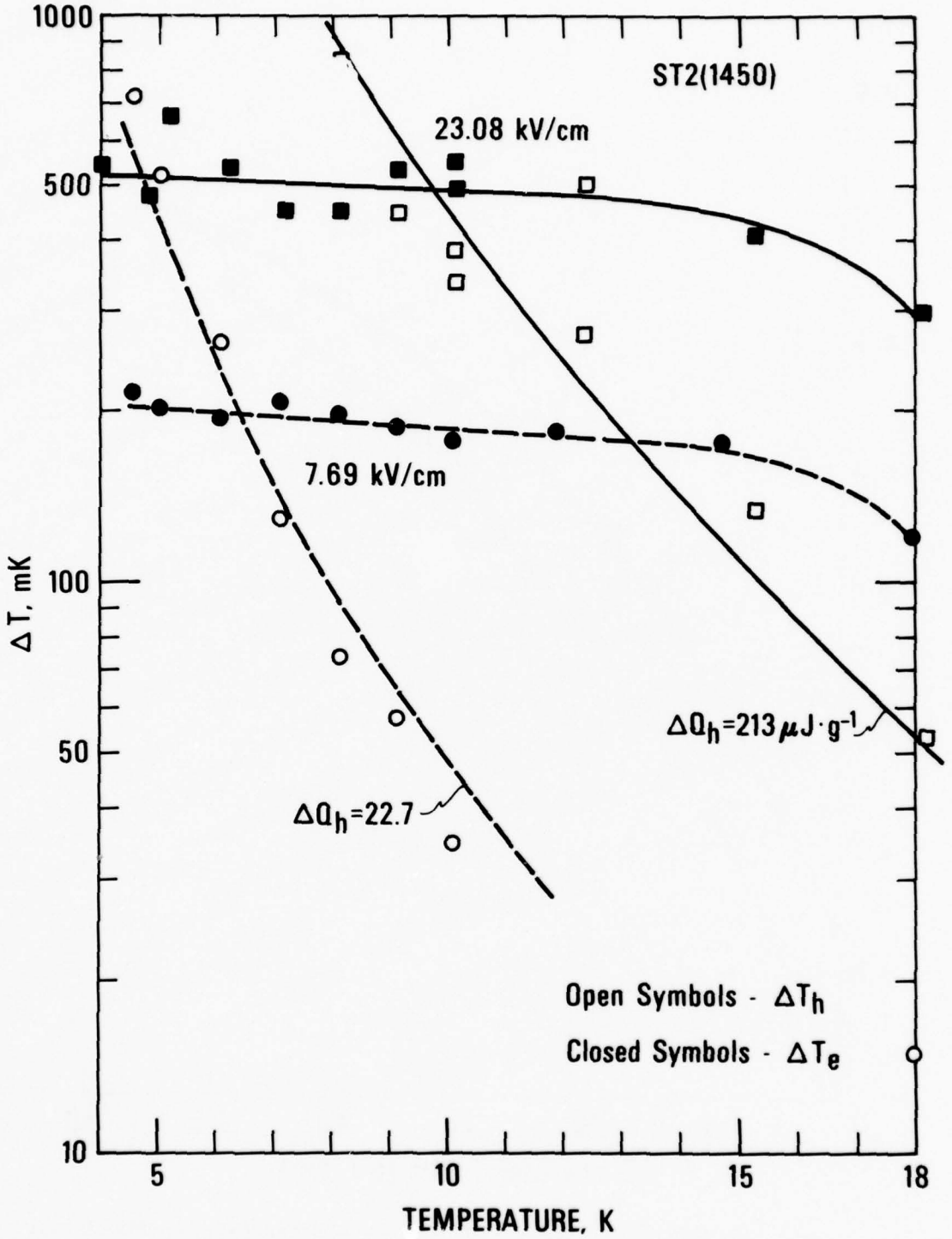

Figure 62. Electrocaloric and hysteretic effects in $SrTiO_3$ ceramic as a function of temperature for two different values of field change.

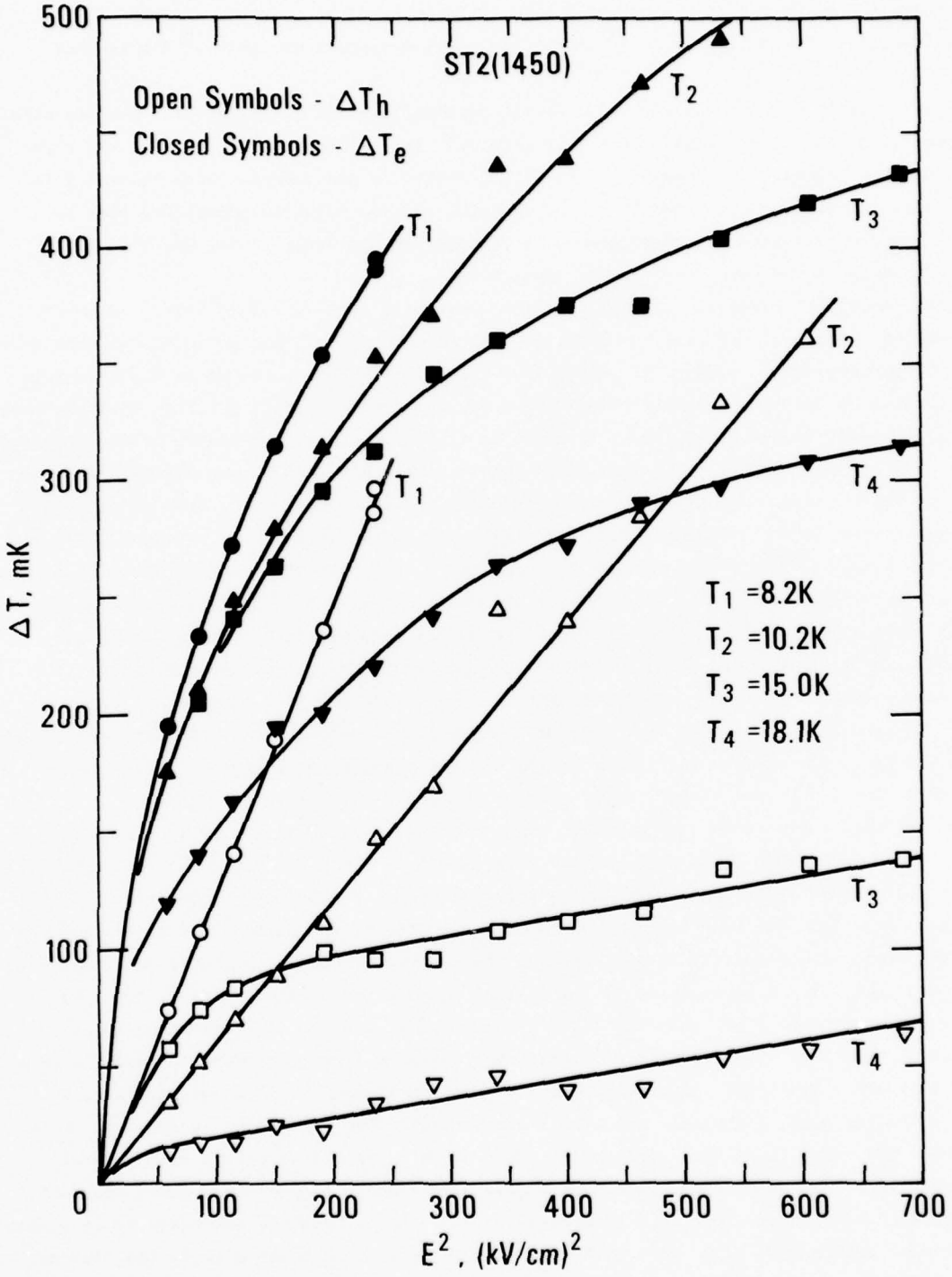

Figure 63. Electrocaloric and hysteretic effects in $SrTiO_3$ ceramic as a function of electric field change for several temperatures.

is somewhat larger than that seen in $KTaO_3$ single crystal, as predicted by the polarization results. Total cooling effects of about 0.1 K were seen at 10 K. Without the hysteretic component, a cooling effect of about 0.5 K would be expected at 10 K for a field of 23 kV/cm. Because of the hysteretic component, no cooling appears possible at 4 K in this sample.

The specific heat of the ST2(1450) $SrTiO_3$ ceramic is shown in figure 64. For the sake of comparison, the specific heat of single crystal[81] and polycrystal[82,83] $SrTiO_3$ are also shown in this figure. The reason for the slight upturn in the ceramic curve below 4 K is not clear, but it could be a result of the specific heat of metallic impurities such as iron. The impurity level in this ceramic is probably on the order of 1%, which is large enough to account for the upturn in the specific heat.

Also shown in figure 64 are specific heat curves for vanadium doped $SrTiO_3$ ceramics. This doping appears to increase the specific heat to some extent, though anomalous effects begin to dominate below about 4 K. The higher specific heat of the vanadium doped samples could mean a higher entropy would be available for refrigeration at 4 K. That would be true only if the additional specific heat is electric field sensitive. Polarization measurements would be able to indicate if the additional specific heat and entropy are field dependent.

The $SrTiO_3$ ceramics containing various amounts of SrV_2O_6 or $SrNb_2O_6$ show dc polarizations that have less T dependence than nominally pure $SrTiO_3$ ceramics. Curves of $P_t(T)$ are shown in figure 65 for STV(10) and STV(20) compared to nominally pure $SrTiO_3$ and in figure 66, curves for STN(10), STN(20) and STN(30) are shown compared to a nominally pure $SrTiO_3$ ceramic made at the same T. A couple of points on the remanent curve for a few of the samples were measured. The STV(10) and STN(30) specimens have very large remanents. The polarization measurement was repeated a second time for STV(10) to measure P_r in more detail. The results are plotted in figure 65 along with the earlier data. The temperature at which the field was applied was higher in the earlier measurement so both P_t and P_r were reduced at 4 K. The fact that P_r seems to drop below 0 will be discussed later.

Hysteresis curves were then measured for the STV(10) sample at 4 K, 39.4 K and 70 K, figure 67. The maximum field applied at 4 K is almost 10 times the field that was applied at 70 K to measure $P_t(T)$ while cooling. After cooling the sample to 4 K, however, the two remanents are about the same size. This was observed before for some of the glass ceramics.

The magnitude of $P_t(4\ K)$ is dependent on the temperature at which the field is applied. This was noted but not appreciated in the initial glass ceramic measurements. The first actual measurement of $P_t(T)$ when the field was applied at 4 K for the first time was for this STV(10) sample. The dielectric constant was measured first and found to have a peak at about 45 K about 1.5 times larger than the 4 K value in figure 68. The polarization, P_t', shows a similar peak, figure 68, when the field is applied at 4 K and P_t is measured while warming. The curve is a quasi equilibrium curve since P_t increases slowly with time at temperatures below the peak and decreases slowly with time at temperatures above the peak. The curve of $P_t(T)$ after the field is applied at the high temperature end seems to be stable with time. Subtracting $P_r(T)$ from $P_t(T)$ measured while cooling gives a curve the same as $P_t(T)$ warming. Measurements of $K'(T)$ for four frequencies between 0.01 Hz and 10 kHz are shown in figure 69 for the STV(10) sample. The applied maximum field was 10 times larger

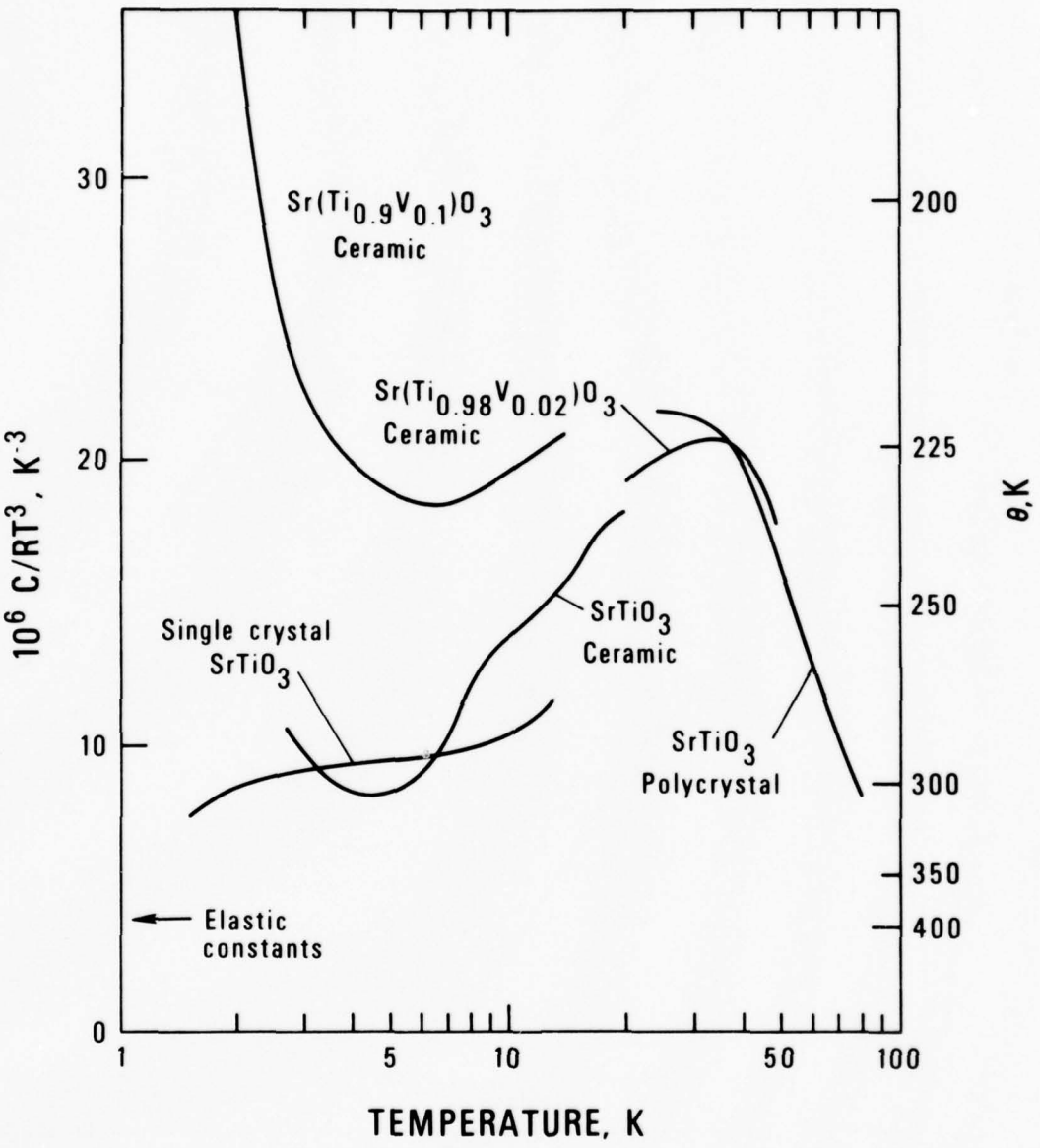

Figure 64. The specific heat of $SrTiO_3$ ceramic and $SrTiO_3$ ceramic doped with various amounts of V. The behavior of single crystal[81] and polycrystal[82,83] $SrTiO_3$ from other measurements are shown for comparison.

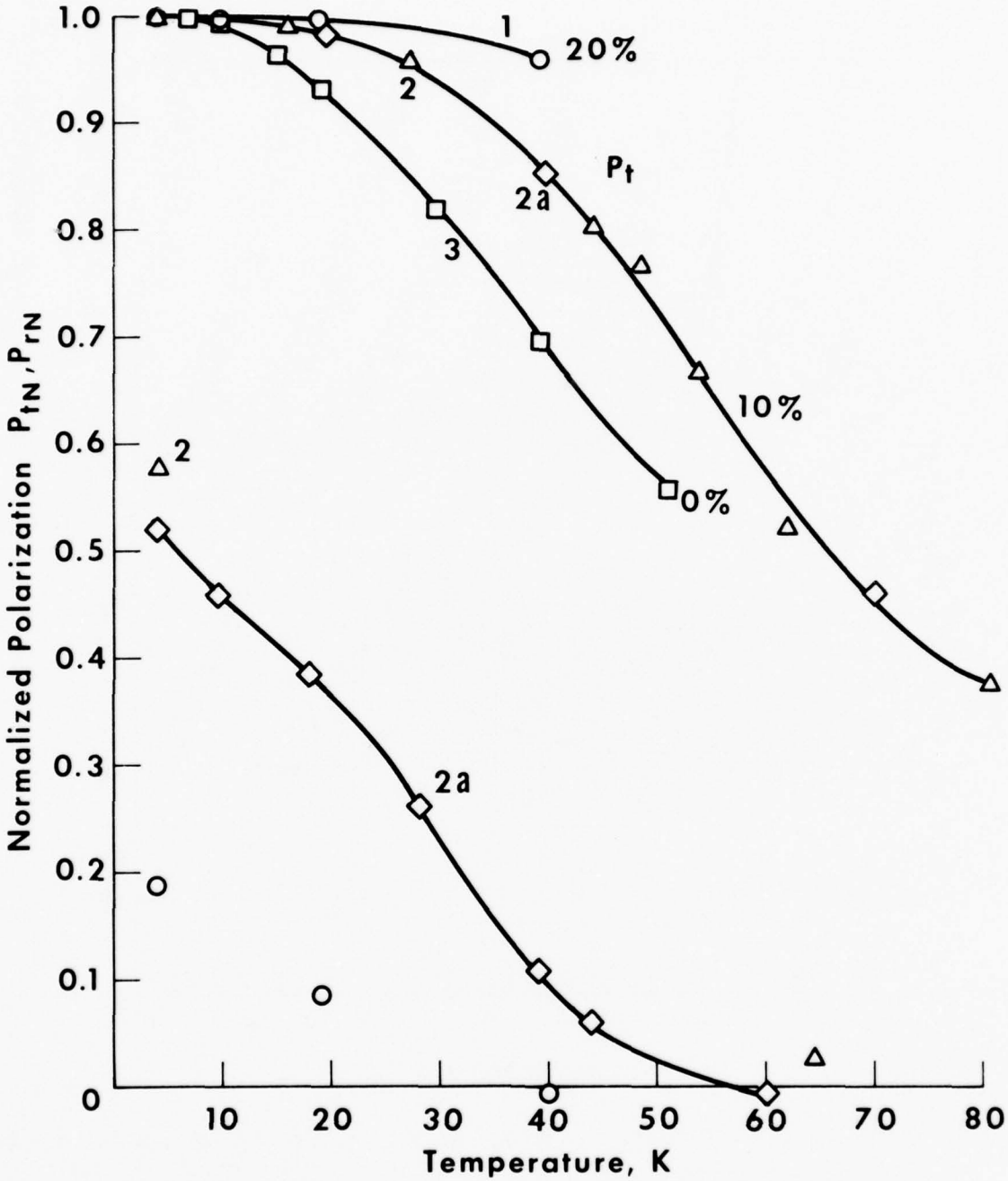

Figure 65. $P_{tN}(T)$ and $P_{rN}(T)$ for two vanadium doped $SrTiO_3$ ceramics compared to a nominally pure $SrTiO_3$ ceramic. Curve 1, STV(20)-2(1350), P = 0.046 μcoul/cm^2, E = 1.57 kV/cm; Curve 2, STV(10)-2(1350), P = 0.084 μcoul/cm^2, E - 0.36 kV/cm; Curve 2a, STV(10)-2(1350), P = 0.083 μcoul/cm^2, E - 0.36 kV/cm; Curve 3, ST-2(1350), P = 0.064 μcoul/cm^2, E = 0.39 kV/cm.

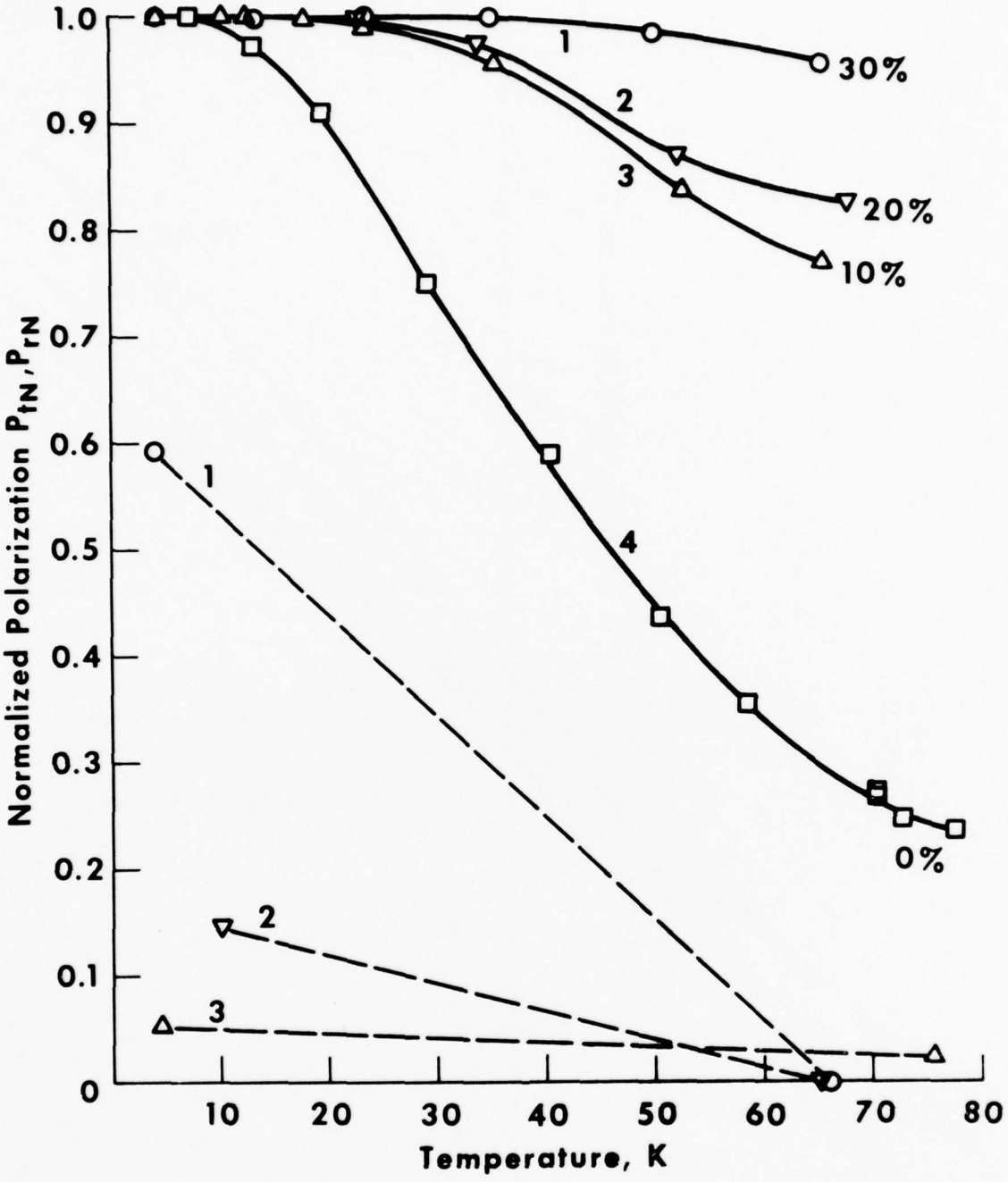

Figure 66. P_{tN} and P_{rN} for $SrTiO_3$ containing $SrNb_2O_6$ compared to a nominally pure $SrTiO_3$ ceramic.

Curve No.	Specimen	P_t(4 K) μcoul/cm^2	E(kV/cm)
1	STN(30)-1(1450)	0.031	0.37
2	STN(20)-1(1450)	0.028	0.35
3	STN(10)-1(1450)	0.026	0.39
4	ST2-(1450)	0.33	0.46

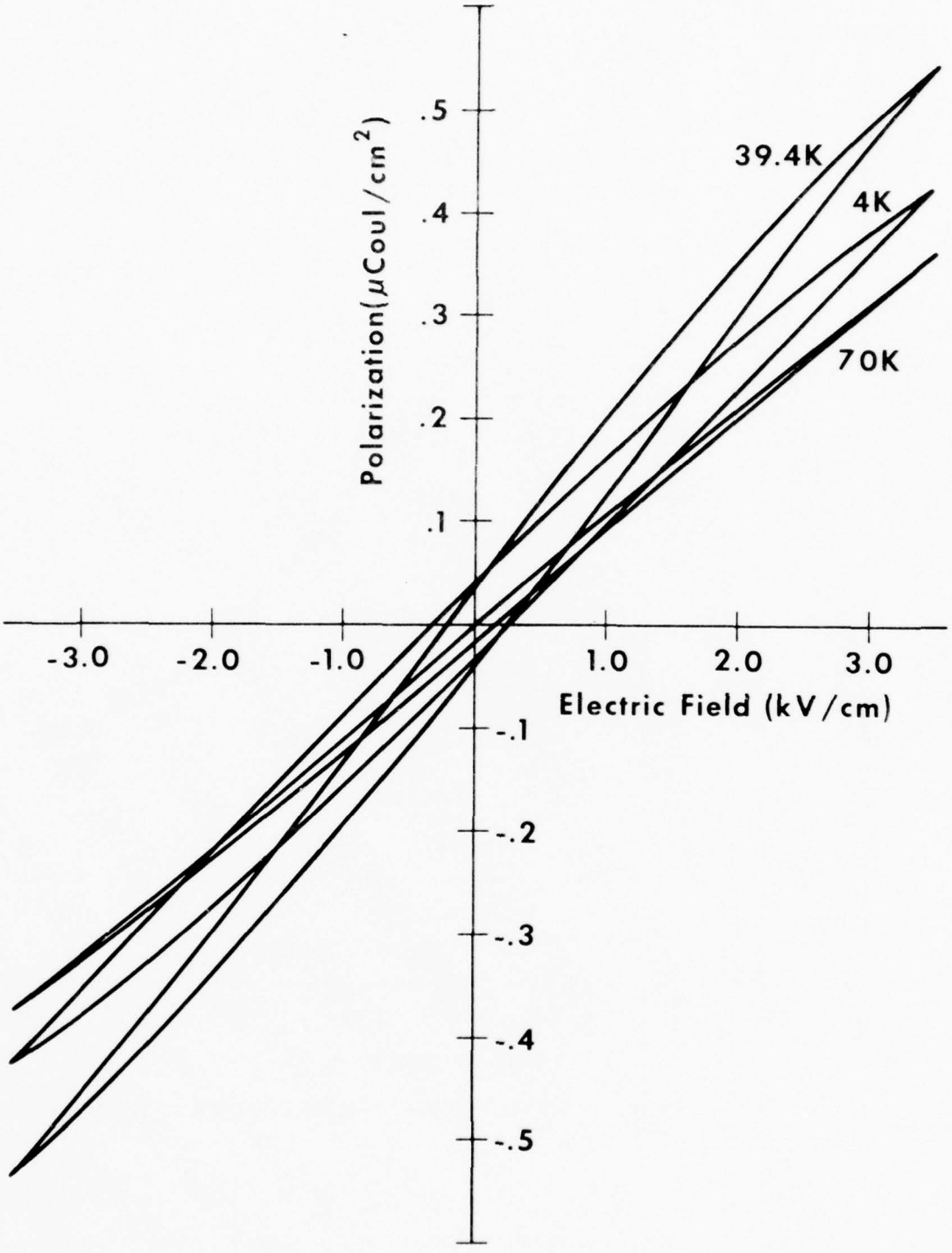

Figure 67. $P_t(E)$ hysteresis curve for STV(10) at 4, 39.5 and 70 K. The 39.4 K loop opening is the same as the opening at 4 K. At 70 K the loop opening was only 1/5 that at lower T.

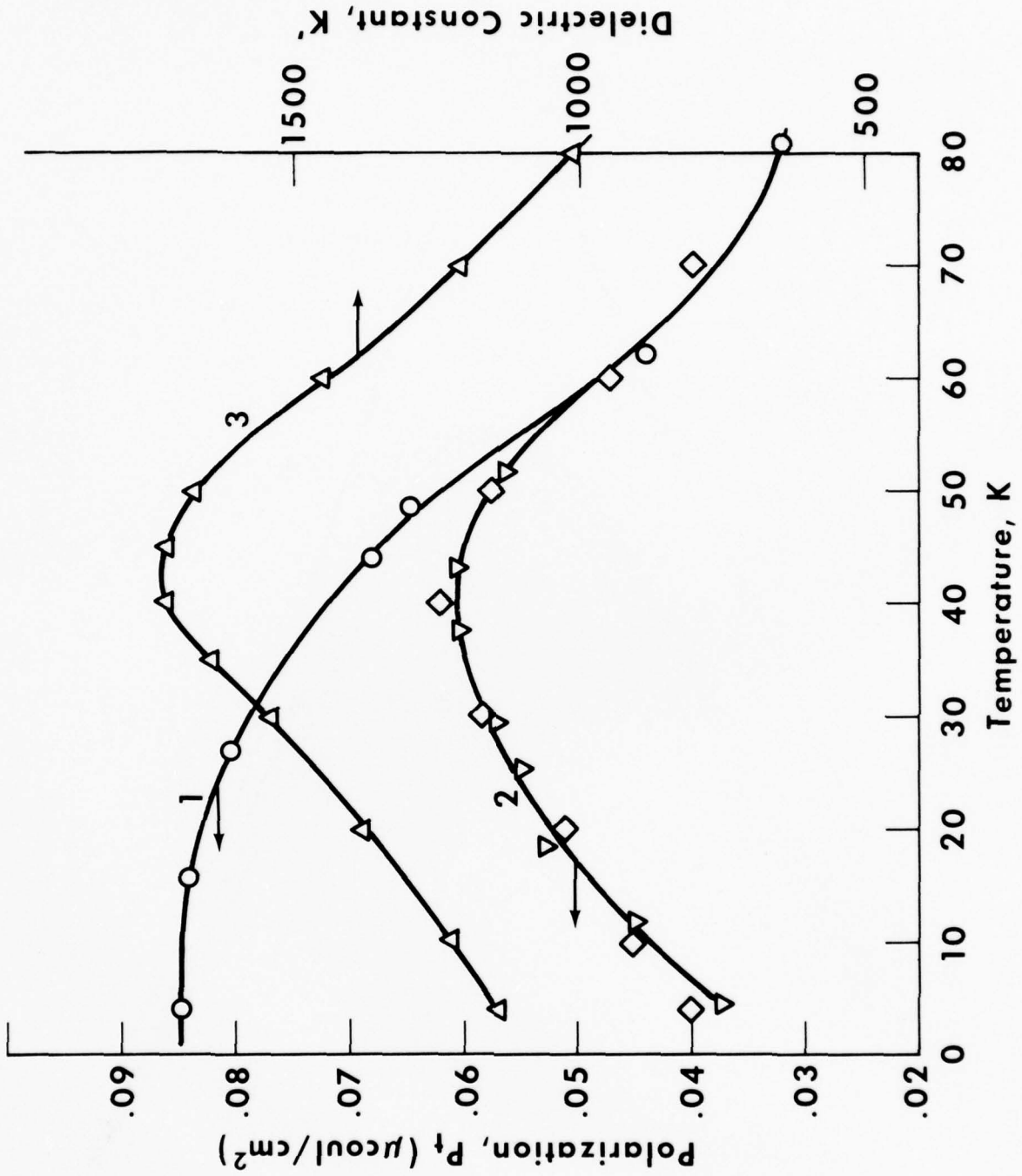

Figure 68. The $P_t(T)$ curves for STV-10 for E = 0.36 kV/cm. Curve 1, field applied at 81 K then the sample was cooled. Curve 2, field applied at 4 K then the sample was warmed. The diamond points on curve 2 are from $P_t(T) - P_r(T)$ for curve 2a of figure 65. Curve 3, K' measured at 10^{-3} Hz.

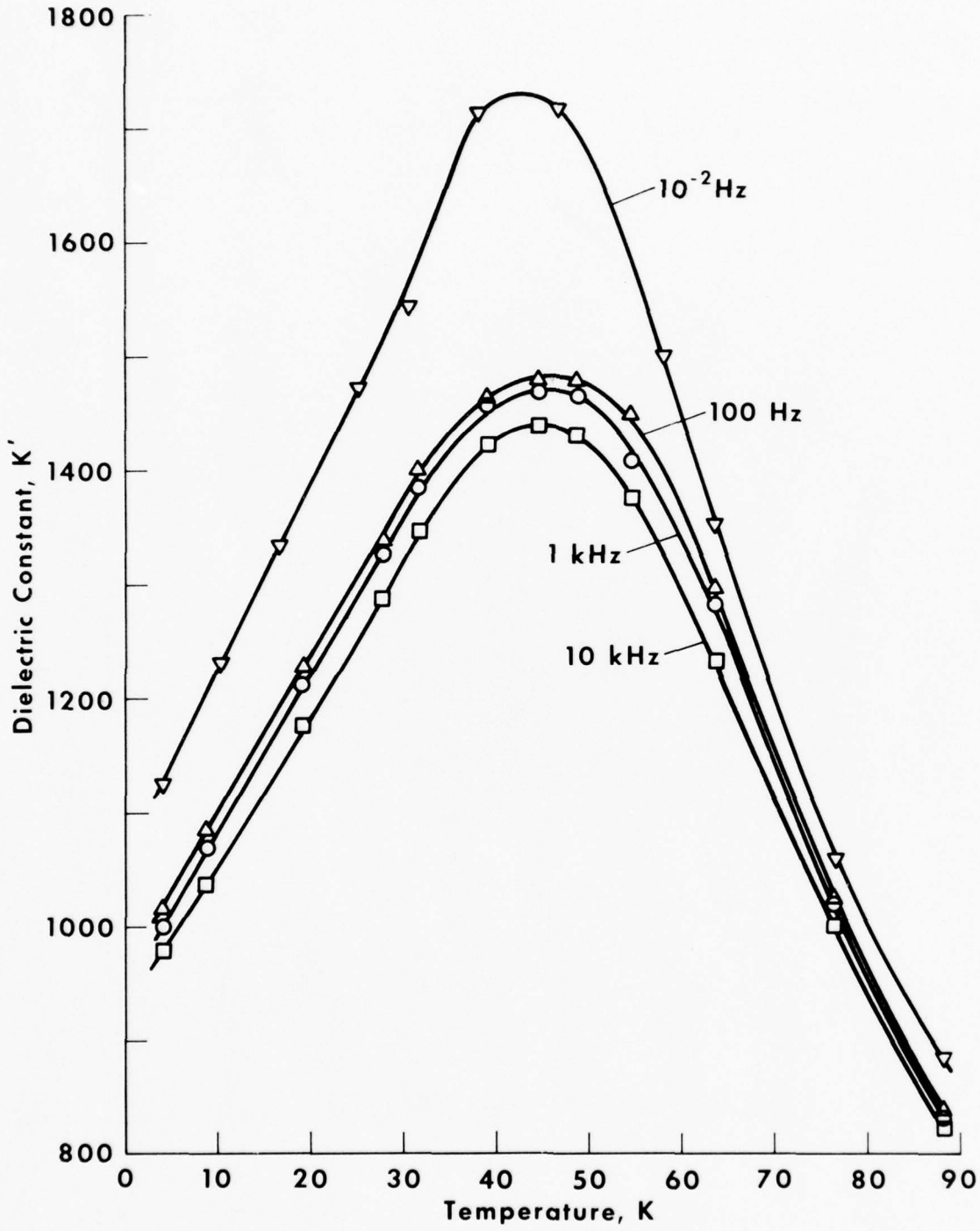

Figure 69. Curves of K'(T) at four frequencies between 0.01 Hz and 10 kHz for STV(10). E = 0.35 kV/cm max at 0.01 Hz and 0.02 kV/cm max. at the higher frequencies.

for the 0.01 Hz measurement but since P(E) is fairly linear at least at these low fields, the K'(T) curve should not be shifted significantly by a lower amplitude measurement. There is definitely a frequency dependence in K'(T).

The dielectric constants of a $SrTiO_3$ ceramic, STV(2), STV(10), and STV(20) are shown in figure 70 normalized to the 4 K value. The peak occurs at a lower temperature for STV(2) than for STV(10) though the peak to 4 K ratio of P_t is about the same. The peak is flattened for STV(20). There appeared to be some change in K' when a dc field was applied.

The dielectric constant of an $SrTiO_3$ ceramic prepared at 1350°C was then measured to see if an observable peak exists in the dielectric constant. The results for P_t and K' are shown in figure 71. A peak exists in K' but the peak value is only about 0.5% higher than the 4 K value.

The peak to 4 K ratios of K' were largest for the vanadium doped $SrTiO_3$. The 20% niobium doped $SrTiO_3$ has a peak 6% higher than the 4 K value as shown in figure 72. The shape of the curve appears to be slightly different than most of the K(T) data in that $\partial P/\partial T$ seems to decrease in magnitude as 4 K is approached. The STN(5) specimen shows a peak only about 0.3% higher than the 4 K value and at a much lower T.

One $SrTiO_3$ ceramic with 5% antimony doping also had a small peak in K'(T) at about 10 K. The peak was only about 0.2% higher than the 4 K value.

$KTaO_3$ and solid solutions: Polarization of a number of the $KTaO_3$ ceramics were measured. The $P_t(T)$ curves for those measured are shown in figure 73. In only one case were the ceramics superior to the single crystal. Sample KT(1)1 had a larger polarizability, P_t/E, by a factor of 3-1/2 than did the single crystal. Also, P_r was a considerably larger percent of P_t. This results in a larger value of $\partial P/\partial T$ at intermediate temperatures but not much improvement below about 10 K as can be seen in the figure. The behavior of the remanent was significantly different from that of the single crystal. At about 29 K, P_r drops with time at constant temperature. This behavior was still observed at 42 K. This sample broke down when a field of about 5 kV/cm was applied. The value of P_t/E at 4 K was not as large for sample KT-1(1300) and the remanent was almost half of P_t at 4 K. The remanent is only $\sim$ 10% for KT-1(1200). The remanent was only measured at the two extremes of T for most for the remaining samples. There would be a peak in ITC for both the KT(1) and the single crystal though perhaps the temperature of the peaks differ. The ceramic materials all had P_r values that were a higher percentage of P_t than did the single crystal.

The single crystal had a rather poor dielectric strength which was definitely undesirable for an electrocaloric refrigerator. The breakdown strength of a ceramic such as KT (1)-1 appeared to be even lower than the single crystal, although no effort was made to improve the ceramic.

The dc polarization of some of a series of $KTaO_3$ ceramics containing 10 and 20% vanadium in place of tantalum were measured and the results of the P_t and P_r measurements on three samples of vanadium doped $KTaO_3$ are shown in figure 74 along with the $P_t(T)$ and $P_r(T)$ measurements of a nominally pure $KTaO_3$ ceramic. A small amount of data were taken on three samples. The data for KTV(10)-1(1250) was taken on warming. The magnitude of P_t(4 K) would presumably be larger and $\partial P_t/\partial T$ would be increased some if $P_t(T)$ was measured from high T. None have as large a value of P_t at 4 K as the nominally pure $KTaO_3$ ceramics or as large a value of

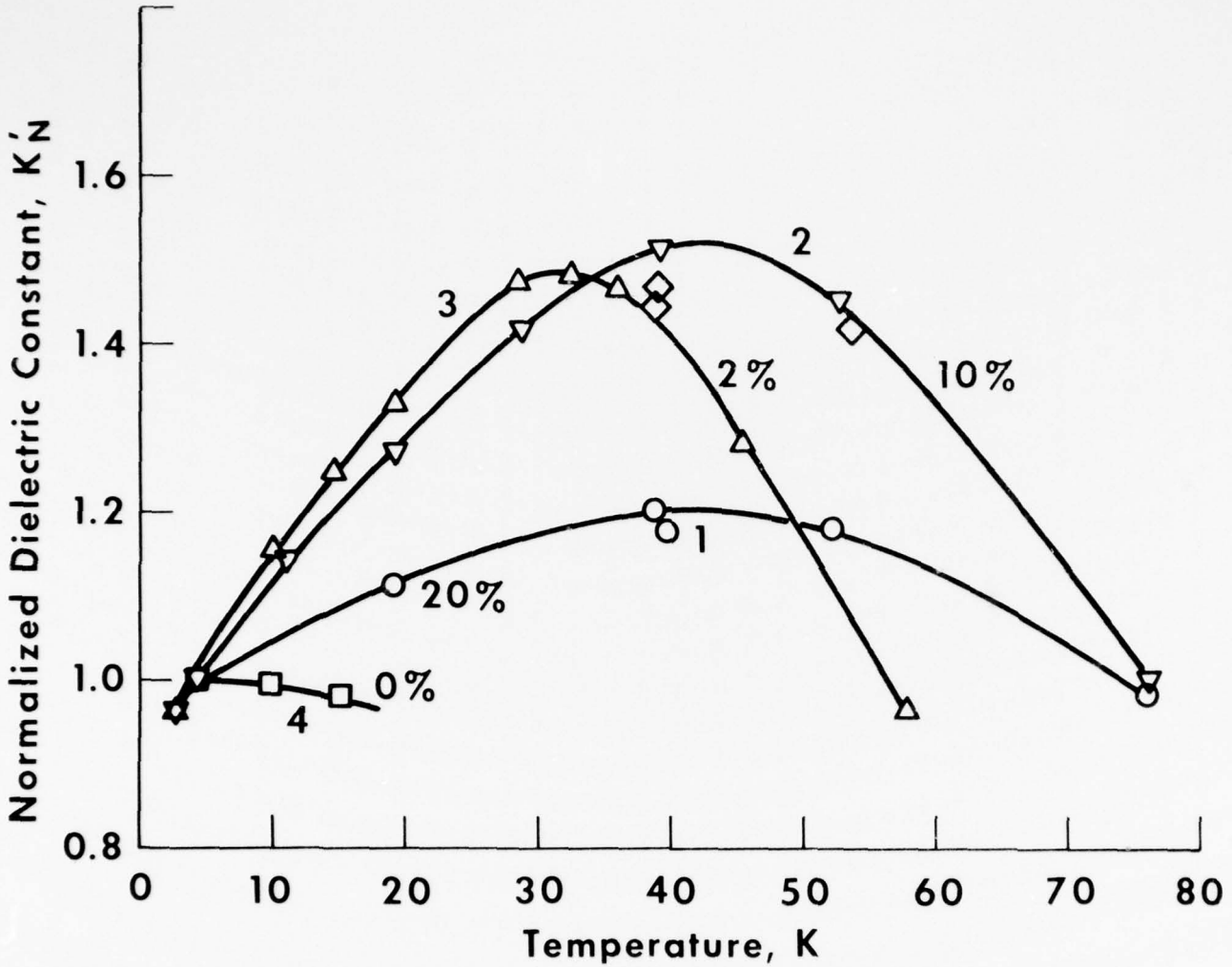

Figure 70. Curves of K' normalized to 1 at 4 K for $SrTiO_3$ containing 0, 2%, 10%, and 20% vanadium replacing titanium. The diamond points are the K' of STV(20) with E_{DC} = 0.36 kV/cm, K' (4 K) = 590; STV(10), K' (4 K) = 1790; STV(2), K' (4 K) = 3170; ST 2(1350), K' (4k) = 4780.

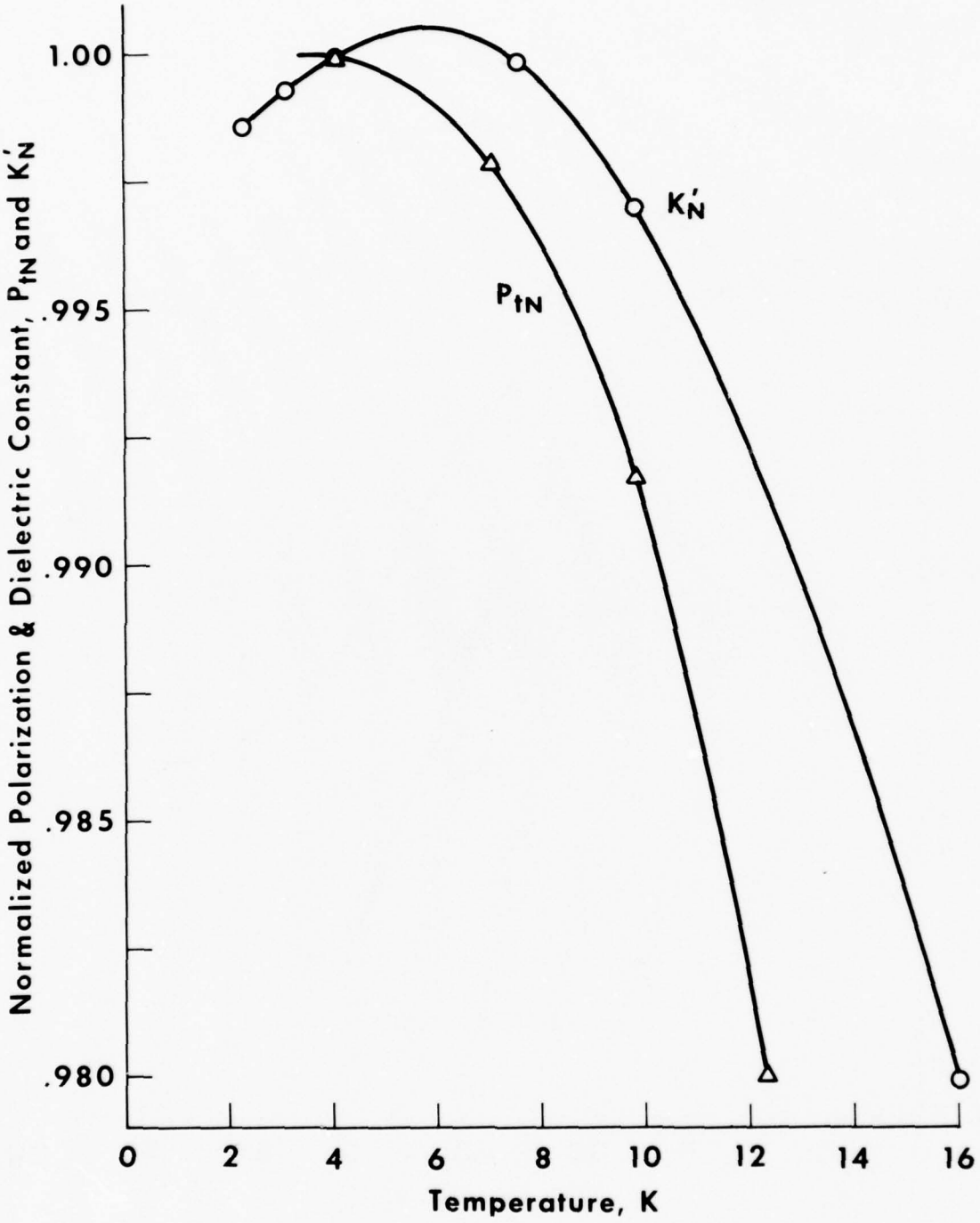

Figure 71. K'(T) and $P_t(T)$ curves of ST 2(1350) normalized to 1 at 4 K. There is a very small peak at about 6 K observed in K'.

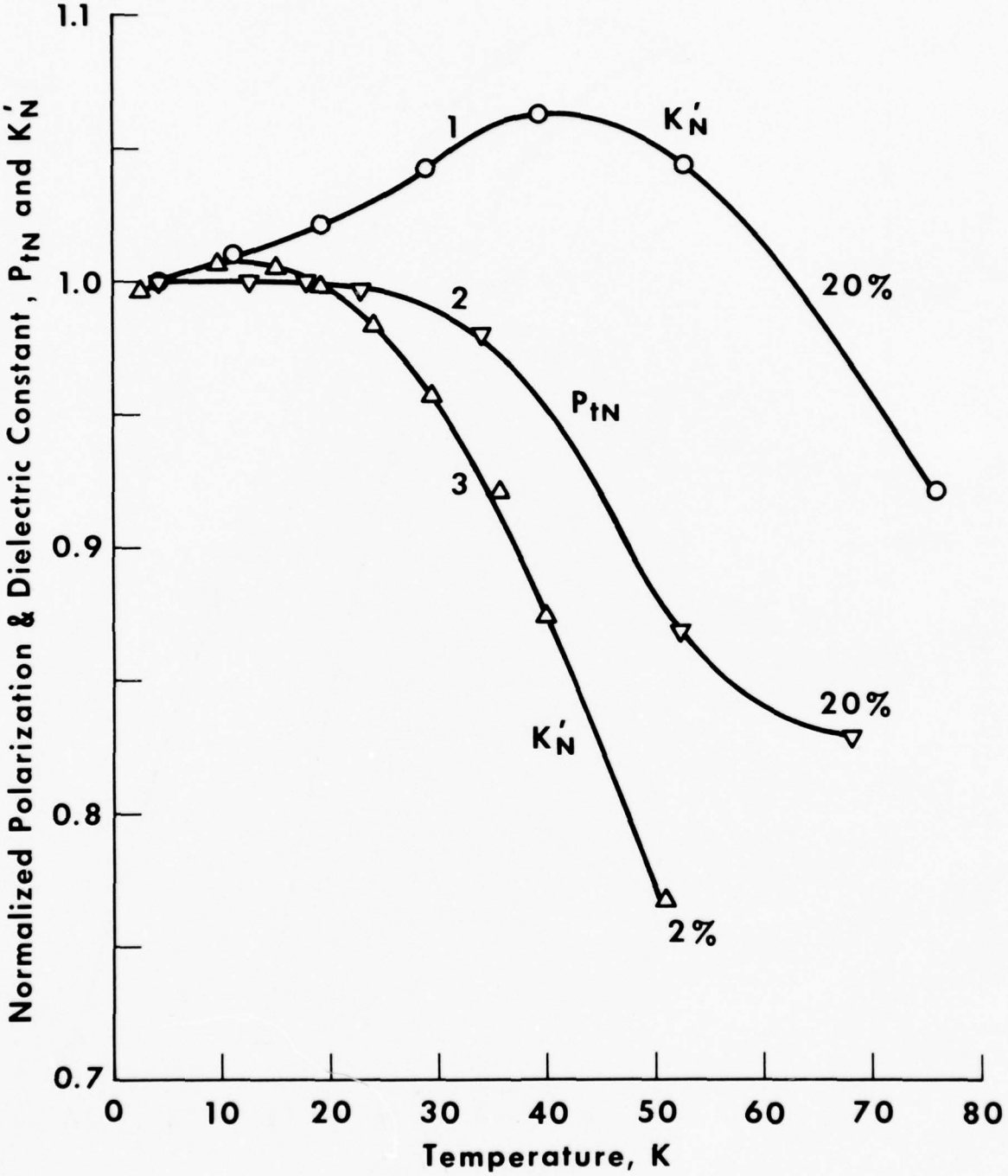

Figure 72. $P_t(T)$ and K'(T) for STN ceramics. Curve 1, K'(T) of STN(20), K' (4 K) = 1370. Curve 2, $P_t(T)$ of STN(20), E = 0.35 kV/cm, P_t(4 K) = 0.0028 μcoul/cm^2. Curve 3, K'(T) of STN2. K' (4 K) = 1702.

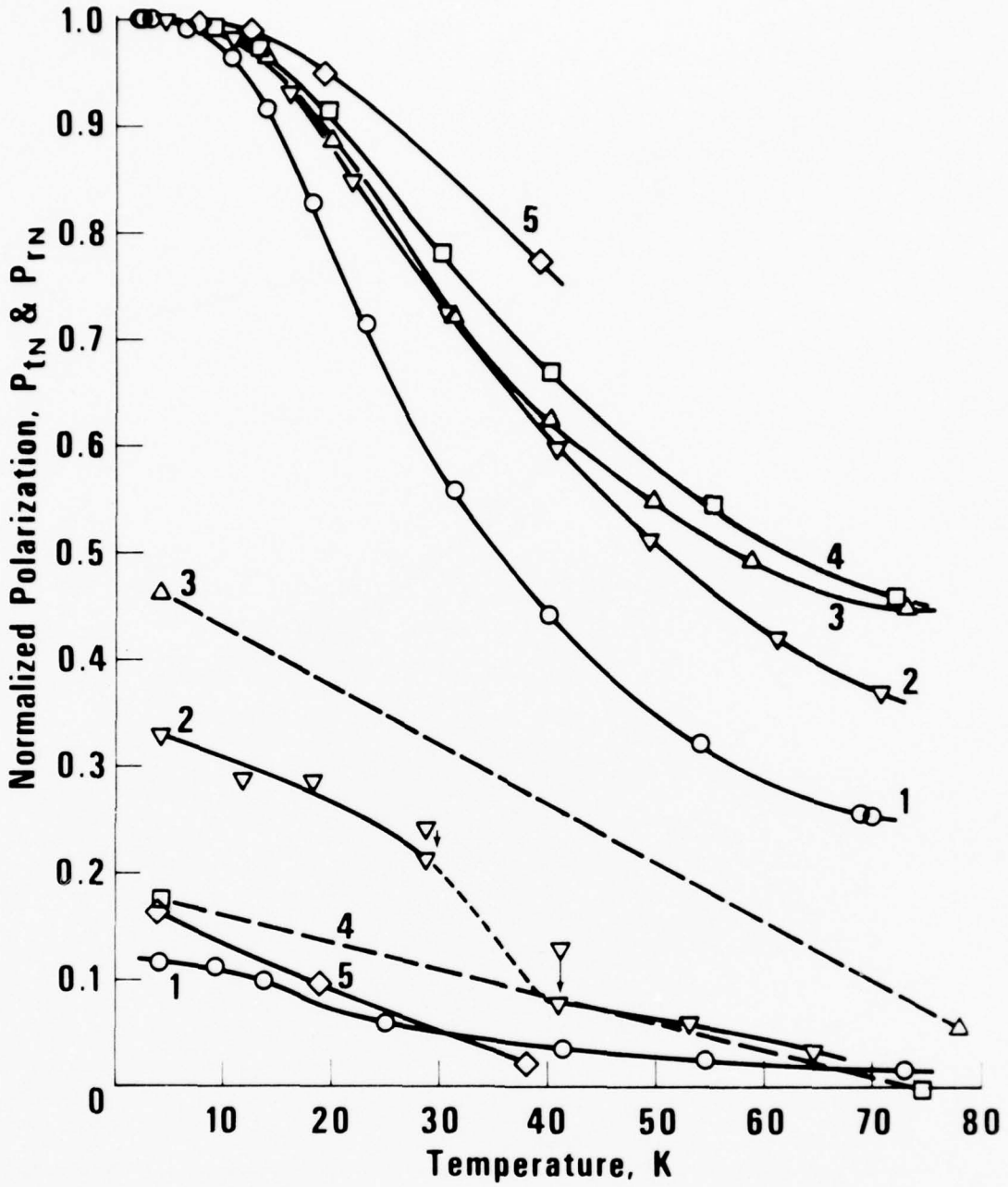

Figure 73. $P_{tN}(T)$ and $P_{rN}(T)$ curves for various $KTaO_3$ specimens.

Curve No.	Specimen	E(kV/cm)	P_t(4 K) (μCoul/cm^2)	P_t(4 K)/E (μCoul/kV·cm)
1	Single crystal	0.25	0.76	0.3
2	Ceramic KT(1)-1	0.38	0.35	0.92
3	Ceramic KT-1(1300)	0.37	0.106	0.29
4	Ceramic KT-1(1200)	1.7	0.072	0.043
5	Ceramic KTV(20) (1300)	1.4	0.041	0.029

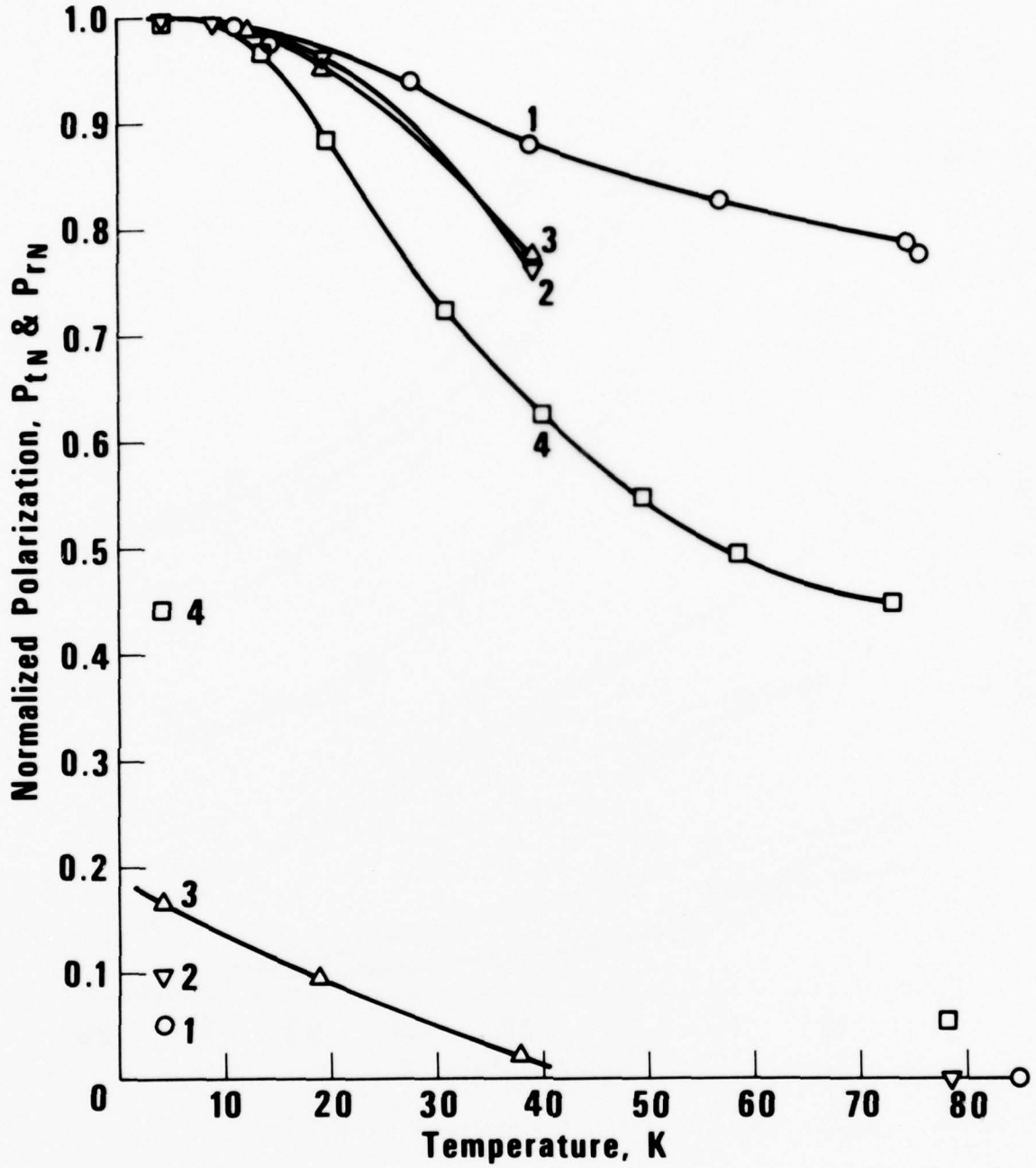

Figure 74. P_{tN} and P_{rN} for vanadium doped $KTaO_3$ ceramics compared to a nominally pure $KTaO_3$ ceramic, curve #4.

Curve No.	Specimen	P_t(4 K) μ Coul/cm^2	E(kV/cm)
1	KTV(20)-1(1250)	.0093	0.42
2	KTV(10)-1(1250)	.027	1.38
3	KTV(20)-1(1300)	.041	1.40
4	KT-1(1300)	.106	0.37

$\partial P/\partial T$. The dielectric constant of KTV(20)-1(1300) was measured at 1 kHz. The normalized curve of K'(T) is shown in figure 75 and compared to P_{tN}. There is a peak in K' at about 12 K. The dielectric constant shows a field dependence.

Polar ceramics: A well known series of polar ceramics is that of the $PbZr_xTi_{1-x}O_3$ (PZT) system. The system is ferroelectric at room temperature for $x \leq 93\%$ but for $x \geq 93\%$ the system is antiferroelectric.[84] The antiferroelectric 95/5 PZT is interesting for this program since hysteresis effects should be small. Polarization measurements at low temperatures had not been done previously. However, the high ordering temperature would suggest that $\partial P/\partial T$ is small at 4 K.

Measurements of P(T) below 77 K were made for both 65/35 PZT and 95/5 PZT with very similar results. Both showed negative $\partial P/\partial T$ values, but for the antiferroelectric 95/5 PZT the slope should be positive. We have no explanation for the observed behavior except to say that 95/5 PZT appears to be a ferroelectric below 77 K.

Electrocaloric measurements were made on the 95/5 PZT sample with depolarization resulting in cooling. Such an effect is consistent with the observed negative $\partial P/\partial T$. Figure 76 shows the results of the electrocaloric measurements made at 12 K and figure 77 shows the temperature dependence of the electrocaloric effect. This material showed only heating effects at 4 K. The specific heat is shown in figure 78. The effective Debye temperature varies from 185 K at low temperatures to 119 K at the peak in C/T^3.

$Pb_2Nb_2O_7$ type ceramics: The dc polarizations of PCTT ($Pb_2Cd_{1/2}Ti_{1/2}TaO_6$), PN ($Pb_2Nb_2O_7$), and CCN ($Cd_2CrNbO_6$) are shown in figure 79. The remanent was measured at only one temperature on each. Only CCN showed appreciable P_r and that was measured only at 48 K. The remanent for PN is zero at 4 K to within the limits of the resolution of the measuring system. Both PCTT and PN exhibit the typical $P_t(T)$ curve. The magnitude of $P_t(T)$ asymptotically approaches the limiting valve at 4 K. It has been suggested that PCTT is an antiferroelectric below the peak in K'(T) at 40 K.[85] A discontinuity appears in the $P_t(T)$ of CCN somewhere between 31 and 42.5 K. A discontinuity appears in the K'(T) measurements also[86] but at a temperature of about 25 K.

Detailed measurements were made on $Pb_2Nb_2O_7$. A peak was noted in K'(T) at 15.4 K for a 1 kHz measuring frequency.[87] In figure 80, $P_t(T)$ and K'(T) at a number of frequencies are plotted as a function of T on a much expanded scale. This work shows a peak at about 17 K but the percent decrease of the 1 kHz value of K'(T) at 2 K from the peak value is almost exactly the same as measured by Hulm,[87] about 2.6%. This peak has been attributed to an antiferroelectric phase transition. If an antiferroelectric transition takes place, then $P_t(T)$ should decrease with decreasing temperature. There was no apparent decrease in $P_t(T)$ except in one measurement, curve P, figure 80 which rules out an antiferroelectric transition. Perhaps the measuring field used destroyed the antiferroelectric ordering. Measurements of P_t were made at a field less than 1/3 the field used for the data in figure 80. No peak was observed in $P_t(T)$. Also, neither the slope or magnitude of K'(T) were changed by applying a steady electric field during the measurement. Furthermore, a hysteresis loop was measured at 4 K to E = ± 7 kV/cm, figure 81. $P_t(E)$ is linear with E over this range and there is no loop opening to within the uncertainty of the instruments. If an antiferro- to ferroelectric transition is caused by the dc field, there should be hysteresis loops above some value of E.

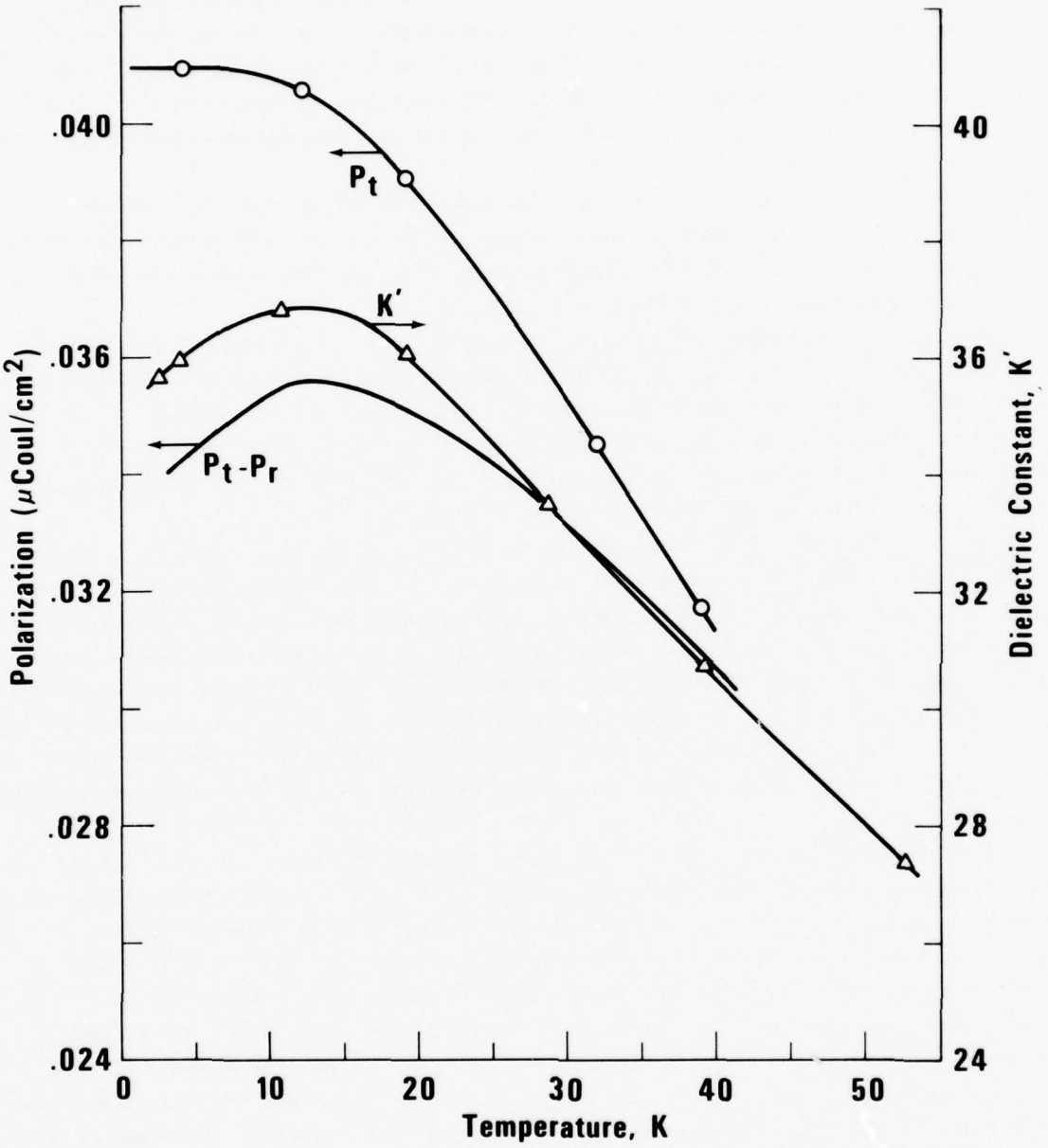

Figure 75. Details of P_{tN} and K'_N for KTV(20)-1(1300). The P_t-P_r curve is calculated from the data for curves 3, figure 73. A steady state field applied reduces K'.

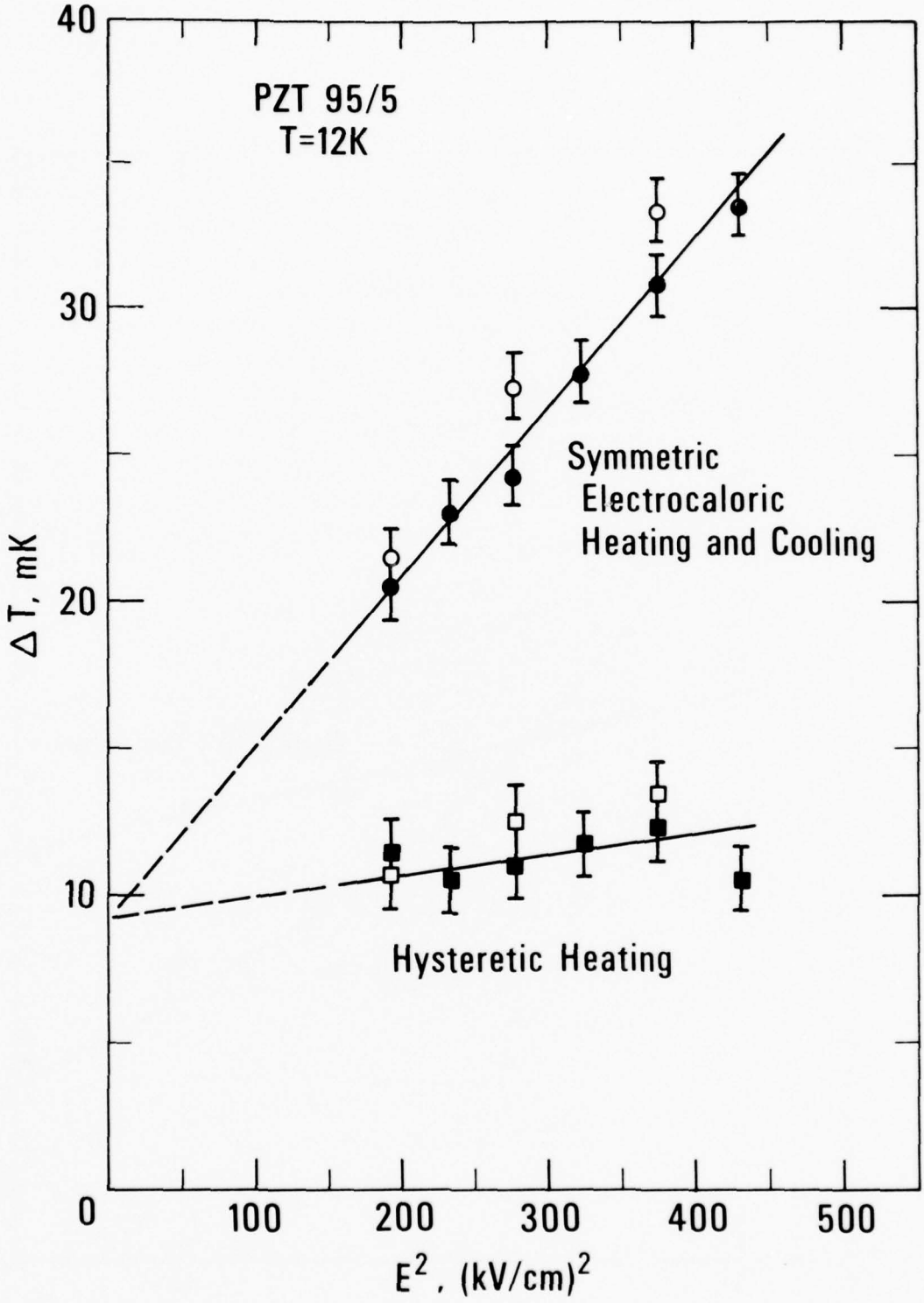

Figure 76. Electrocaloric and hysteretic effects in 95/5 PZT at 12 K as a function of electric field change.

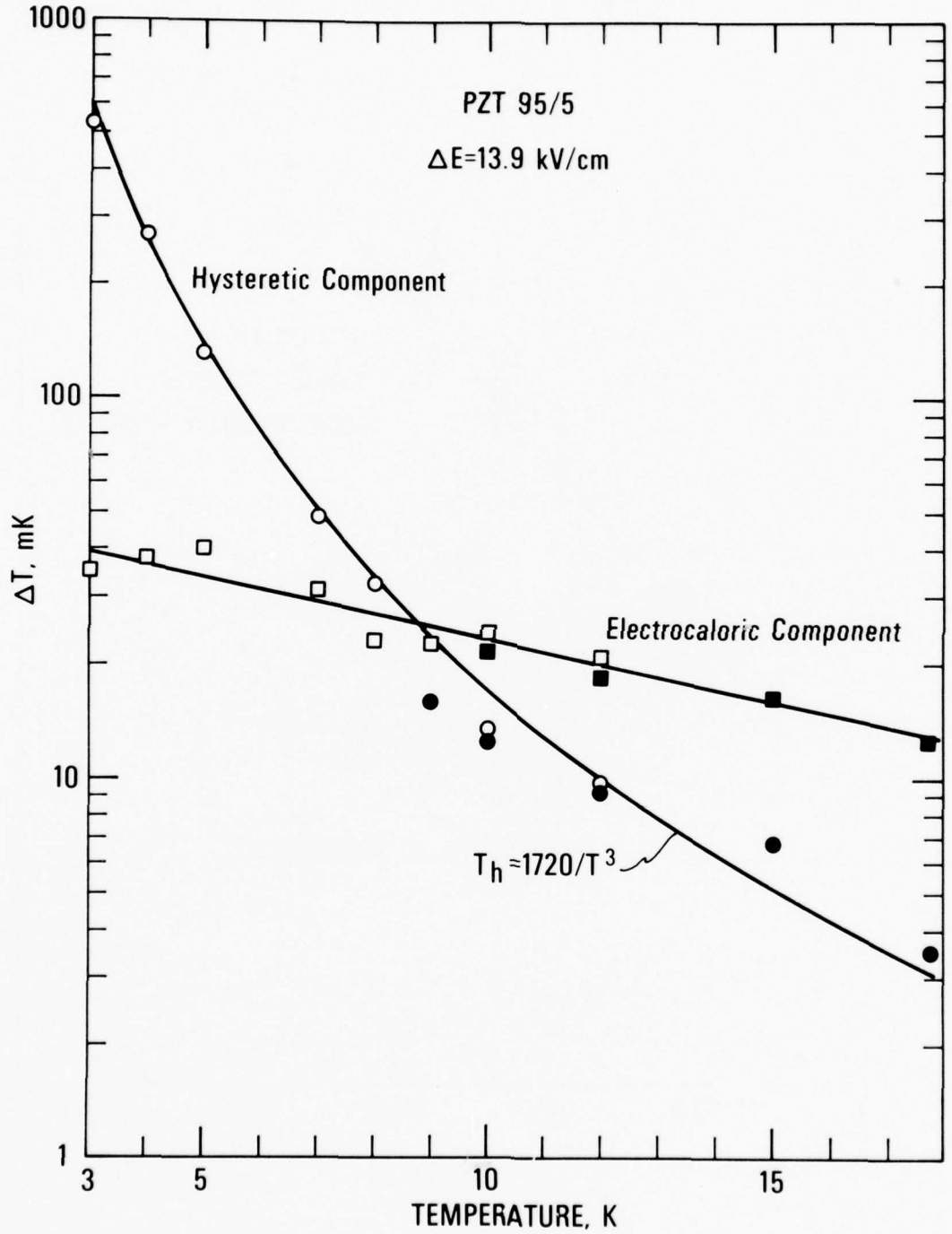

Figure 77. Electrocaloric and hysteretic effects in 95/5 PZT as a function of temperature for a field change of 13.9 kV/cm.

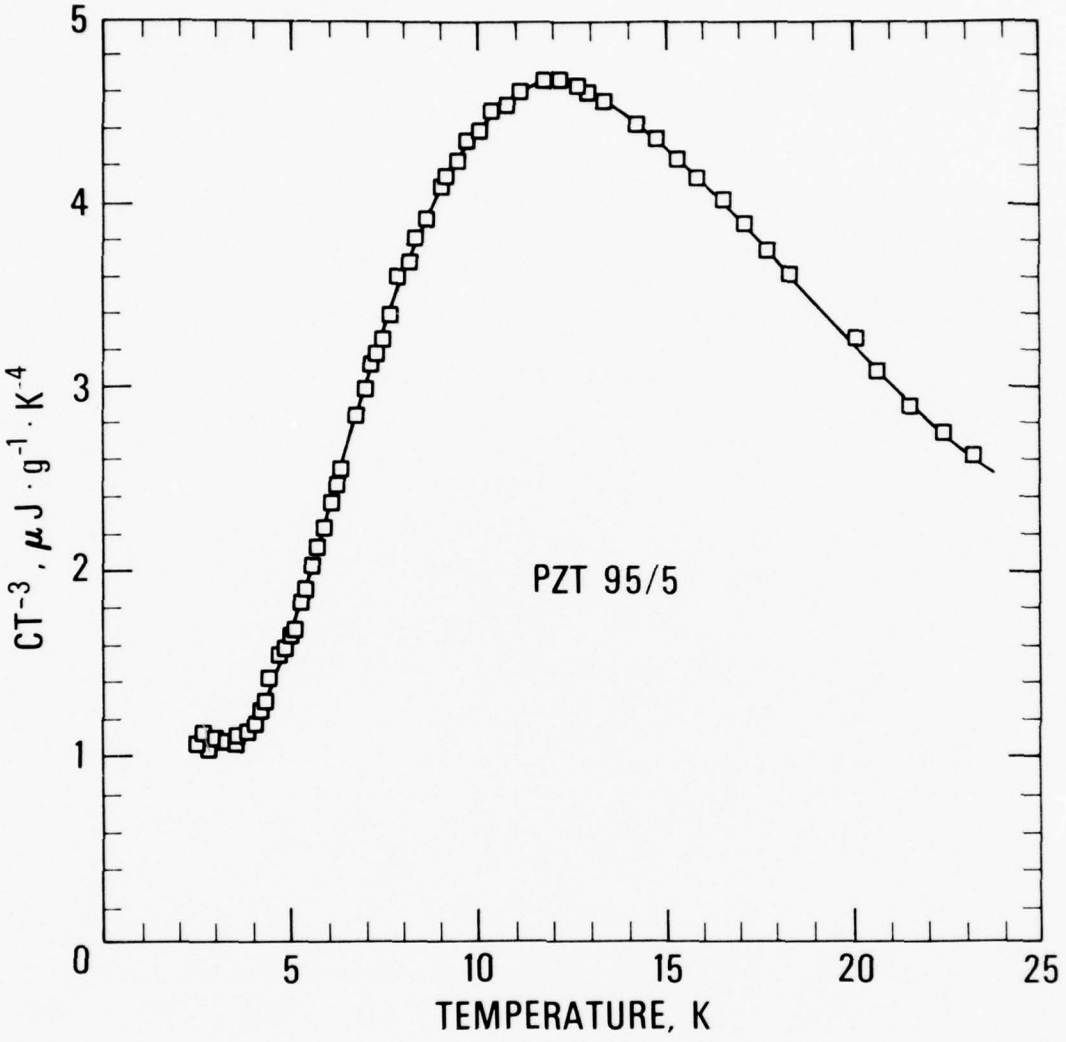

Figure 78. Specific heat of PZT 95/5 between 2 and 23 K.

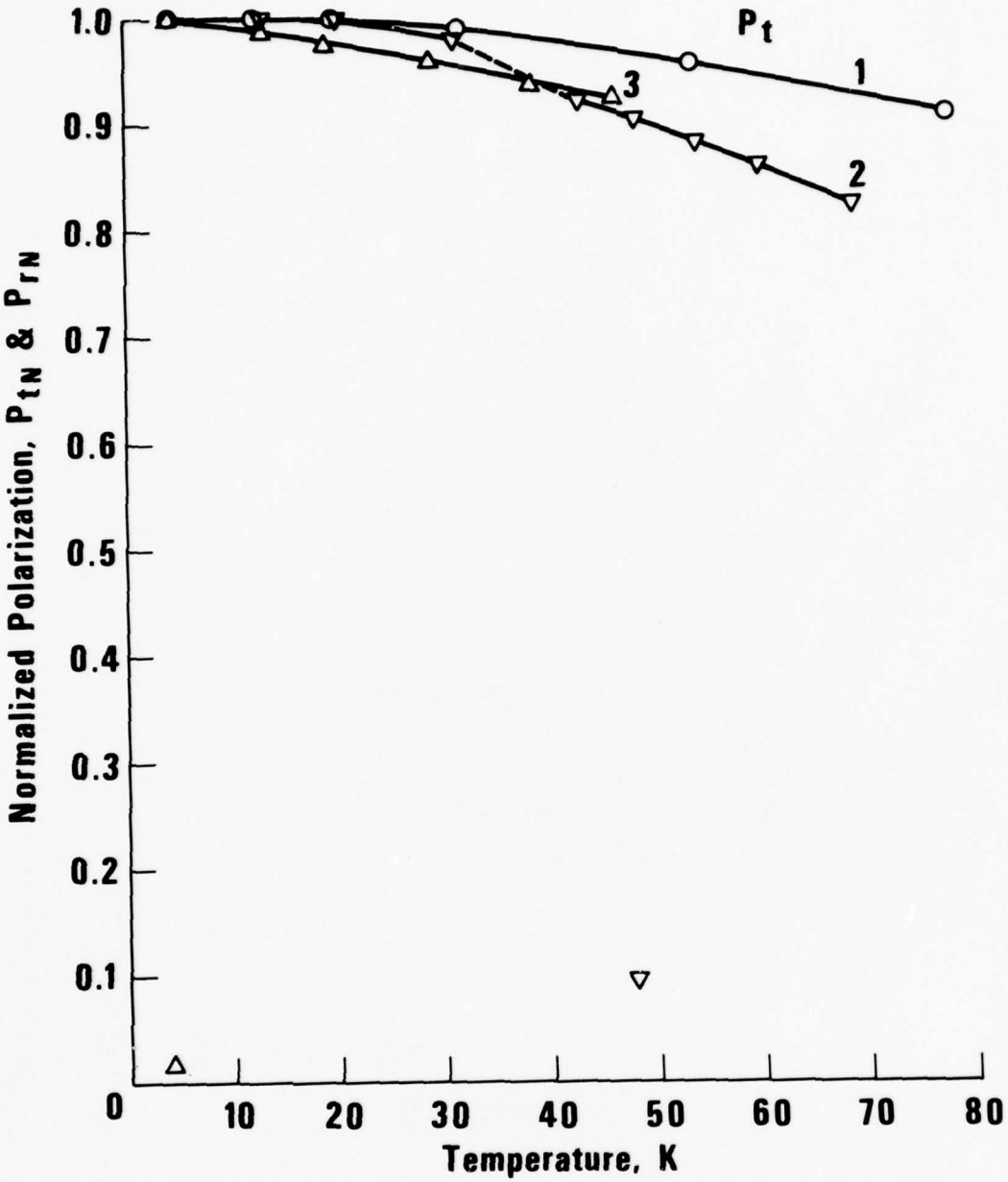

Figure 79. $P_t(T)$ of the pyrochlores $Pb_2Nb_2O_7$ and Cd_2CrNbO_6, and the antiferroelectric perovskite $Pb_2Cd_{1/2}Ti_{1/2}TaO_6$. This latter material shows no evidence of any antiferroelectric ordering over the range measured.

Curve No.	Specimen	$P_t(4\ K)_2$ ($\mu Coul/cm^2$)	E(kV/cm)
1	$Pb_2Nb_2O_7$	0.0066	1.47
2	Cd_2CrNbO_6	0.016	0.30
3	$Pb_2Cd_{1/2}Ti_{1/2}TaO_6$	0.021	1.0

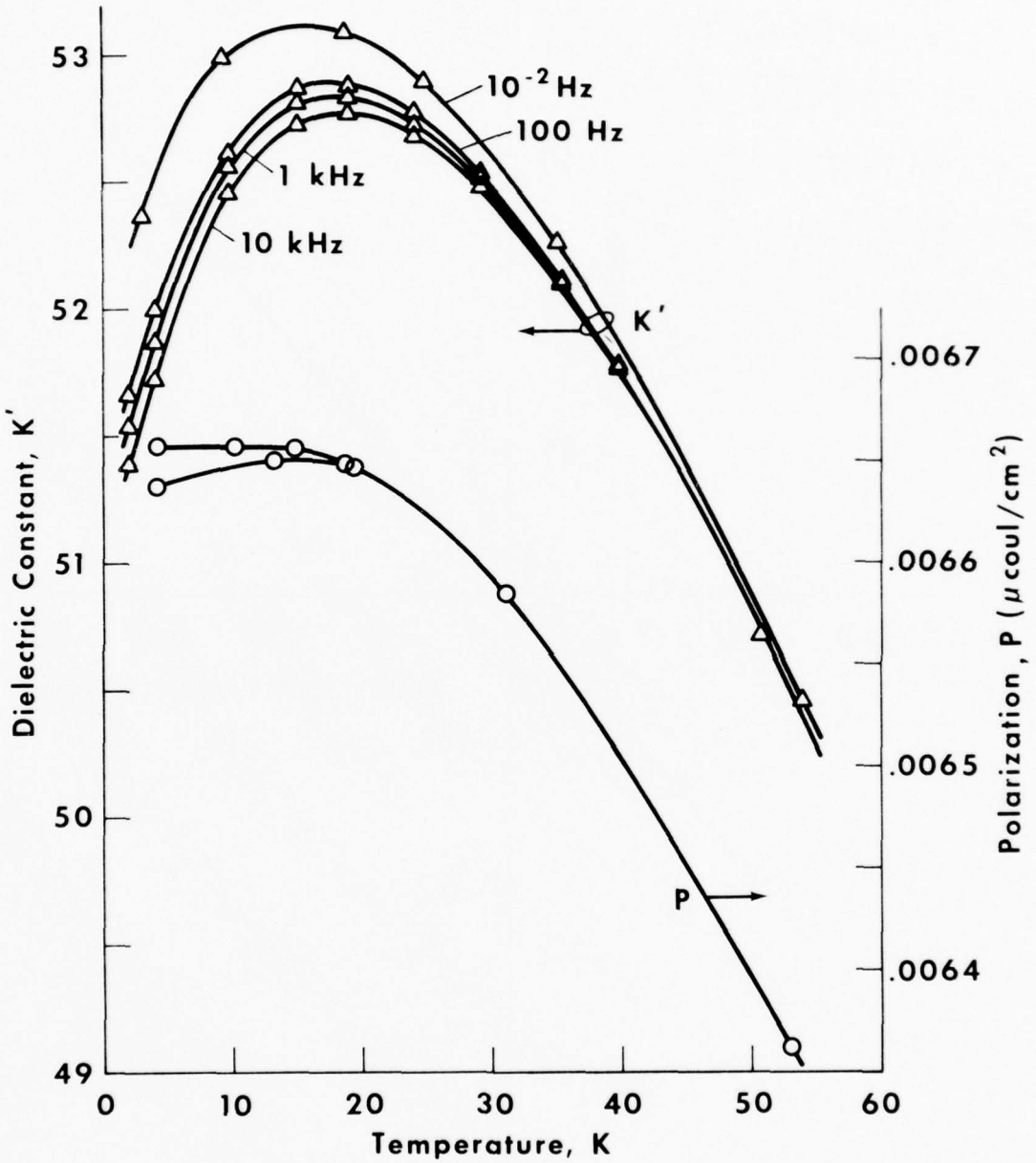

Figure 80. Polarization and dielectric constant of $Pb_2Nb_2O_7$ on an expanded axis. The polarization curve is for a 1.47 kV/cm electric field. The K'(T) curve at 1 kHz and E_{max} = 0.44 kV/cm was unchanged from the zero steady state field curve when a 1.47 kV/cm field was applied. The other K'(T) curves were measured at the same field amplitude except the 0.01 curve, for which E_{max} = 1.47 kV/cm.

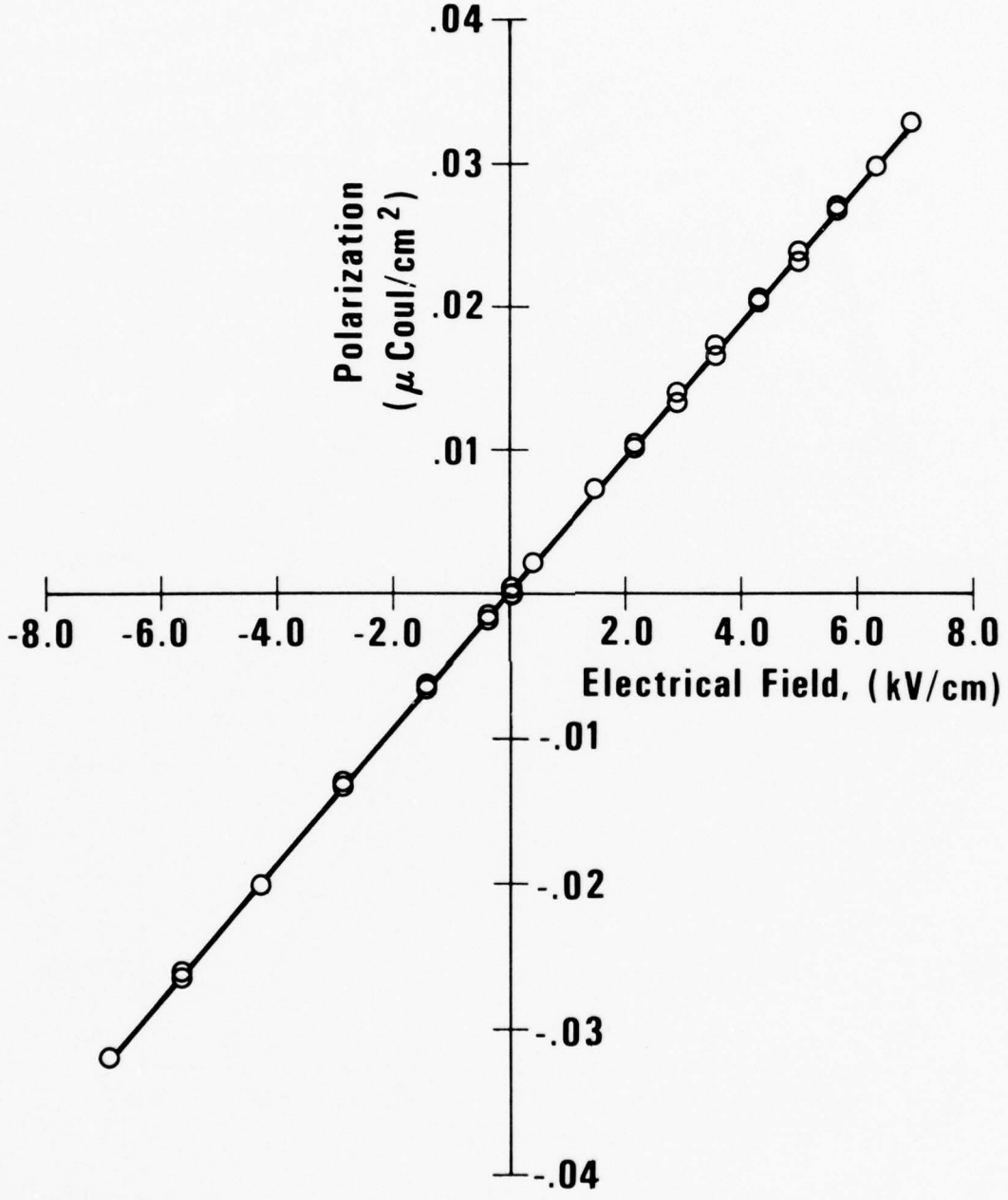

Figure 81. $P_t(E)$ for $Pb_2Nb_2O_7$ at 4 K, E = $\pm$ 7.0 kV. The curve is a straight line. There is no observable loop.

This result along with the lack of a maximum in $P_t(T)$ suggests that neither a ferro- nor antiferroelectric transition takes place around the maximum of K'(T). In figure 80, K'(T) is shown for frequencies of 10, 1, and 0.1 kHz as well as for a frequency of about 0.01 Hz. The curve of K'(T) at 0.01 Hz was determined by measuring hysteresis loops at a series of temperatures with the dc polarization instrument. The dielectric constant measured using the dc system gave a slightly lower value for K' at higher T. This curve is raised by 0.8% to place it slightly above the higher frequency K' values at 52 K. The voltage out of the electrometer read by the DVM was found to be $\sim$ 1% low for one polarity which agrees with the correction made. The observed loss tangents are quite small but increase monotonically with decreasing T by about a factor of 100 when an estimated lead loss is subtracted. The increase in tan δ and the dispersion in the K'(T) curves along with the dc polarization measurements suggest that the peak in K'(T) is the result of a dielectric relaxation mechanism rather than an ordering transition.

The specific heat of the $Pb_2Nb_2O_7$ ceramic is shown in figure 82. Measurements were made for E = 0 and E = 27.3 kV/cm. To within the precision of about 1%, there is no difference in specific heat for the two electric field values. Such behavior argues against the material being in an antiferroelectric state below 15 K. Also, the lack of an anomaly in the specific heat seems to suggest no transition to the antiferroelectric state. Thus, both the polarization measurements and the specific heat measurements are consistent with each other and indicate the material remains in the paraelectric state down to at least 3 K.

3.8. Discussion of Experimental Results

Several questions have been brought to light by the measurements in this program. In this section we discuss and attempt to explain the following observations, (i) the lack of cooling in $SrTiO_3$ glass ceramics at 4 K, (ii) the agreement between polarization and electrocaloric measurements, (iii) the peak in the dielectric constant in most dielectrics at low temperatures, (iv) the reason for the remanent polarization in most dielectrics at low temperatures, and (v) the specific heat and its relation to electrocaloric refrigeration. Then finally we make some general conclusions regarding the low temperature behavior of dielectrics and the potential of electrocaloric refrigeration.

Adiabatic polarization cooling of $SrTiO_3$ glass ceramics was predicted because of large positive values of $\partial K'/\partial T$ at 4 K. The polarization calculated from K', assuming no remanent, would also have this positive slope. However, actual measurements of P on glass ceramics, ceramics, and single crystals not only showed the presence of hysteresis, but also no sign of a positive slope in P(T) when cooled in a field. Electrocaloric measurements agreed well with that predicted from measured P(T) data. What then gives rise to the peak in the dielectric constant and the remanent polarization?

3.8.1. Dielectric properties

Earlier measurements of the electrical properties of $SrTiO_3$ by Weaver[66] have shown hysteresis in the P-E data up to 45 K. Burke and Pressley[88] saw hysteresis in the P-E curves with stress applied and attributed the hysteresis to surface charge build up. Saifi and Cross[67] have measured apparent antiferroelectric hysteresis loops in some cases. Earlier work on ceramic $SrTiO_3$ showed a peak in K'(T) in one case but not in another.[89]

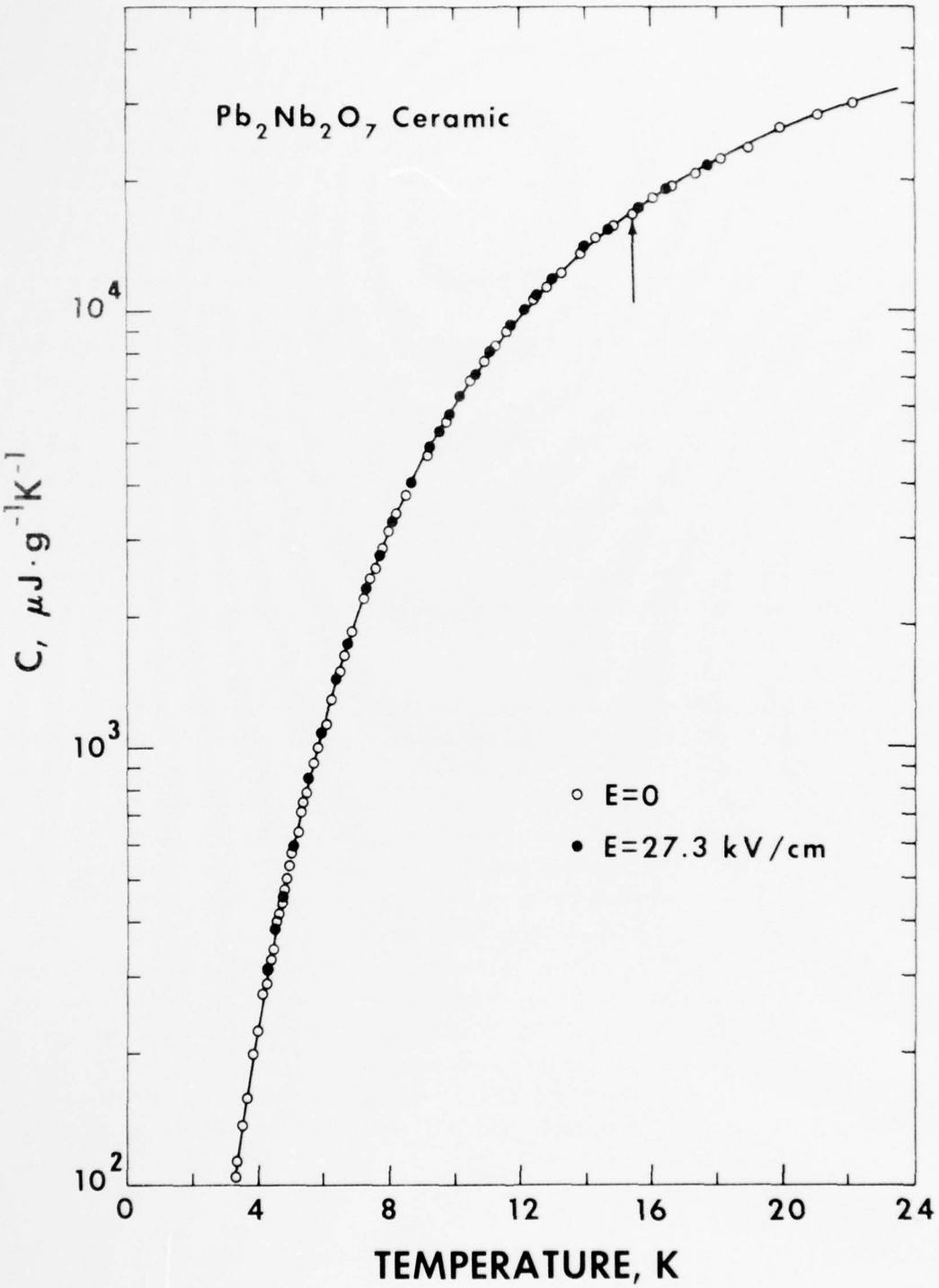

Figure 82. Specific heat of $Pb_2Nb_2O_7$ ceramic between 3 and 23 K in zero field and in a field of 27.3 kV/cm. The arrow indicates the temperature of the observed peak in K'(T).

Similar results have been obtained for $KTaO_3$. A peak in K'(T) was observed originally by Hulm, et al.[90] Recent measurements by Demurov and Venevtsev[91] have shown a peak at 10 K. Dielectric measurements in this laboratory on the single crystal of Samara and Morosin[92] showed a slight peak in K'(T) at 3 K. Hysteresis loops have been observed in P-E curves up to 56 K.[91]

There exists no model of electrical behavior for $SrTiO_3$ or $KTaO_3$ that explains hysteresis or peaks in K'(T) without assuming a ferroelectric or an antiferroelectric transition. In this section, a model consisting of permanent dipoles, due to impurities, that have an electret state and give rise to dielectric relaxation effects will be proposed and used to explain the behavior of the materials measured here. The model also explains the presence of apparent ferroelectric hysteresis curves without requiring an ordering transition.

The total polarization per unit volume, P_t, can be described as the sum of three parts,[93]

$$P_t = P_e + P_a + P_d,$$

where P_e is the polarization due to displacement of the electrons, P_a is the polarization due to displacement of the atoms, and P_d is the polarization due to alignment of any permanent dipoles. For many substances, all the temperature dependence of P_t comes from the dipole term. Any T dependence in P_e is negligible. For many materials the only T dependence in P_a would be expected to come from lattice transformations or thermal expansion. The thermal expansion contribution would be expected to be small compared to the T dependence of the dipole term. For the soft mode materials such as $SrTiO_3$ and $KTaO_3$, however, P_a can have a larger T dependence than the dipole term. The $P_t(T)$ measurements reported here show $\partial P_t(T)/\partial T \doteq 0$ for all specimens at 4 K so both P_a and P_d are T independent at 4 K. The $P_t(E)$ data taken at 4 K should only measure the stretch of the electronic and atomic dipoles. If the dipoles are in harmonic potential wells, the $P_t(E)$ curves should be linear until electrical breakdown occurs. The fact that the curves deviate from linearity at high fields suggests anharmonicity due to a flat bottomed potential well, which would be expected for soft mode materials. The shape of the P(E) curves in the T independent region tell nothing about the electrocaloric cooling capabilities of the material.

Measurements of $P_t(T)]_E$ for a number of applied fields should have been made to higher fields to determine $\partial P/\partial T$ as a function of E in the temperature region of interest. The data on the $KTaO_3$ single crystal show only that P_t is about proportional to E up to E = 4 kV/cm for all temperatures. Some correction may be required for the temperature dependence of the remanent since it adds a nonreversible part to P_t. This correction would be expected to be large for the glass ceramic where most of the T dependence is associated with the remanent.

Because of the lattice symmetry, there are presumably no permanent dipoles in pure $SrTiO_3$ and $KTaO_3$. Since remanent polarizations and hysteresis effects are present in the materials, permanent dipoles of some sort must exist in these samples.

Usually, a peak in K'(T) is assumed to indicate a transition to ferroelectric or antiferroelectric ordering. If the ordering is antiferroelectric then both $P_t(T)$ and K'(T)

should decrease below the transition temperature. Since $P_t(T)$ does not decrease with T for any of the specimens measured here, an antiferroelectric state is immediately ruled out. The observed T dependence of K' and P_t do not exclude a ferroelectric phase, but $P_r(T)$ does not behave as would be expected. The remanent would be expected to remain nearly constant as T increases then decrease rapidly to zero at the Curie temperature, T_c, as seen by Gesi[71] using the same dc technique. The polarization must go to zero around the same temperature that the peak of K'(T) occurs, though there can be some asymtotic behavior at T_c if there is a spread of transition temperatures in the material. Contrary to the expected behavior, the $SrTiO_3$ and $KTaO_3$ materials showed the most rapid decrease of $P_r(T)$ with increasing T at the lowest temperatures. Then $P_r(T)$ asymtotically approaches zero at temperatures well above 77 K, though the peaks of K'(T) occur from 6 K to 45 K. In addition, some of the $P_r(T)$ data reverse sign. Only a formation of domains that proceeds rapidly at low T then slows down at higher T could account for such behavior. If domains form and the domain walls move so easily, then the walls should move easily under fields. The P(E) data, however, show no sign of saturation at the highest fields applied indicating that domain walls do not move easily or do not exist.

An alternative cause of the K'(T) peaks might be dielectric relaxation. A simple model for the peak in K'(T) is that motion of the dipoles in the material is increasingly inhibited as the temperature decreases and also they are less able to follow a field at constant T as the frequency increases. A decrease in dielectric constant and an increase in dissipation results. This was first reported by Skanavi and Matveeva[94] for impurity doped $SrTiO_3$ and was later observed by Tien and Cross[95] and Johnson, Cross and Hummel[96] for a number of different impurities in $SrTiO_3$. Nomura and Kojima[97] have observed similar effects in some tantalates and niobates containing potassium, bismuth and magnesium. The dielectric relaxation effects in solids have been observed mainly in the perovskites. The peaks in the dielectric constant are accompanied by a large increase in dissipation. The loss tangents observed in the specimens measured in this work increased as T decreased. Detailed results were not obtained because the loss tangents were small and apparently dominated by lead losses. There was some insensitivity to the dissipation factor also, perhaps because of the poor lead shielding in the cryostat.

The observed remanent polarization is not a necessary result of relaxation effects but is probably the cause of them. The perovskites are nonpolar prior to a ferroelectric transition. There is another common source of polarization in dielectrics known as the electret state. There is not a large number of papers in the literature dealing with the electrets probably because they are commercially important. Some review papers on electrets have been published.[98-101]

Electrets are sometimes specified by the activating process used in their formation. Those formed by lowering the specimen temperature in a field are called thermoelectrets. Their formation is thought to result from the trapping of charge or dipoles in a material after it had been cooled in the presence of an electric field. The dipoles would be trapped so they cannot freely rotate, or charge may be trapped on the surface, at defects or on grain boundaries. It may be difficult to establish which mechanism or how many of the mechanisms are causing the remanent polarization. An electret can be formed without raising

the temperature of the material though the polarization is not as large. The electret may have a final charge after the field is removed that gives a field the same direction as (homocharge) or opposite to (heterocharge) the forming electric field. The heterocharge is due to the induced polarization while the homocharge results from charge leaking from the electrodes on to the surface of the dielectric. The polarization of an electret can actually reverse if both charges are formed initially and the heterocharge leaks off more rapidly. This polarization reversal is common, especially after poling in high fields.

The reviews do not make a distinction between an electret and a ferroelectric. For this discussion, we will make the distinction that a ferroelectric is the result of a collective interaction that reduces the lattice energy by reducing the symmetry in such a way that polarization results. The electret, on the other hand, is a mechanical trapping of dipoles or charge and a polarization results only if a field has been applied. If only one dipole or charge existed in the whole of the material an electret can be formed.

Gubkin and Skanavi[102] reported thermoelectric behavior in a number of ceramics, including $SrTiO_3$, at room temperature. The apparent sign reversal on some of the P_r measurements in this work indicate an electret behavior where both homocharge and heterocharge are present. The fact that a much higher value of P_r at 4 K results when the specimen is cooled in a field rather than when the field is applied at 4 K suggests the electret state also. If this was due to refusal of domain walls to move at 4 K under a field, then P_r would not have the high T dependence around 4 K that was generally noted for these specimens.

The model being suggested here is that of a thermoelectret formed from permanent dipoles. Grain boundary charging is assumed negligible since a similar $P_r(T)$ was observed even for single crystal $KTaO_3$. Space and surface charge effects may contribute but such effects are considered negligible because the remanent seems to be repeatable. The dependence on impurities suggest permanent dipoles similar to the impurity-vacancy (I-V) dipole that has been studied extensively in alkali halides.[78,103-105] The I-V dipole in alkali halides consists of a divalent metal ion accompanied by the metal ion vacancy required to maintain charge neutrality. Permanent dipoles consisting of impurities and vacancies should be considerably more complex in the perovskites because the impurity valancy is not a simple 2 to 1 ratio with the lattice cation and the valancy of both the lattice cation and the impurity are variable. Because of the range of valances available, the electret properties should vary depending on the temperature, and atmosphere present when the material is manufactured as well as on the impurity included.

Dreyfus[106] measured polarization current vs. time and found a charging current decaying as the sum of two exponentials. He interpreted the double exponential as being the sum of at least two different rate processes, one being the alignment of impurity-nearest neighbor vacancy dipoles and the other with impurity-next nearest neighbor vacancy dipoles. The polarization current of FEL (1090) is the time derivative of the polarization $P_t(\infty) - P_t(T)$ and is shown in figure 46. This polarization current is approximately the sum of two exponentials. In this respect, at least, an I-V dipole model seems compatible with the measured results.

The presence of permanent dipoles with long relaxation times can cause the hysteresis loops observed for almost all the specimens measured. Since electrets can be formed at low

temperatures by field application, there is a source of polarization of long relaxation time.

The suggested model is one in which I-V type dipoles in $SrTiO_3$ and $KTaO_3$ base materials are sufficiently free to move and contribute to the ac dielectric constant. As the temperature is reduced, these dipoles freeze out. The dispersion noted arises from the freezing out process. A low frequency field can move more of the dipoles at any given T.

The remanent in STV(10) is quite large but a fairly large amount of vanadium was added. The peaks in K'(T) in the glass-ceramics are very similar but the $SrTiO_3$ crystallites are supposed to be pure. The crystals are grown in glass which certainly can be a source of impurities. If it is assumed that the dipoles in STV(10), for instance, are a positive and negative electronic charge one lattice spacing apart then around 10 parts per million impurities, if all form dipoles, are all that is required to give the observed P_r at 4 K. This impurity level for the precipitated crystals is quite conceivable. The electrical behavior of the glass ceramics is similar to that of STV(10), suggesting that the glass matrix is making no significant contribution to the behavior of the glass ceramics.

Curves of $K'_N(T)$, $P_{tN}(T)$, and $P_{rN}(T)$ are shown in figure 83 for the simple model just discussed. The model assumes that the dielectric constant due to the soft mode effects, K'_{smN}, varies as 1/T down to 20 K whereupon it curves over and becomes constant at $\sim$ 5 K. This polarization is normalized to 1 at 0 K and is arbitrarily set to be 0.2 at 80 K. The dielectric constant due to permanent dipoles, K'_{dN}, is assumed to be proportional to $e^{-T_o/(T-T_c)}$ where T_o is 14 K and T_c is zero for the K'_{dN} curve shown. This quantity divided by K'_{dN} at $T = \infty$ is the fraction of dipoles not trapped by the potential kT_o. The trapped dipoles can no longer contribute to the ac dielectric constant, but can contribute to the remanent if polarized. The ac polarization measured is the $K'_N(T)$ curve of figure 83, which is the sum of K'_{dN} and K'_{smN}. This gives a peak in K'_N at 12.5 K that is 1.066 times the 0 K dielectric constant. This peak is changed in temperature and size when T_o, or K_{dN} at $T = \infty$, or the value of T for which K'_{sm} departs from 1/T behavior, is changed. A wide range of peak temperatures and peak to 0 K ratios of K'_N are possible by varying all three parameters.

The remanent polarization could be proportional to $K_{dN}(\infty) - K_{dN}(T)$ if all dipoles are aligned by the applied field while cooling the specimen. Since the ac dielectric constant, K'_N, has a strong T dependence, the measured polarization would be expected to be proportional to K' also. Thus,

$$P_r \propto [K_d(\infty) - K_d(T)]K'(T).$$

This relation gives the $P_{rN}(T)$ curve shown in figure 83. This assumes a long lifetime for trapped dipoles and that any dipoles falling into the traps align with the remainder. It is not obvious what mechanism might produce such dipole alignment but the curve is similar to the remanent polarization observed when heating the specimen.

When a specimen is cooled in an applied field, E, a polarization $\varepsilon_o EK'(T)$ is observed. Assuming that the remanent contribution is the same cooling as observed in 0 field while heating, then

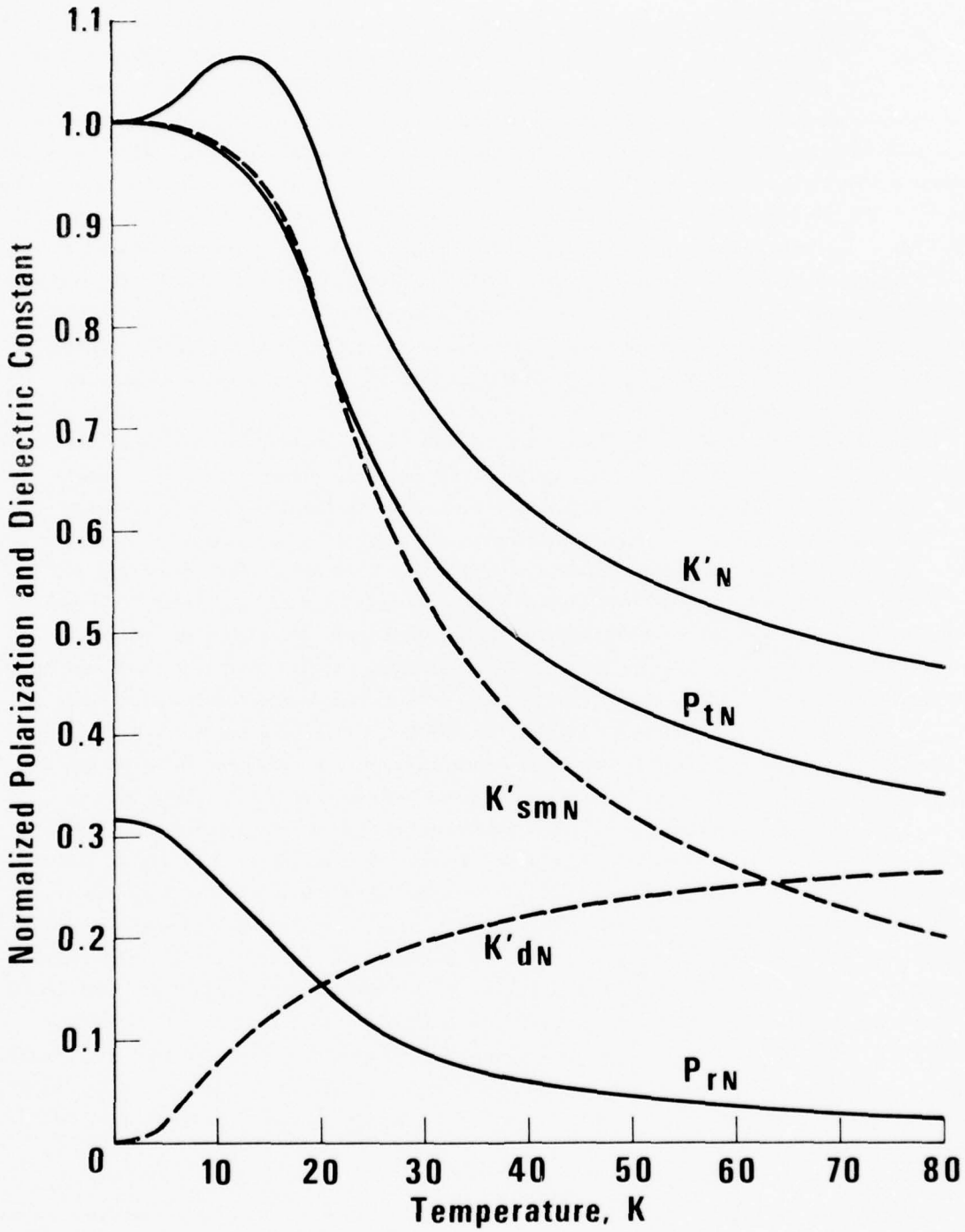

Figure 83. Normalized dielectric constant, K'_N, and polarization, P_{rN} and P_{tN}, as a function of temperature based on the mathematical model described in the text.

$$P_t(T) = \varepsilon_o E K'(T) + P_r(T).$$

The $P_{tN}(T)$ curve in figure 83 is derived from the above equation by assuming a value for $\varepsilon_o E$ such that $\varepsilon_0 E K'_N(0) + P_{rN}(0) = 1$. No peak is generated in $P_t(T)$ regardless of the T dependence of $P_r(T)$ and $K'(T)$ because of the relationship between K'_d and P_r. The curves obtained from this simple model have temperature dependences for P_r, P_{tN}, and K'_N similar to those observed, though the model doesn't specifically fit any particular specimen. For the ceramic materials containing additives, K'_{sm} probably deviates from 1/T at a much higher T, then the peak in $K'(T)$ and the peak temperatures are increased. The T dependence of P_{rN} is probably less than calculated since all the dipoles would presumably not align in the applied field.

Of the materials measured in any detail, only $Pb_2Nb_2O_7$ differed significantly from the behavior discussed above. The peak in $K'(T)$ is probably due to dielectric relaxation but there is no significant remanent at 4 K or hysteresis in the P-E curve. Apparently the relaxing dipoles are not sufficiently inhibited to form an electret state even at 2 K.

3.8.2. Thermal properties

For temperatures somewhat above 4 K, the term $\partial P/\partial T$ in most materials studied became reasonably large and negative, expecially for $SrTiO_3$ and $KTaO_3$ (single crystal, ceramic, or glass-ceramic). The largest $\partial P/\partial T$ values, and hence largest entropy changes, occur in the 20-50 K temperature range. The observed adiabatic depolarization cooling in this temperature range agreed well with that predicted from the measured $\partial P/\partial T$ and specific heat via eq. (3.3). The actual tmeperature changes were always less than 1 K for the field strengths used. It was uncertain how much further the temperature could be reduced by using much larger fields, since $\partial P/\partial T$ was not known at higher fields. If $\partial P/\partial T$ could be measured in sufficiently high fields to make $\partial P/\partial T$ apprach zero, then the maximum entropy change could be calculated. Since all the materials studied had $\partial P/\partial T<0$, an applied electric field always decreases the entropy. The maximum entropy change then would be just the value of the field dependent entropy of the material, or the dipolar entropy in zero field. When that is subtracted from the zero field entropy, the remainder is the intrinsic lattice entropy, which is field independent. As will be discussed later the lattice entropy can be influenced slightly by an electric field in some cases. In those cases the maximum entropy change can be larger than the case where the lattice entropy is field independent. In any case the maximum entropy change can be no larger than the total entropy in zero field. Such a limit indicates the maximum refrigeration power which can be expected from a material, even though the material could cool itself down from any temperature.

At this point we are faced with the problem of determining the total zero field entropy and then separating that into the dipolar and lattice contributions. Equation (3.6) can be used to determine the total zero field entropy if the specific heat is measured to a sufficiently low temperature.

For low enough temperatures, $\partial P/\partial T = 0$ and $\partial^2 P/\partial T^2 = 0$, and the dipolar contribution to the specific heat should be negligible. According to eq. (3.4) the specific heat is independent of field in that temperature region. For all the materials studied in this program, 2 K was a sufficiently low temperature to insure $\partial P/\partial T$ and $\partial^2 P/\partial T^2$ were zero. Specific heat

results on these samples showed that C/T^3 was beginning to level off in the range 2 ~ 4 K and approach the value predicted by elastic constants. For some of the materials, such as $SrTiO_3$ and $KTaO_3$, it would be desirable to have specific heat measurements down to 1 K or below to accurately extrapolate C/T^3 to 0 K. However, because $C \propto T^3$, the temperature range below 1 K contributes only about 2% to the entropy at 4 K. Considerable uncertainties in C/T^3 below 1 - 2 K are then of little consequence.

The only cause for concern in extrapolating the specific heat to 0 K is that an anomaly in the specific heat may be present in that temperature interval. Only an anomaly which is influenced by an electric field is of any consequence since any other type would simply shift all the curves in figure 1 by the same amount. For the case of $SrTiO_3$ the dielectric constant shows no anomaly down to 0.025 K.[49] The dielectric constant of $SrTiO_3$ glass-ceramics goes through a minimum at about 0.1 K[8] and continues to increase as the temperature is decreased even to 7 mK.[107] Similar behavior has been seen in measurements in this laboratory on a $KTaO_3$ single crystal. Because other work in this laboratory has shown that in $SrTiO_3$ glass-ceramics the minimum in dielectric constant is a function of the ac measuring field amplitude and frequency, it is probable that a thermodynamic anomaly does not occur there. That also is consistent with the specific heat measurements on a $SrTiO_3$ glass-ceramic sample at 4 K as a function of electric field. Since the change in specific heat at 4 K was only 5% or less in a field of 220 kV/cm, the entropy at 4 K is little affected by such a field. That suggests that if any anomaly did exist, it must be orders of magnitude lower in temperature than 4 K and thus has no influence on the relative entropy at 4 K and above. In addition, there is no theoretical reason to expect any anomaly in the range below 1 K.

Separation of the total entropy into the lattice and dipolar parts could be done experimentally if a sharp transition occurred. The dipolar part would simply be the transition entropy and the lattice part would be the background entropy. This separation is commonly done for materials with ferroelectric transitions near room temperature.[88] When the dipolar entropy is small and there are no sharp transitions, it becomes difficult to separate the two from experimental specific heat results. Such is the case with all the materials studied in this program. To help in the separation, we will make use of theoretical models.

Order-disorder materials: Ferroelectric and antiferroelectric transitions are usually classified into order-disorder or displacive type transitions.[88,108] For order-disorder materials a permanent dipole moment exists even in the non-polar phase which implies the existence of a double potential well for the ion or group of ions. This kind of dielectric material is very much analogous to magnetic substances. The elementary magnetic moment of a material is independent of temperature and exists both above and below the transition temperature. In such materials the thermal energy tends to randomize the direction of each moment so that no net moment exists in the material above the transition temperature. In magnetic materials short range forces of the exchange, super-exchange, or double exchange type bring about an ordering of the dipoles below the transition temperature. For dielectric and ferroelectric materials long range forces, such as the Columb interaction, are just as important as the short range forces in bringing about ordering of the moments. Nevertheless

the thermodynamic treatment of the magnetic and dielectric cases is identical. Thus depolarization cooling with an order-disorder dielectric should be completely analogous to adiabatic demagnetization of a paramagnetic material. In paramagnetic materials with total angular momentum of j there are 2j + 1 possible orientations of the magnetic moment and so the entropy in the disordered state is S = Rln(2j + 1). A pseudo-spin model may be used to describe order-disorder dielectrics.[109] For a material with two minimums in the single particle potential well, spin 1/2 operators are used in the description. Because of the two equilibrium positions of the particle in the disordered state, the dipolar entropy is S = Rln2 in the disordered state. Sufficiently high electric fields can order the dipole moments and so maximum entropy changes of the order of Rln2 are possible with order-disorder dielectrics above the transition temperature.

There are a few materials such as potassium dihydrogen phosphate and tri-glycine sulfate, which are typically order-disorder type ferroelectrics. Specific heat measurements do indeed show entropy changes on the order of Rln2 at the transition from the ferroelectric to the paraelectric state. The transitions, however, occur at much too high a temperature to be useful for refrigeration at 4 K. The lowest transition temperature for a known order-disorder ferroelectric is 96 K for KH_2AsO_4[108] and 122 K for KH_2PO_4.[108] The theoretical entropy and spontaneous polarization of such materials were derived by Devonshire[109] and are shown in figure 84 as a function of the reduced temperature. According to that calculation S/R falls below 10^{-2} for $T/T_c < 0.3$ and continues to drop exponentially. Thus for KH_2AsO_4 below about 30 K the dipolar entropy is too small to make a useful refrigerator. In order to meet the requirement of $S/R \geq 10^{-2}$ at 4 K, it would be necessary to have an order-disorder material with a transition lower than about 13 K. If the ordered state is ferroelectric, then there still would be the problem of hysteretic heating during field changes.

The material lithium thallium tartrate ($LiTlC_4H_4O_6 \cdot H_2O$), hereafter abbreviated as LTT, has shown indications of a ferroelectric transition at about 11 K.[110-113] A fairly pronounced peak in the dielectric constant occurs at 11 K for semi-transparent electrodes as well as a rapid softening of the lattice.[112] Both the elastic compliance and dielectric constant are strong functions of electric field in the region around 11 K. The structural similarity to Rochelle salt indicates it may be an order-disorder ferroelectric. Unfortunately there was not time to measure the specific heat and electrocaloric effects of this material because of the difficulties in obtaining a sample. Existing measurements[113] of the spontaneous polarization P_s can be used to give estimates of the entropy change near the transition. This estimate is done via the Clapeyron equation,

$$\Delta S = P_s^2/2\varepsilon_o C, \tag{3.24}$$

where ε is the dielectric constant and C is the Curie constant in the Curie-Weiss expression

$$K' = C/(T - T_o). \tag{3.25}$$

If we use $C = 1.4 \times 10^3$ K and $P_s = 2 \times 10^{-7}$ C/cm^2 and a molar volume of about 40 cm^3/mole, the entropy change is only $\Delta S/R = 8 \times 10^{-4}$. Such a change would be too small for useful

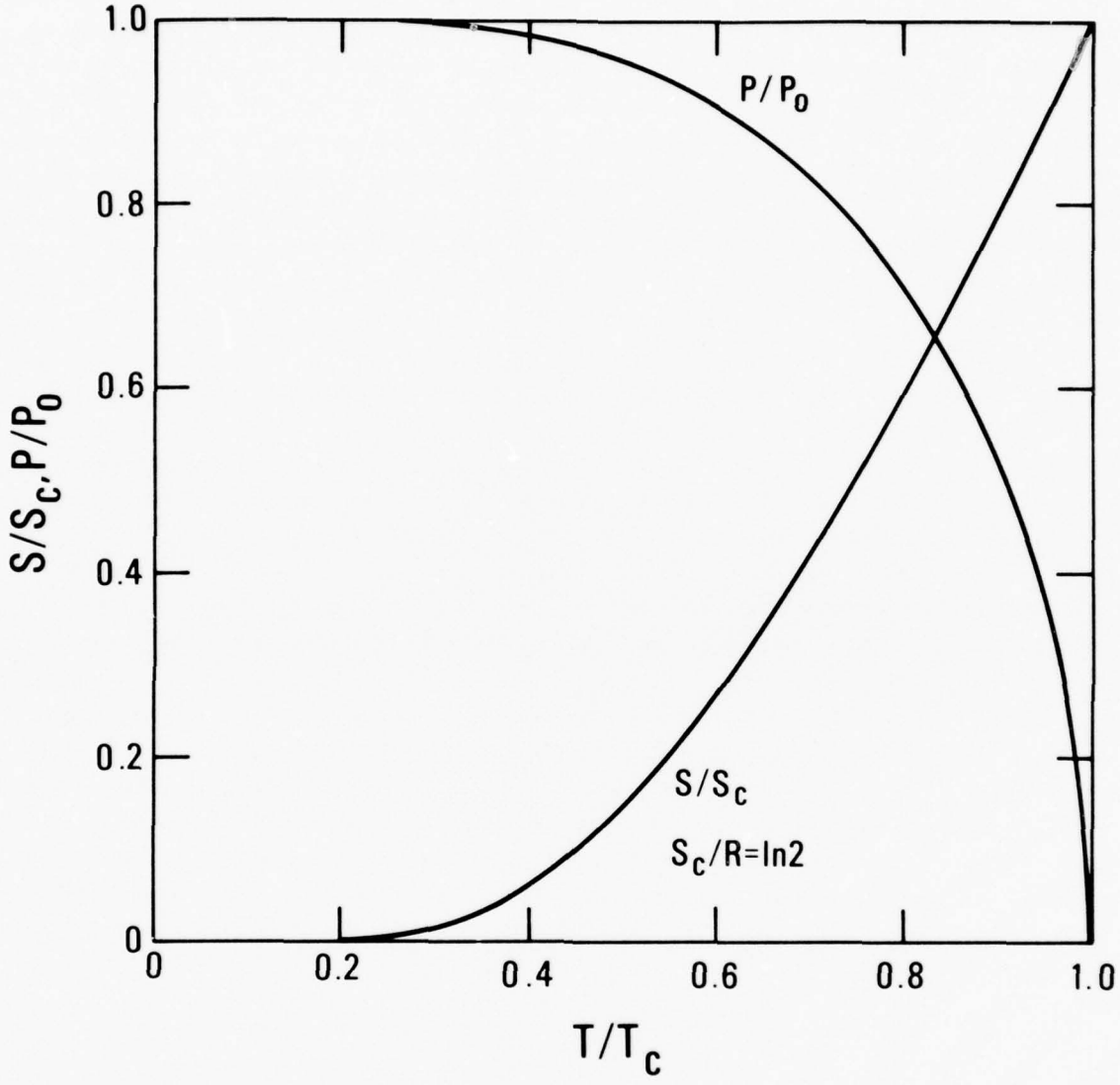

Figure 84. The reduced entropy and spontaneous polarization as a function of reduced temperature for an order-disorder ferroelectric. The curves are based on calculations by Devonshire.[109]

refrigeration but further measurements on LTT would be useful.

Displacive materials: The other class of dielectric transitions is the displacive type. In these materials the potential well, V(X), has only one minimum and is only slightly anharmonic. A permanent dipole moment does not exist in these materials above the transition temperature, but the application of an electric field induces a moment. As the temperature is lowered in such a dielectric, the long and short range forces on the ion can change in such a way that they tend to cancel each other at some termperature. When this occurs, $\partial^2 V/\partial X^2 = 0$ at $X = 0$ and the ion becomes unstable at $X = 0$. A small displacement of the ion can occur at and below that temperature and the material becomes a displacive ferroelectric or antiferroelectric. A lattice dynamic description of such materials, as introduced by Cochran,[114] and Anderson[115] has proven very useful.[108] In this description the frequency, ω, of the optic phonon mode decreases as the temperature is lowered. At the transition temperature ω becomes zero at some value of the wave number q. The process is called a condensation of a soft mode. If the condensation occurs at $q = 0$, the transition is to the ferroelectric state, whereas if it occurs at the Brillouin zone boundary, an antiferroelectric transition occurs. An electric field has a strong effect on the soft mode.

The ABO_3 compounds having the perovskite structure usually display the displacive type transitions. The material $PbTiO_3$ is the most ideal example in the sense that the soft optic mode is sharp and underdamped in contrast to $BaTiO_3$ where the soft optic mode is highly overdamped.[116] Both $SrTiO_3$ and $KTaO_3$ are good examples of displacive or soft optic materials though the optic mode never quite condenses at $q \approx 0$ even for $T = 0$ K. These materials could be called incipient ferroelectrics. All of the materials studied in this program are probably of the displacive type.

The lattice dynamic description of the displacive materials provides a simple way of separating the lattice and dipolar entropies. In such a model the lattice entropy is that associated with the acoustic modes and the dipolar entropy is that of the optic mode. Recent neutron scattering experiments using high flux reactors have been valuable for mapping out the phonon dispersion curves of several of the materials studied in this program. Various thermodynamic properties of the material can then be calculated from these phonon dispersion curves. For instance, when the phonon dispersion curves are independent of the temperature, the specific heat is given as[117]

$$C = \frac{Vk}{8\pi^3} \sum_p \iiint \frac{x^2 e^x}{(e^x - 1)^2} \, dq^3, \tag{3.26}$$

where V is the volume, k is Boltzmann's constant, q is the wave number, p refers to summation over all polarizations, and x is given by

$$x(q,T) = \hbar\omega(q)/kT. \tag{3.27}$$

The summation over the polarizations refers to the various transverse and longitudinal modes in the acoustic and optic branches. The transverse modes are doubly degenerate in both the acoustic and optic branches. In general, the phonon dispersion curves have not been measured in enough directions or in enough detail to warrant solving eq. (3.26) exactly. Instead we

make the assumption that the phonon dispersion curves are the same in all directions and approximate the Brillouin zone with a sphere. With those approximations we get

$$\frac{C}{3R} = \sum_p \int_0^1 \frac{x^2 e^x}{(e^x - 1)^2} y^2 dy, \tag{3.28}$$

where $y = q/q_{max}$. For a cubic crystal with a zone boundary of $q_{B.Z}$ along a [100] direction, q_{max} for the spherical approximation is

$$q_{max} = \sqrt[3]{6/\pi}\, q_{B.Z}. \tag{3.29}$$

With these approximations the entropy is given as

$$\frac{S}{3R} = \sum_p \int_0^1 \left[\frac{x}{e^x - 1} - \ln(1 - e^{-x}) \right] y^2 dy. \tag{3.30}$$

If the dispersion curves are functions of temperature, the entropy is still given by eq. (3.30), but then the specific heat must be calculated from

$$C = T\partial S/\partial T. \tag{3.31}$$

The materials studied in this program had phonon dispersion curves that were nearly temperature independent below 15 K. Thus, eqs. (3.28) and (3.30) were used in all the calculations since the region of main interest in this program is that below 15 K. The calculations for C and S were carried out to 40 K and, in general, the error introduced in C at that temperature by not using the exact technique of eq. (3.31) is probably the order of 10%. That uncertainty is still smaller than that of the complete phonon dispersion curves.

Figure 85 shows the phonon dispersion curves for $SrTiO_3$ used for the thermodynamic calculations. For low q the curves are based on the neutron scattering work of Yamada and Shirane.[118] The slopes of the acoustic modes at q = 0 are consistent with the elastic constant measurements of Bell and Rupprecht.[119] The Debye temperature, normalized to one atom per molecule, derived from the elastic constants is 390 K. The double valued part of the transverse optic (TO) curve at low q and E = 0 indicates the uncertainty of the curve. The upper curve is based on the neutron work[118] and the lower curve is based on Raman scattering work.[120] The difference is outside experimental error and has been attributed to thermal aging which causes an increase in the energy with time. The lower curve was used in our calculations because it is more consistent with that derived from dielectric constants using the Lyddane-Sachs-Teller relation,

$$K'_o/K'_\infty = \omega_{LO}^2/\omega_{TO}^2, \tag{3.32}$$

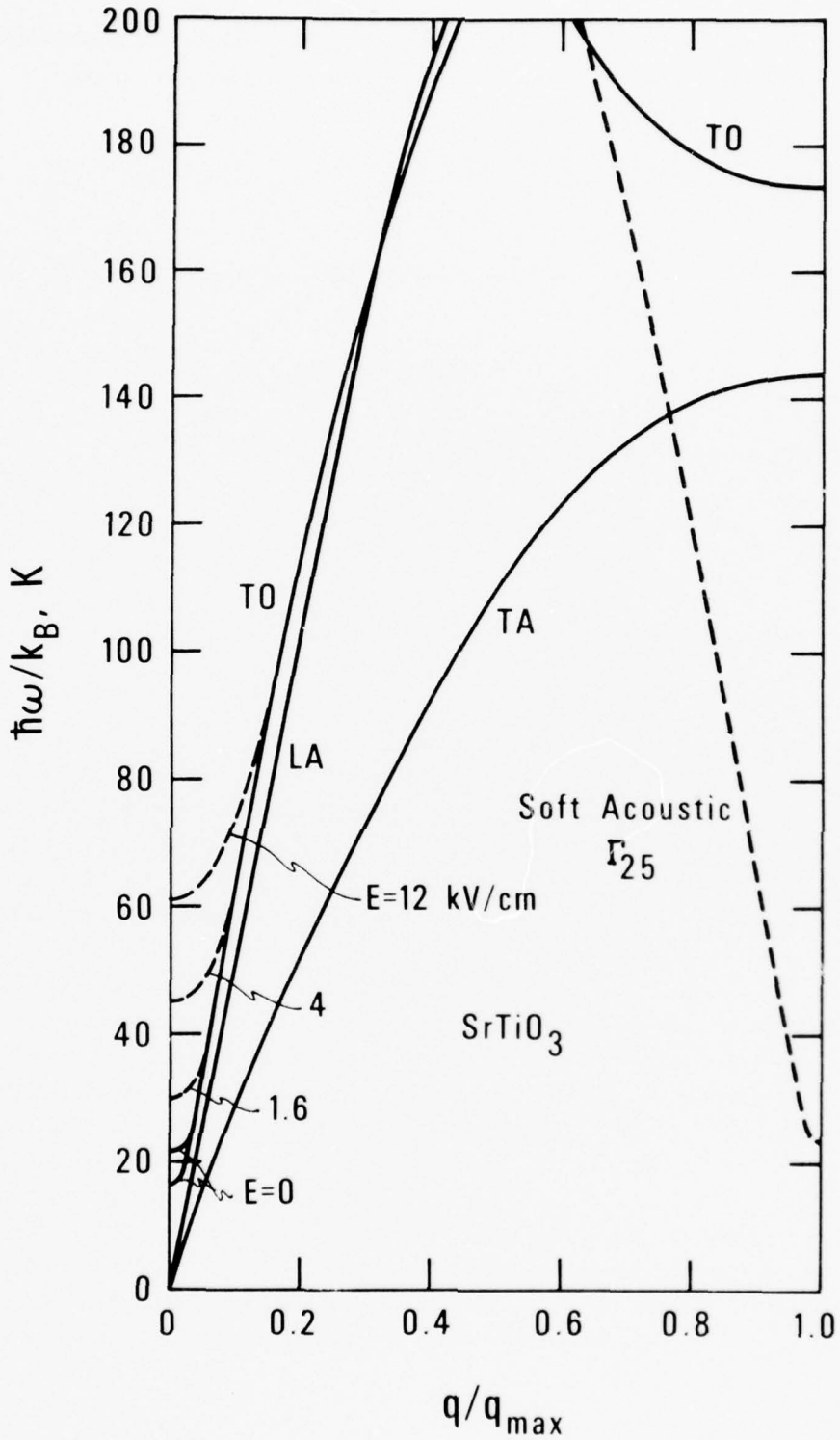

Figure 85. Phonon dispersion curves for $SrTiO_3$ used for thermodynamic calculations. The curves are based on neutron and Raman scattering work.

where K'_o and K'_∞ are the static and high frequency dielectric constants, ω_{LO} and ω_{TO} refer to the longitudinal and transverse optical phonon frequencies. In any case the total entropy or specific heat would be reduced by less than 1% if the upper curve was used. The dispersion curves for various values of electric field are estimates based on the q = 0 values from Raman scattering data.[120]

For high values of q the dispersion curves in figure 85 are based on the work of Shirane and Yamada[121] and of Cowley.[122] The dashed line in figure 85 shows the soft acoustic mode, Γ_{25}, along the [111] direction which is responsible for the antiferrodistortive structural transition at 105 K. The curve as drawn is the position of the mode below about 40 K. The highly anisotropic nature of the Γ_{25} mode means that its contribution to the specific heat and entropy cannot be calculated by eqs. (3.28) and (3.30) since they assume an isotropic mode. Its contribution, however, is probably small and so a crude estimate was made. This was done by using eqs. (3.28) and (3.30) and multiplying the resultant C and S by a constant factor to give reasonable agreement with experiment. The factor used here turned out to be 10^{-2}.

Figure 86 shows the calculated specific heat curves for $SrTiO_3$, plotted as C/RT^3 to remove most of the units and the temperature dependence. The lower dashed curve is the contribution from the three acoustic modes. The middle dashed curve is the specific heat after adding on the contribution from the soft Γ_{25} mode. Notice the hump it tends to give near 5-6 K, which is in reasonable agreement with that seen experimentally in $SrTiO_3$ ceramic. The top dashed line is the specific heat after the addition of the contribution from the doubly degenerate soft TO mode for E = 0. For E = 12 kV/cm the specific heat contribution from the TO mode is decreased. The maximum effect occurs between 5 and 10 K but the total specific heat is lowered only about 2-3%. Such a small change in specific heat with field is consistent with our observation of less than 5% change at 4.4 K for a field of 220 kV/cm on a $SrTiO_3$ glass-ceramic. It is also consistent with the results of Lombardo, et al.,[123] who found no change within 3% in the specific heat of single crystal $SrTiO_3$ for a field of 1.8 kV/cm. Shown in the same figure are the results of measurements on a ceramic in this laboratory, a single crystal,[81] and a polycrystal.[82,83] The agreement between the theoretical and experimental curves is very good over most of the temperature range. The difference is largest below 4 K, which could be a result of impurity contributions and an uncertainty in the details of the acoustic dispersion curves for $h\omega/k < 20$ K. The elastic constant value is based on measurements above the 105 K transition and may not be correct for the 4 K value.

The phonon dispersion curves for $KTaO_3$ have been measured by Shirane, et al.[124] and Axe, et al.[125] The curves shown in figure 87 are based on their work. The slopes of the LA and TA modes are consistent with elastic constant measurements made at 2 K[126] and give a Debye temperature, normalized to one atom per molecule, of 327 K. A slight flattening of the TA mode occurs at about $q/q_{max} = 0.2$, which has been attributed to an interaction between the TO and TA modes.[125] Figure 88 shows the calculated specific heat of $KTaO_3$ in comparison with the measured value. The agreement is good except for the region of 10-15 K. The discrepancy there indicates the TA mode is too low near $q/q_{max} = 1$. That may be possible since the TA mode shown in figure 87 is based on neutron measurements only along the [100] direction. The TA mode could be higher along other directions which would mean the average value shown in

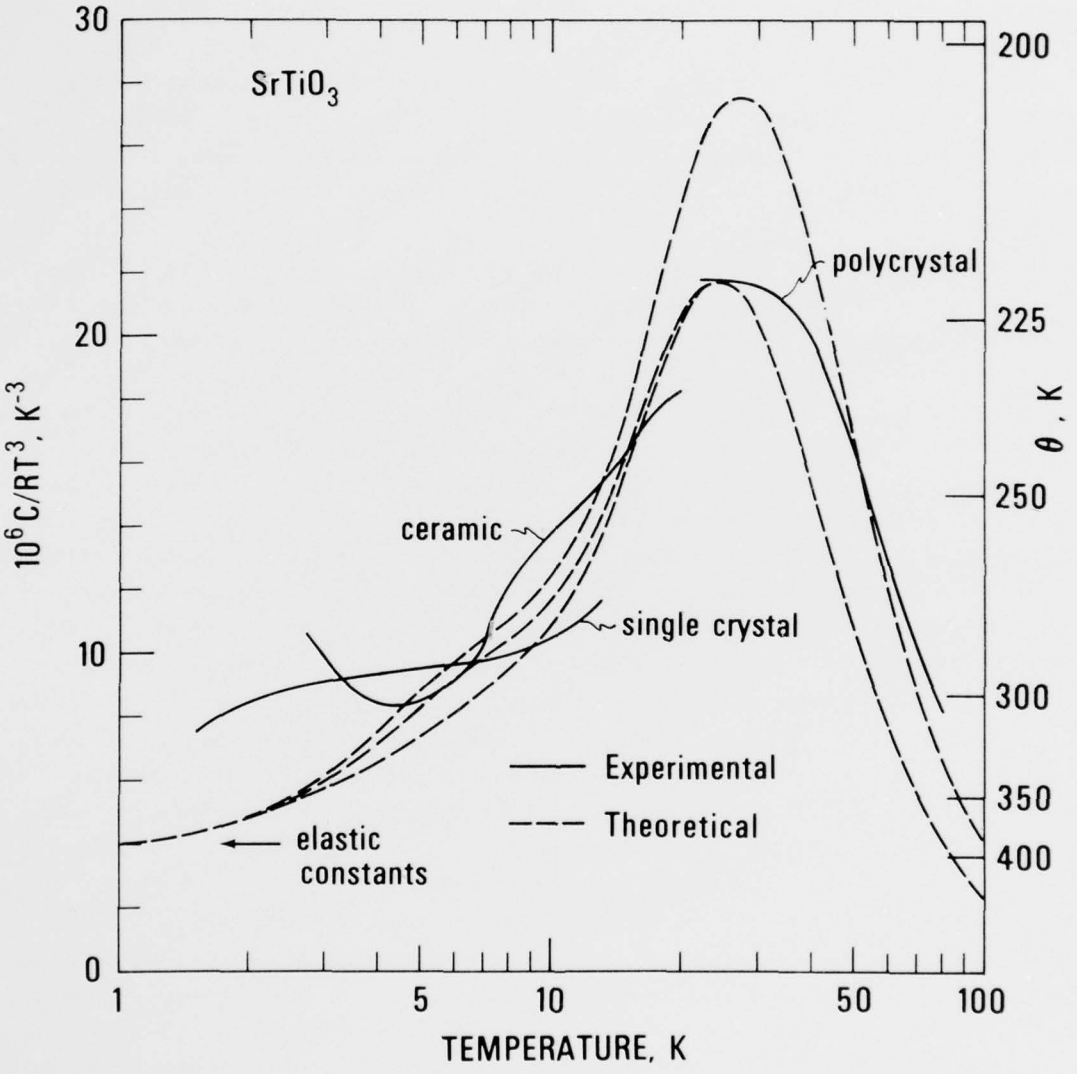

Figure 86. Specific heat of $SrTiO_3$ calculated from the phonon dispersion curves as compared with experimental measurements. See text for explanation of the three theoretical curves.

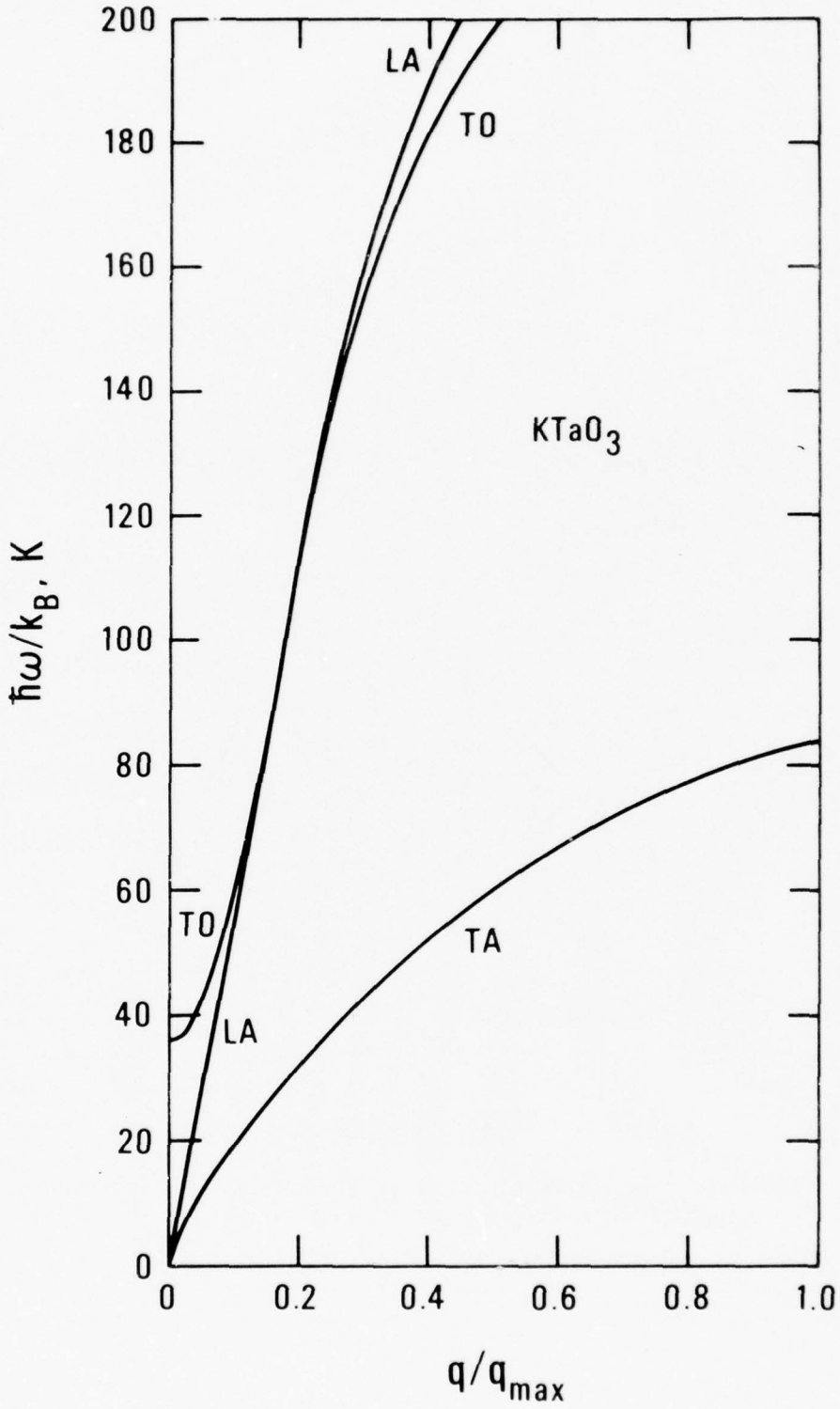

Figure 87. Phonon dispersion curves for $KTaO_3$ used for thermodynamic calculations. The curves are based on neutron scattering work.

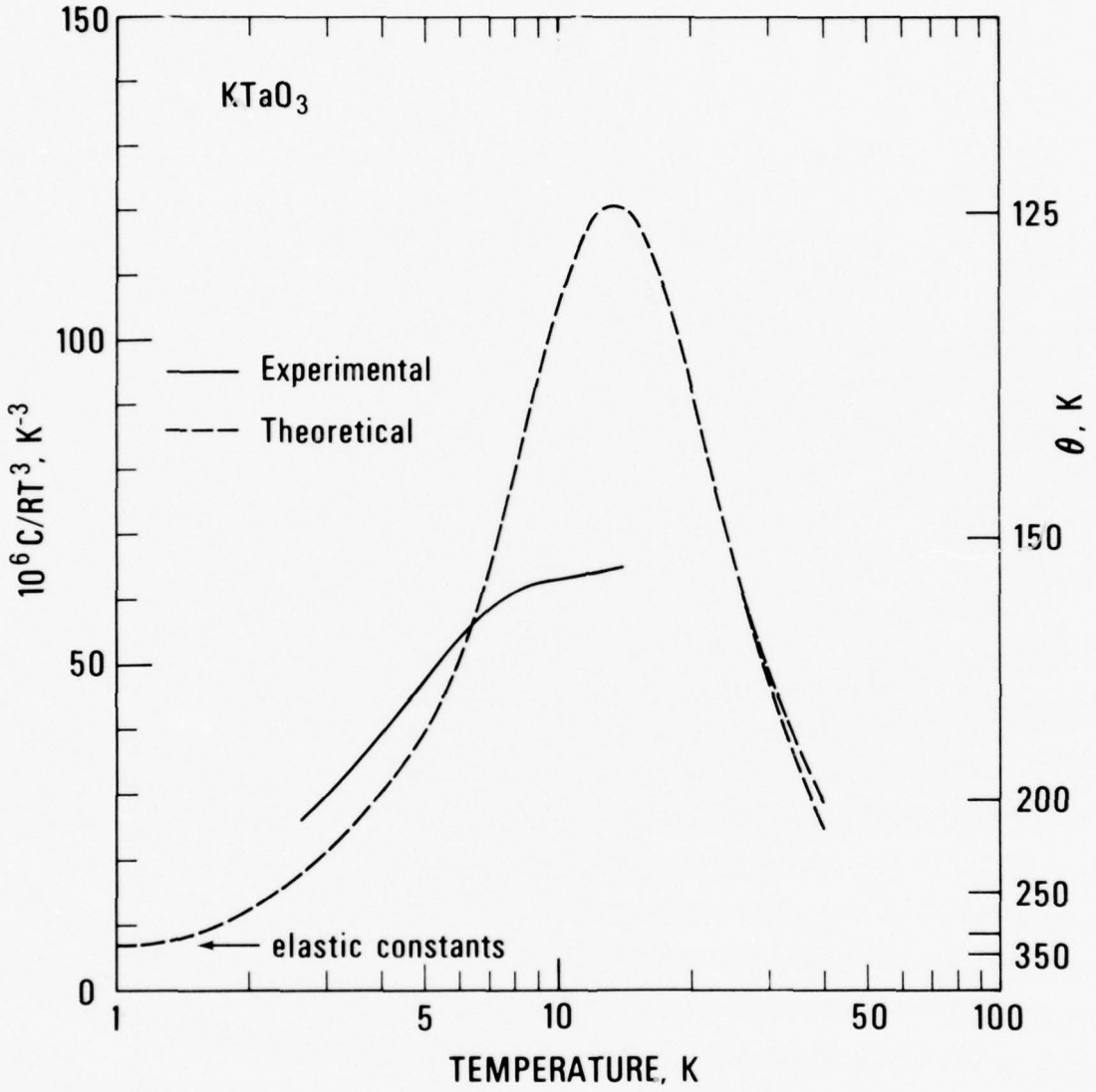

Figure 88. Specific heat of $KTaO_3$ calculated from the phonon dispersion curves as compared with experimental measurements.

figure 87 would have to be raised. The TO mode contribution to the specific heat is much less than that in $SrTiO_3$. It is only for temperatures above about 30 K where the TO mode begins to contribute significantly to the total specific heat (see upper dashed line in figure 88).

A material studied in this program which showed no cooling effects was TlBr. For the sake of comparison we also have calculated the thermodynamic properties of this material. Figure 89 shows the phonon dispersion curve, which are based on the neutron scattering work of Cowley and Okazaki.[127] The TA mode is fairly anisotropic with the (0,0,1) direction giving the lowest values and the (1,1,1) direction the highest. Thus, instead of considering the TA mode doubly degenerate as for $SrTiO_3$ and $KTaO_3$, these two curves were used in the thermodynamic calculations. Such a process tends to average the two curves. As drawn, the acoustic modes are consistent with a Debye temperature, normalized to one atom per molecule, of 100 K. Elastic constant measurements yield a Debye temperature of 131 K,[128] which is rather high to be consistent with the dispersion curves. The TO mode is quite high and independent of temperature and would not be considered a soft mode. The dielectric constant obeys a Curie-Weiss law but the temperature dependence is a result of anharmonic lattice effects rather than a softening of the TO mode.[80] The material is paraelectric for all temperatures and never even approaches a ferroelectric transition as do $SrTiO_3$ and $KTaO_3$.

The calculated specific heat is shown in figure 90 and compared with the experimental curve. There is excellent agreement between the two curves. This material has a rather large specific heat which is a result of the fairly soft acoustic modes. As shown by the upper dashed line, the TO mode contributes little to the total specific heat.

Theoretical calculations for the thermodynamic properties of PZT and $P_2Nb_2O_7$ cannot be done since there have been no measurements of the phonon dispersion curves. The three specific heat comparisons ($SrTiO_3$, $KTaO_3$, and TlBr) between theory and experiment indicate that the lattice dynamic model gives a good description of the thermodynamic properties of the displacive type materials. In all three cases, however, the TO mode contributed only a small part to the total specific heat. Thus the specific heat measurements are not a very sensitive measure of the thermodynamic properties associated with the TO mode. The TO mode contribution could be factors of 2-5 higher before the agreement with experiment is deteriorated. Nevertheless, because of the good agreement in the total specific heat, we shall proceed with the assumption that both the acoustic and TO mode contributions to the thermodynamic properties are well described by the lattice dynamic model.

With the lattice dynamic model, we now have the means for separating the dipolar and lattice entropies for the displacive type materials. The soft transverse optic (TO) mode is in general strongly temperature dependent and is responsible for the polarization of the material. We then assign the dipolar entropy as that associated with the soft TO mode and the lattice entropy as that of the acoustic modes. Electric fields have a strong effect on the static dielectric constant and by the LST relation in eq. (3.32) they also have a strong effect on the frequency of the soft TO mode. An applied electric field has the effect of hardening the TO mode, i.e., increasing the frequency of the mode. The effect is greatest for that part of the Brillouin zone with the lowest frequency of the TO mode. This is the zone center for ferroelectric type materials and the zone edge for antiferroelectric type

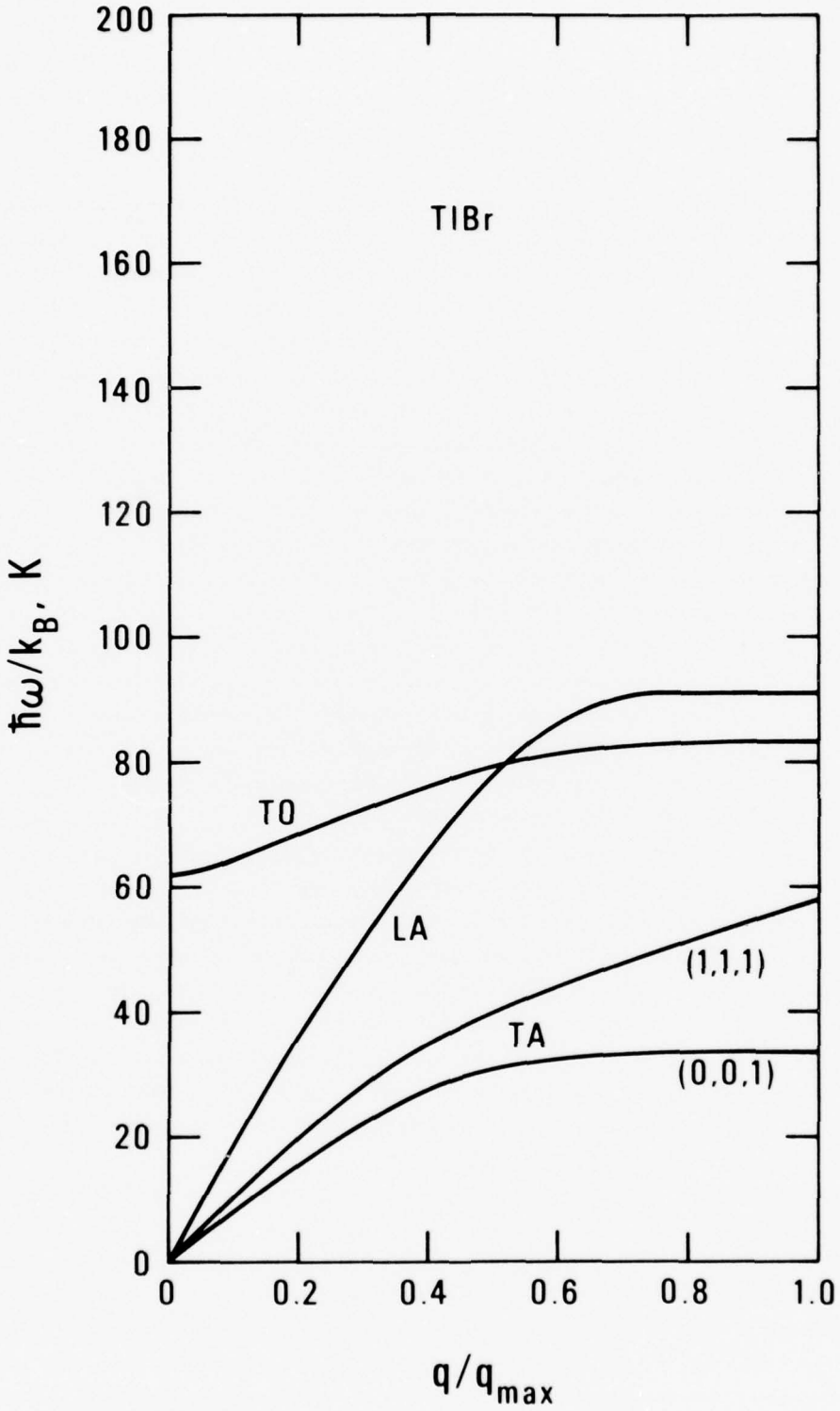

Figure 89. Phonon dispersion curves for TlBr used for thermodynamic calculations. The tranverse acoustic mode, TA, is shown in two principle directions. These curves are based on neutron scattering work.

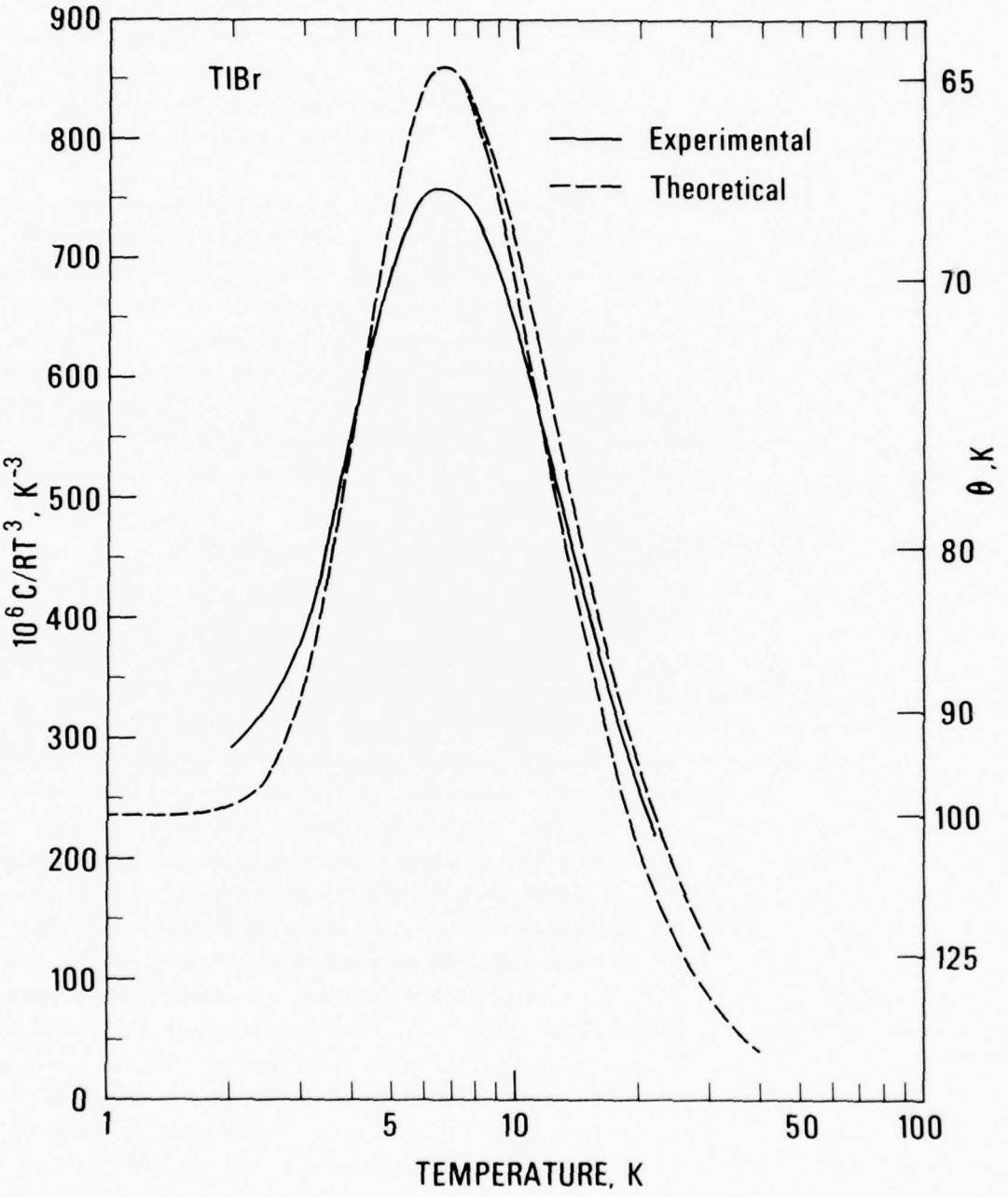

Figure 90. Specific heat of TlBr calculated from the phonon dispersion curves as compared with experimental measurements.

materials. At the other extreme of the zone, the electric field should have little effect on the TO mode. The materials studied here are of the ferroelectric type so that an electric field increases the frequency at the zone center, but has little effect on the frequency at the zone edge. We then expect that as the electric field increases to infinity the soft TO mode hardens and becomes nearly constant for all wave numbers. This constant value is just that of the original soft mode at the zone edge. These two extreme positions for the TO mode then can be used for the dipolar entropies at E = 0 and E = ∞. We have made the assumption that the electric field has no effect on the acoustic modes, though we show later that this is not entirely correct.

Figure 91 shows the entropy of the acoustic and optic modes calculated via eq. (3.30) for $SrTiO_3$. For E = ∞ we have taken the value $h\omega/k$ = 185 K for the TO mode, which tends to level out the hump in that mode. The calculated entropy for that case is just two-thirds the Einstein entropy of a material with an Einstein temperature of 185 K. The difference between the E = 0 and E = ∞ curves gives the maximum entropy change possible, provided the acoustic mode is unaffected by the field. We recall that it was desirable to have entropy changes on the order of $\Delta S/R \approx 10^{-2}$ at 4 K for a practical refrigerator. As shown in figure 91, the maximum dipolar entropy change is over three orders of magnitude less than the desired amount. Because the dipolar entropy is also so much less than the lattice entropy, temperature changes during adiabatic depolarization would be expected to be small. For small temperature changes, i.e., $\Delta T/T \ll 1$, we calculate these changes by

$$\frac{\Delta T}{T} \approx \frac{\Delta S}{T(\partial S/\partial T)} = \frac{\Delta S}{C}, \qquad (3.33)$$

where C is the total specific heat of the material in zero electric field.

Figure 92 shows the calculated temperature changes possible in $SrTiO_3$ when depolarizing from various E values. Shown for comparison are some experimental measurements. The work of Hegenbarth[53] was for a field of 10 kV/cm on a single crystal and that of Kikuchi and Sawaguchi[52] was for 7 kV/cm on a single crystal. The experimental work shown for this program was for a field of 26 kV/cm on a ceramic sample. The open symbols indicate actual observed cooling effects, whereas the solid circles indicate the reversible cooling effect which would occur if the hysteretic heating component is subtracted. According to the theoretical curves, higher electric fields would not significantly increase ΔT below 15 K.

We note that some of the observed cooling effects are somewhat larger than the theoretical maximum. If this is a real effect, then the electric field must affect the entropy not only of the optic mode but of the acoustic modes as well. An interaction between the TO and the TA modes must then exist in order for the electric field to influence the TA mode. A TO-TA mode interaction is known to exist in the case of $KTaO_3$,[125] as discussed earlier in regard to a flattening of part of the TA mode at low temperatures. It would be very desirable to study this interaction further by such means as observing the field dependence of the phonon dispersion curves. It is probably a general occurrence that as the TO mode softens and approaches the TA mode, the TA mode also softens in part of the Brillouin zone because of the interaction between the two modes. The existence of electrostrictive or

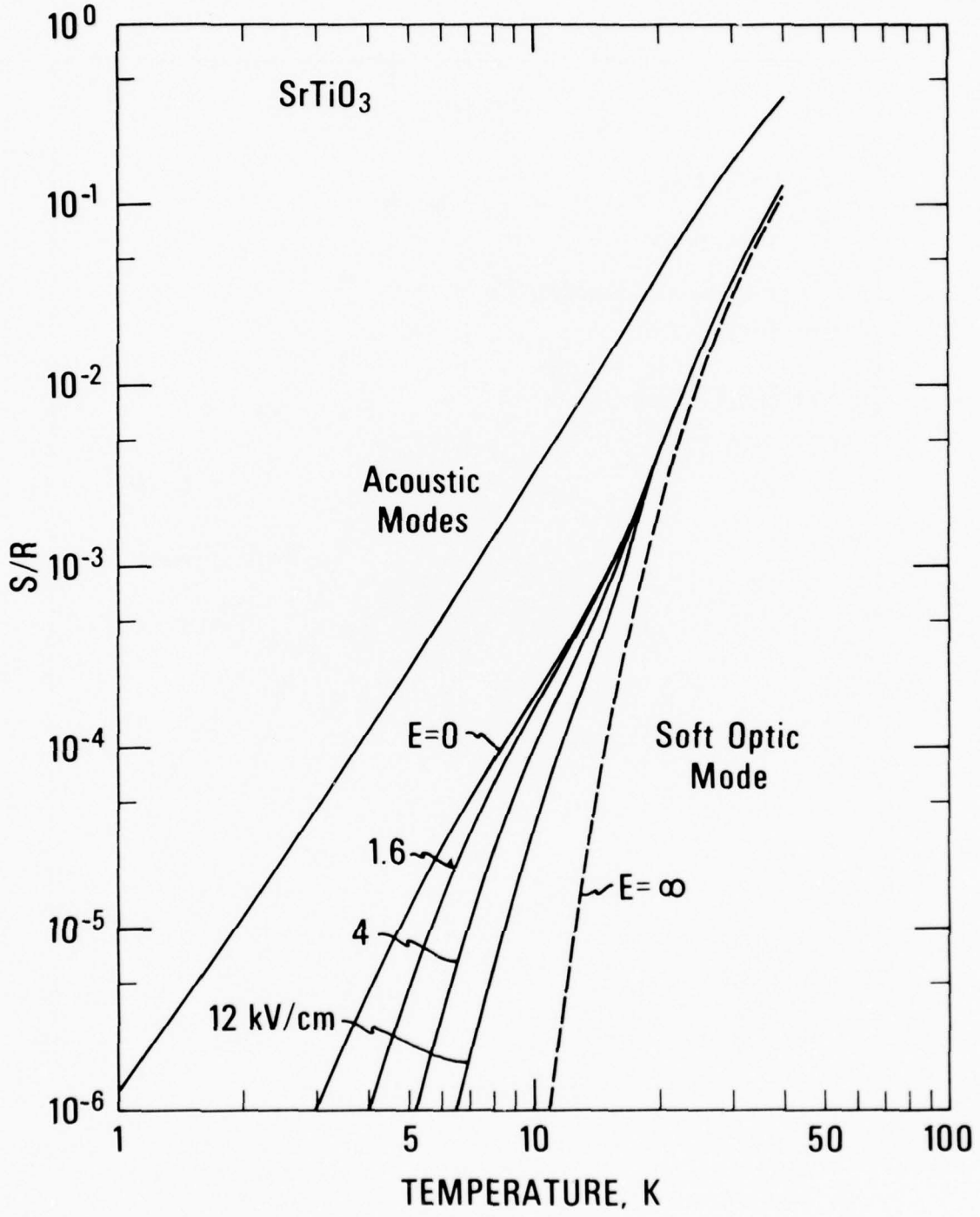

Figure 91. Entropy of the acoustic and optic modes of $SrTiO_3$ calculated from the phonon dispersion curves.

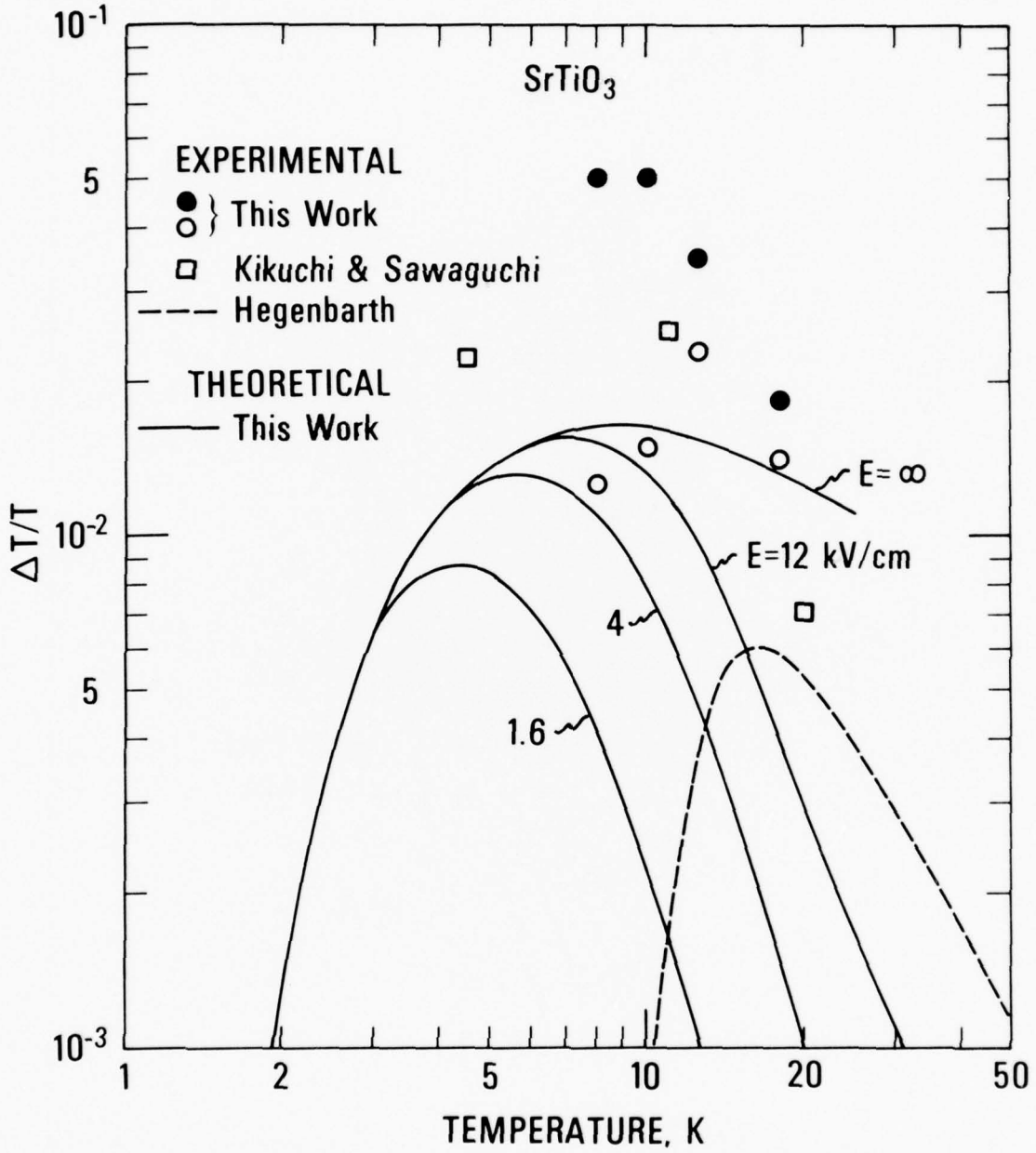

Figure 92. Calculated maximum temperature change due to optic mode during depolarization of $SrTiO_3$. Experimental values are shown for comparison.

piezoelectric effects in a material is an indication of coupling between optic and acoustic modes. It is known that an electric field does have an effect on the elastic constants,[119] i.e., the slopes of the acoustic modes at the zone center. A field of 20 kV/cm decreases the slope by 4% at 125 K, which is the opposite direction for the effect we are looking for. Presumably the field increases the acoustic phonon frequency farther out from the zone center. Because the entropy associated with the acoustic mode is so much higher than that of the TO mode, a rather small shift of the acoustic mode with electric field can make a large correction to calculated temperature changes. In the case of $SrTiO_3$ a shift of the acoustic mode entropy by 15% would account for the observed high values of $\Delta T/T$. Even if the total entropy of the acoustic modes is completely removed by the electric field, the resulting entropy change of $\Delta S/R = 10^{-4}$ is still two orders of magnitude less than the desirable amount for a practical refrigerator.

Figure 93 shows the calculated optic and acoustic mode entropies for $KTaO_3$. The soft optic mode entropy is less than that for $SrTiO_3$, whereas the acoustic mode entropy is higher than that of $SrTiO_3$. The entropies at 4 K are much less than the desired value of $S/R = 10^{-2}$. The calculated electrocaloric temperature changes for field changes from $E = \infty$ to $E = 0$ are shown in figure 94. Experimental results on a $KTaO_3$ single crystal with a depolarizing field of 15 kV/cm are shown for comparison. Both the experimental results and the calculated limit are less than for $SrTiO_3$. As for the case of $SrTiO_3$, the experimental values for $\Delta T/T$ are higher than the theoretical limit. A 10% reduction of the acoustic mode entropy in an applied field would account for the larger observed $\Delta T/T$.

The entropies of the acoustic and TO modes for TlBr are shown in figure 95. The TO mode (shown in figure 89) for TlBr, unlike $SrTiO_3$ and $KTaO_3$, does not soften at the zone center, i.e., the phonon frequency is nearly independent of wave number. Thus an electric field should have little effect on the TO mode and its entropy, as is indicated by the calculated curves in figure 95. The entropy of the acoustic mode is on the order of $S/R = 10^{-2}$, but little interaction would be expected between the TO and acoustic modes because of the large difference in energy between the two modes. Thus, the electric field should have little effect on the acoustic mode. Theoretically the temperature changes during adiabatic depolarization are very small (about 1 mK at 7 K) and probably not observable. As expected, no temperature changes could be detected experimentally.

Except for PZT, none of the displacive type materials showed a transition to the ferroelectric or antiferroelectric state. Instead they remained incipient ferroelectrics down to 0 K. If a displacive transition to the ferroelectric state did occur at a low-temperature, would the dipolar entropy then be high enough for a practical refrigerator? To answer this question we look at the general behavior of the soft TO mode dispersion curve. For the TO mode we consider a fairly simple but reasonable[129] dispersion curve of the form

$$\omega^2(q) = \Delta_o^2 + s^2q^2, \qquad (3.34)$$

where Δ_o is the phonon frequency at $q = 0$ and s is a constant. Putting this equation in temperature units and in units of $y = q/q_{max}$ gives

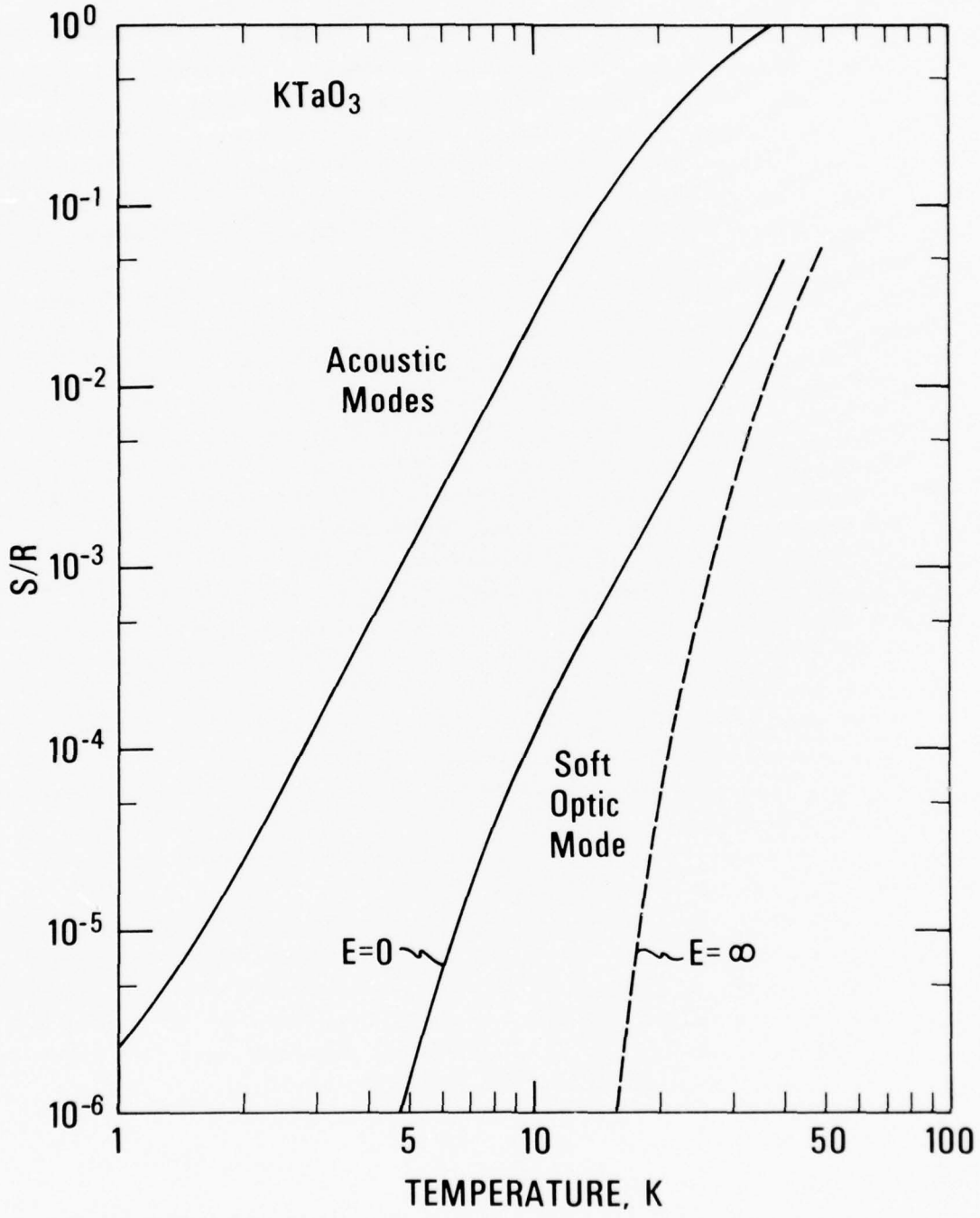

Figure 93. Entropy of the acoustic and optic modes of $KTaO_3$ calculated from the phonon dispersion curves.

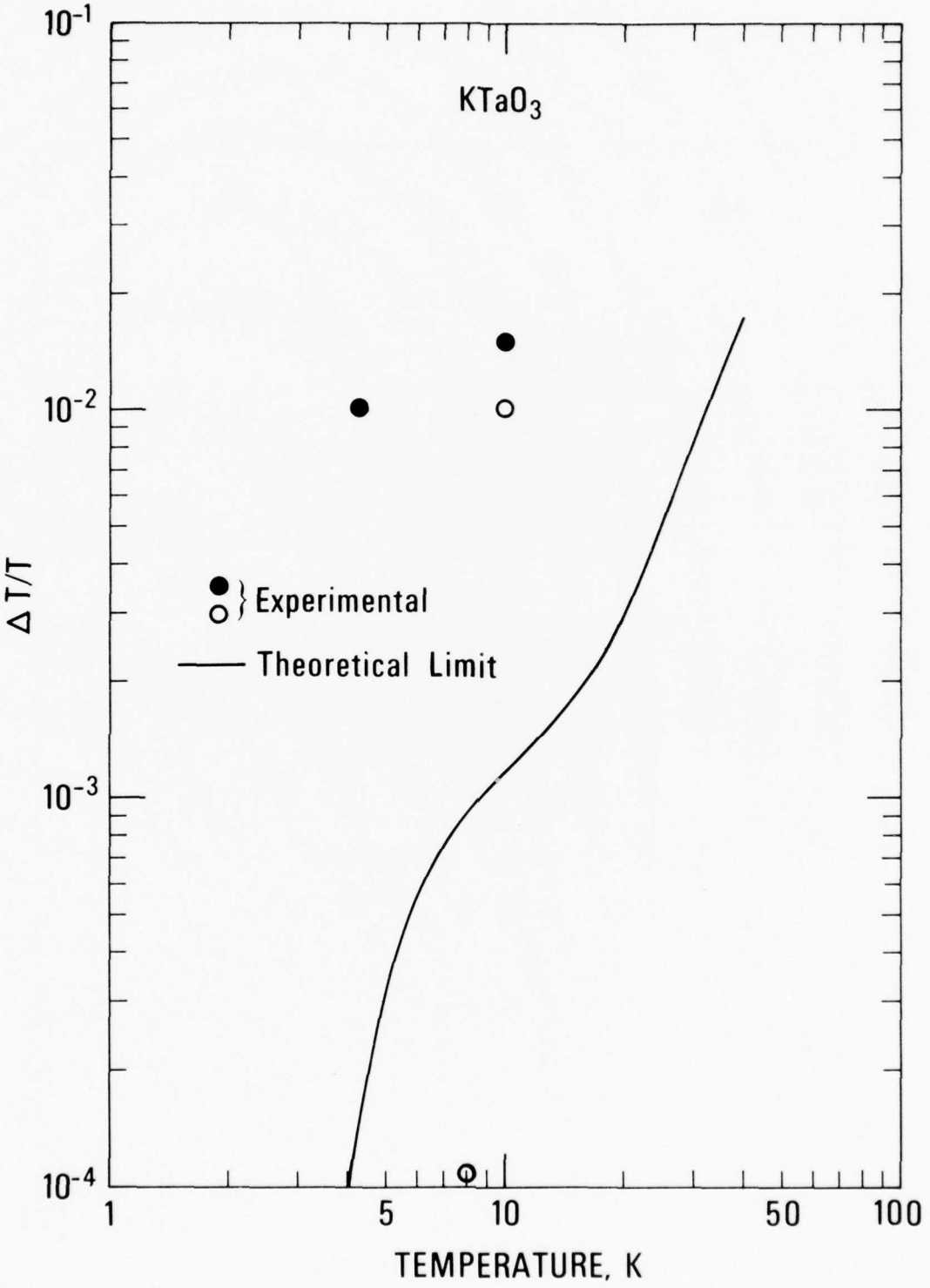

Figure 94. Calculated maximum temperature change due to optic mode during depolarization of $KTaO_3$. Experimental values are shown for comparison.

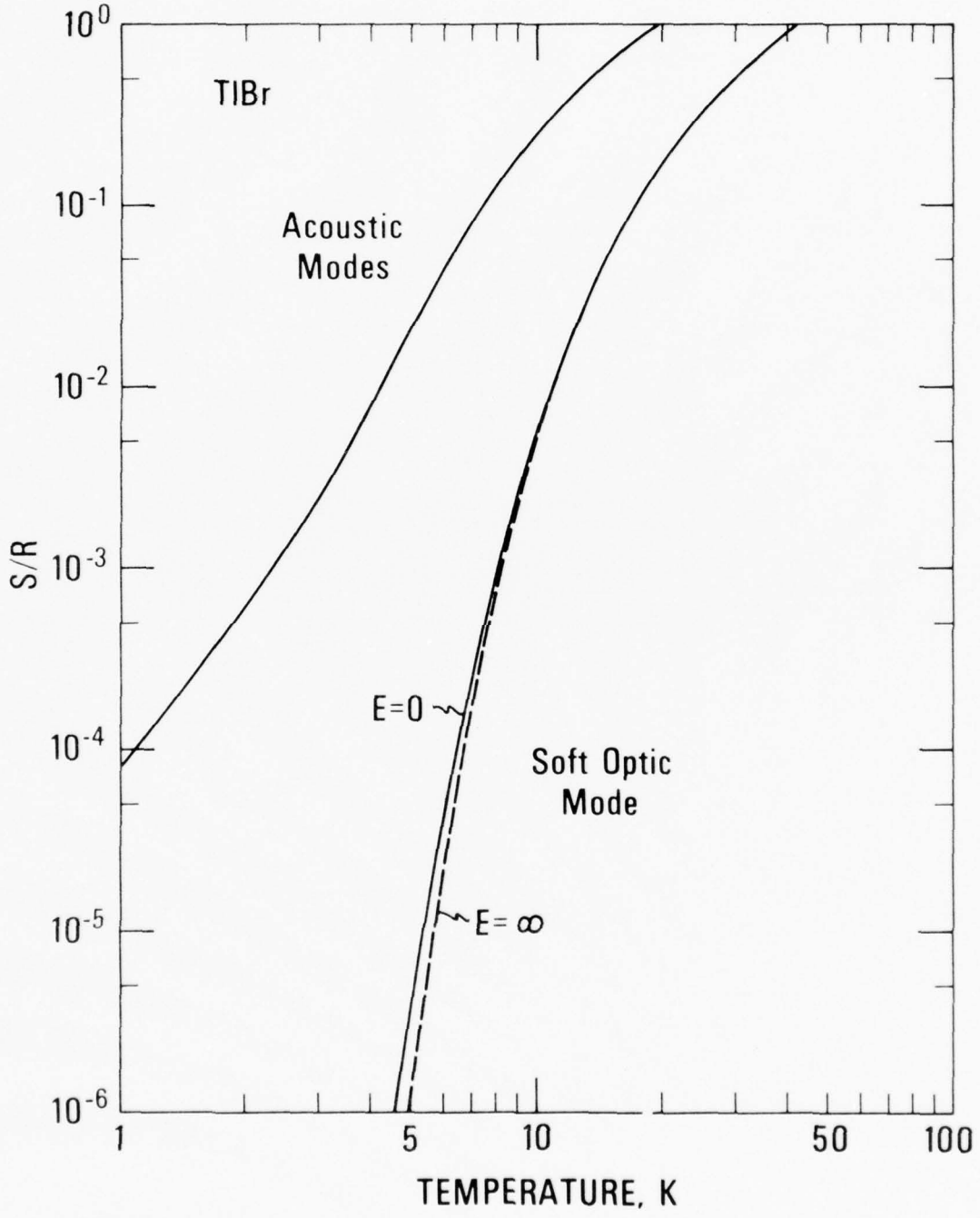

Figure 95. Entropy of the acoustic and optic modes of TlBr calculated from phonon dispersion curves.

$$\hbar\omega/k = \left[(\hbar\Delta_o/k)^2 + (cy)^2\right]^{1/2}. \qquad (3.35)$$

Figure 96 is a plot of equation (3.35) for various values of Δ_o as c is varied to keep $\hbar\omega/k$ at 200 K for y = 1. Condensation of the TO mode would follow the behavior of these curves as Δ_o approaches zero. The condensation of the mode, which gives rise to a ferroelectric transition, can occur at any temperature.

Figure 97 shows the entropy of the TO mode, calculated via equation (3.30), at various temperatures as a function of $\hbar\Delta_o/k$. From these curves we note that the dipolar entropy at the transition ($\Delta_o = 0$) increases with temperature. Whereas S/R is significantly greater than 10^{-2} for a transition at 50 K, it is significantly less than 10^{-2} for a transition at 5 K. In $SrTiO_3$ a transition does not occur and instead $\hbar\Delta_o/k$ comes down to only 16 K. At 5 K the dipolar entropy for this case as shown in figure 97 is about 3×10^{-4} R. If the transition did occur, the entropy is increased by only a factor of three as seen in figure 97. Thus a transition in $SrTiO_3$ to the ferroelectric state would not significantly increase the dipolar entropy. The entropy change which can be brought about by an electric field change from E = 0 to E = ∞ is just the entropy at a given value of $\hbar\Delta_o/k$ minus the entropy at $h\Delta_o/k$ = 200 K. For $\hbar\Delta_o/k \geq 200$ K the phonon dispersion curve is independent of phonon momentum (see figure 96) and probably cannot be raised any further by an electric field. The maximum entropy change an electric field causes on the mode occurs when the model undergoes a transition ($\hbar\Delta_o/k = 0$). This maximum entropy change caused by a change in field from E = 0 to E = ∞ is the entropy at $\hbar\Delta_o/k = 0$ minus the entropy at $\hbar\Delta_o/k$ = 200 K. The curve marked displacive material in figure 98 shows this entropy change as a function of temperature. The significance of the curve is apparent when it is compared with the region of practical refrigeration, also shown in figure 98. The lower boundary for that region is defined by $\Delta T/T_f = 1$ below about 20 K and gradually decreasing to $\Delta T/T_f = 1/3$ at higher temperatures. In this expression T_f is the final temperature reached after cooling from some higher temperature. The curve was calculated using the Debye specific heat of a material with Debye temperature of 200 K. This definition of practical refrigeration pertains only to the ability of a material to cool itself to T_f and says nothing about the refrigeration power once T_f is reached. If the refrigeration power were also considered, the lower limit of the practical refrigeration would be at least a factor of two higher, depending on the specific refrigeration requirements. In any case it is clear that the lower boundary for practical refrigeration is in reality a somewhat fuzzy band with a width of at least a factor of two centered on the sharp line drawn in figure 98.

The example worked out for figure 98 is for a material with a Debye temperature of 200 K. The low temperature part of the $\Delta S/R$ curves for the displacive material and the region of practical refrigeration will change for different Debye temperatures. However, each of the two curves will change by the same percentage amount so the relative position of the curves in figure 98 remains unchanged. It is evident from figure 98 that the possible entropy change in a displacive material is much too small to be useful for practical refrigeration at any temperature. This results from the fact that the TO mode is always higher than the TA mode and thus the dipolar entropy is always less than the lattice entropy. This means

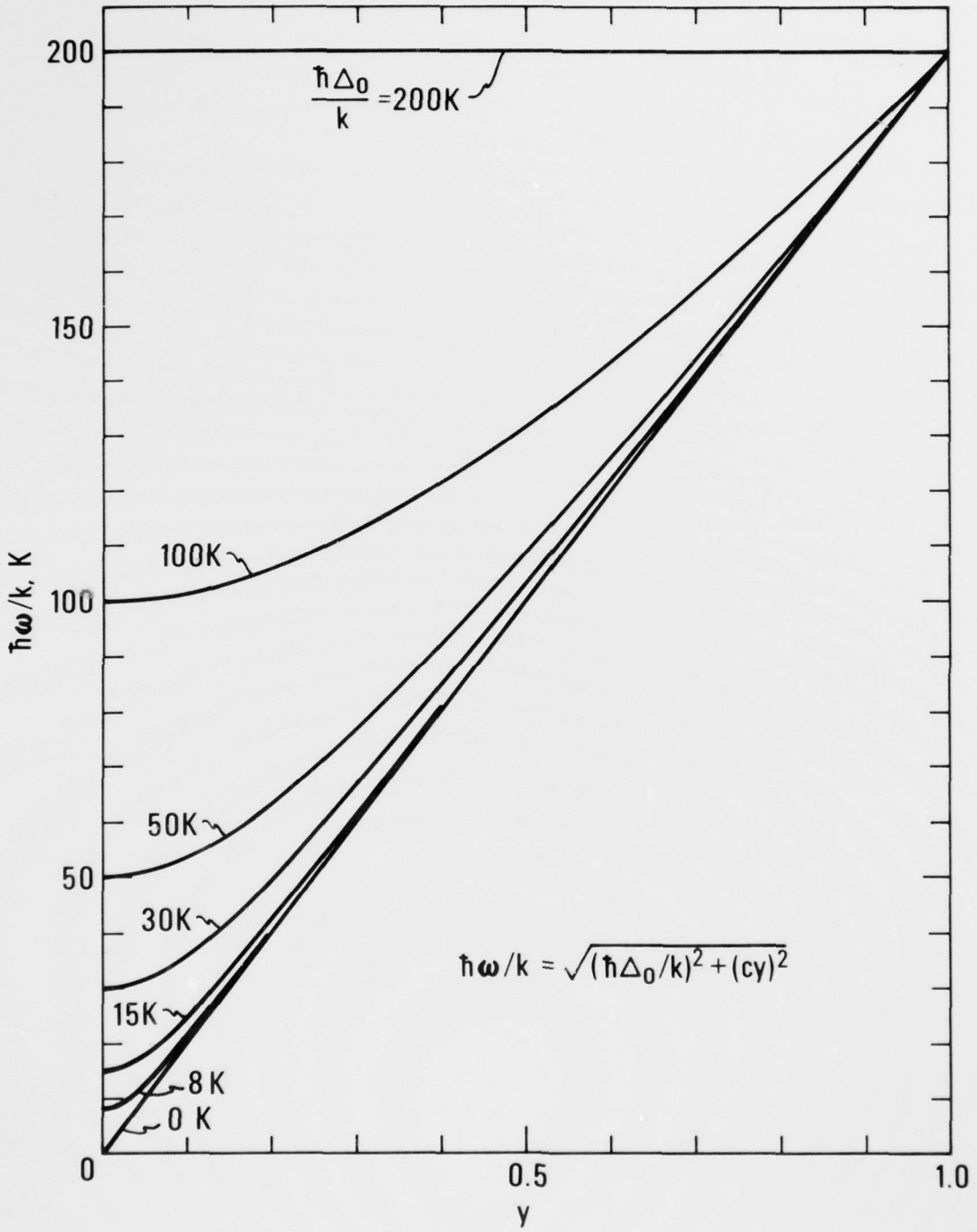

Figure 96. Plot of equation (3.35) for various values of Δ_o and c. These curves are typical of the dispersion curves for transverse optic modes as they soften and condense.

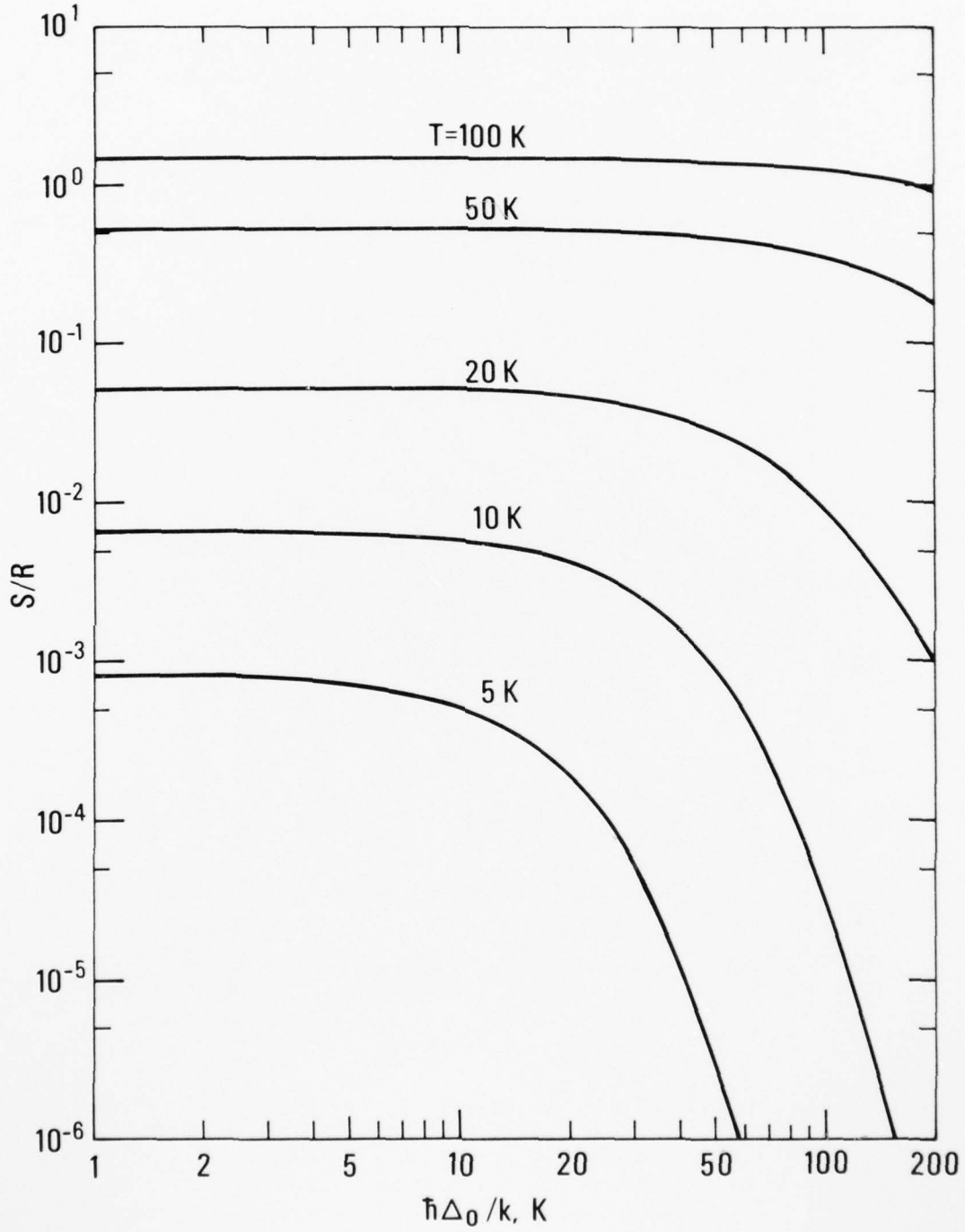

Figure 97. Calculated entropy of a transverse optic mode from the dispersion curves of figure 96 as a function of $h\Delta_o/k$ for various temperatures.

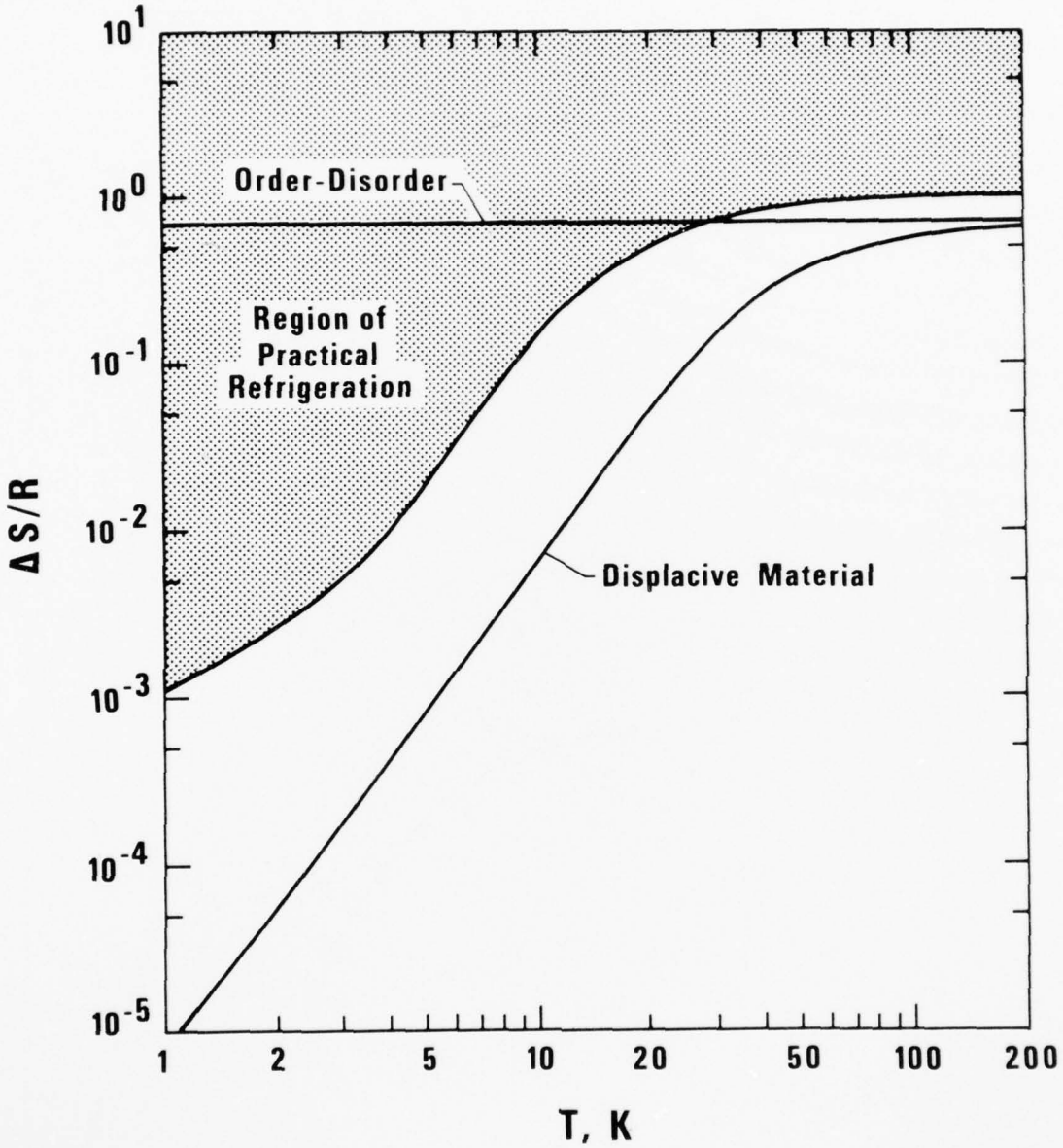

Figure 98. Calculated maximum entropy change for a field change from E=0 to E=∞ in a model displacive material in which the TO mode has condensed at the zone center. The dispersion curves used in the calculations are from Figure 96. Shown for comparison are the maximum entropy change expected in an order-disorder material and the region of practical refrigeration.

that a displacive material cannot cool itself significantly in any temperature range, unless the TO-TA mode interaction is large. In a material with a large TO-TA mode interaction the Debye temperature would have to be less than about 80 K (normalized to one atom per molecule) to provide enough lattice entropy for practical refrigeration. No such a material is known to exist.

For an order-disorder material with a two position dipole the maximum dipolar entropy change is simply $\Delta S/R = \ell n2$ for all temperatures. The ordering temperature must be below the desired refrigeration temperature in order for the entropy to be changed by $R\ell n2$. As shown by figure 98 an order-disorder material could provide practical refrigeration below about 30 K. Adiabatic demagnetization of a paramagnetic salt below 1 K is a classic example of the practicality of the magnetic order-disorder materials. Because of the many spin orientations possible in some magnetic substances, e.g., gadolinium, the entropy changes may be as high as $R\ell n8$. In that case the order-disorder line in figure 98 is moved up into the region of practical refrigeration even at room temperature. It should be noted however that the removal of most of the $R\ell n8$ entropy at 200-300 K requires extremely high magnetic fields. In the case of dielectric materials, either order-disorder or displacive, extremely high electric fields are required to remove most of the dipolar entropy at room temperature, whereas at lower temperatures more moderate fields would be sufficient.

3.8.3. Recommendations for further work.

We consider here one final possibility in the search for materials useful for electrocaloric refrigeration at 4 K. Suppose we use an order-disorder material and by some means we lower the transition temperature down to about 5 K. There are a couple of methods whereby this can be done. One method uses hydrostatic pressure to lower the transition temperature and the other uses an electric field bias on an antiferroelectric material. Samara[130] has measured the transition temperature as a function of pressure for the ferroelectric material KH_2PO_4 and the antiferroelectric material $NH_4H_2PO_4$. The transition temperatures decrease to 0 K at 17 kbar for KH_2PO_4 and 33 kbar for $NH_4H_2PO_4$. The transition temperatures in zero pressure are 122 K for KH_2PO_4 and 151 K for $NH_4H_2PO_4$. What happens then to the transition entropy, or the dipolar entropy, as the transition temperature is lowered? To answer this we use the Clapeyron equation,

$$\Delta S = \Delta v \frac{dp}{dT_c}, \qquad (3.36)$$

where Δv is the change in molar volume at the transition from the ferroelectric to the paraelectric state and dp/dT_c is the slope of the pressure vs. temperature curve separating the two phases. At $p = 0$ the entropy change is[89] $\Delta S/R = 0.37$. This number is used with Samara's[130] value for dp/dT at $p = 0$ to calculate Δv at $p = 0$. Then if Δv is assumed independent of temperature, we get the following expression for the entropy change below 50 K by using Samara's data for T_c vs p:

$$\Delta S/R = 6.0 \times 10^{-3} T_c. \qquad (3.37)$$

At $T_c \approx 5$ K the entropy change is then $\Delta S/R = 3 \times 10^{-2}$, which is sufficiently high for a refrigerator. For $NH_4H_2PO_4$ we expect the entropy change at 5 K to be about $\Delta S/R = 2 \times 10^{-2}$. Because $NH_4H_2PO_4$ is antiferroelectric, it would not have the problem of hysteresis. However, the need for a pressure of 33 kbars probably makes such a method impractical.

In the case of an antiferroelectric, such as $NH_4H_2PO_4$, an electric field also reduces the transition temperature. For that case the Clapeyron equation is

$$\Delta S = -P_s \frac{dE}{dT_c}, \tag{3.38}$$

where P_s is the sublattice polarization and E is the electric field along the transition from the antiferroelectric to the paraelectric state. No data exists for dE/dT_c, but we assume it falls off linearly with temperature below about 50 K, just as for the case of dp/dT_c. At 5 K we then expect the entropy change to be about $\Delta S/R = 2 \times 10^{-2}$. The field necessary to lower the transition to 5 K may be on the order of 100 kV/cm. The application of a field to an antiferroelectric in some cases may introduce a ferroelectric state between the antiferroelectric and paraelectric states. If this occurs in $NH_4H_2PO_4$ the entropy change at 5 K would be reduced but the field required to push the transition down to 5 K would also be reduced. A study of $NH_4H_2PO_4$ in an electric field would be very desirable in establishing its usefulness as a refrigerator material.

For a material to have a transition to a ferroelectric or antiferroelectric state at a very low temperature requires a very small dipole moment. In fact the transition temperature will be proportional to the square of the distance between ions. At some point the zero point motion of the atoms would tend to make smaller displacements, and hence lower transition temperatures, unstable. Kurtz[131] has shown that 20 K is an approximate cutoff temperature below which a transition to a dielectrically ordered state cannot occur. Naturally a lower transition could occur in dilute materials, but the entropy per unit volume is also decreased by the dilution.

4. CONCLUSIONS

This study showed that the $SrTiO_3$ and $KTaO_3$ glass-ceramics and doped ceramics have more pronounced peaks in the dielectric constant vs. temperature curves than do the other nominally pure dielectric materials studied. The positive slope at temperatures below the peak cannot be used for electrocaloric refrigeration as originally believed. The fundamental thermodynamic quantity, the dc polarization, had only negative values for $\partial P/\partial T$ when the sample was cooled in the applied field. The slope was nearly zero for temperatures below about 5 K in all samples tested. It was concluded that the peaks in the dielectric constant were a result of the thermal electret behavior of impurity-vacancy dipoles.

Electrocaloric cooling effects could be seen in many of the samples tested for the temperature range 10-30 K where $\partial P/\partial T$ is large and negative. The largest effects were seen in $SrTiO_3$ ceramics rather than glass-ceramics with similar effects seen in a $KTaO_3$ single crystal. The observed cooling effects were the order of 0.5 K or less for fields of 27 kV/cm. Such effects were not large enough for a practical refrigerator, although the fields were not very high.

In this study, glass-ceramics, ceramics, and single crystals were investigated to better understand the general principles of dielectric behavior and to search for possible cooling materials. All of the materials studied for possible cooling materials were of the soft optic phonon mode (displacive) type dielectrics. Theoretical calculations using the phonon dispersion curves were made of the thermodynamic quantities and showed good agreement with the experimental results. From these calculations it was concluded that the entropy in such materials is one to three orders of magnitude too small for practical refrigeration at 4 K even with infinitely high electric fields. However, discovery of a material with a low Debye temperature and a large TO-TA mode interaction would warrent further investigation.

Dielectric materials of the order-disorder type have orders of magnitude higher entropy ($\Delta S/R \approx 1$) above their transition to the paraelectric state than do the displacive type materials. Unfortunately, an order-disorder dielectric with a low enough transition temperature has not been found. It is recommended that the material lithium thallium tartrate, which has anomalous dielectric behavior at 11 K, be investigated further. Further low temperature studies are also needed on $NH_4H_2PO_4$, which from theoretical estimates could have enough entropy change remaining at 5 K in a high field to make a useful refrigerator.

Both mechanical and magnetothermal types of heat switches can be used successfully for a cyclic refrigerator operating between 15 and 4 K. Multiple leaf contact switches are useful for loads up to the order of 5 W/K. The magnetothermal switches where a transverse magnetic field alters the thermal conductivity of a metal single crystal are particularly useful because they have no moving parts. Single crystal beryllium can be used for both the upper and lower switch. It is also possible to use tungsten, but for the lower switch only.

Further engineering work on an electrocaloric refrigerator is not practical at this time. Instead more basic research on the thermodynamic behavior of dielectrics must be done to find a suitable refrigeration material or to show that such a material cannot exist because of certain fundamental reasons.

5. REFERENCES

1. Strobridge, T. R., Cryogenic Refrigerators - An Updated Survey, Nat. Bur. Stand. (U.S.) Tech. Note 655 (1974).

2. Lawless, W. N., Dielectric Cooling Technology: 15-4.2 K, Proc. Cryo. Cooler Conf. (1973), Tech. Report AFFDL-TR-73-149, vol. 1, p. 417.

3. Garrett, C. G. B., Magnetic Cooling (John Wiley and Sons, Inc., New York, 1954).

4. Kobeko, P. and Kurtschatov, J., Dielektrische Eigenschaften der Seignettesalzkristalle, Zeit, fur Physik 66, 192 (1930).

5. van Geuns, J. R., a Study of a New Magnetic Refrigerating Cycle, Philips Res. Repl Suppl. No. 6 (1966); U.S. Patent 3,413,814 (1968), Method and Apparatus for Producing Cold.

6. Lawless, W. N., A Low Temperature Glass-Ceramic Capacitance Thermometer, Rev. Sci. Instrum. 42, 561 (1971).

7. Rubin, L. G. and Lawless, W. N., Studies of a Glass-Ceramic Capaciance Thermometer in an Intense Magnetic Field at Low Temperatures, Rev. Sci. Instrum. 42, 571 (1971).

8. Lawless, W. N., Radebaugh, R., and Soulen, R. J., Studies of a Glass-Ceramic Capacitance Thermometer between 0.025 and 2.4 K, Rev. Sci. Instrum. 42, 567 (1971).

9. Lawless, W. N., Low-Temperature Dielectric Bolometer, J. Opt. Soc. Am. 62, 1449 (1972); Improvements on "Low-Temperature Dielectric Bolometer," J. Opt. Soc. Am. 64, 820 (1974).

10. Lawless, W. N., Closed-Cycle Electrocaloric Refrigerator and Method, U.S. Patent No. 3,638,440 (1972).

11. Steigmeier, E. F., Field Effect on the Cochran Modes in $SrTiO_3$ and $KTaO_3$, Phys. Rev. 168, 523 (1968).

12. See, for example, Colwell, J. H., The Performance of a Mechanical Heat Switch at Low Temperatures, Rev. Sci. Instrum. 40, 1182 (1969), and references cited therein.

13. Berman, R., Some Experiments on Thermal Contact at Low Temperatures, J. Appl. Phys. 27, 318 (1956).

14. Berman, R. and Mate, C. F., Thermal Contact at Low Temperatures, Nature 182, 1661 (1958).

15. Jacobs, R. B. and Starr, C., Thermal Conductance of Metallic Contacts, Rev. Sci. Instrum. 10, 140 (1939).

16. Kopp, F. J. and Ashworth, J., Carbon Resistors as Low Temperature Thermometers, Rev. Sci. Instrum. 43, 327 (1972).

17. Childs, G. E., Ericks, L. J., and Powell, R. L., Thermal Conductivity of Solids at Room Temperature and Below, NBS Monograph 131 (1973).

18. McCarty, R. D., Thermophysical Properties of Helium-4 from 2 to 1500 K with Pressures to 1000 Atmospheres, Nat. Bur. Stand. (U.S.) Tech. Note 631 (1972).

19. Aschermann, Von G., and Justi, E., Elektrische Leitfähigkeit, magnetische Widerstandsvermehrung, Hall-effekt und Supraleitung von Rhenium, Phys. Z. 43, 207 (1942).

20. Rosenberg, H. M., Low Temperature Solid State Physics (Oxford at the Clarendon Press, 1963) Chapter 5.

21. Engels, J. M. L., Gorter, F. W., and Miedema, A. R., Magnetoresistance of Gallium - A Practical Heat Switch at Liquid Helium Temperatures, Cryogenics 12, 141 (1972).

22. Boughton, R. I. and Yaqub, M., Anisotropy of the Electron Mean Free Path in the Thermal Conductivity of Very Pure Gallium, Phys. kondens. Materie 9, 138 (1969).

23. Yaqub, M. and Cochran, J. F., Mean Free Path of Electrons and Magnetomorphic Effects in Small Single Crystals of Gallium, Phys. Rev. 137, A1182 (1965).

24. DeHaas, W. J. and DeNobel, J., The Thermal and the Electrical Resistance of a Tungsten Single Crystal at Low Temperatures and in Magnetic Fields, Physica 5, 449 (1938); DeNobel, J., Thermal and Electrical Resistivity of Some Tungsten Single Crystals at Low Temperatures and in Strong Magnetic Fields, Physica 23, 261 (1957).

25. Long, J. R., Thermal and Electrical Transport in a Tungsten Crystal for Strong Magnetic Fields and Low Temperatures, Phys. Rev. B3, 1197 (1971).

26. Grüneisen, E. and Adenstedt, H., Enfluss Transversaler Magnetfelder auf Elektrizitäts-und Wärmeleitung reiner Metalle bei tiefer Temperatur, Ann. Physik [5] 31, 714 (1938).

27. Grüneisen, E. and Erfling, H. S., Electrischer und Thermischer Widerstand von Berylliumkristallen im Transversalen Magnetfeld, Ann. Physik [5] 38, 399 (1940).

28. Sparks, L. L. and Powell, R. L., Low Temperature Thermocouples: KP, "Normal" Silver, and Copper versus Au-0.02 at %Fe and Au-0.07 at %Fe, Journal of Research NBS 76A, 263 (1972).

29. Powell, R. W., The Thermal and Electrical Conductivities of Beryllium, Phil. Mag. 44, 645 (1953).

30. Reich, R., Kink, V. Q., and Bonmarin, J., Etude de la resistivite d'echantillons de beryllium de differentes puretes en fonction de la temperature et determination de la temperature de Debye de ce metal, Compt. Rend. Acad. Sci. 256, 5558 (1963).

31. Powell, R. L., Harden, J. L., and Gibson, E. F., Low Temperature Transport Properties of Commercial Metals and Alloys. IV. Reactor Grade Be, Mo, and W, J. Appl. Phys. 31, 1221 (1960).

32. Meaden, G. T., Electrical Resistance of Metals (Plenum Press, New York, 1965) p. 132.

33. Friedberg, C. B., Effects of Alloying in the Dilute Limit on the Quantum States of Electrons in Magnesium, J. Low Temp. Phys. 14, 147 (1974).

34. Anderson, A. C. and Peterson, R. E., Selection of a Thermal Bonding Agent for Temperatures below 1 K, Cryogenics 10, 430 (1970).

35. Steyert, W. A., Thermal Transport Across Superconducting Solder Joints Near 0.1 K, Rev. Sci. Instrum. 38, 964 (1967).

36. Challis, L. J. and Cheeke, J. D. N., Thermal Conduction Across Copper-Leand-Copper Sandwiches at Helium Temperatures, Proc. Phys. Soc. (London) 83, 109 (1964).

37. Barnes, L. J. and Dillinger, J. R., Thermal Resistivity at Pb-Cu and Sn-Cu Interfaces between 1.3 and 3.1 K, Phys. Rev. 141, 615 (1966).

38. Yovanovich, M. M. and Tuarze, M., Experimental Evidence of Thermal Resistance at Soldered Joints, J. Spacecraft 6, 855 (1969); Yovanovich, M. M., A Correlation of the Minimum Thermal Resistance at Soldered Joints, J. Spacecraft 7, 1013 (1970).

39. Ashworth, T., Loomer, J. E., and Kreitman, M. M., Thermal Conductivity of Nylonds and Apiezon Greases, Adv. Cry. Eng. 18, 271 (1973).

40. McTaggart, J. H. and Slack, G. A., Thermal Conductivity of General Electric No. 7031 Varnish, Cryogenics 9, 384 (1969).

41. Sauer, H. J., Jr., Remington, C. R., Stewart, W. E., Jr., and Lin, J. T., Thermal Contact Conductance with SEveral Interstitial Materials, XI Int'l. Thermal Cond. Conf., Albuquerque, NM, 1971, p. 22.

42. Sauer, H. J., Jr., Remington, C. R., and Heizer, G. A., Thermal Contact Conductance of Lubricant Films, XI Int'l. Thermal Cond. Conf., Albuquerque, NM, 1971, p. 24.

43. Gmelin, E., A Cryostat for Measuring Heat Capacities from 1.2 to 300 K and Measurements of the Specific Heat of Magnesium Oxide below 36 K, Cryogenics 7, 225 (1967).

44. Bitter, F., Water-Cooled Magnets, Proc. Int'l. Conf. High Magnetic Fields, M.I.T., 1961, p. 85.

45. Lawless, W. N., Thermodynamics of Electrocaloric Phenomena in KCl:OH. Paraelectric Cooling, J. Phys. Chem. Solids 30, 1161 (1969).

46. Weiss, P. and Forrer, R., Ann. Phys. Pariz 5, 153 (1926).

47. See, For example, Thacher, P. D., Electrocaloric Effects in Some Ferroelectric and Antiferroelectric Pb(Zr, Ti)O_3 Compounds, J. Appl. Phys. 39, 1996 (1968), and references cited therin.

48. Gränicher, H., Induzierte Ferroelektrizität von $SrTiO_3$ bei sehr tiefen Temperaturen und über die Kälteerzeugung durch adiabatische Entpolarisierung, Helv. Phys. Acta 29, 210 (1956).

49. Frenzel, C., Gladun, A., Gladun, C., Hegenbarth, E., and Knorn, M., Measurement of the Dielectric Constant of $SrTiO_3$ in the Temperature Range from 1.2 to 0.025 K, phys. stat. sol. (a)15, K61 (1973).

50. Barrett, J. H., Dielectric Constant in Perovskite Type Crystals, Phys. Rev. 86, 118 (1952).

51. Hegenbarth, E., Studies of the Electrocaloric Effect of Ferroelectric Ceramics at Low Temperatures, Cryogenics 1, 242 (1961).

52. Kikuchi, A. and Sawaguchi, E., Electrocaloric Effect in $SrTiO_3$, J. Phys. Soc. Japan 19, 1497 (1964).

53. Hegenbarth, E., Die Temperaturabhängigkeit des elektrokalorischen Effects bei $SrTiO_3$-Einkristallen, phys. stat. sol. 8, 59 (1965).

54. Sawaguchi, E., Kikuchi, A., and Kodera, Y., Dielectric Constant of Strontium Titanate at Low Temperatures, J. Phys. Soc. Japan 17, 1666 (1962).

55. Kanzig, W., Hart, H. R., Jr., and Roberts, S., Paraelectricity and Ferroelectricity Due to Hydroxyl Ions in Alkali Halides; Paraelectric Cooling, Phys. Rev. Letters 13, 543 (1964).

56. Kuhn, U. and Lüty, F., Paraelectric Heating and Cooling with OH^--Dipoles in Alkali Halides, Solid State Commun. 4, 31 (1965).

57. Shepherd, I. and Feher, G., Cooling by Adiabatic Depolarization of OH^- Molecules in KCl, Phys. Rev. Letters 15, 194 (1965); Shepherd, I. W., Electrocaloric Properties of OH^- Molecules in KCl, J. Phys. Chem. Solids 28, 2027 (1967).

58. Lawless, W. N., Ideal Paraelectric Refrigeration in KCl;OH and RbCl:CN, J. Appl. Phys. 40, 4448 (1969).

59. Lombardo, G. and Pohl, R. O., Electrocaloric Effect and a New Type of Impurity Mode, Phys. Rev. Letters 15, 291 (1965).

60. Pohl, R. O., Taylor, V. L., and Gouban, W. M., Electrocaloric Effect in Doped Alkali Halides, Phys. Rev. 178, 1431 (1969).

61. Korrovits, V. Kh., Luud'ya, G. G., and Mikhkel'soo, V. T., Thermostating Crystals at Temperatures Below 1 K by Using the Electrocaloric Effect, Cryogenics 14, 44 (1974).

62. Lawless, W. N., Paraelectric Refrigeration Method and Apparatus, U. S. Patent 3,436,924 (1969).

63. Robinson, M. C. and Wertheimer, M. R., Paraelectric Refrigerator, U. S. Patent 3,650,117 (1972).

64. Stookey, S. D., Glastech. Ber., 32K, 5th Int'l. Congress on Glass (Verlay der Deutschen Glastechnischen Gesellschaft, Frankfurt am Main, 1959), p. 574.

65. Herczog, A., Microcrystalline $BaTiO_3$ by Crystallization from Glass, J. Amer. Ceram. Soc. 47, 107 (1964); Layton, M. M. and Herczog, A., Nucleation and Crystallization of $NaNbO_3$ from Glasses in the Na_2O-Nb_2O_5-SiO_2 System, ibid. 50, 369 (1967).

66. Weaver, H. E., Dielectric Properties of Single Crystals of $SrTiO_3$ at Low Temperatures, J. Phys. Chem. Solids 11, 274 (1959).

67. Saifi, M. A. and Cross, L. E., Dielectric Properties of Strontium Titanate at Low Temperature, Phys. Rev. 82, 677 (1970).

68. Sakudo, T. and Unoki, H., Dielectric Properties of $SrTiO_3$ at Low Temperatures, Phys. Rev. LEtters 26, 851 (1971).

69. Neville, R. C. Hoeniesen, B., and Mead, C. A., Permittivity of Strontium Titanate, J. Appl. Phys. 43, 2124 (1972).

70. McBrayer, R. D., Peters, F. I., and Smith, R. D., Method of Making a Capacitor, U. S. Patent 3,604,082 (1971).

71. Gesi, K., Pyroelectric Study on the Spontaneous Polarization in $AgNa(NO_2)_2$, J. Phys. Soc. Japan 33, 108 (1972).

72. Knop, K., Pfister, G., and Känzig, Dielectric Relaxation of KBr Doped with KOH and KOD, Phys. kondene. Materie 7, 107 (1968); Kapphan, S. and Liity, F., Electro-Caloric Effects of Li^+, OH^- and Ag^+ Dipoles in Alkali Halides, Solid State Commun. 6, 907 (1968).

73. Pandorf, R. C., Chen, C. Y., and Daunt, J. G., Heat Transport Through Carbon Radio Resistors at Low Temperatures and Their Use in Conjunction with Superconducting Thermal Valves, Cryogenics 2, 239 (1962).

74. Neighbor, J. E., Leads Power Calorimentry, Rev. Sci. Instrum. 37, 497 (1966).

75. White, G. K. and Birch, J. A., Thermal Properties of Silica at Low Temperatures, Phys. Chem. Glasses 6, 85 (1965).

76. Flubacher, P., Leadbetter, A. J., Morrison, J. A., and Stoicheff, B. P., The Low Temperature Heat Capacity and the Raman and Brillouin Spectra of Vitreous Silica, J. Phys. Chem. Solids 12, 53 (1959); Simon, F., Untersuchungen, über die spezifische wärme bei tiefen temperaturen, Ann. Physik 68, 241 (1922).

77. Leadbetter, A. J., The Thermal Properties of Glasses at Low Temperatures, Phys. Chem. glasses 9, 1 (1968).

78. Bucci, C., Fieschi, R., and Guidi, G., Ionic Thermocurrents in Dielectrics, Phys. Rev. 148, 816 (1966).

79. Gopal, E. S. R., Specific Heats at Low Temperatures, (Plenum Press, New York, 1966).

80. Samara, G. A., Temperature and Pressure Dependence of the Dielectric Constants of the Thallous Halides, Phys. Rev. 165, 959 (1968).

81. Colwell, J. H., private communication, 1975.

82. Hegenbarth, E., Dielecktrische und kalorische Untersuchungen an ferroelektrischen Keramiken bei tiefen Temperaturen, phys. stat. sol. 2, 1544 (1962).

83. Todd, S. S. and Lorenson, R. E., Heat Capacities at Low Temperatures and Entropies at 298.16 K of Metatitanates of Barium and Strontium, J. Amer. Chem. Soc. 74, 2043 (1952).

84. Sawaguchi, E., Ferroelectricity versus Antiferroelectricity in the Solid Solutions of $PbZrO_3$ and $PbTiO_3$, J. Phys. Soc. Japan 8, 615 (1953).

85. Demurov, D. G., Nikiforov, L. G., Viskov, A. S. and Venevtsev, Yu. N., New Antiferroelctrics Having the Pyrochlore Structure, Soviet Physics-Solid State 11, 3089 (1970).

86. Venevtsev, Yu. N., Kapyshev, A. G., Shvorneva, L. I., et al., New Ferroelectrics and Seignettomagnets of the Perovskite and Pyrochlore Type: Synthesis and Study of the Crystal Structure and Properties, Proc. 2nd Int'l. Meeting on Ferroelectricity, 1969, J.Phys. Soc. Japan, Supplement 28, 139 (1970).

87. Hulm, J. K., Low-Temperature Dielectric Properties of Cadmium and Lead Niobates, Phys. Rev. 92, 504 (1953).

88. Burke, W. J. and Pressley, R. J., Stress Induced Ferroelectricity in $SrTiO_3$, Solid State Commun. 9, 191 (1971).

89. Jona, F. and Shirane, G., Ferroelectric Crystals (Macmillan, New York, 1962), p. 251.

90. Hulm, J. K., Matthias, B. T., and Long, E. A., A Ferromagnetic Curie Point in $KTaO_3$ at Very Low Temperatures, Phys. Rev. 79, 885 (1950).

91. Demurov, D. G., and Venevtsev, Yu. N., Character of Phase Transition of Ferroelectric $KTaO_3$, Sov. Phys. Solid State 13, 553 (1971), [Fiz. Tverd. Tela. 13, 669 (1971)].

92. Samara, G. A., and Morosin, B., Anharmonic Effects in $KTaO_3$: Ferroelectric Mode, Thermal Expansion, and Compressibility, Phys. Rev. B8, 1256 (1973).

93. Dekker, A. J., Solid State Physics (Prentice Hall, NJ, 1957), p. 144.

94. Skanavi, G. I., and Matveeva, E. N., New Nonpiezoelectric Dielectrics with Very High Dielectric Permeability and Small Conductivity, Sov. Phys. JETP. 3, 905 (1957).

95. Tien, T. Y., and Cross, L. E., Dielectric Relaxation in Strontium Titanate Solid Solutions Containing Lanthania, Jap. J. Appl. Phys. 6, 459 (1967).

96. Johnson, D. W., Cross, L. E., and Hummel, F. A., Dielectric Relaxation in Strontium Titanates Containing Rare-Earth Ions, J. Appl. Phys. 41, 2828 (1970).

97. Nomura, S., and Kojima, F., Dielectric Relaxation and Thermal Stimulated Current in $(K_{3/4}Bi_{1/4})(Zn_{1/6}Nb_{5/6})O_3$ and Its Solid Solutions, Jap. J. Appl. Phys. 12, 205 (1972); Dielectric Properties of Perovskite-Type $(K_{3/4}Bi_{1/4})(Mg_{1/6}Ta_{5/6})O_3$ and $(K_{3/4}Bi_{1/4})(Mg_{1/6}Nb_{5/6})O_3$ Ceramics, ibid. 14, 907 (1975).

98. Gutmann, F., The Electret, Rev. Mod. Phys. 20, 457 (1948).

99. Fridkin, V. M. and Zheludev, I. S., Photo Electrets and the Electrophotographic Process, (Consultants Bureau, New York, 1960).

100. Pillai, P. K. C., Jain, K., and Jain, V. K., Thermoelectrets and Their Applications, phys. stat. sol. (a)13, 341 (1972).

101. Gross, B., Electret Devices for Pollution Control, T. Kallard, Ed., (Optsonic Press, New York, 1974).

102. Gubkin, A. N., and Skanavi, G. I., Akad. Nauk SSSR, Bulletin, Phys. Ser. 22, 327 (1958).

103. Cook, J. S., and Dryden, J. S., An Investigation of the Aggregation of Divalent Cationic Impurities in Alkali Halides by Dielectric Absorption, Proc. Phys. Soc. (London) 80, 479 (1962).

104. Crawford, J. H., Jr., Aggregation of Divalent Metal Impurity in Alkali Halide Crystals, J. Phys. Chem. Solids 31, 399 (1970).

105. Stoebe, T. G. and Watanabe, S., Thermoluminescence and Lattice Defects in LiF, phys. stat. sol. (a)29, 11 (1975).

106. Dryefus, R. W., Dielectric Relaxation Due to Impurity-Vacancy Complexes in NaCl Crystals, Phys. Rev. 121, 1675 (1961).

107. Bakalyar, D., Swinehart, R., Weyhmann, W., and Lawless, W. N., Studies of a Glass-Ceramic Capacitance Thermometer between 0.007 and 0.040 K, Rev. Sci. Instrum. 43, 1221 (1972).

108. Blinc, R., and Zeks, B., Soft Modes in Ferroelectrics and Antiferroelectrics, Selected Topics in Solid State Physics, Vol. 13 (North-Holland, New York, 1974).

109. Devonshire, A. F., Theory of Ferroelectrics, Adv. Phys. 3, 85 (1954).

110. Matthias, B. T. and Hulm, J. K., New Ferroelectric Tartrates, Phys. Rev. 82, 108 (1951).

111. Sawaguchi, E., and Cross, L. E., Electric Field Control of the Elastic Compliance in Lithium Thallium Tartrate, Appl. Phys. Letters 18, 1 (1971); Control of the Elastic Compliance of Ferroelectric $LiTlC_4H_4O_6\cdot H_2$) by Electric field, Ferroelectrics 3, 327 (1972).

112. Sawaguchi, E. and Cross, L. E., Electromechanical Coupling Effects on the Dielectric Properties and Ferroelectric Phase Transition in Lithium Thallium Tartrate, Ferroelectrics 2, 37 (1971).

113. Abe, R., Kamiya, N., and Matsuda, M., Dielectric Behavior of LLT and Calculation of Dipole-Dipole Interaction Energy in LAT, Ferroelectrics 8, 557 (1974).

114. Cochran, W., Crystal Stability and the Theory of Ferroelectricity, Adv. Phys. 9, 387 (1960); Crystal Stability and the Theory of Ferroelectricity, Part II. Piezoelectric Crystals, Adv. Phys. 10, 401 (1961).

115. Anderson, P. W., *Proceedings of the Conference* on the Physics of Dielectrics (Academy of Science, USSR, Moscow, 1958), p. 290.

116. Burns, G. and Scott, B. A., Lattice Modes in Ferroelectric Perovskites: $PbTiO_3$, Phys. Rev. B7, 3088 (1973).

117. Ziman, J. M., Principles of the Theory of Solids, 2nd. ed. (Cambridge University Press, 1972).

118. Yamada, Y., and Shirane, G., Neutron Scattering and Nature of the Soft Optical Phonon in $SrTiO_3$, J. Phys. Soc. Japan 26, 396 (1969).

119. Bell, R. O. and Rupprecht, G., Elastic Constants of Strontium Titanate, Phys. Rev. 129, 90 (1963).

120. Worlock, J. M. and Fleury, P. A., Electric Field Dependence of Optical-Phonon Frequencies, Phys. Rev. Letters 19, 1176 (1967).

121. Shirance, G. and Yamada, Y., Lattice-Dynamical Study of the 110 K Phase Transition in $SrTiO_3$, Phys. Rev. 177, 858 (1969).

122. Cowley, R. A., Lattice Dynamics and Phase Transitions of Strontium Titanate, Phys. Rev. A134, 981 (1964).

123. Lombardo, G., Sievers, A. J., and Pohl, R. O., Low-Temperature Heat Capacity of $SrTiO_3$, Bull. Am. Phys. Soc. 10, 44 (1965).

124. Shirane, G., Nathans, R., and Minkiewicz, V. J., Temperature Dependence of the Soft Ferroelectric Mode in $KTaO_3$, Phys. Rev. 157, 396 (1967).

125. Axe, J. D., Harada, J., and Shirane, G., Anomalous Acoustic Dispersion in Centrosymmetric Crystals with Soft Optic Phonons, Phys. Rev. B1, 1227 (1970).

126. Barrett, H. H., Ultrasonic Propagation Velocity in $KTaO_3$, Phys. Letters 26A, 217 (1968).

127. Cowley, E. R., and Okazaki, A., The Lattice Dynamics of Thallous Bromide, Proc. Roy. Soc. (London) A300, 45 (1967).

128. Vallin, J., Marklund, K. and Sikström, J. O., Second Nordic Solid State Conference, Tylösand, Sweden, 1966.

129. Khmel'nitskii, D. E., and Sheneerson, V. L., Phase Transitions of the Displacement Type in Crystals at Very Low Temperatures, Sov. Phys.-JETP 37, 164 (1973).

130. Samara, G. A., Vanishing of the Ferroelectric and Antiferroelectric States in KH_2PO_2 Type Crystals at High Pressure, Phys. Rev. Letters 27, 103 (1971).

131. Kurtz, S. K., Electrooptic Materials, Trans. Amer. Crystallographic Assoc., Vol. II on Appl. Crystal Chem. 1975.

AD-A037 412 DEVELOPMENT OF SANDWICH STRUCTURED PHOTOSENSITIVE FILMS FOR APPLICATION TO NON-CONTACT POTENTIOMETERS(U) NAVAL AVIONICS FACILITY INDIANAPOLIS IND G A MAGEE NOV 76

UNCLASSIFIED NAFI-TR-2148-REV-1 F/G 14/2 NL

3/3

END
DATE FILMED
10-84
DTIC

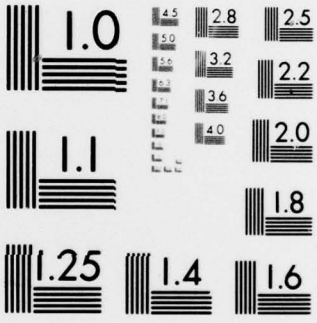

MICROCOPY RESOLUTION TEST CHART
NATIONAL BUREAU OF STANDARDS-1963-A

NBS-114A (REV. 7-73)

U.S. DEPT. OF COMM. BIBLIOGRAPHIC DATA SHEET	1. PUBLICATION OR REPORT NO. NBSIR 76-847	2. Gov't Accession No.	3. Recipient's Accession No.

4. TITLE AND SUBTITLE

ELECTROCALORIC REFRIGERATION FOR SUPERCONDUCTORS

5. Publication Date: February 1977

6. Performing Organization Code: 275.08

7. AUTHOR(S)
Ray Radebaugh, J. D. Siegwarth, W. N. Lawless & A. J. Morrow

8. Performing Organ. Report No.

9. PERFORMING ORGANIZATION NAME AND ADDRESS

NATIONAL BUREAU OF STANDARDS
DEPARTMENT OF COMMERCE
WASHINGTON, D.C. 20234

10. Project/Task/Work Unit No.: 2750489

11. Contract/Grant No.: NAonr-1-75 and ARPA 2535

12. Sponsoring Organization Name and Complete Address (Street, City, State, ZIP)

Advanced Research Projects Agency
Arlington, VA 22209

13. Type of Report & Period Covered: Final
May 1973 - June 1975

14. Sponsoring Agency Code

15. SUPPLEMENTARY NOTES

16. ABSTRACT (A 200-word or less factual summary of most significant information. If document includes a significant bibliography or literature survey, mention it here.)

A solid state type of refrigeration, which utilizes the electrocaloric effect in certain dielectric materials, has been investigated. Such a refrigerator would operate with a load at 4 K and reject heat to a reservoir at 15 K. Heat switches for such a refrigerator were studied. One type was a multiple leaf contact switch. The other type was a magnetothermal switch utilizing single crystal beryllium. Based upon earlier preliminary work, the refrigeration material was to be a $SrTiO_3$ glass-ceramic. It was found here that such a material has no useful electrocaloric effect at 4 K. Many other materials were studied but none were found with sufficiently high electrocaloric effects for a practical refrigerator. The largest effects were seen in $SrTiO_3$ ceramics, followed by $KTaO_3$ single crystal. Termperature reductions of about 0.5 K at 10 K were observed during depolarization. A theoretical model, based on the electret behavior of impurity-vacancy dipoles, was developed to explain the observed dielectric behavior in the materials investigated. Another theoretical model, based on the lattice dynamics of displacive dielectrics, was used to explain the observed entropy and temperature changes seen in such materials. The model points out that displacive type materials have too low entropies at 4 K for practical refrigeration. An investigation of certain order-disorder dielectrics is suggested.

17. KEY WORDS (six to twelve entries; alphabetical order; capitalize only the first letter of the first key word unless a proper name; separated by semicolons) Beryllium; ceramics; cryogenics; dielectric-constant; electrets; electrocaloric effect; entropy; ferroelectrics; glass-ceramics; heat switches; magnetothermal conductivity; polarization; potassium tantalate; refrigeration; specific heat; strontium titanate.

18. AVAILABILITY

[x] Unlimited

[ ] For Official Distribution. Do Not Release to NTIS

[ ] Order From Sup. of Doc., U.S. Government Printing Office Washington, D.C. 20402, SD Cat. No. C13

[x] Order From National Technical Information Service (NTIS) Springfield, Virginia 22151

19. SECURITY CLASS (THIS REPORT): UNCLASSIFIED

21. NO. OF PAGES: 194

20. SECURITY CLASS (THIS PAGE): UNCLASSIFIED

22. Price: $7.50

USCOMM-DC 29042-P74

D
B4